

Supplement of Atmos. Chem. Phys., 17, 10535–10563, 2017
<https://doi.org/10.5194/acp-17-10535-2017-supplement>
© Author(s) 2017. This work is distributed under
the Creative Commons Attribution 3.0 License.



Atmospheric
Chemistry
and Physics
Open Access
EGU

Supplement of

A quantitative analysis of the reactions involved in stratospheric ozone depletion in the polar vortex core

Ingo Wohltmann et al.

Correspondence to: Ingo Wohltmann (ingo.wohltmann@awi.de)

The copyright of individual parts of the supplement might differ from the CC BY 3.0 License.

Contents

1 Results for other years and altitudes than shown in the paper

- 1.1 Northern hemisphere 2004/2005 (Figure 1 – Figure 24)
- 1.2 Northern hemisphere 2009/2010 (Figure 25 – Figure 48)
- 1.3 Southern hemisphere 2006 (Figure 49 – Figure 72)
- 1.4 Southern hemisphere 2011 (Figure 73 – Figure 96)

2 Results for runs not corrected for the HCl discrepancy

- 2.1 Northern hemisphere 2004/2005 (Figure 97 – Figure 120)
- 2.2 Southern hemisphere 2006 (Figure 121 – Figure 144)

3 Comparison to measurements of MLS and ACE-FTS

MLS at 46 hPa (northern and southern hemisphere)
ACE-FTS at all altitudes (only southern hemisphere)

- 3.1 Northern hemisphere 2004/2005 (Figure 145 – Figure 152)
- 3.2 Southern hemisphere 2006 (Figure 153 – Figure 172)

**1 Results for other years and altitudes than shown
in the paper**

1.1 Northern Hemisphere 2004/2005

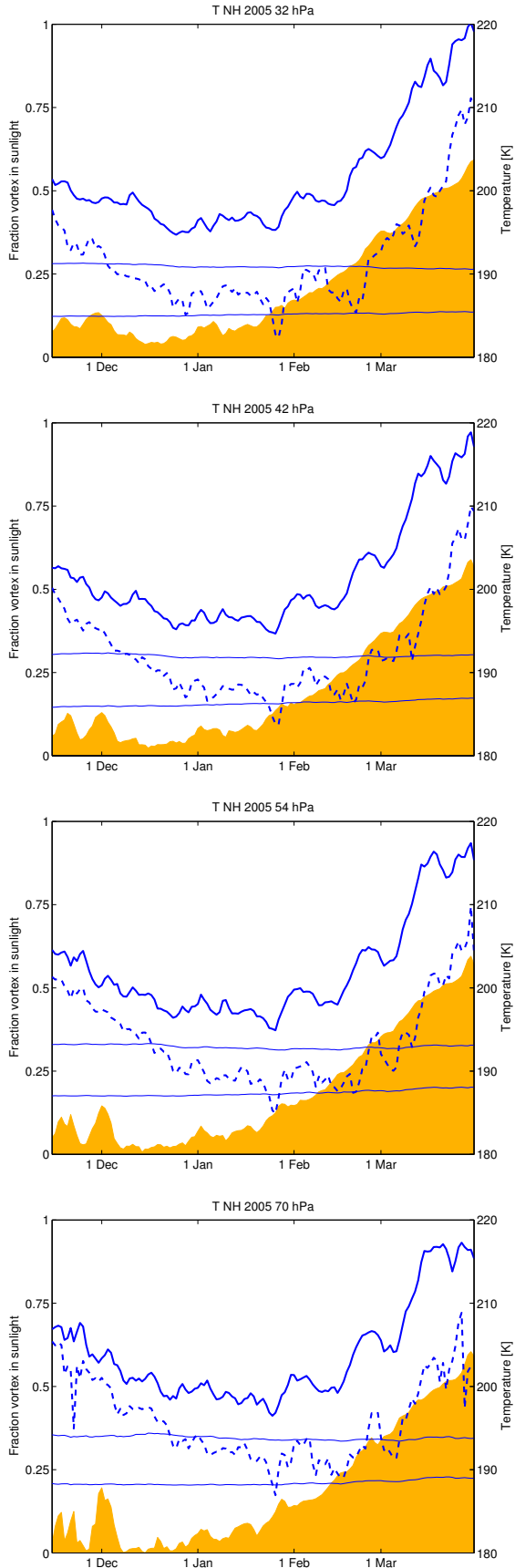


Figure 1: Vortex-averaged temperature (blue), vortex minimum temperature (dashed blue) and fraction of the vortex in sunlight (yellow). The upper thin blue line shows the threshold temperature for the formation of NAT clouds used in the model (based on vortex mean mixing ratios and considering supersaturation), and the lower thin blue line shows the same for ice clouds. The vortex tracer criterion is not applied (in contrast to all other figures).

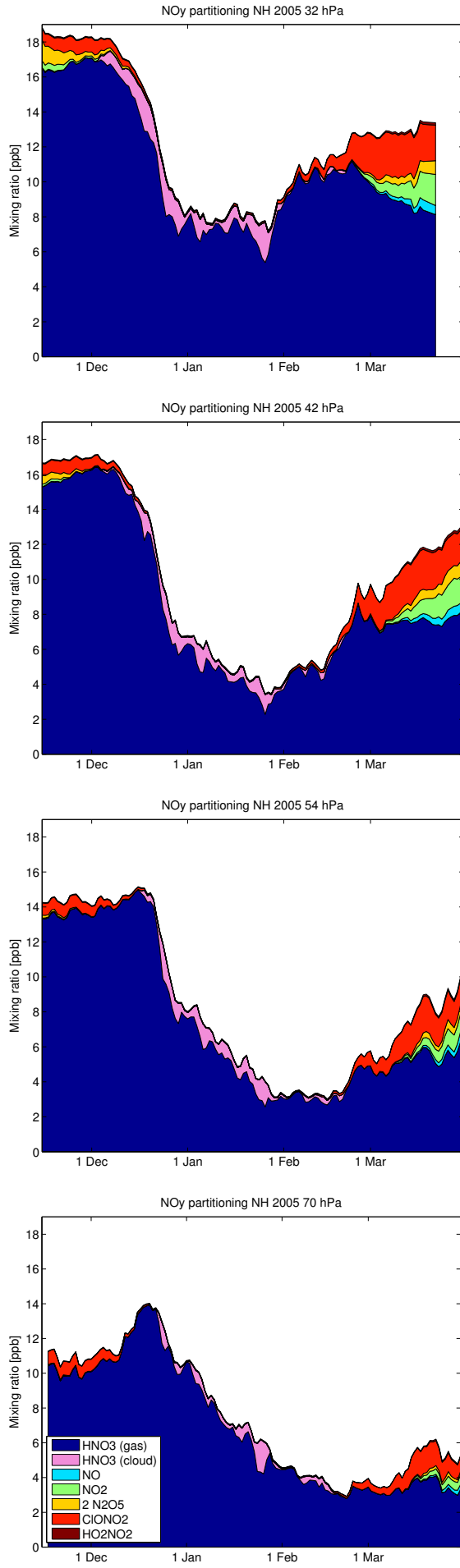


Figure 2: Vortex-averaged partitioning of NO_y species. Species NO₃, BrONO₂, ClONO₂ and N are not shown due to their small mixing ratios.

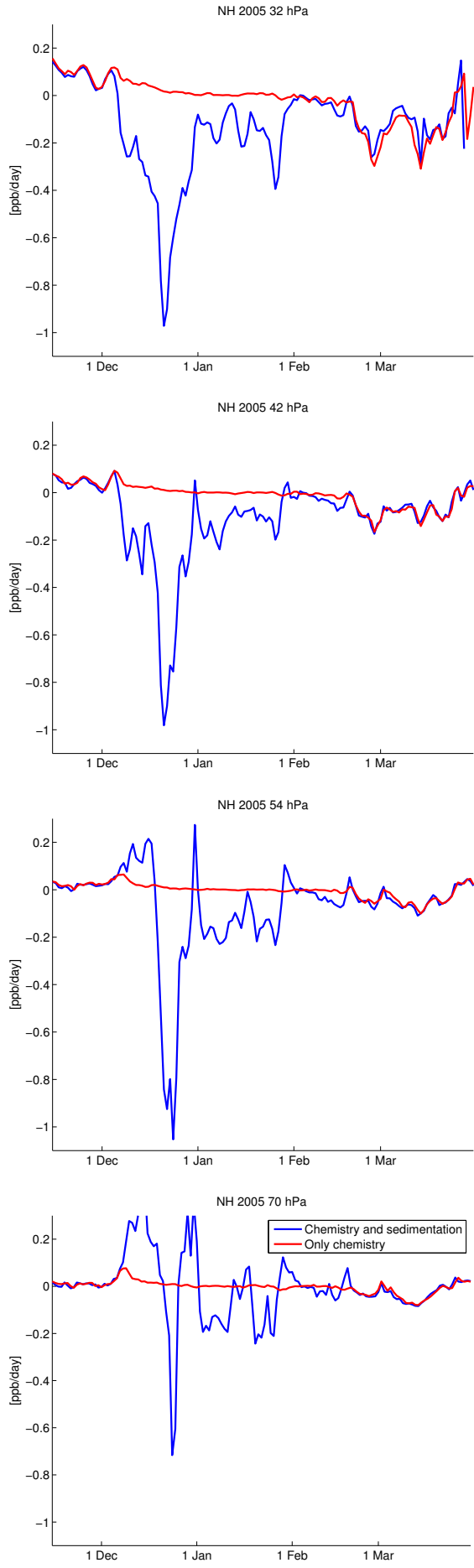


Figure 3: Vortex-averaged net chemical reaction rate of HNO₃ (red) and sum of the vortex-averaged change by sedimentation and the net chemical reaction rate (blue).

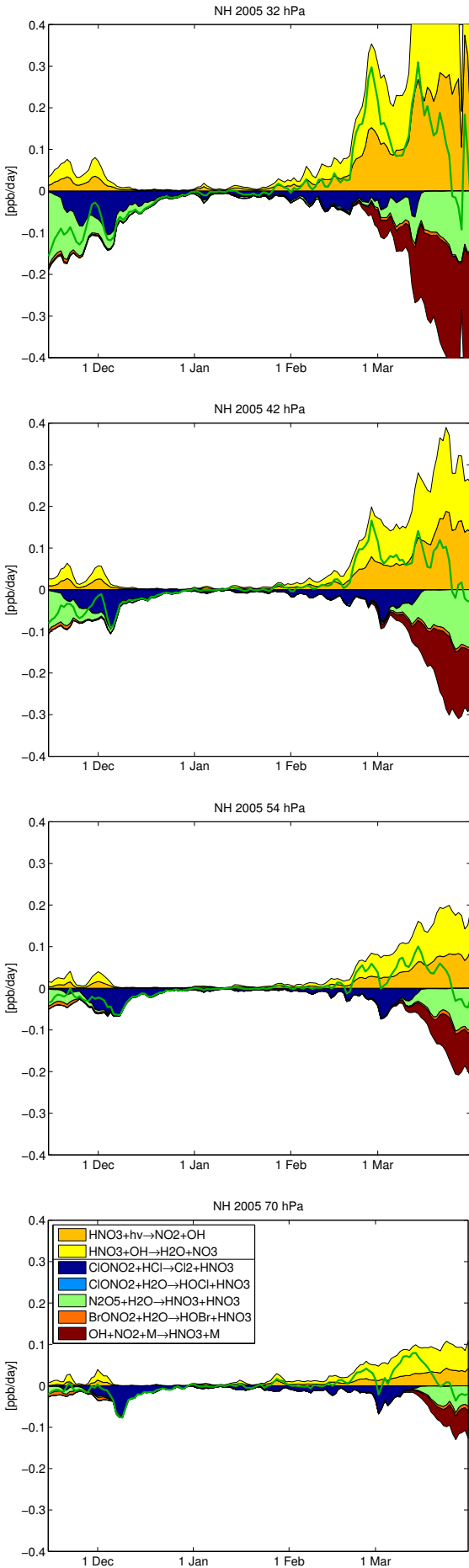


Figure 4: Vortex-averaged chemical reaction rates of reactions changing extended NO_x ($\text{NO} + \text{NO}_2 + \text{NO}_3 + 2\text{N}_2\text{O}_5 + \text{ClONO}_2 + \text{BrONO}_2 + \text{HO}_2\text{NO}_2$). Production reactions are shown positive and are separated by a line in the legend from the loss reactions, which are shown negative. The net change of extended NO_x is shown as a green line.

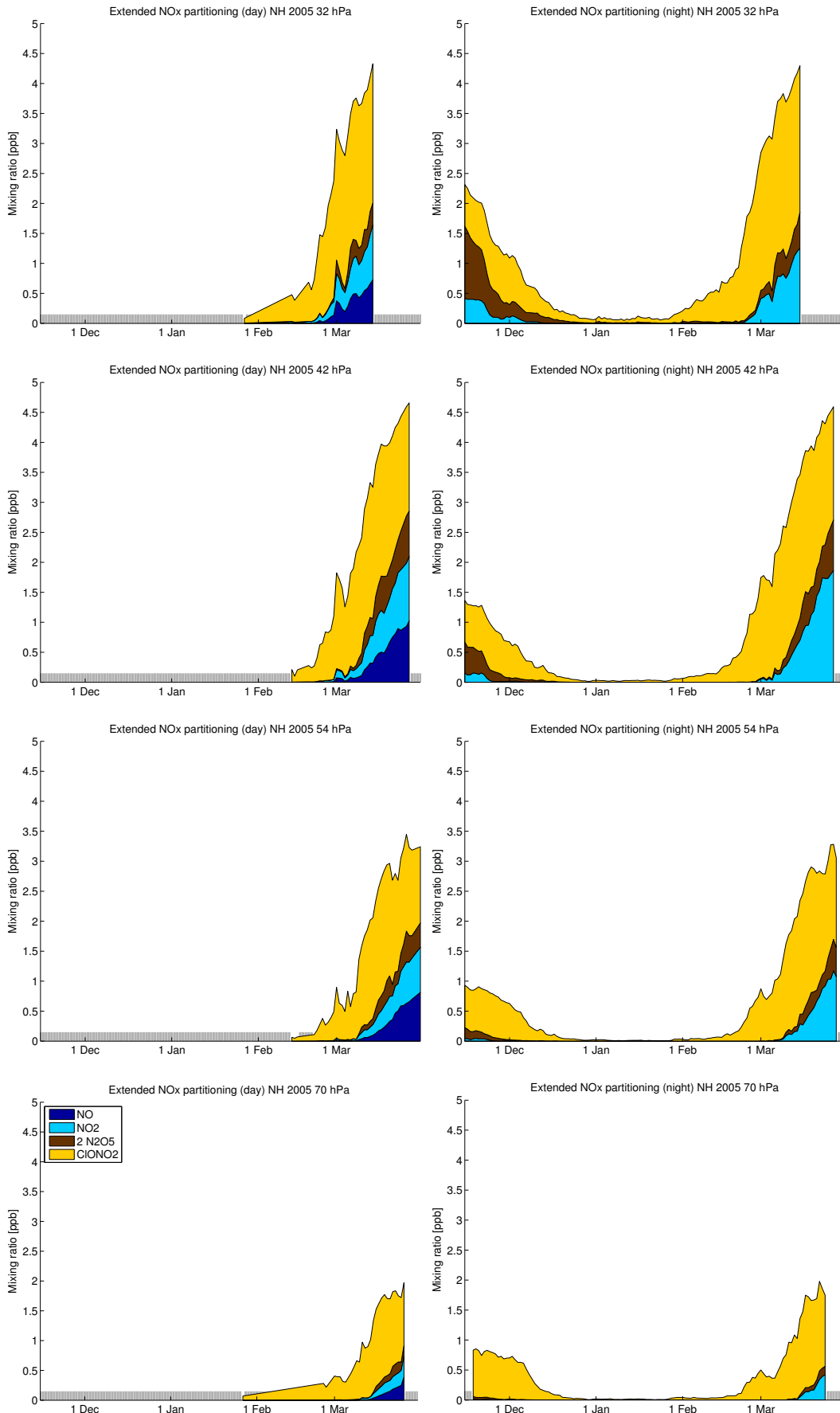


Figure 5: Vortex-averaged partitioning of extended NO_x species. Left: Daytime averages (parts of the vortex where the solar zenith angle is smaller than 80°). Right: Nighttime averages (parts of the vortex where the solar zenith angle is larger than 100°). Days without sufficient data for averaging are not shown (grey bars).

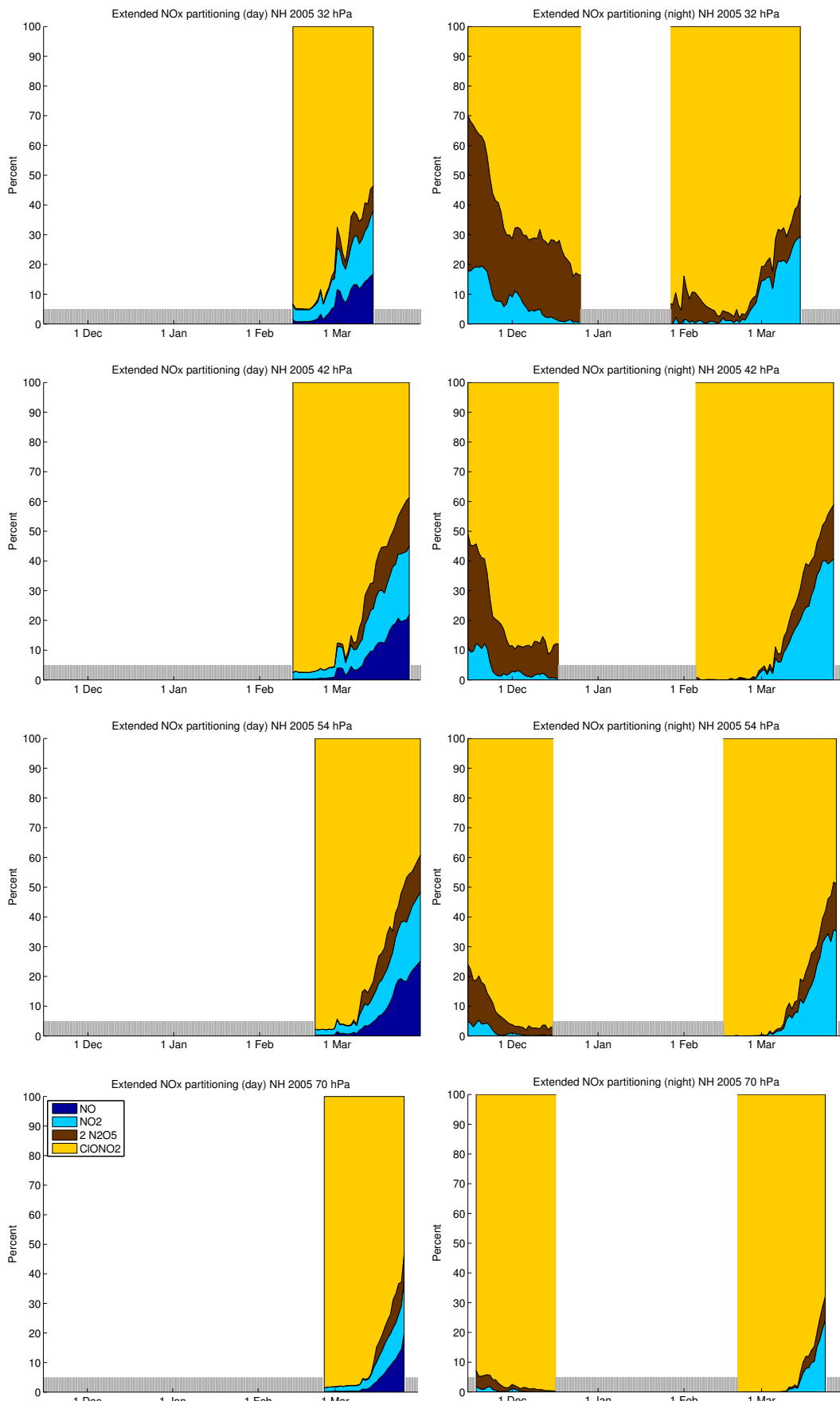


Figure 6: Same as Figure 5, but now in percentages and not in mixing ratios. Percentages are not shown for values of extended NO_x below 0.1 ppb and for days without sufficient data for averaging (grey bars).

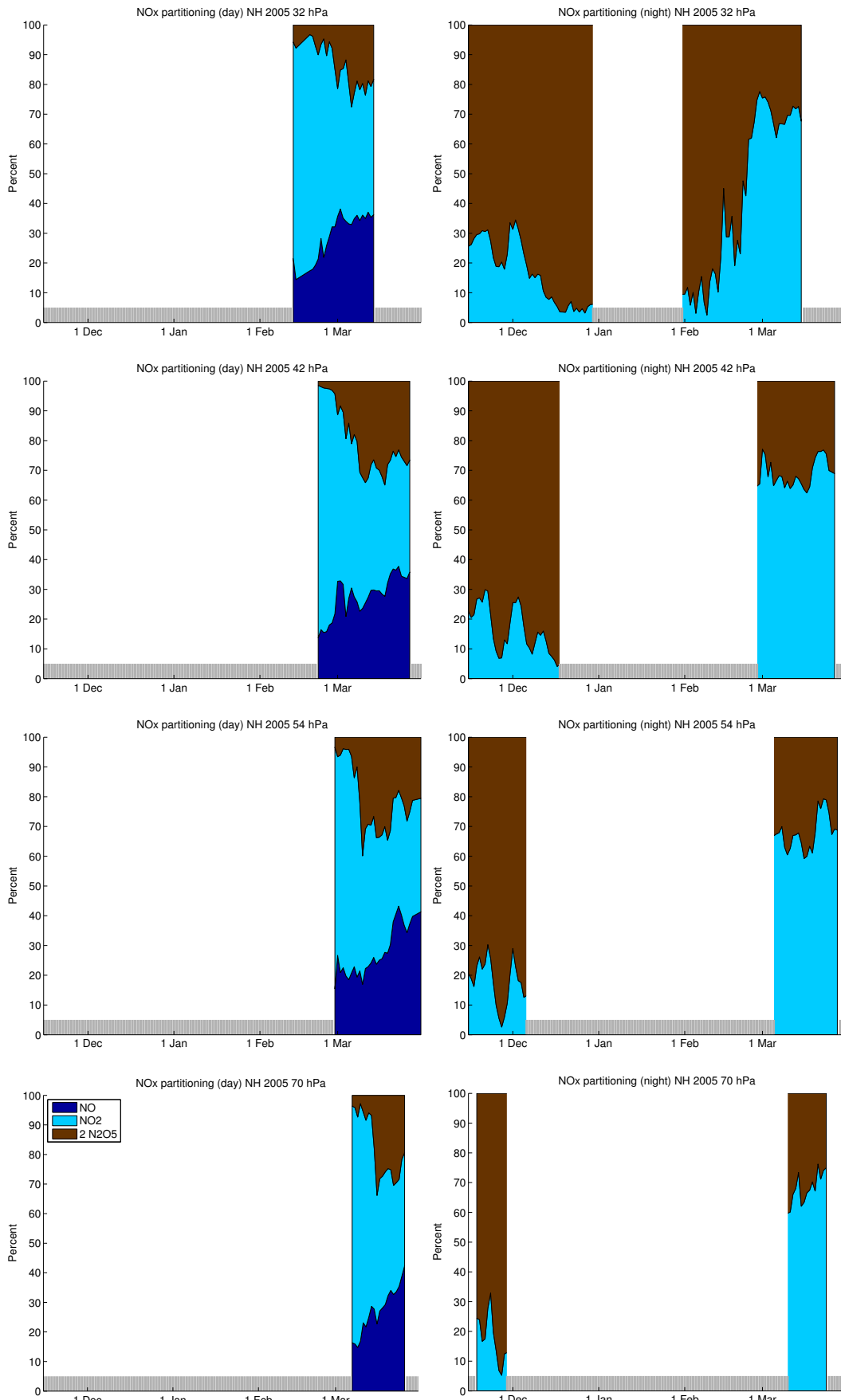


Figure 7: Same as Figure 6, but with only $\text{NO}_x = \text{NO} + \text{NO}_2 + 2\text{N}_2\text{O}_5$ partitioning. Percentages are not shown for values of NO_x below 0.01 ppb and for days without sufficient data for averaging (grey bars).

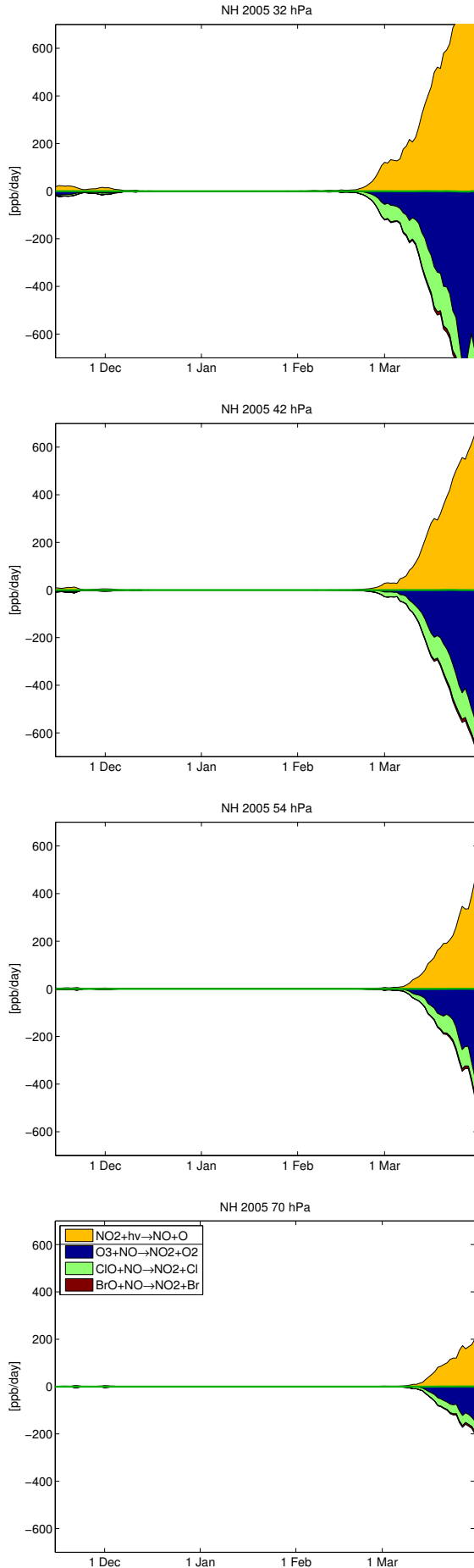


Figure 8: Vortex-averaged chemical reaction rates of reactions changing NO to illustrate NO_x partitioning. Production reactions are shown positive and are separated by a line in the legend from the loss reactions, which are shown negative. The net change of NO is shown as a green line.

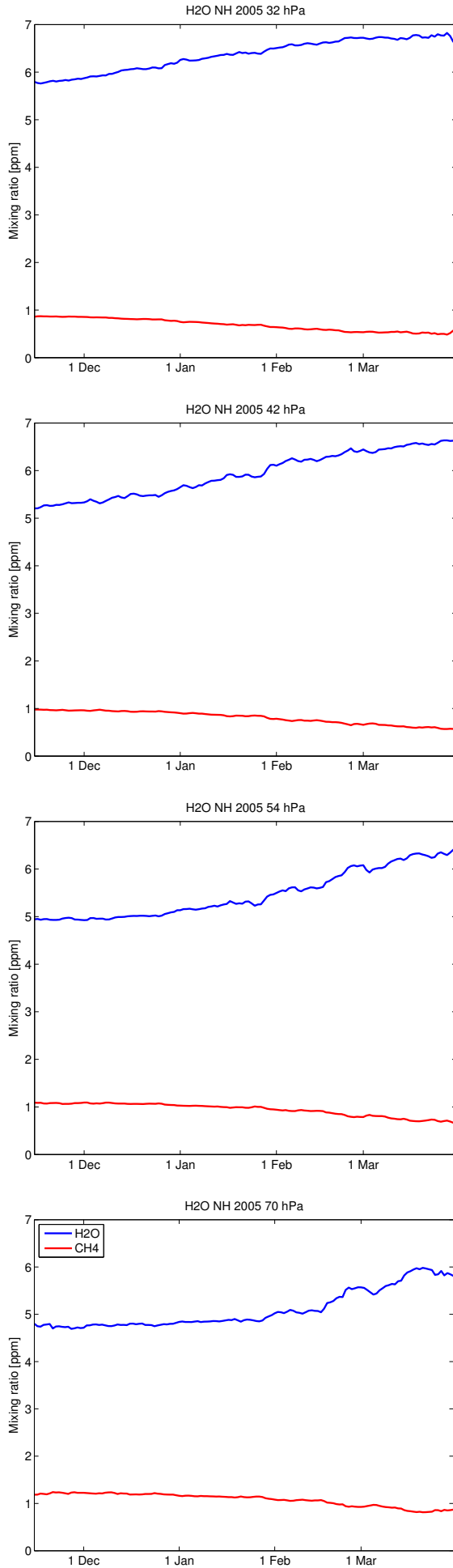


Figure 9: Vortex-averaged mixing ratios of H₂O and CH₄.

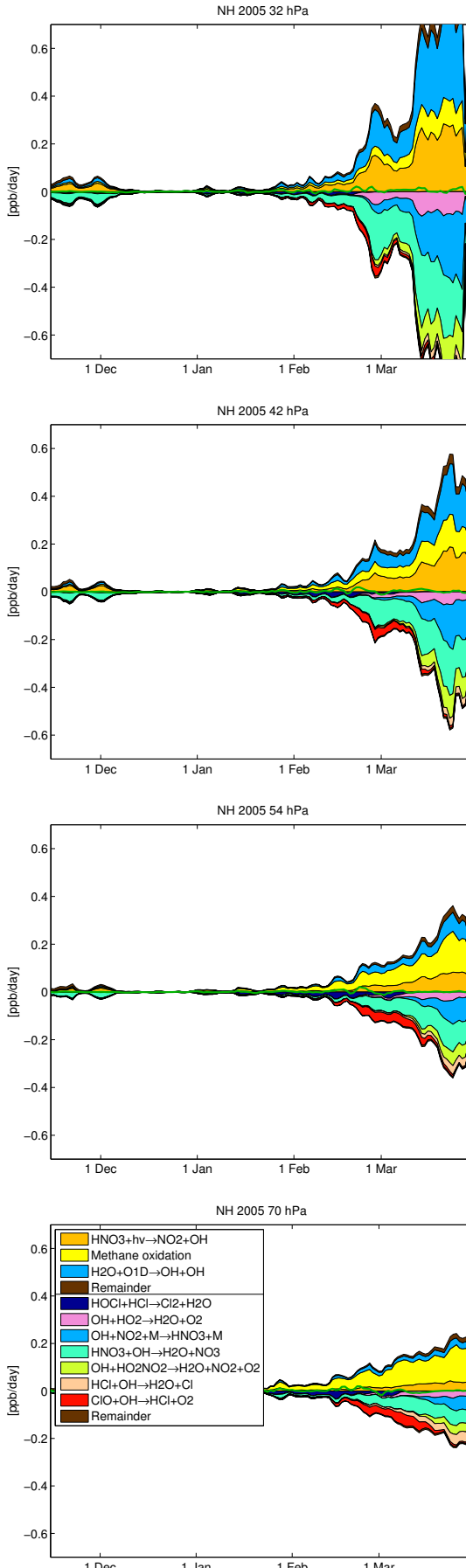


Figure 10: Vortex-averaged chemical reaction rates of reactions changing extended HO_x ($\text{OH} + \text{HO}_2 + \text{H} + \text{HOCl} + \text{HOBr} + \text{HO}_2\text{NO}_2$). Production reactions are shown positive and are separated by a line in the legend from the loss reactions, which are shown negative. The net change of extended HO_x is shown as a green line. Methane oxidation is modelled by simplified net reactions in ATLAS, the reactions denoted as methane oxidation in the legend are $\text{Cl} + \text{CH}_4 \rightarrow \text{HCl} + \text{CH}_2\text{O} + \text{HO}_2$ and $\text{Cl} + \text{CH}_2\text{O} \rightarrow \text{HCl} + \text{CO} + \text{HO}_2$.

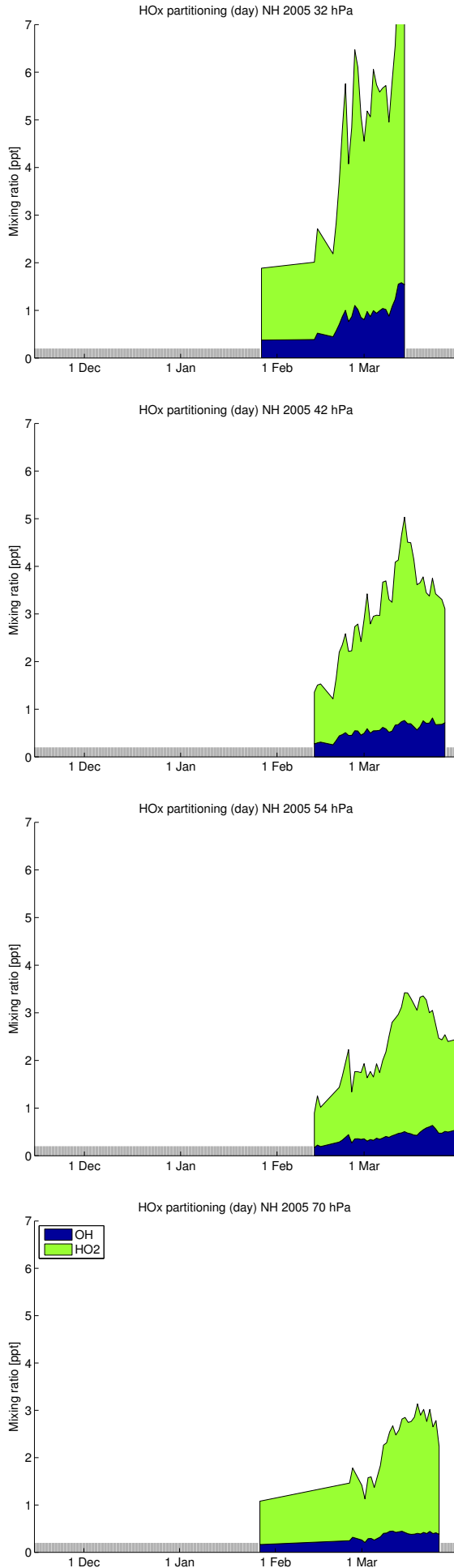


Figure 11: Vortex-averaged partitioning of HO_x species. Daytime averages (parts of the vortex where the solar zenith angle is smaller than 80°). Nighttime averages are near zero and not shown. Data: WRF-Chem (10 km resolution, 40 sigma levels, 1000 m orographic height).

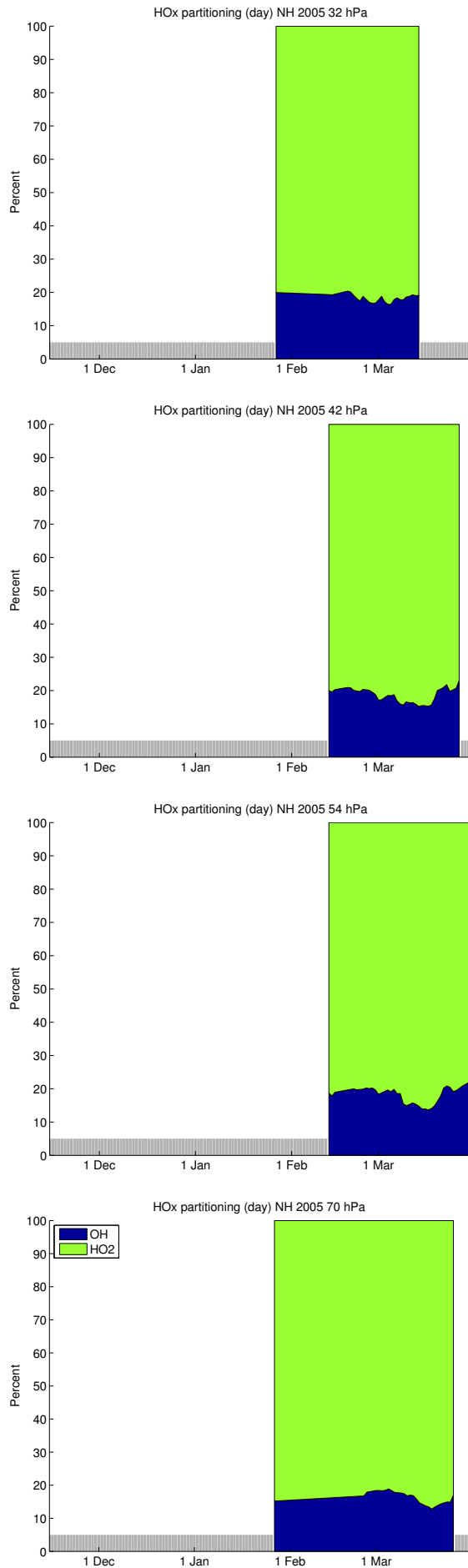


Figure 12: Same as Figure 11, but now in percentages and not in mixing ratios. Days without sufficient data for averaging are not shown (grey bars).

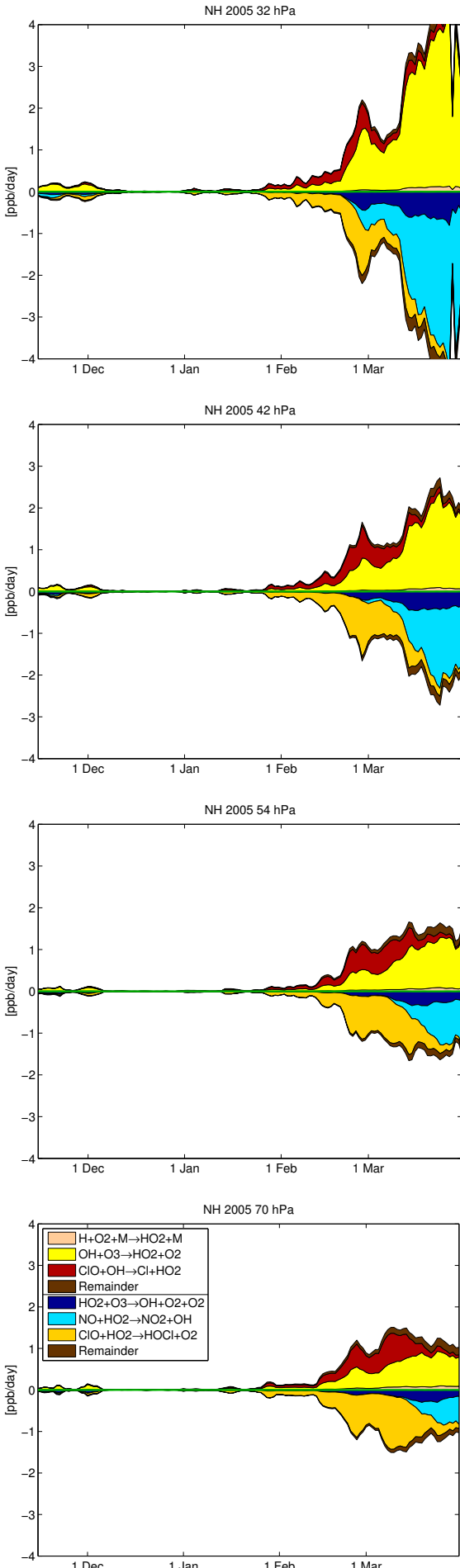


Figure 13: Vortex-averaged chemical reaction rates of reactions changing HO_2 to illustrate HO_x partitioning. Production reactions are shown positive and are separated by a line in the legend from the loss reactions, which are shown negative. The net change of HO_2 is shown as a green line.

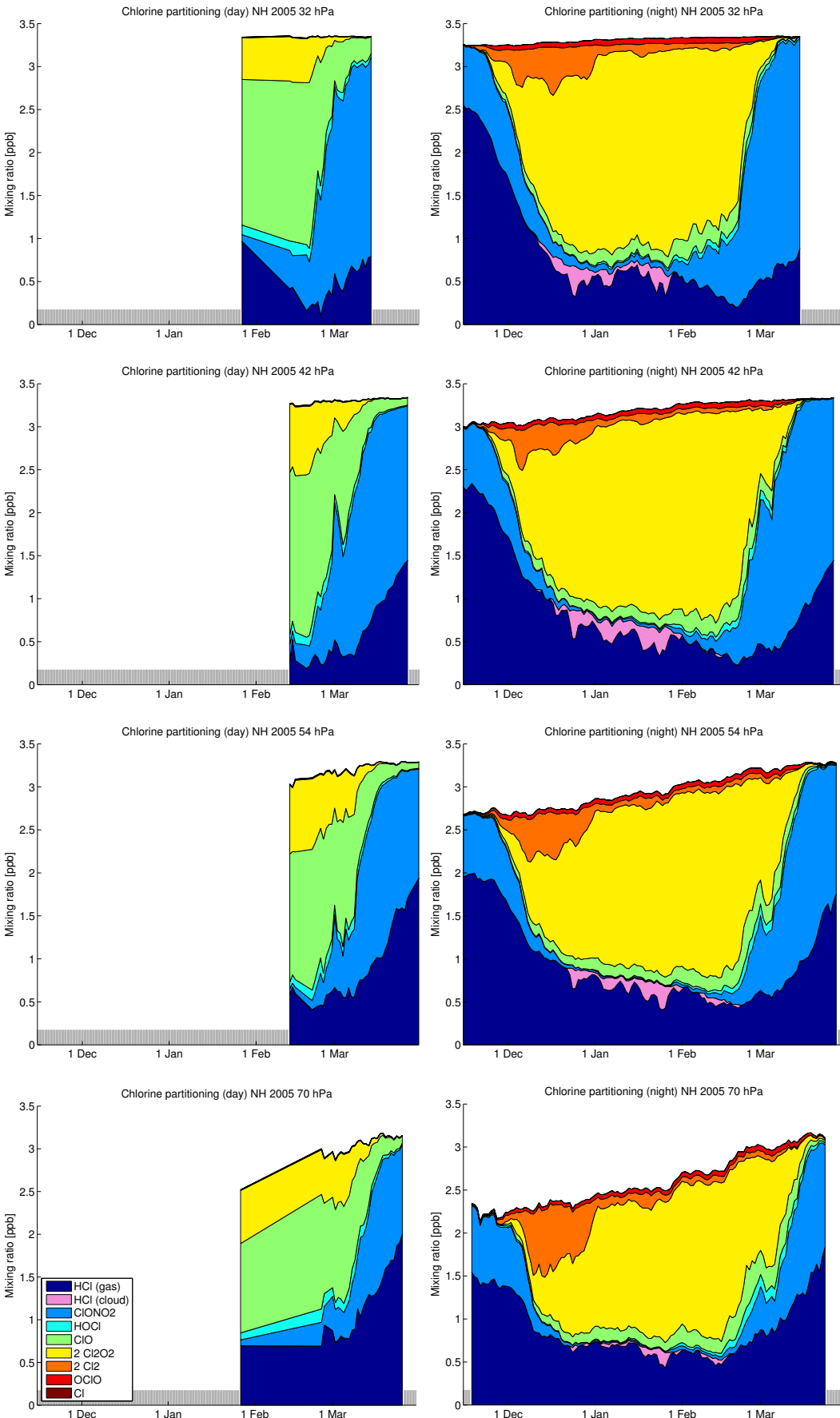


Figure 14: Vortex-averaged partitioning of inorganic chlorine species (Cl_y). Left: Daytime averages (parts of the vortex where the solar zenith angle is smaller than 80°). Right: Nighttime averages (parts of the vortex where the solar zenith angle is larger than 100°). Days without sufficient data for averaging are not shown (grey bars). Species ClNO_2 and BrCl are not shown due to their small mixing ratios. The area labeled “HCl (cloud)” shows HCl dissolved in STS droplets due to the applied correction to the HCl solubility.

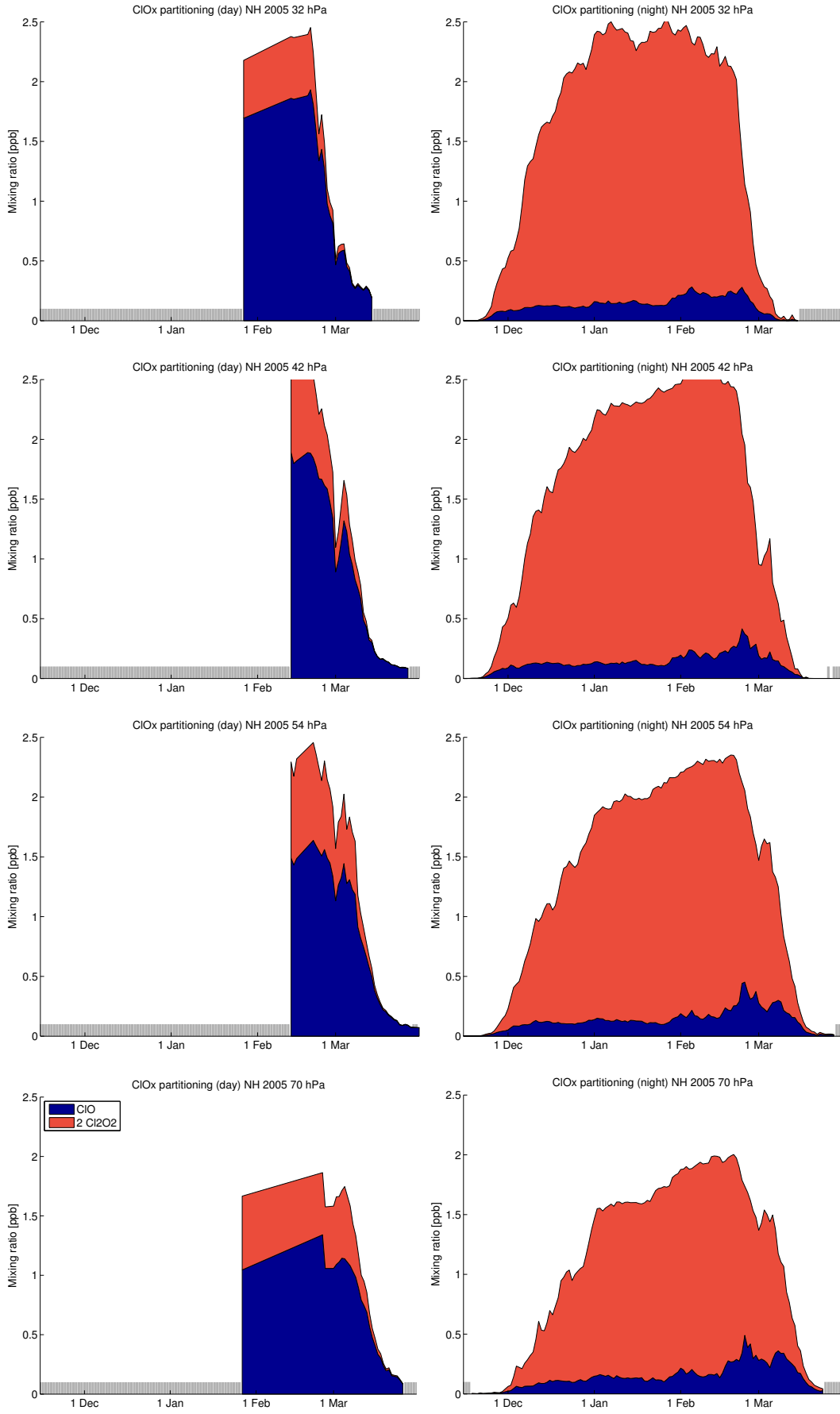


Figure 15: Vortex-averaged partitioning of ClO_x . Left: Daytime averages (parts of the vortex where the solar zenith angle is smaller than 80°). Right: Nighttime averages (parts of the vortex where the solar zenith angle is larger than 100°). Days without sufficient data for averaging are not shown (grey bars).

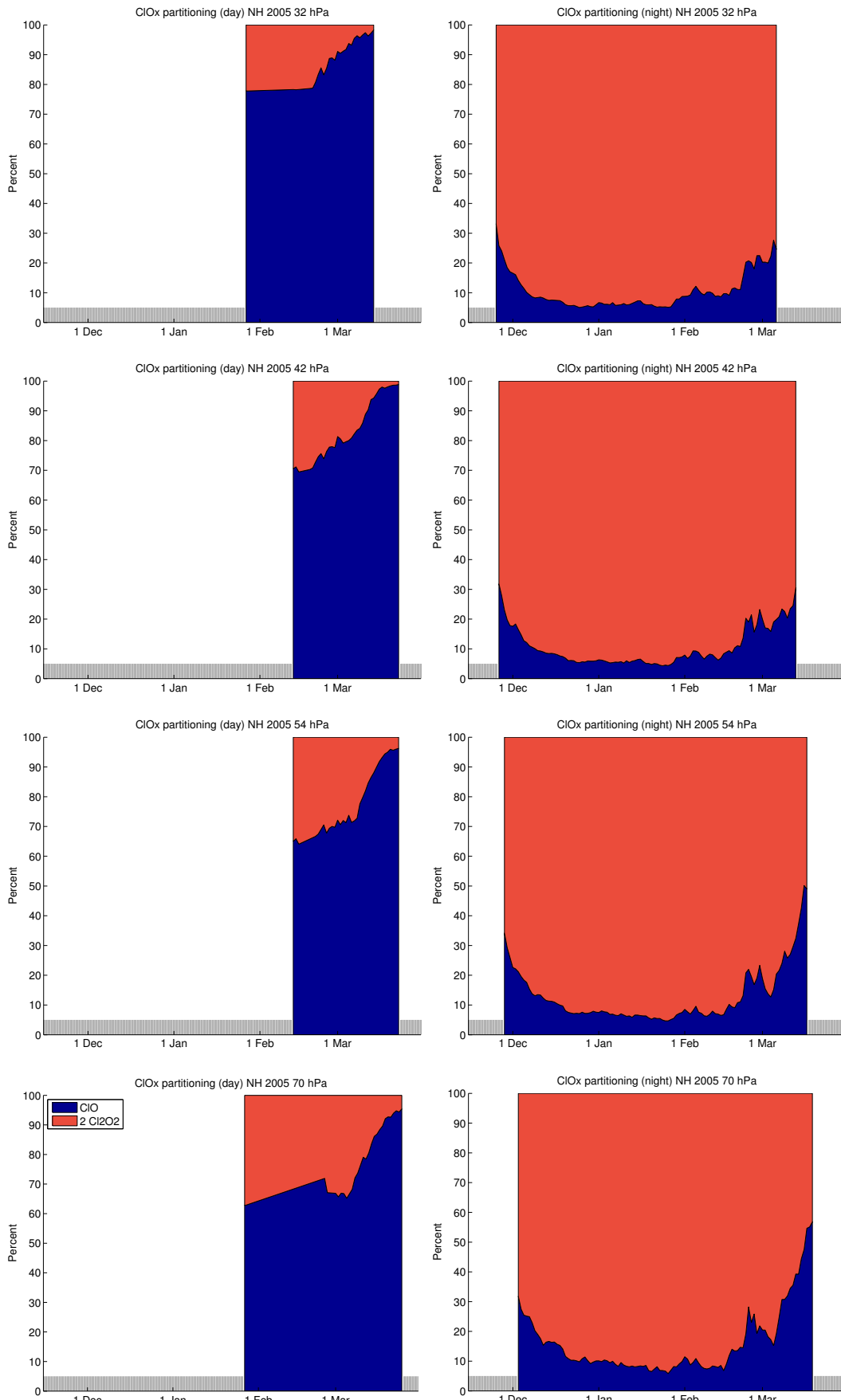


Figure 16: Same as Figure 15, but now in percentages and not in mixing ratios. Percentages are not shown for values of ClO_x below 0.1 ppb and for days without sufficient data for averaging (grey bars).

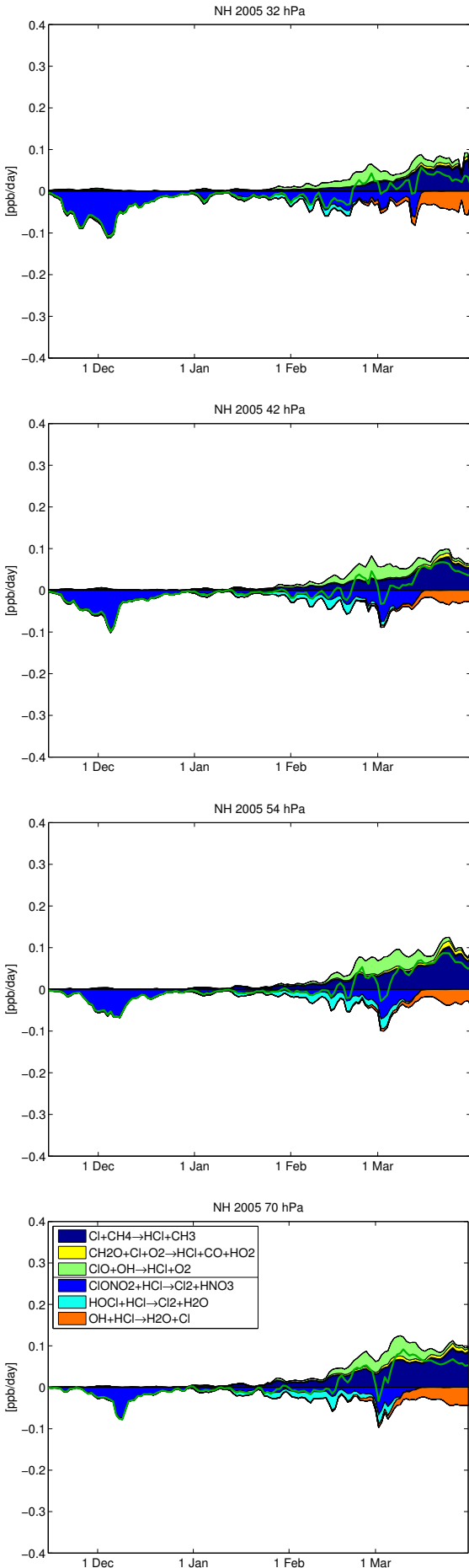


Figure 17: Vortex-averaged chemical reaction rates of reactions involving HCl. Production reactions are shown positive and are separated by a line in the legend from the loss reactions, which are shown negative. The net change of HCl is shown as a green line. Reactions with rates which cannot be distinguished from the zero line at plot resolution are not shown.

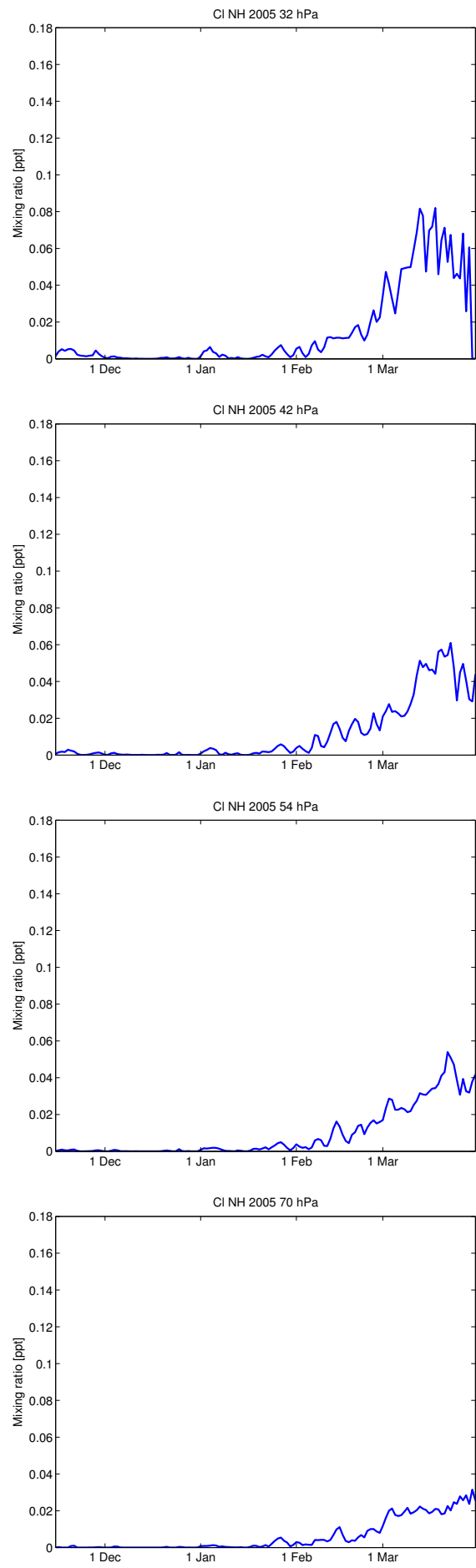


Figure 18: Vortex-averaged Cl mixing ratios.

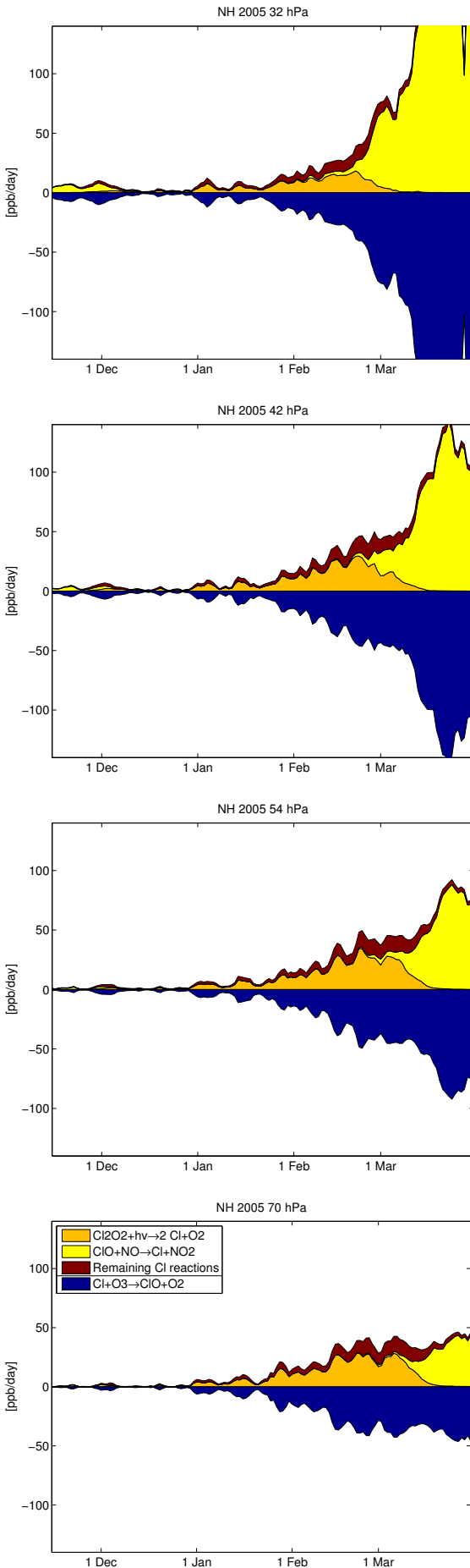


Figure 19: Vortex-averaged chemical reaction rates of reactions involving Cl. Production reactions are shown positive and are separated by a line in the legend from the loss reactions, which are shown negative.

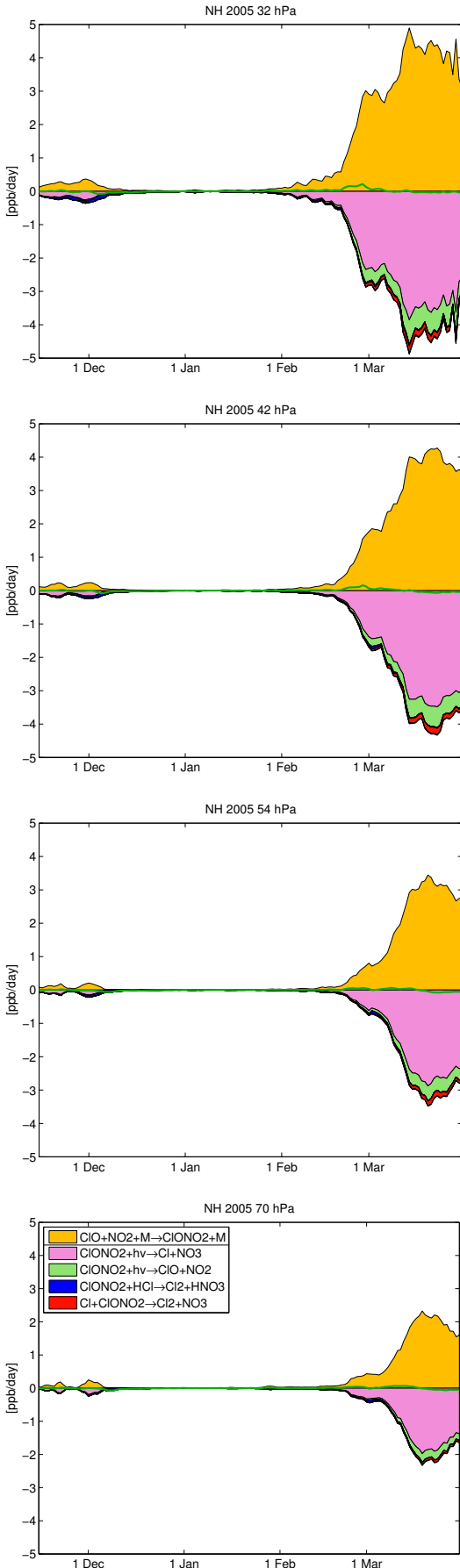


Figure 20: Vortex-averaged chemical reaction rates involving ClONO_2 . Production reactions are shown positive and are separated by a line in the legend from the loss reactions, which are shown negative. The net change of ClONO_2 is shown as a green line. Reactions with rates which cannot be distinguished from the zero line at plot resolution are not shown.

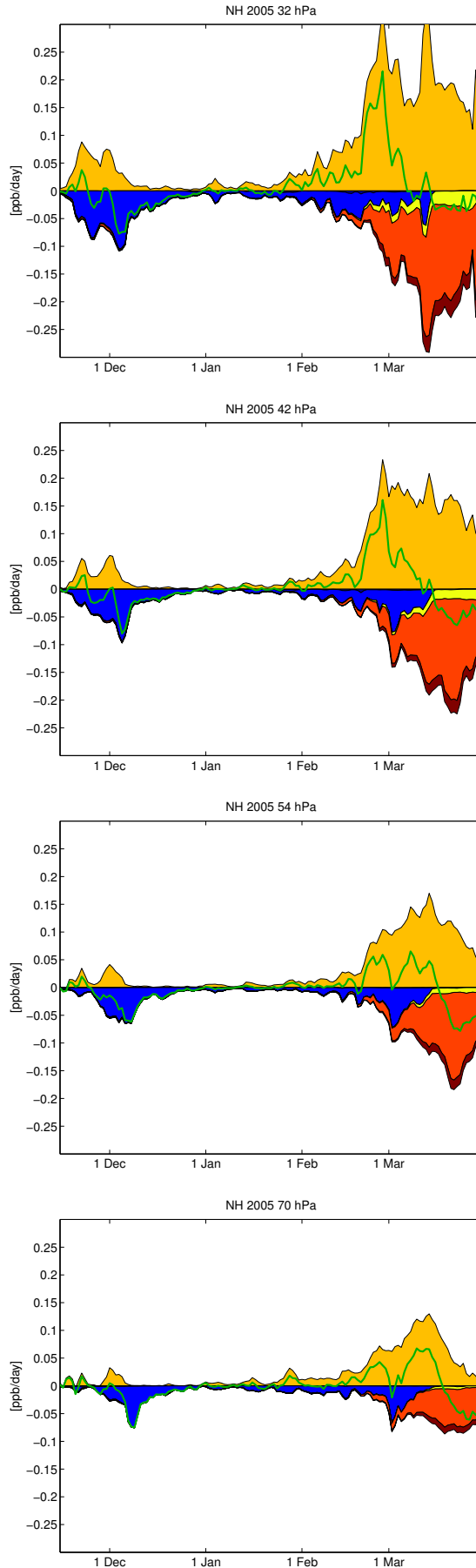


Figure 21: Vortex-averaged chemical reaction rates involving ClONO₂. In contrast to Figure 20, the net production rate of the fast cycle ClONO₂+ $h\nu \rightarrow$ Products / ClO+NO₂+M \rightarrow ClONO₂+M is shown. This cycle is separated by a line in the legend from the loss reactions. The green line shows the net change of ClONO₂ by chemistry. Reactions with rates which cannot be distinguished from the zero line at plot resolution are not shown.

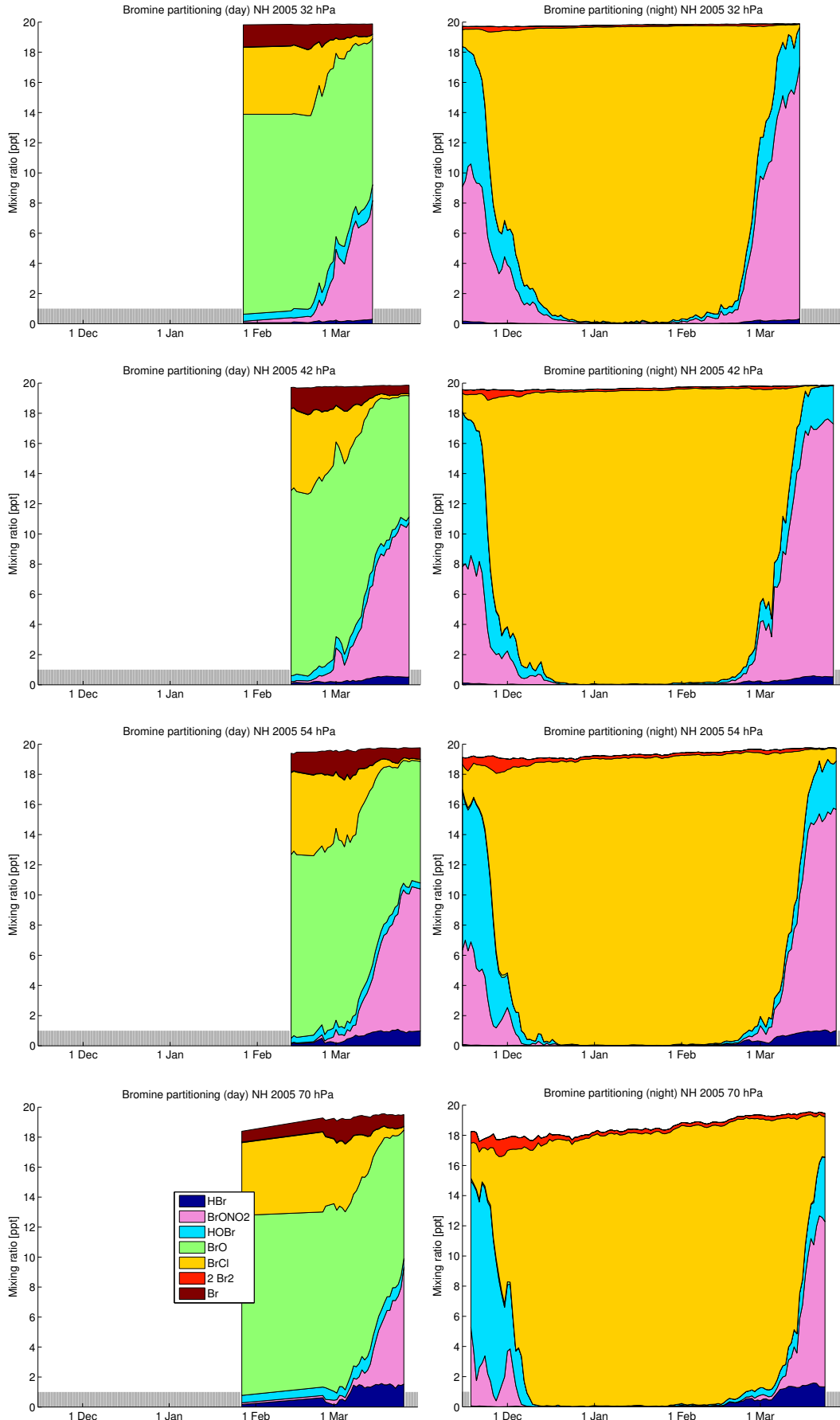


Figure 22: Vortex-averaged partitioning of inorganic bromine species. Left: Daytime averages (parts of the vortex where the solar zenith angle is smaller than 80°). Right: Nighttime averages (parts of the vortex where the solar zenith angle is larger than 100°). Days without sufficient data for averaging are not shown (grey bars).

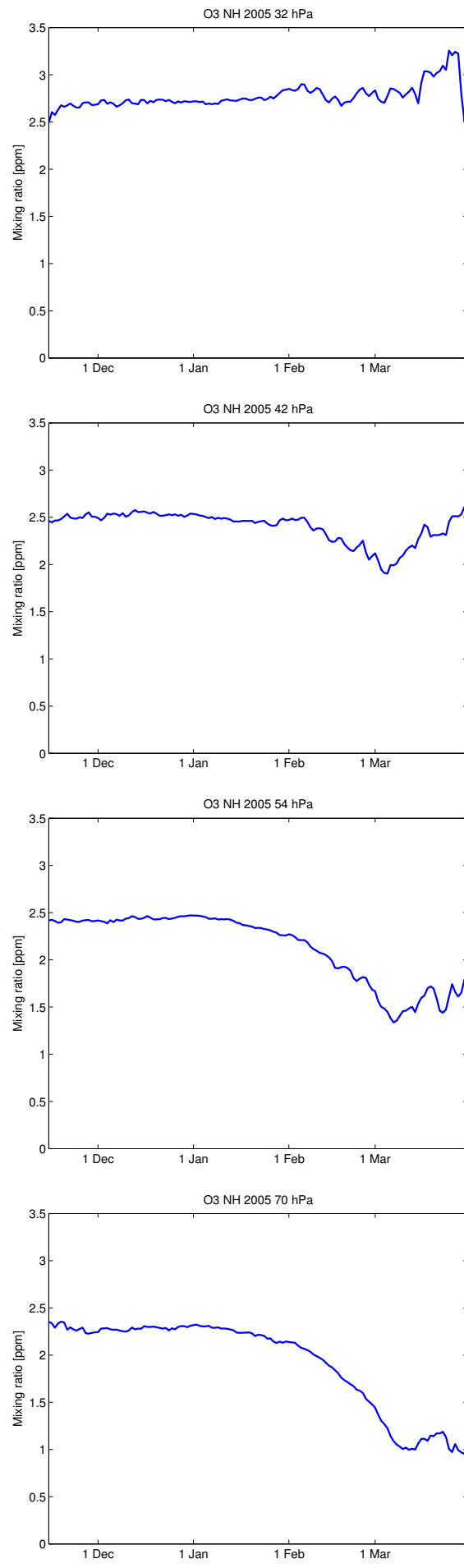


Figure 23: Vortex-averaged ozone mixing ratios.

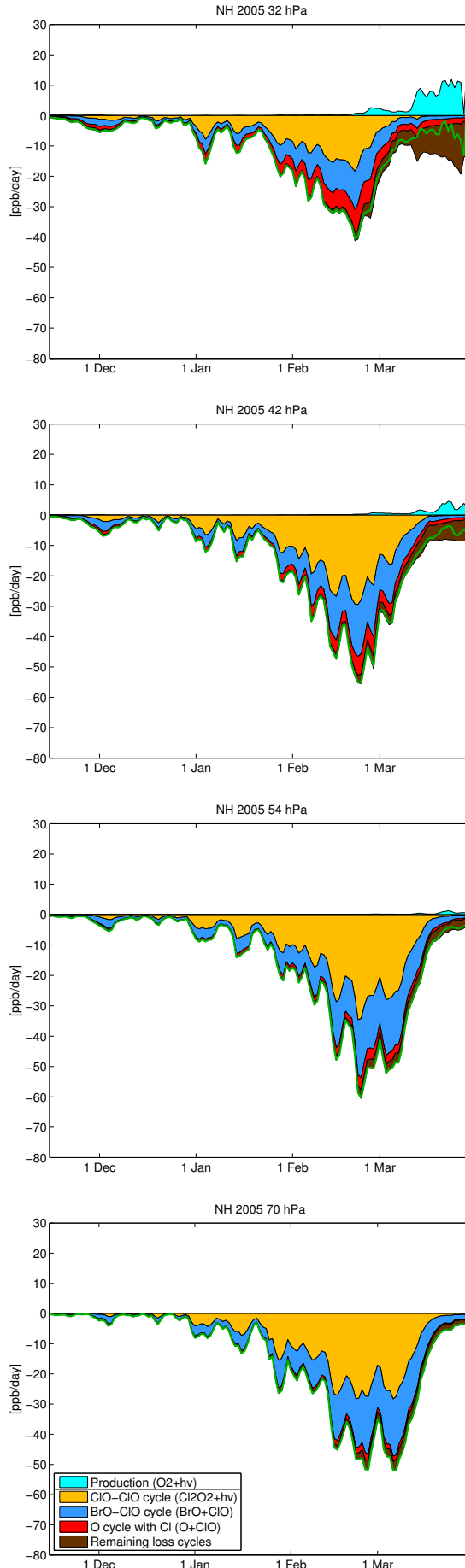


Figure 24: Vortex-averaged net chemical change of odd oxygen. The green line shows the net chemical change rate of ozone, which nearly equals the change rate of odd oxygen. The contribution of different catalytic cycles to the ozone loss is shown by the reaction rates of their rate limiting step. Only the three most important cycles are shown, the contribution of other cycles is small. Ozone production, which is almost exclusively by the $O_2 + h\nu$ reaction, is shown in cyan.

1.2 Northern Hemisphere 2009/2010

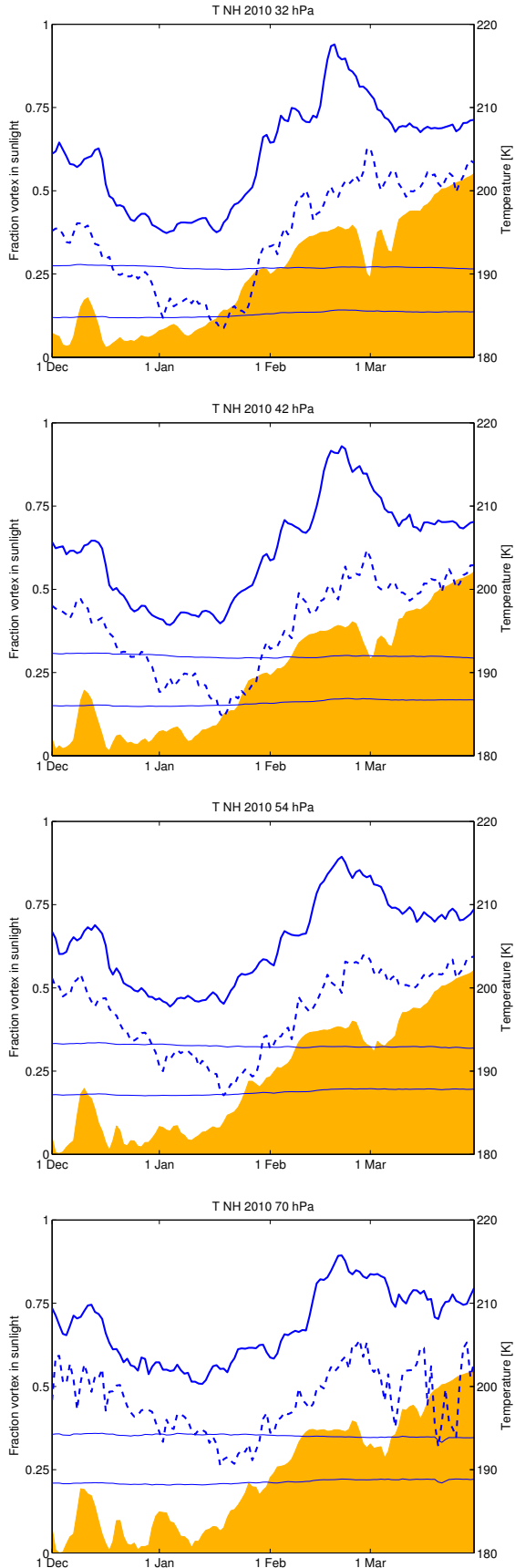


Figure 25: Vortex-averaged temperature (blue), vortex minimum temperature (dashed blue) and fraction of the vortex in sunlight (yellow). The upper thin blue line shows the threshold temperature for the formation of NAT clouds used in the model (based on vortex mean mixing ratios and considering supersaturation), and the lower thin blue line shows the same for ice clouds. The vortex tracer criterion is not applied (in contrast to all other figures).

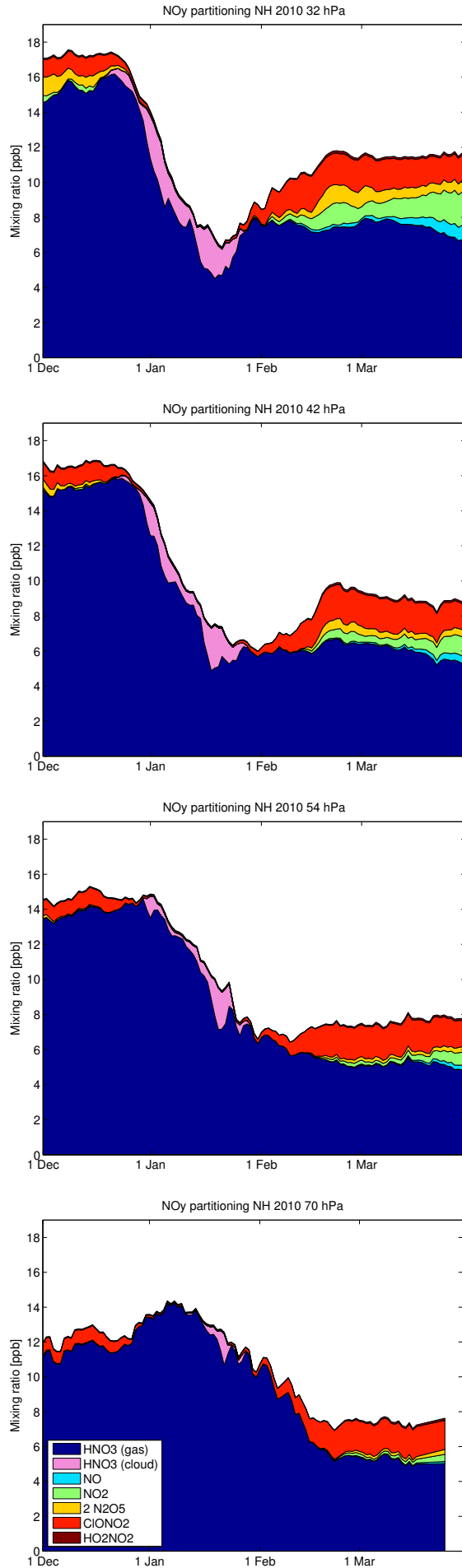


Figure 26: Vortex-averaged partitioning of NO_y species. Species NO₃, BrONO₂, ClONO₂ and N are not shown due to their small mixing ratios.

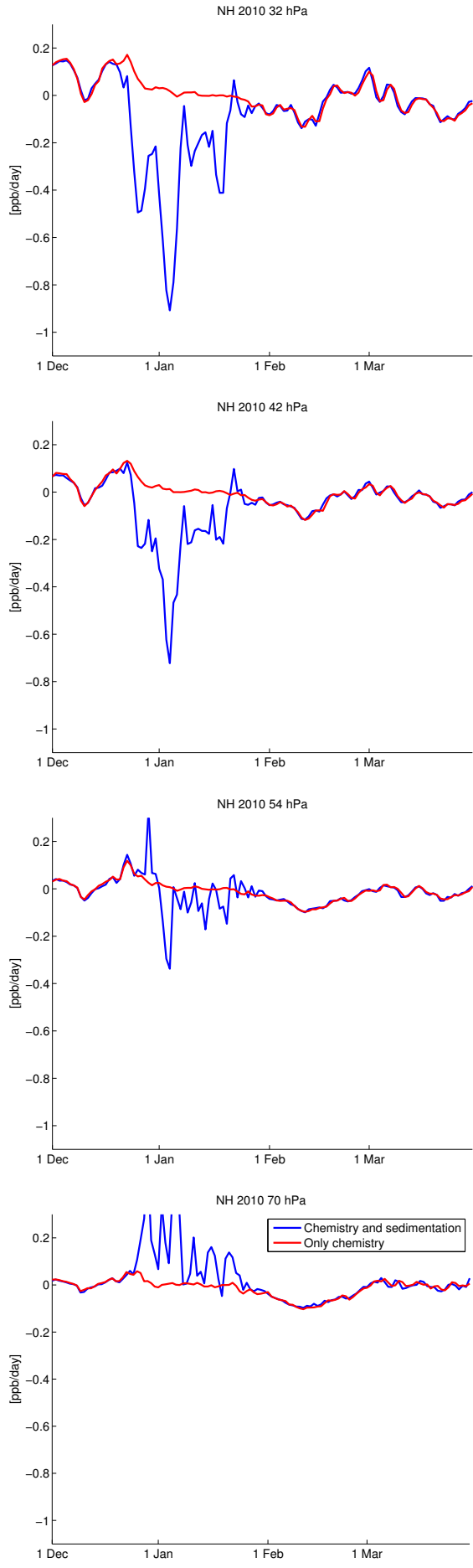


Figure 27: Vortex-averaged net chemical reaction rate of HNO_3 (red) and sum of the vortex-averaged change by sedimentation and the net chemical reaction rate (blue).

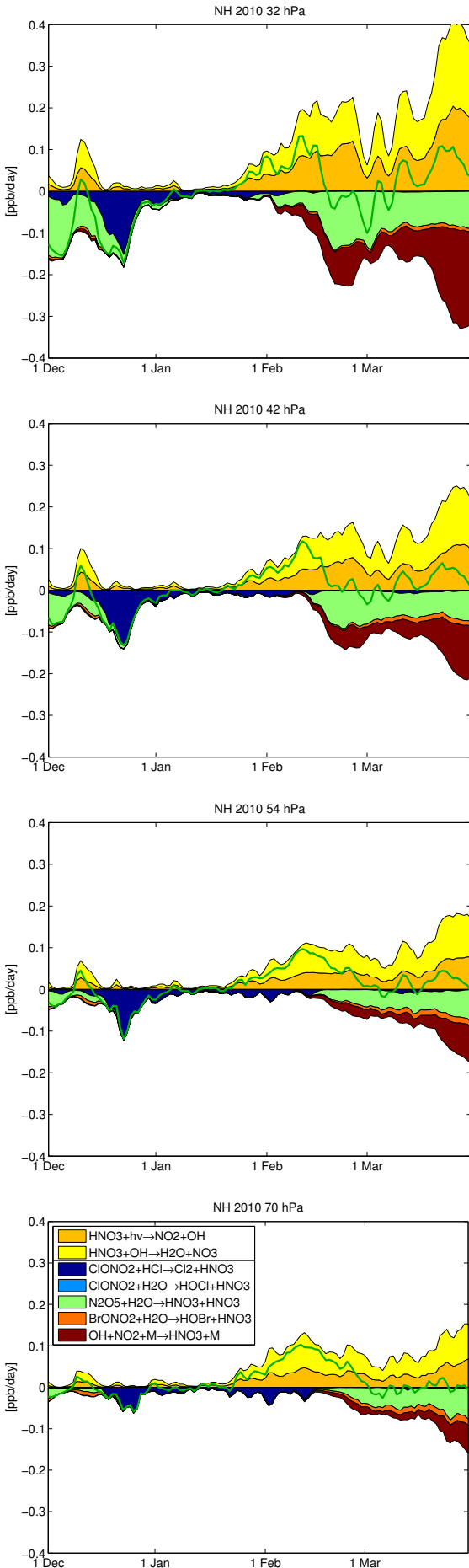


Figure 28: Vortex-averaged chemical reaction rates of reactions changing extended NO_x ($\text{NO} + \text{NO}_2 + \text{NO}_3 + 2\text{N}_2\text{O}_5 + \text{ClONO}_2 + \text{BrONO}_2 + \text{HO}_2\text{NO}_2$). Production reactions are shown positive and are separated by a line in the legend from the loss reactions, which are shown negative. The net change of extended NO_x is shown as a green line.

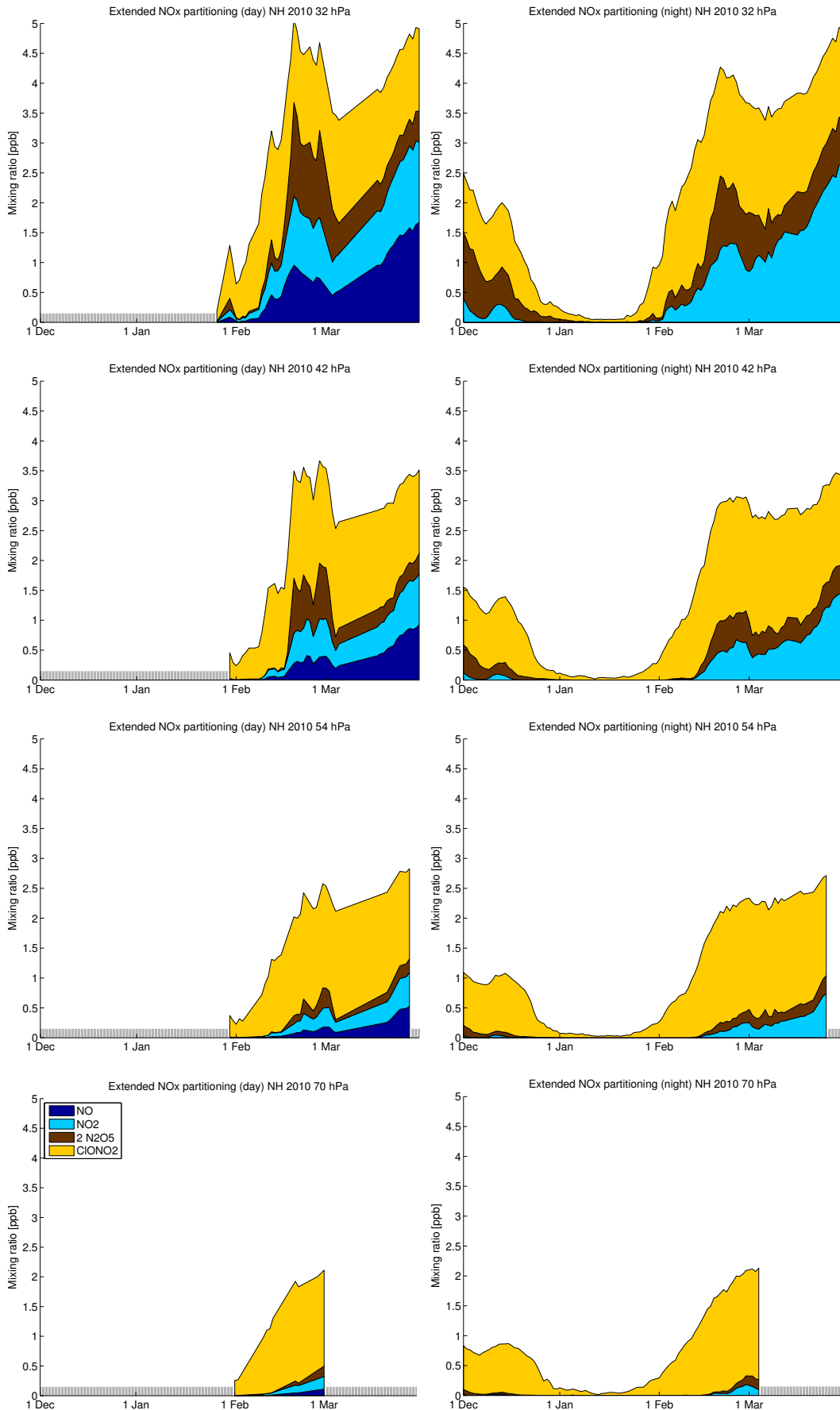


Figure 29: Vortex-averaged partitioning of extended NO_x species. Left: Daytime averages (parts of the vortex where the solar zenith angle is smaller than 80°). Right: Nighttime averages (parts of the vortex where the solar zenith angle is larger than 100°). Days without sufficient data for averaging are not shown (grey bars).

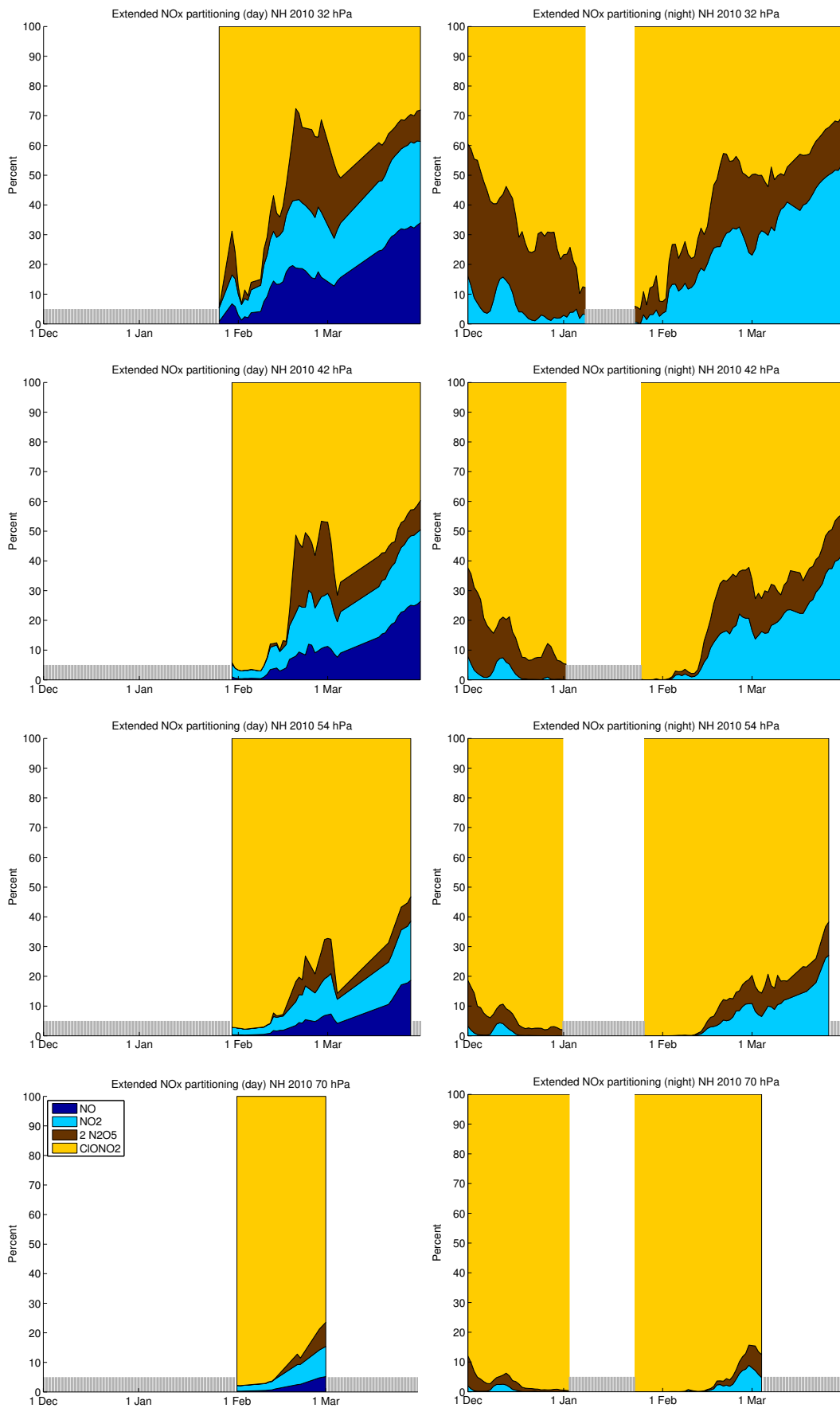


Figure 30: Same as Figure 29, but now in percentages and not in mixing ratios. Percentages are not shown for values of extended NO_x below 0.1 ppb and for days without sufficient data for averaging (grey bars).

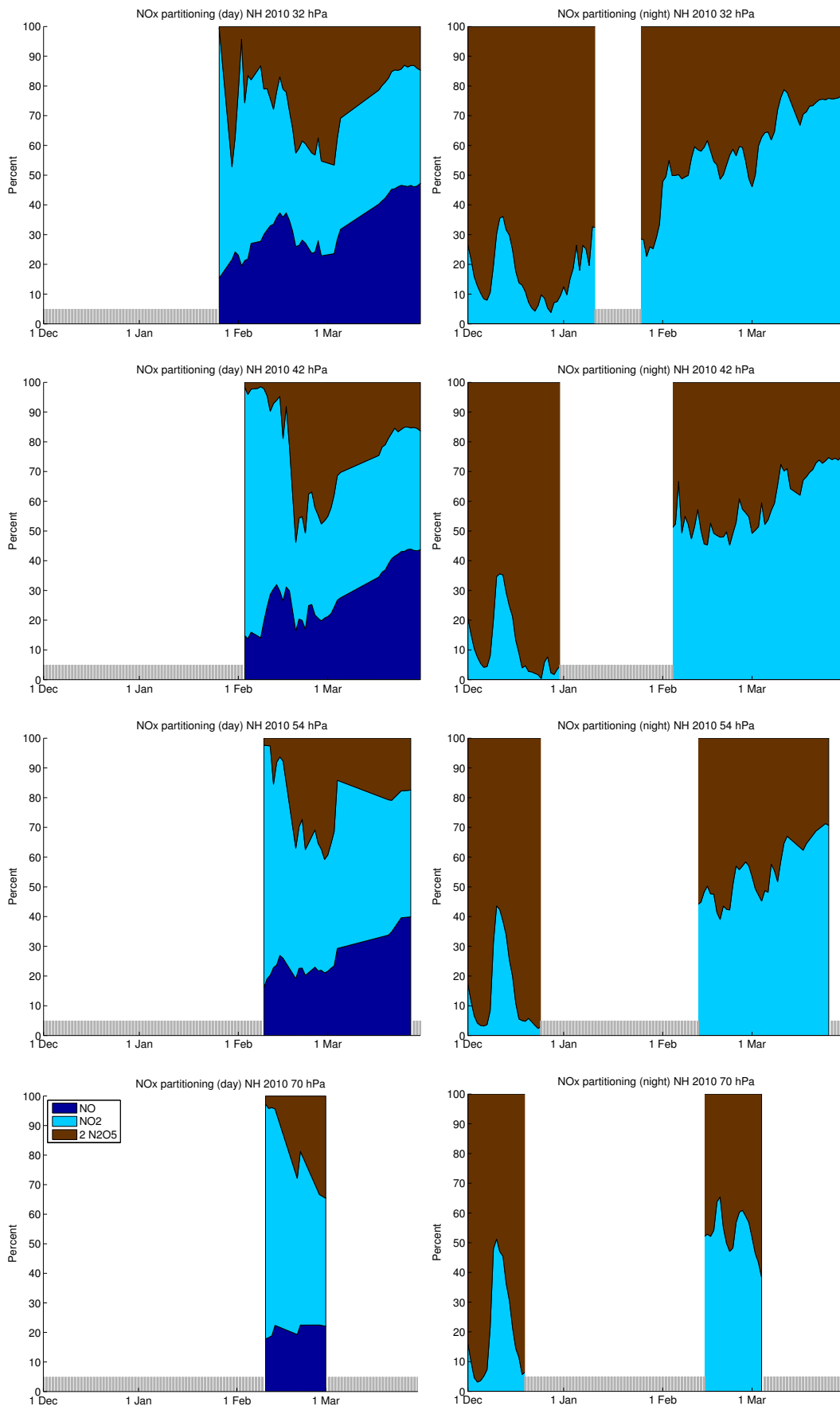


Figure 31: Same as Figure 30, but with only $\text{NO}_x = \text{NO} + \text{NO}_2 + 2\text{N}_2\text{O}_5$ partitioning. Percentages are not shown for values of NO_x below 0.01 ppb and for days without sufficient data for averaging (grey bars).

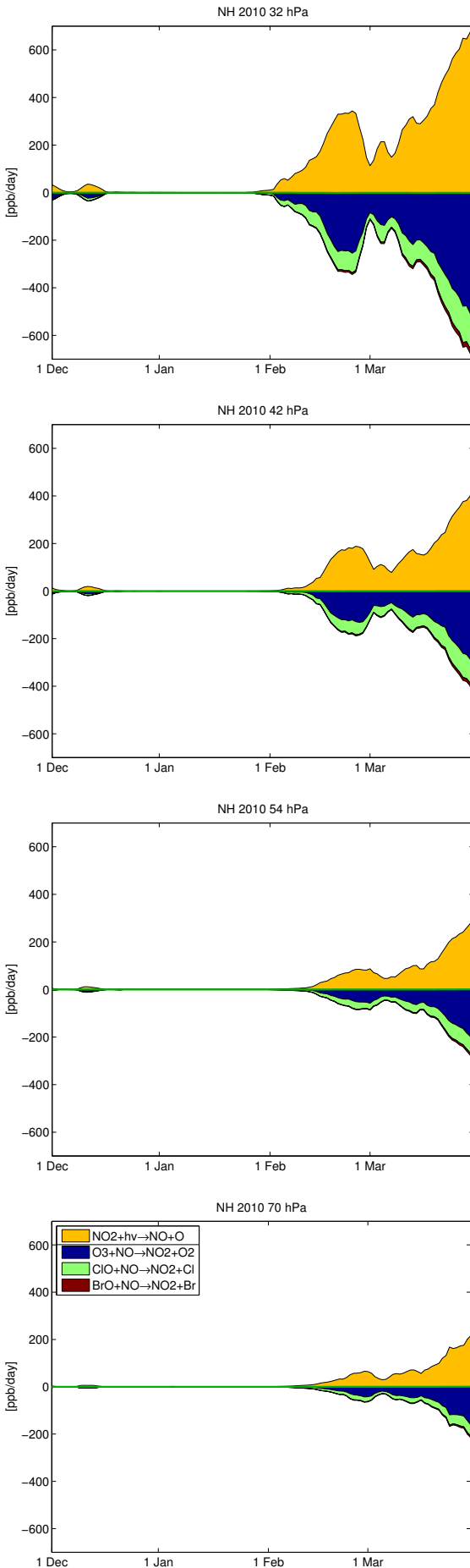


Figure 32: Vortex-averaged chemical reaction rates of reactions changing NO to illustrate NO_x partitioning. Production reactions are shown positive and are separated by a line in the legend from the loss reactions, which are shown negative. The net change of NO is shown as a green line.

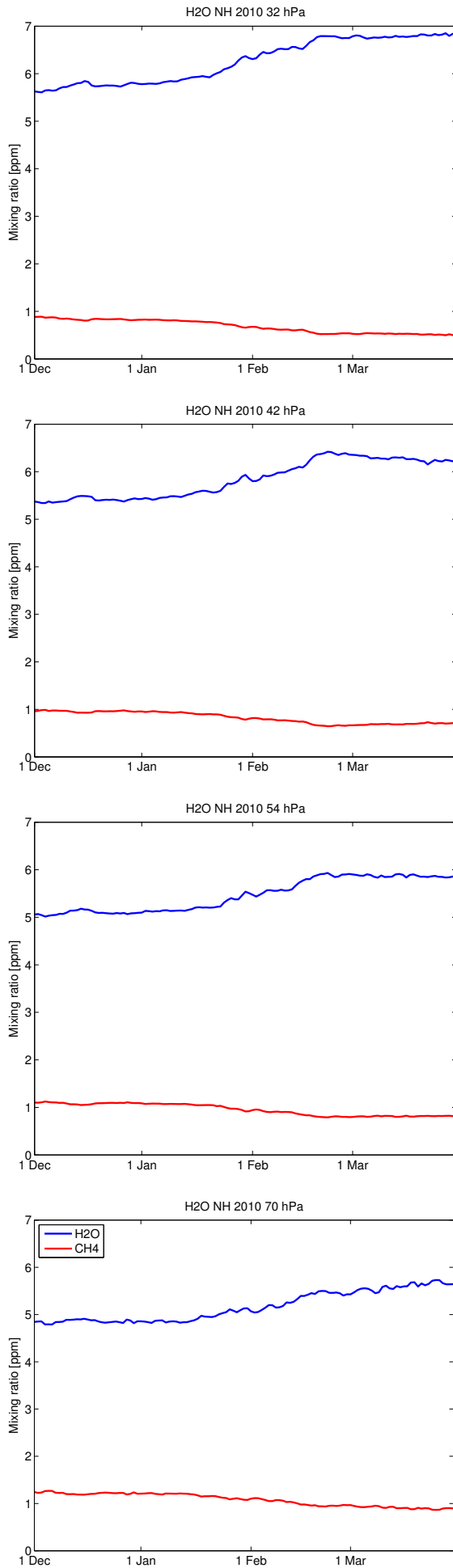


Figure 33: Vortex-averaged mixing ratios of H₂O and CH₄.

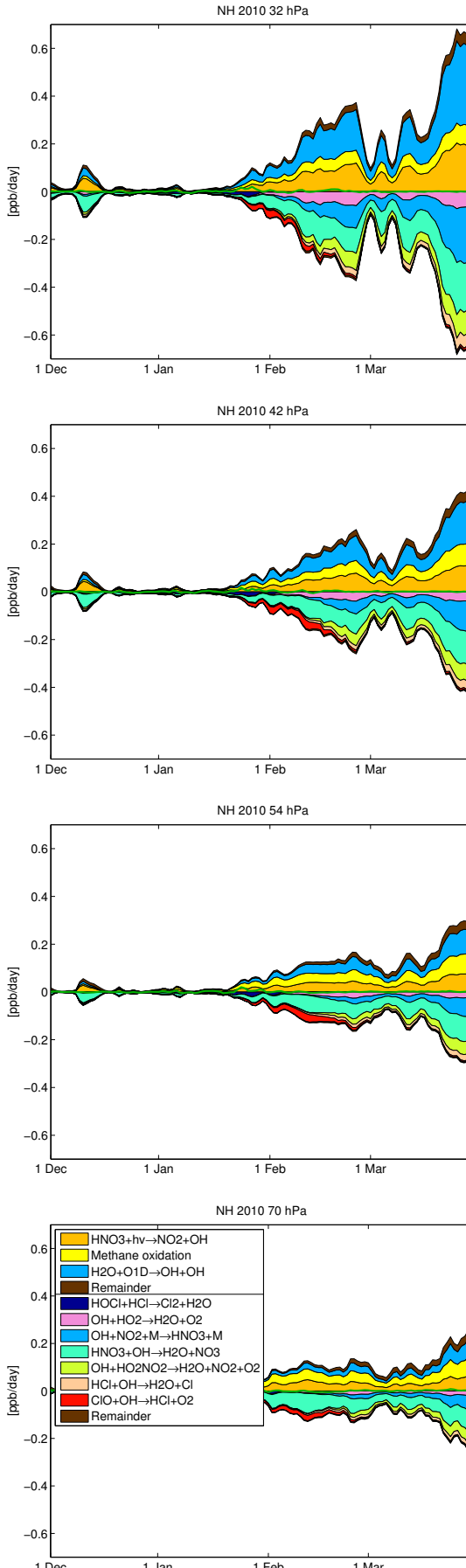


Figure 34: Vortex-averaged chemical reaction rates of reactions changing extended HO_x (OH + HO₂ + H + HOCl + HOBr + HO₂NO₂). Production reactions are shown positive and are separated by a line in the legend from the loss reactions, which are shown negative. The net change of extended HO_x is shown as a green line. Methane oxidation is modelled by simplified net reactions in ATLAS, the reactions denoted as methane oxidation in the legend are Cl + CH₄ → HCl + CH₂O + HO₂ and Cl + CH₂O → HCl + CO + HO₂.

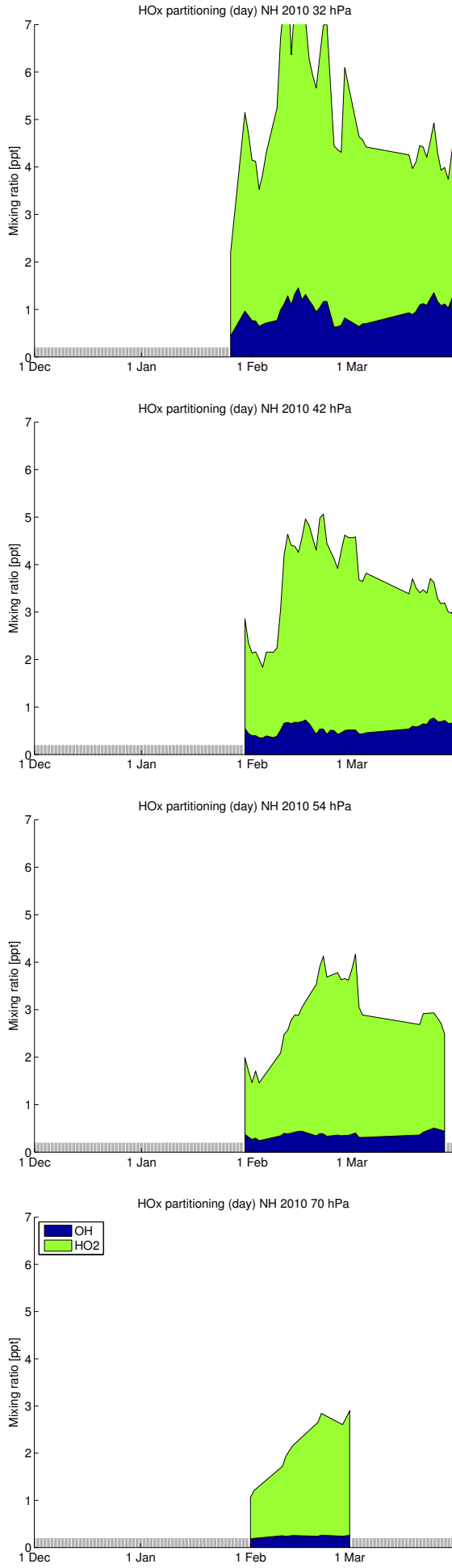


Figure 35: Vortex-averaged partitioning of HO_x species. Daytime averages (parts of the vortex where the solar zenith angle is smaller than 80°). Nighttime averages are near zero and not shown. Data: WMO (2010) Geopotential height from reanalysis (version 1).

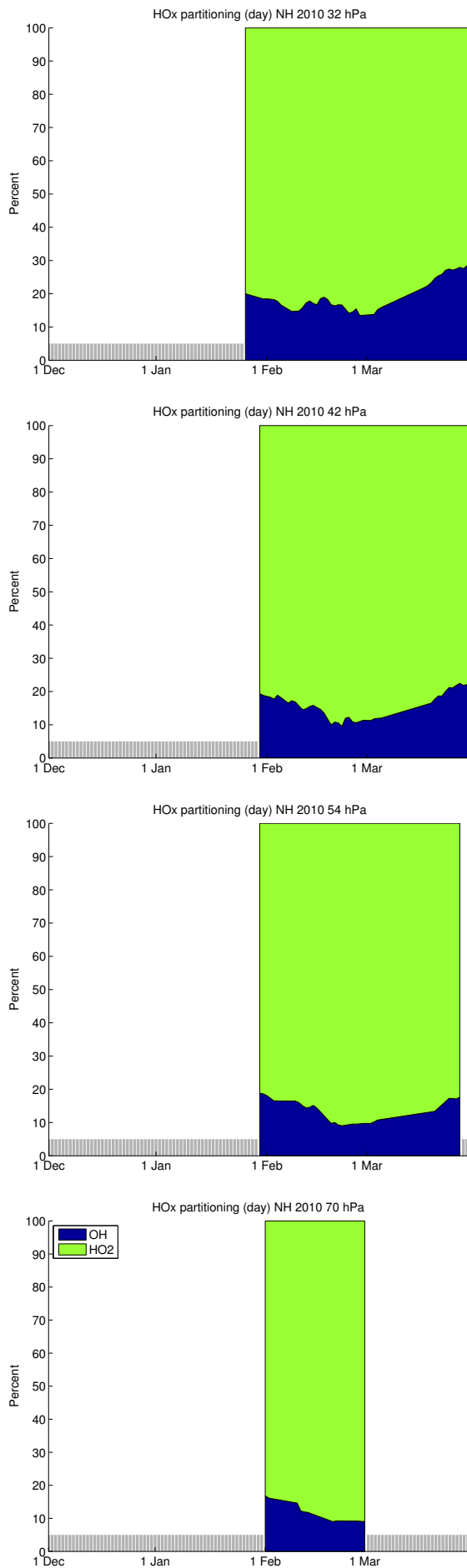


Figure 36: Same as Figure 35, but now in percentages and not in mixing ratios. Days without sufficient data for averaging are not shown (grey bars).

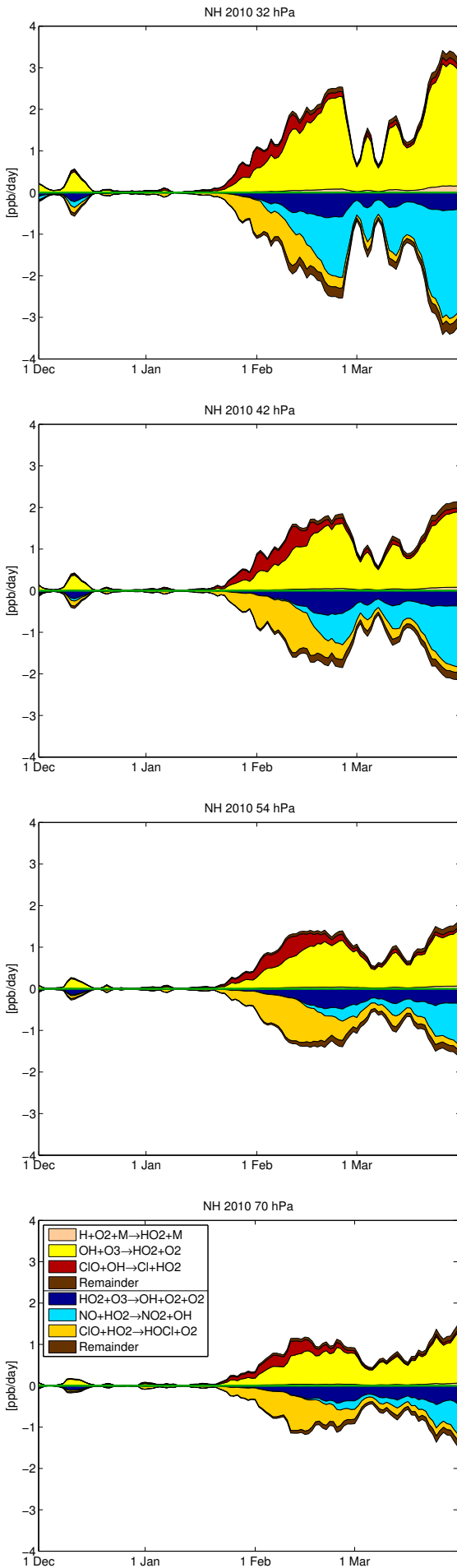


Figure 37: Vortex-averaged chemical reaction rates of reactions changing HO_2 to illustrate HO_x partitioning. Production reactions are shown positive and are separated by a line in the legend from the loss reactions, which are shown negative. The net change of HO_2 is shown as a green line.

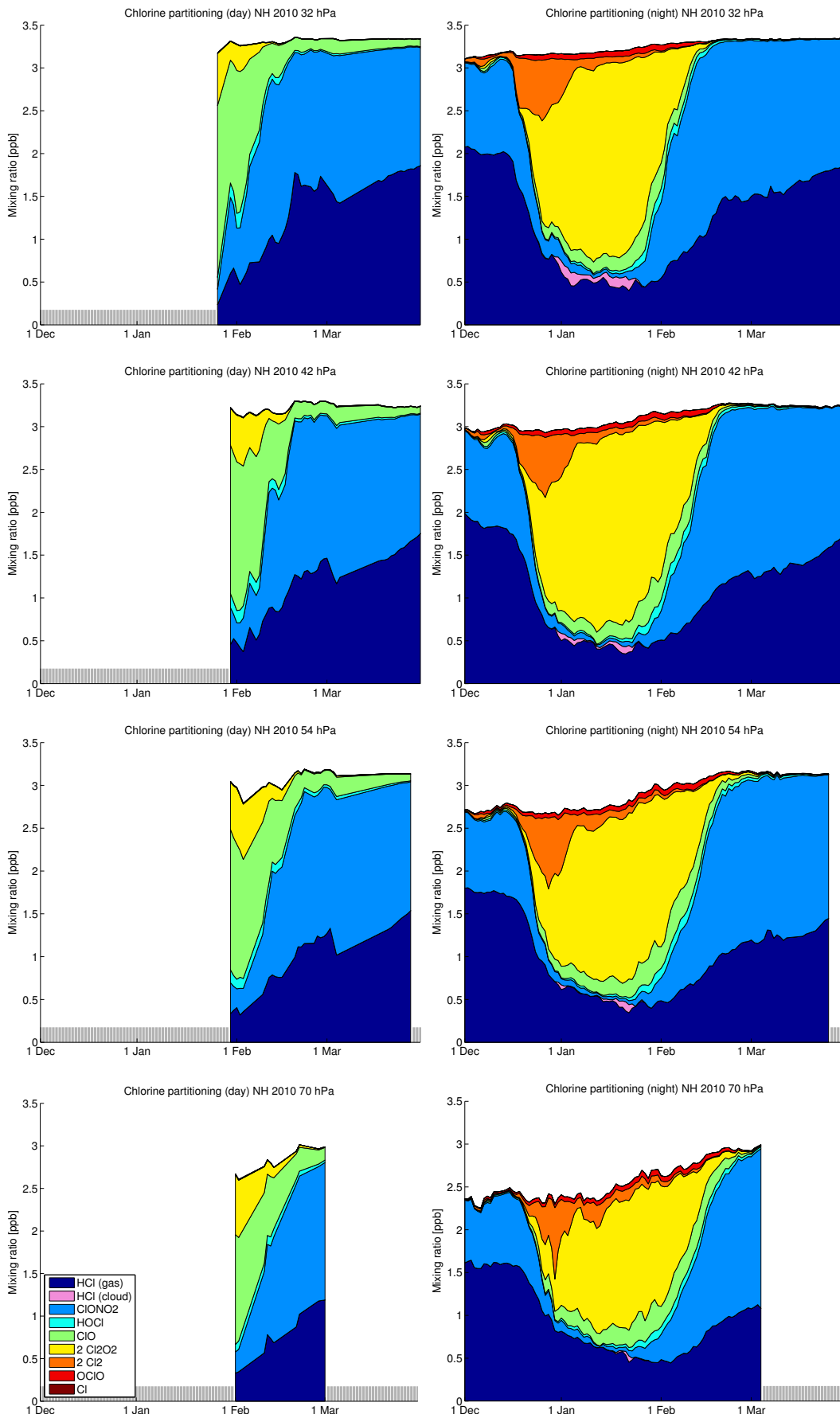


Figure 38: Vortex-averaged partitioning of inorganic chlorine species (Cl_y). Left: Daytime averages (parts of the vortex where the solar zenith angle is smaller than 80°). Right: Nighttime averages (parts of the vortex where the solar zenith angle is larger than 100°). Days without sufficient data for averaging are not shown (grey bars). Species ClNO_2 and BrCl are not shown due to their small mixing ratios. The area labeled “HCl (cloud)” shows HCl dissolved in STS droplets due to the applied correction to the HCl solubility.

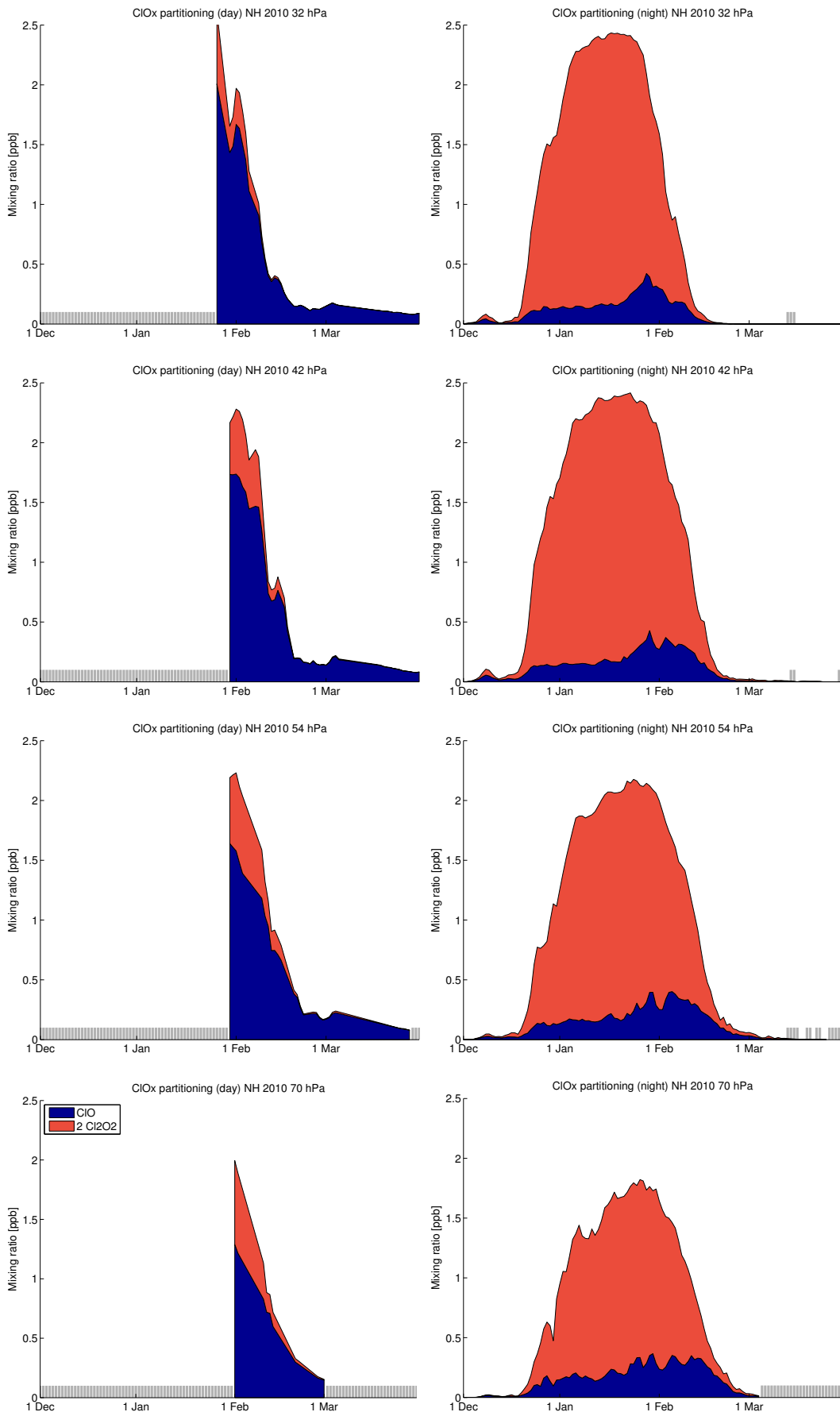


Figure 39: Vortex-averaged partitioning of ClO_x . Left: Daytime averages (parts of the vortex where the solar zenith angle is smaller than 80°). Right: Nighttime averages (parts of the vortex where the solar zenith angle is larger than 100°). Days without sufficient data for averaging are not shown (grey bars).

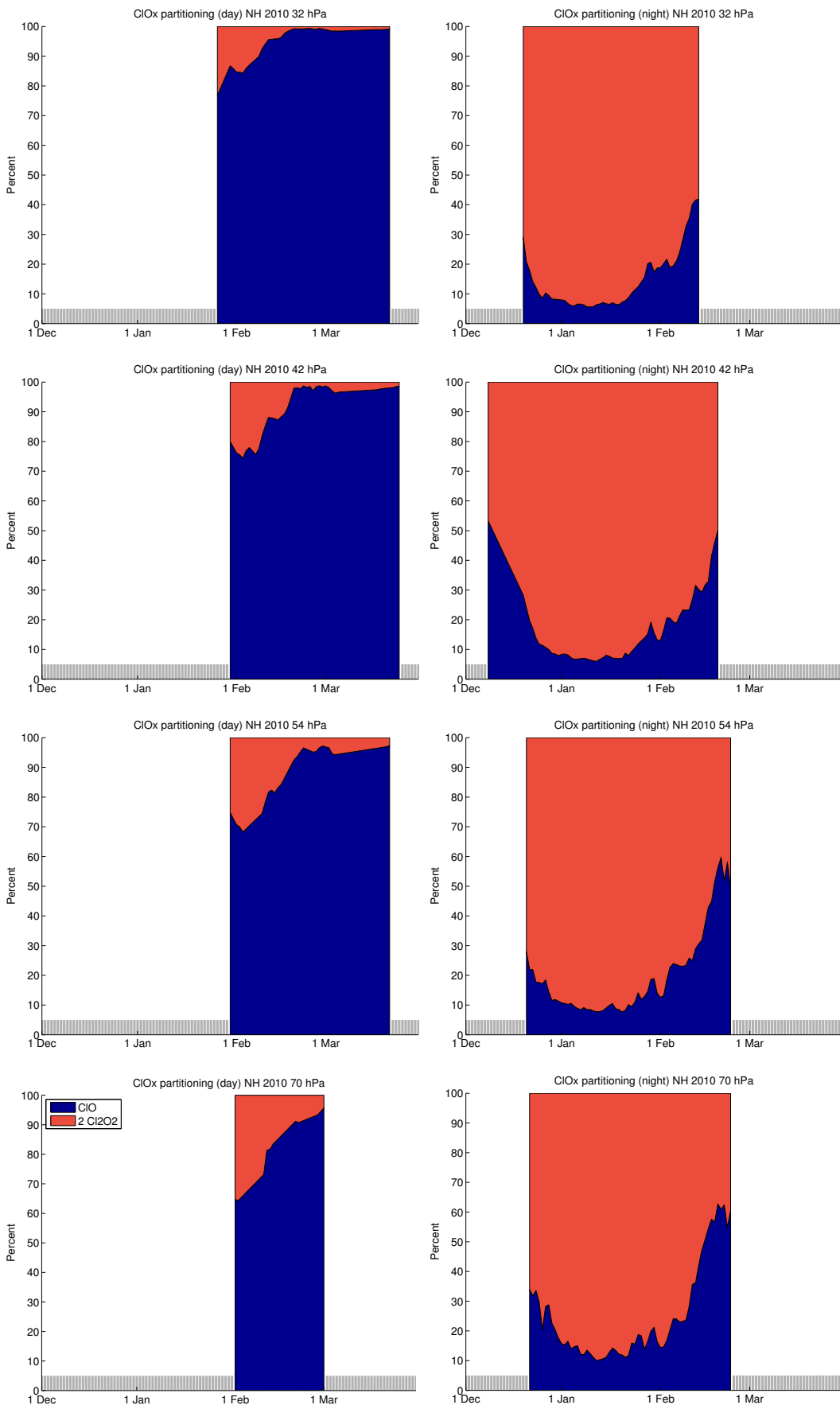


Figure 40: Same as Figure 39, but now in percentages and not in mixing ratios. Percentages are not shown for values of ClO_x below 0.1 ppb and for days without sufficient data for averaging (grey bars).

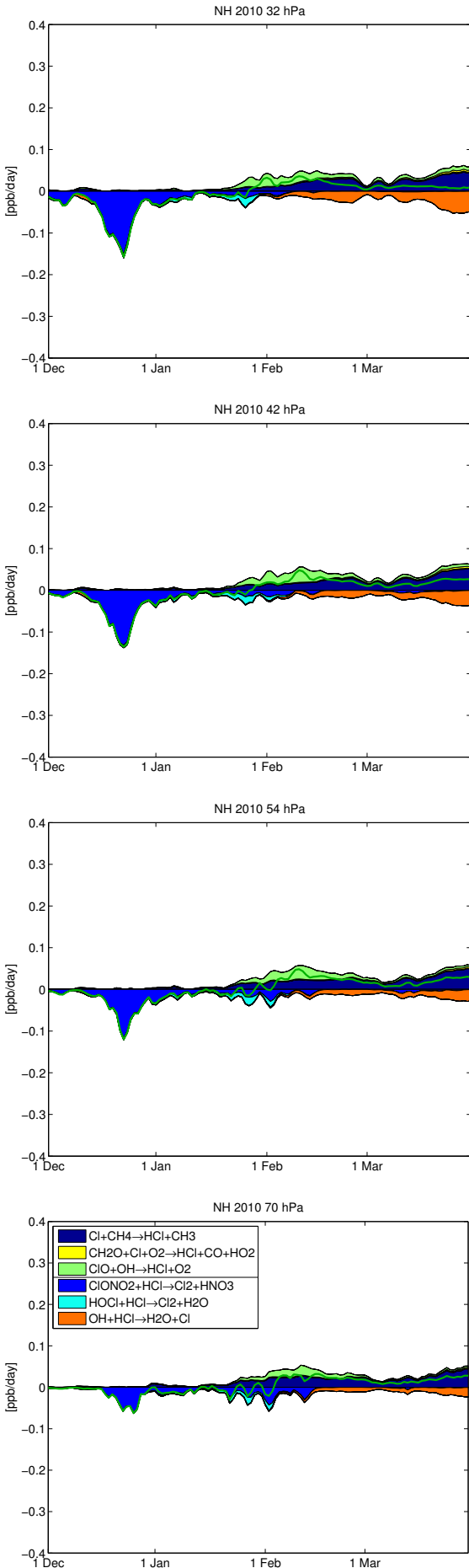


Figure 41: Vortex-averaged chemical reaction rates of reactions involving HCl. Production reactions are shown positive and are separated by a line in the legend from the loss reactions, which are shown negative. The net change of HCl is shown as a green line. Reactions with rates which cannot be distinguished from the zero line at plot resolution are not shown.

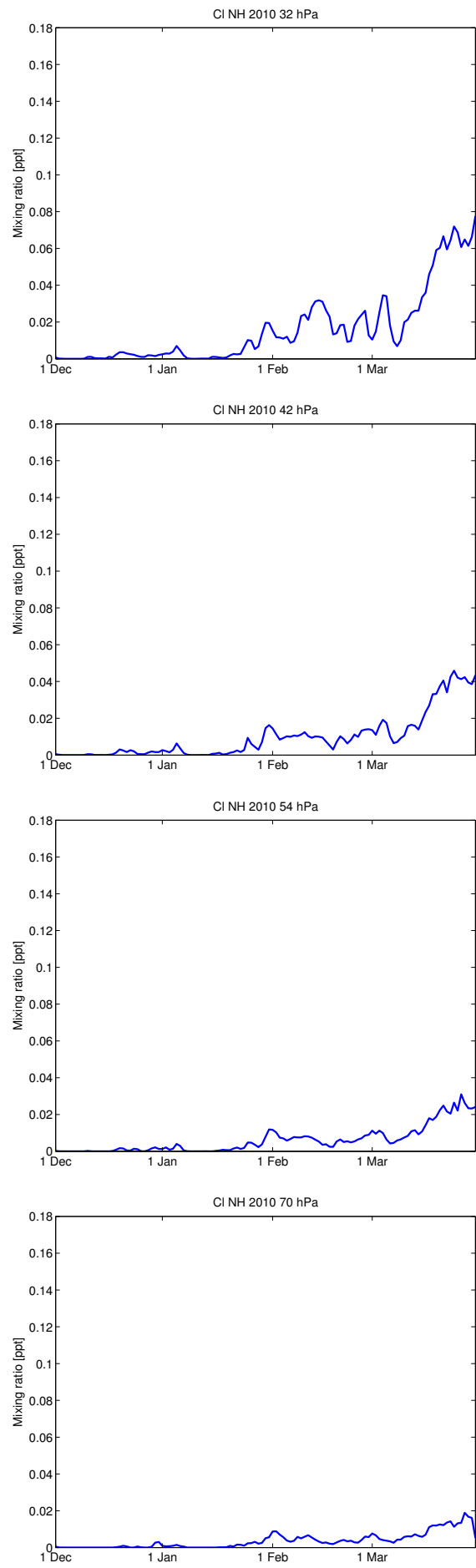


Figure 42: Vortex-averaged Cl mixing ratios.

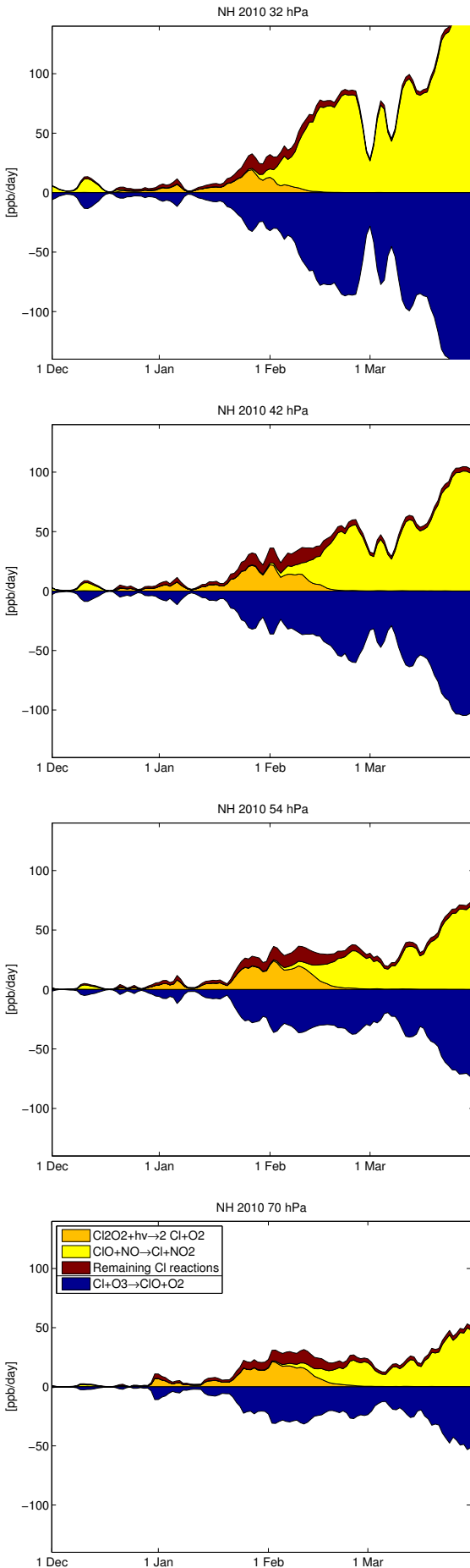


Figure 43: Vortex-averaged chemical reaction rates of reactions involving Cl. Production reactions are shown positive and are separated by a line in the legend from the loss reactions, which are shown negative.

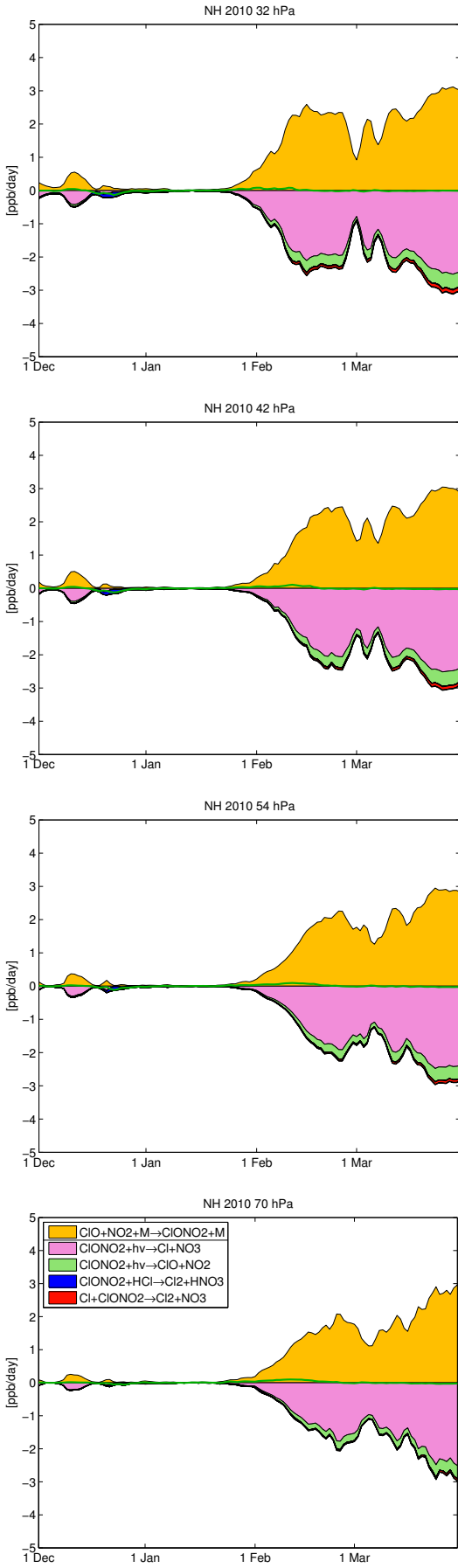


Figure 44: Vortex-averaged chemical reaction rates involving ClONO_2 . Production reactions are shown positive and are separated by a line in the legend from the loss reactions, which are shown negative. The net change of ClONO_2 is shown as a green line. Reactions with rates which cannot be distinguished from the zero line at plot resolution are not shown.

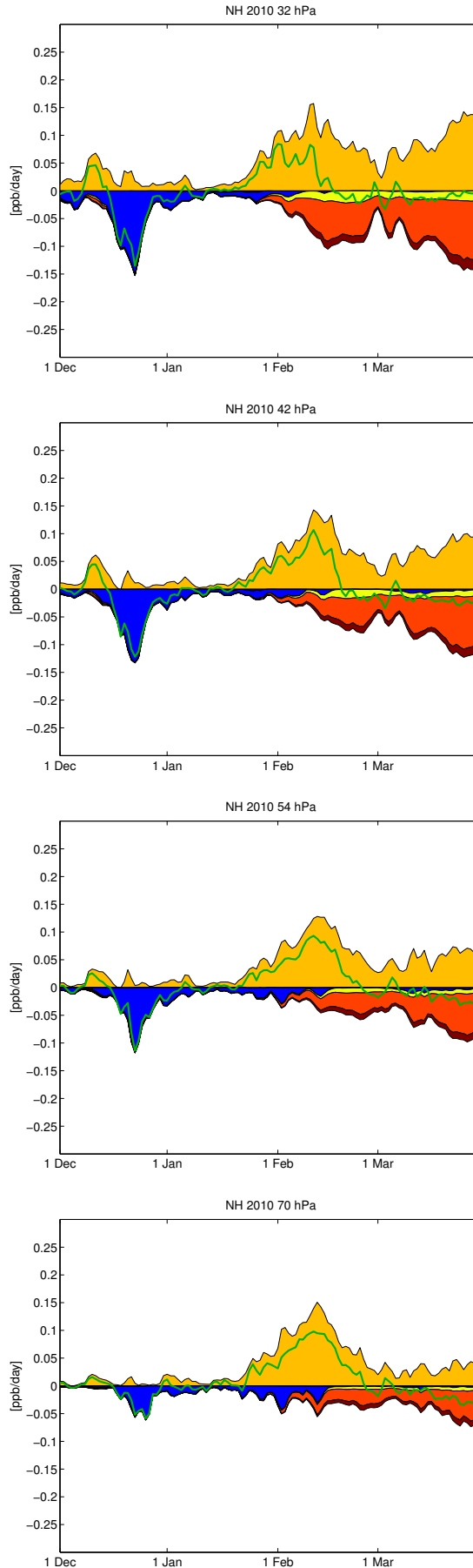


Figure 45: Vortex-averaged chemical reaction rates involving ClONO_2 . In contrast to Figure 44, the net production rate of the fast cycle $\text{ClONO}_2 + h\nu \rightarrow \text{Products}$ / $\text{ClO} + \text{NO}_2 + \text{M} \rightarrow \text{ClONO}_2 + \text{M}$ is shown. This cycle is separated by a line in the legend from the loss reactions. The green line shows the net change of ClONO_2 by chemistry. Reactions with rates which cannot be distinguished from the zero line at plot resolution are not shown.

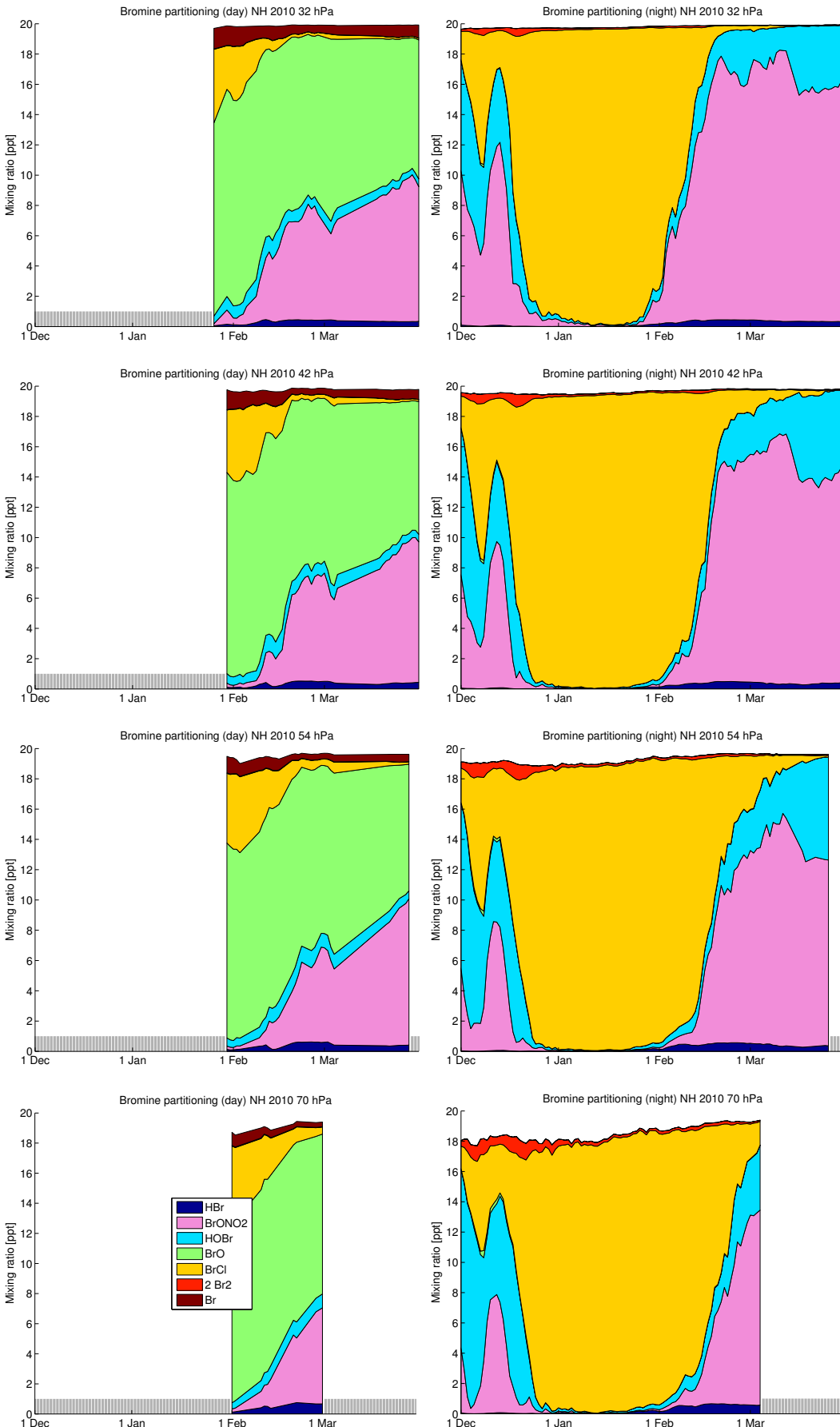


Figure 46: Vortex-averaged partitioning of inorganic bromine species. Left: Daytime averages (parts of the vortex where the solar zenith angle is smaller than 80°). Right: Nighttime averages (parts of the vortex where the solar zenith angle is larger than 100°). Days without sufficient data for averaging are not shown (grey bars).

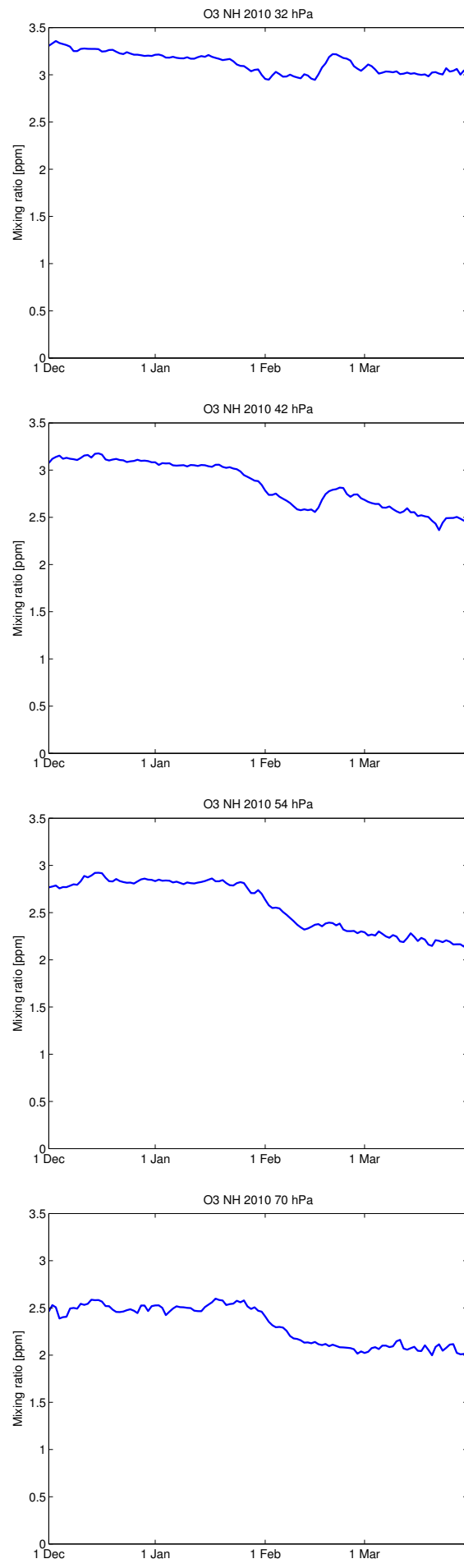


Figure 47: Vortex-averaged ozone mixing ratios.

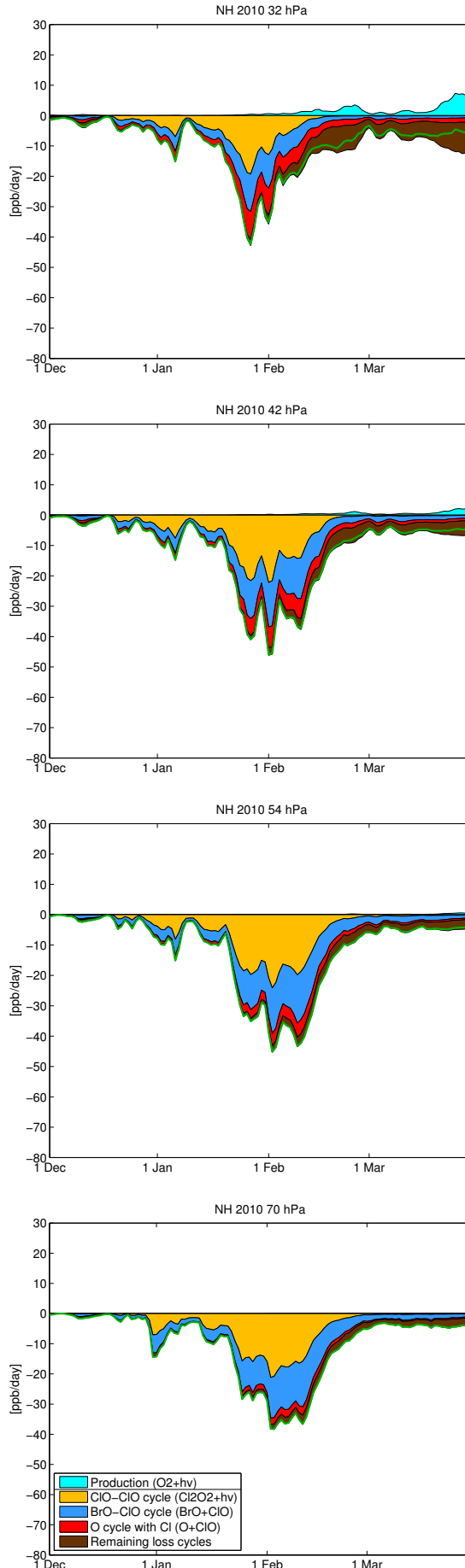


Figure 48: Vortex-averaged net chemical change of odd oxygen. The green line shows the net chemical change rate of ozone, which nearly equals the change rate of odd oxygen. The contribution of different catalytic cycles to the ozone loss is shown by the reaction rates of their rate limiting step. Only the three most important cycles are shown, the contribution of other cycles is small. Ozone production, which is almost exclusively by the $O_2 + hv$ reaction, is shown in cyan.

1.3 Southern Hemisphere 2006

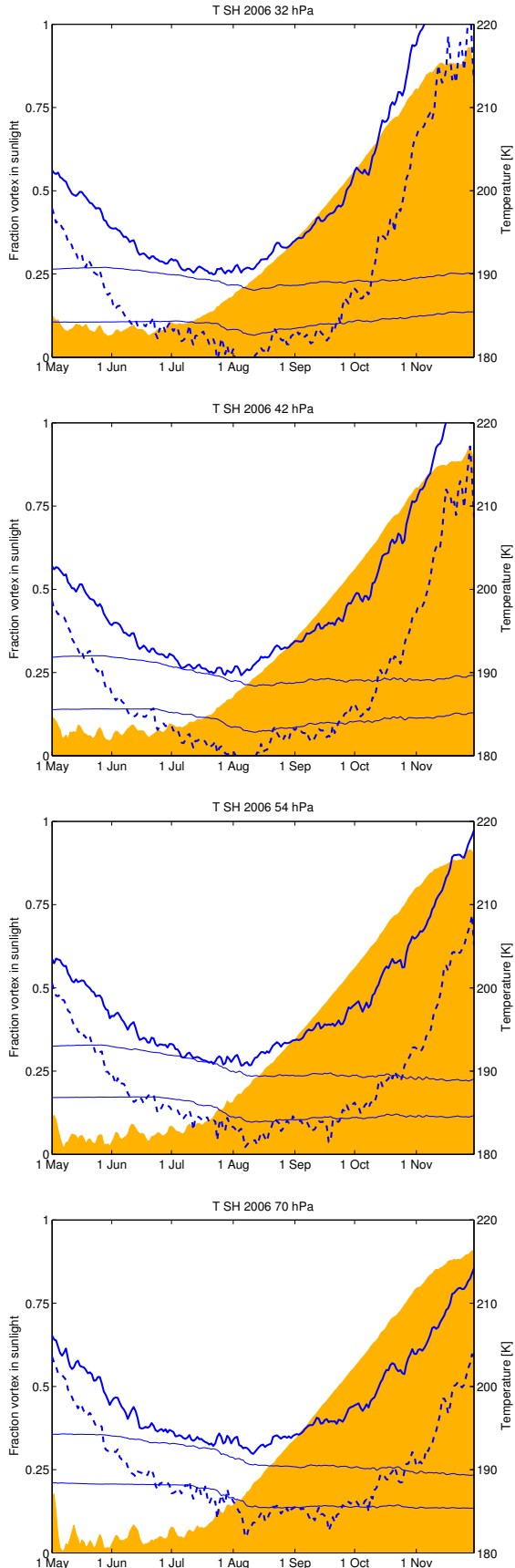


Figure 49: Vortex-averaged temperature (blue), vortex minimum temperature (dashed blue) and fraction of the vortex in sunlight (yellow). The upper thin blue line shows the threshold temperature for the formation of NAT clouds used in the model (based on vortex mean mixing ratios and considering supersaturation), and the lower thin blue line shows the same for ice clouds. The vortex tracer criterion is not applied (in contrast to all other figures).

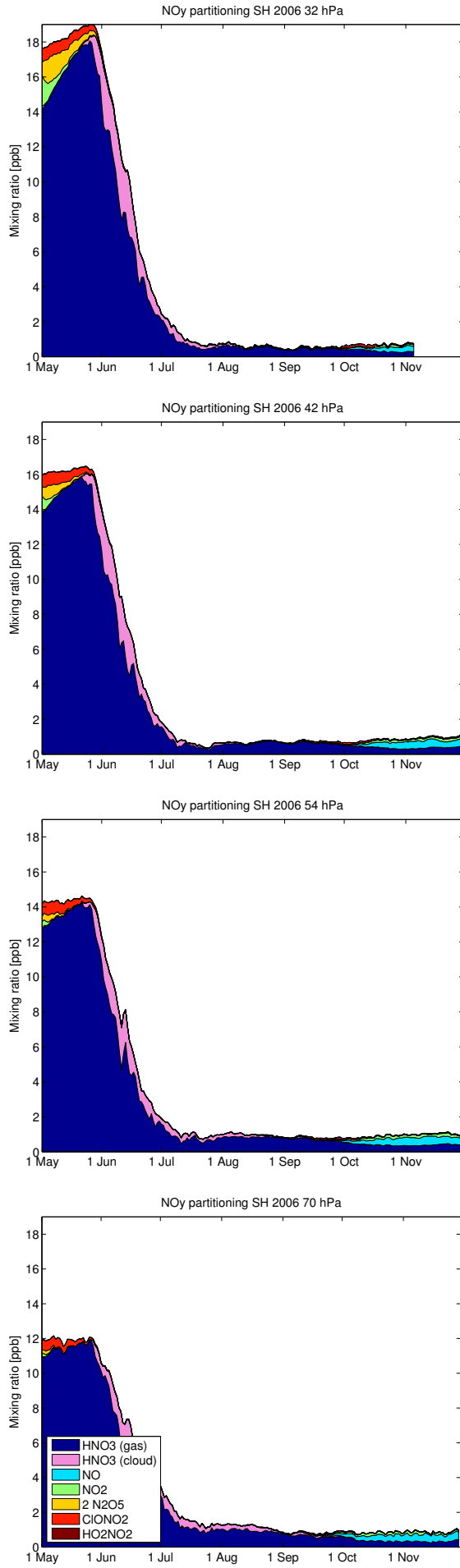


Figure 50: Vortex-averaged partitioning of NO_y species. Species NO₃, BrONO₂, ClONO₂ and N are not shown due to their small mixing ratios.

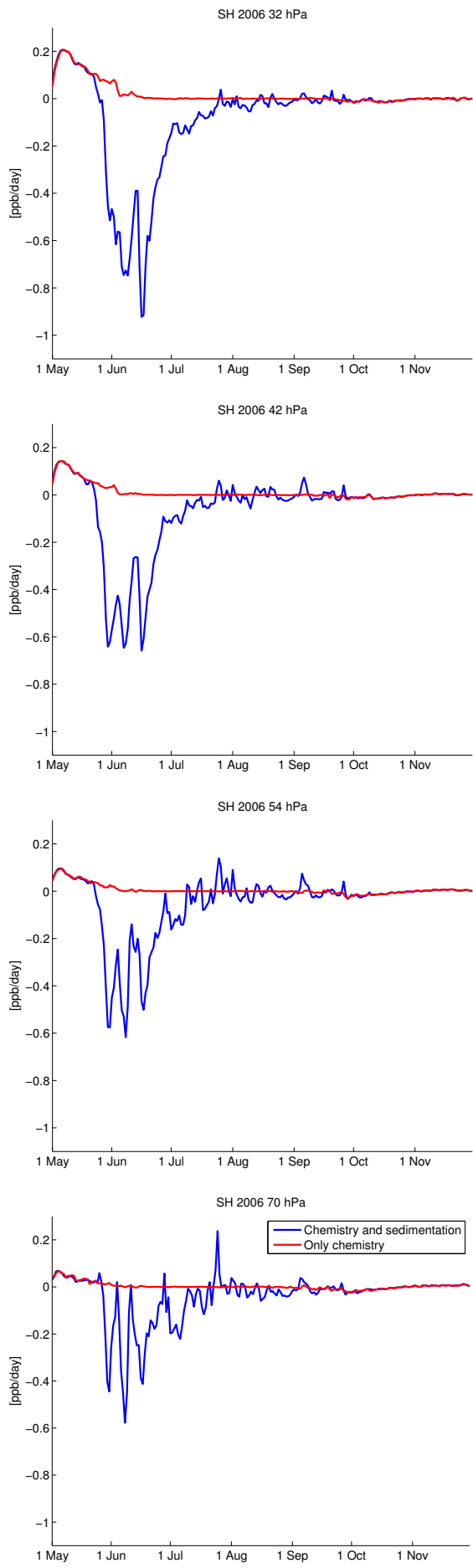


Figure 51: Vortex-averaged net chemical reaction rate of HNO_3 (red) and sum of the vortex-averaged change by sedimentation and the net chemical reaction rate (blue).

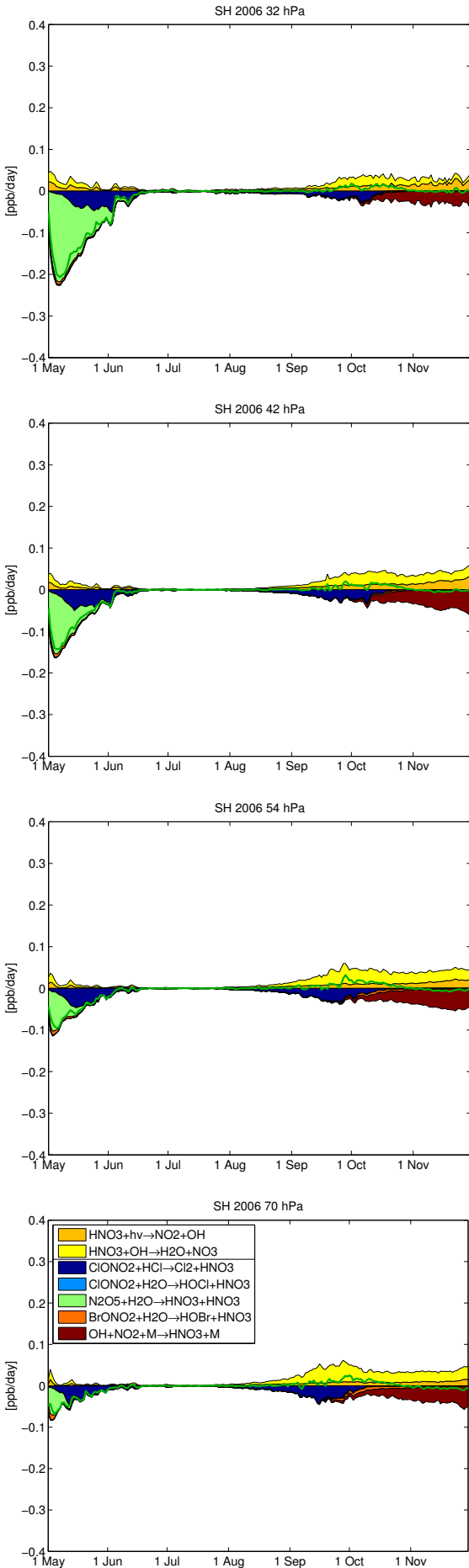


Figure 52: Vortex-averaged chemical reaction rates of reactions changing extended NO_x (NO + NO₂ + NO₃ + 2N₂O₅ + ClONO₂ + BrONO₂ + HO₂NO₂). Production reactions are shown positive and are separated by a line in the legend from the loss reactions, which are shown negative. The net change of extended NO_x is shown as a green line.

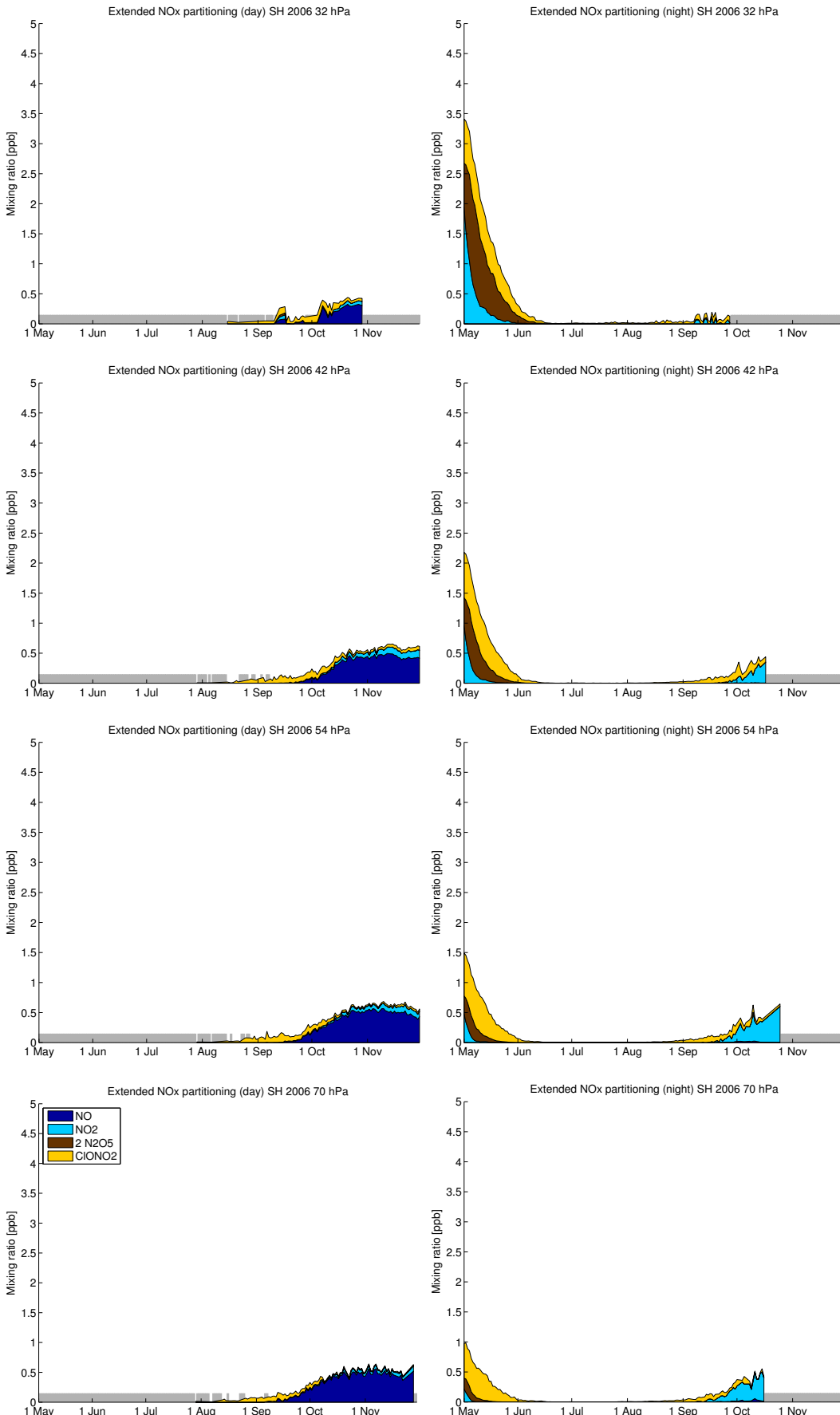


Figure 53: Vortex-averaged partitioning of extended NO_x species. Left: Daytime averages (parts of the vortex where the solar zenith angle is smaller than 80°). Right: Nighttime averages (parts of the vortex where the solar zenith angle is larger than 100°). Days without sufficient data for averaging are not shown (grey bars).

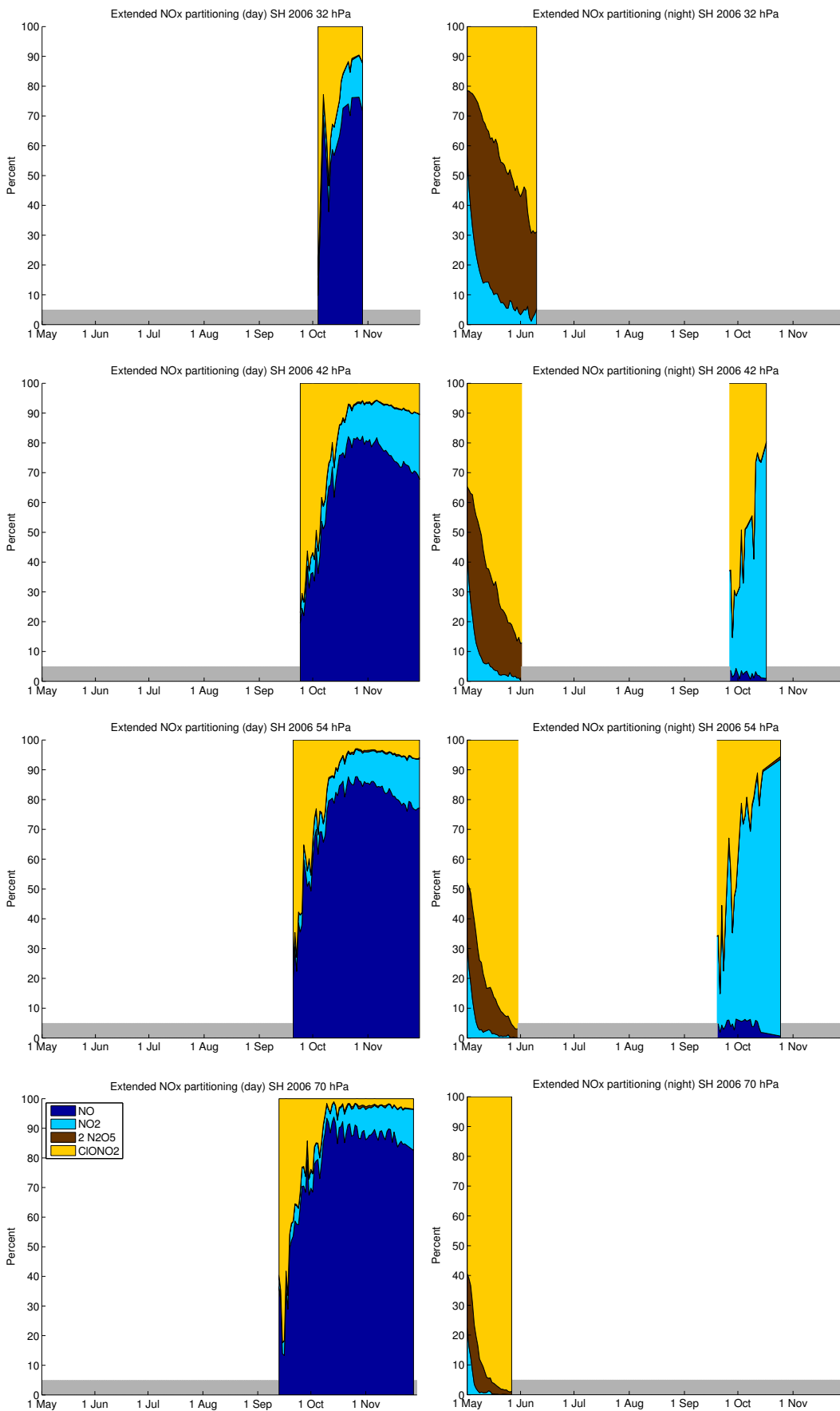


Figure 54: Same as Figure 53, but now in percentages and not in mixing ratios. Percentages are not shown for values of extended NO_x below 0.1 ppb and for days without sufficient data for averaging (grey bars).

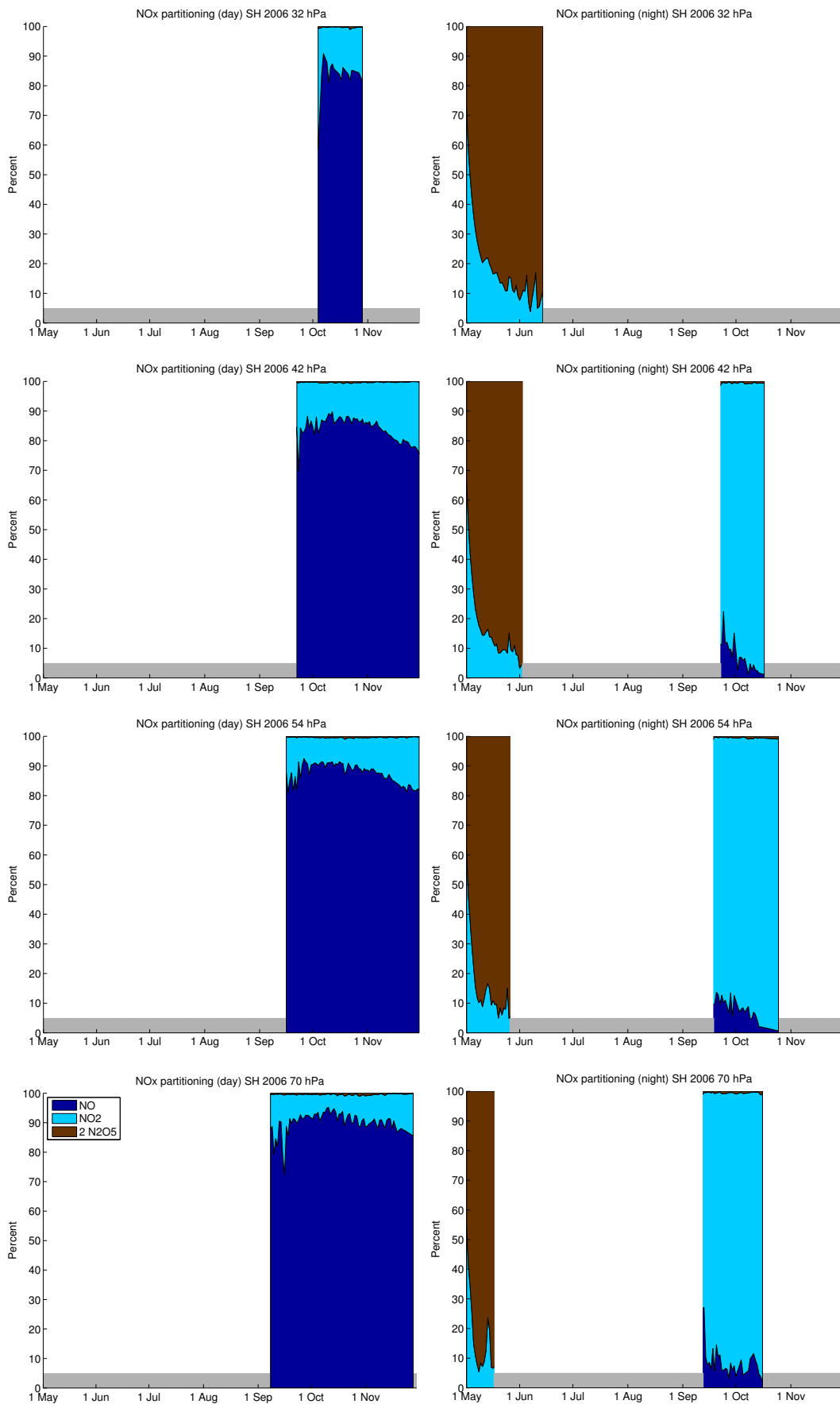


Figure 55: Same as Figure 54, but with only $\text{NO}_x = \text{NO} + \text{NO}_2 + 2\text{N}_2\text{O}_5$ partitioning. Percentages are not shown for values of NO_x below 0.01 ppb and for days without sufficient data for averaging (grey bars).

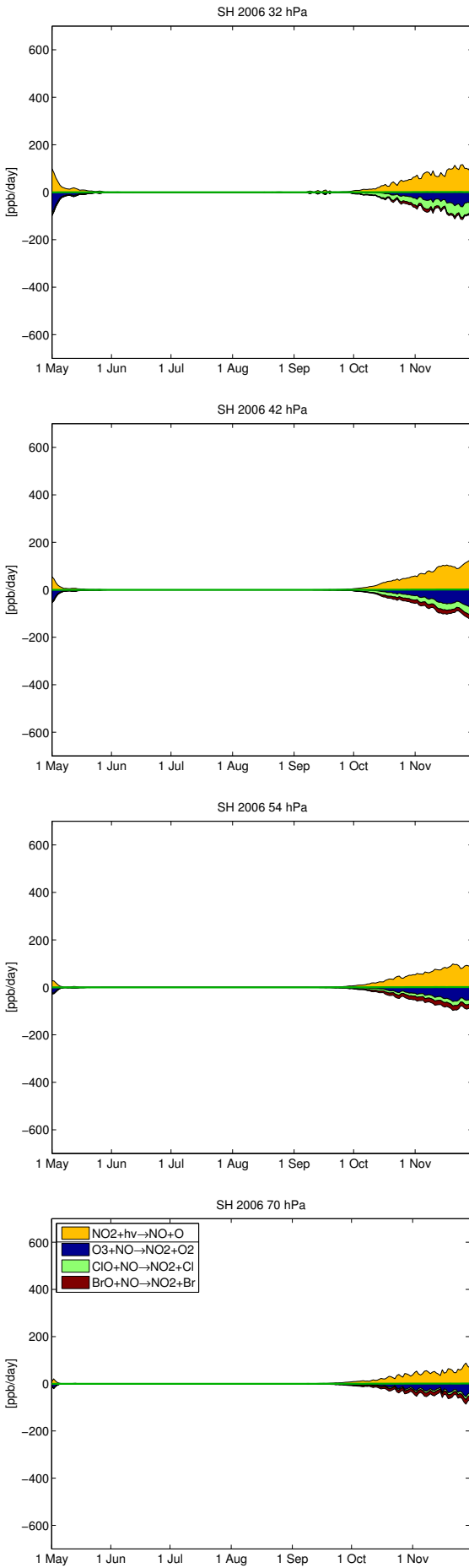


Figure 56: Vortex-averaged chemical reaction rates of reactions changing NO to illustrate NO_x partitioning. Production reactions are shown positive and are separated by a line in the legend from the loss reactions, which are shown negative. The net change of NO is shown as a green line.

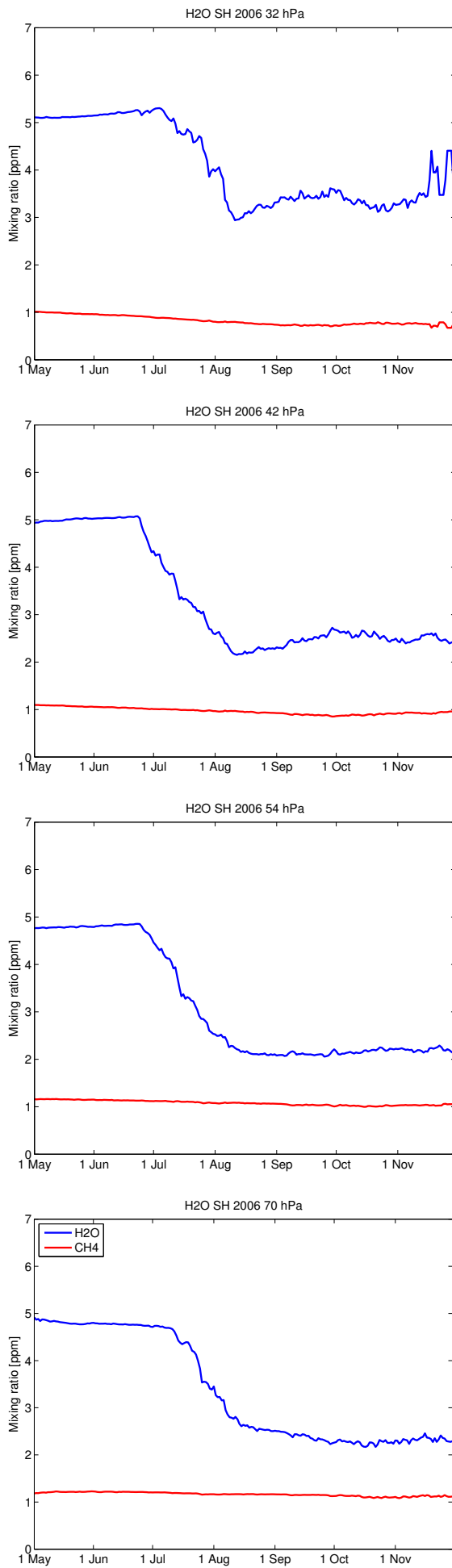


Figure 57: Vortex-averaged mixing ratios of H₂O and CH₄.

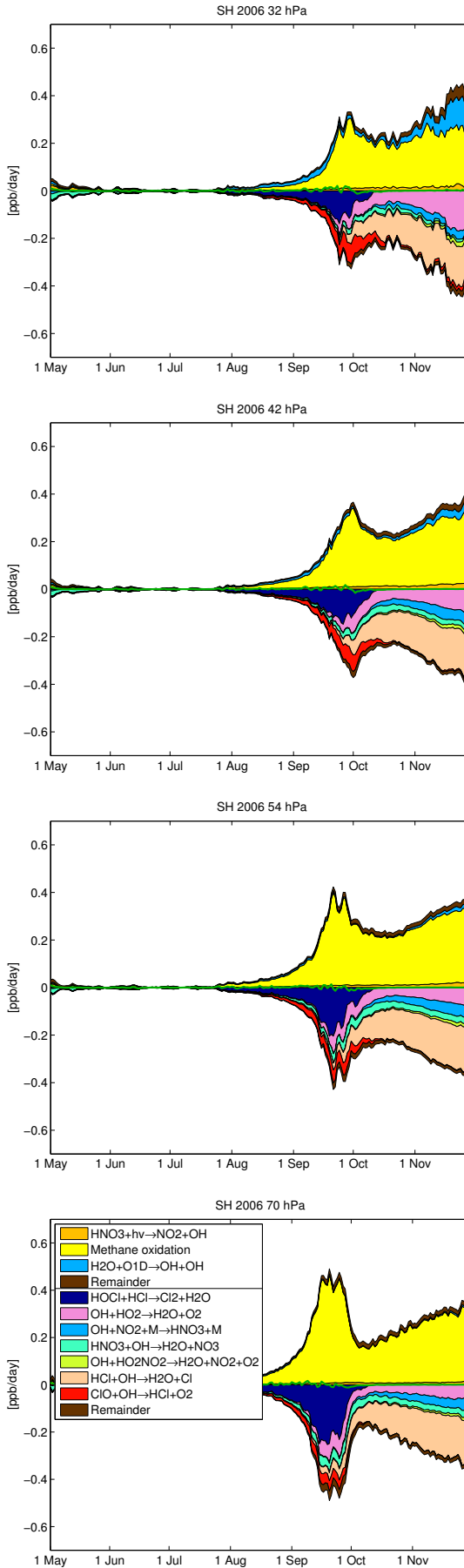


Figure 58: Vortex-averaged chemical reaction rates of reactions changing extended HO_x ($\text{OH} + \text{HO}_2 + \text{H} + \text{HOCl} + \text{HOBr} + \text{HO}_2\text{NO}_2$). Production reactions are shown positive and are separated by a line in the legend from the loss reactions, which are shown negative. The net change of extended HO_x is shown as a green line. Methane oxidation is modelled by simplified net reactions in ATLAS, the reactions denoted as methane oxidation in the legend are $\text{Cl} + \text{CH}_4 \rightarrow \text{HCl} + \text{CH}_2\text{O} + \text{HO}_2$ and $\text{Cl} + \text{CH}_2\text{O} \rightarrow \text{HCl} + \text{CO} + \text{HO}_2$.

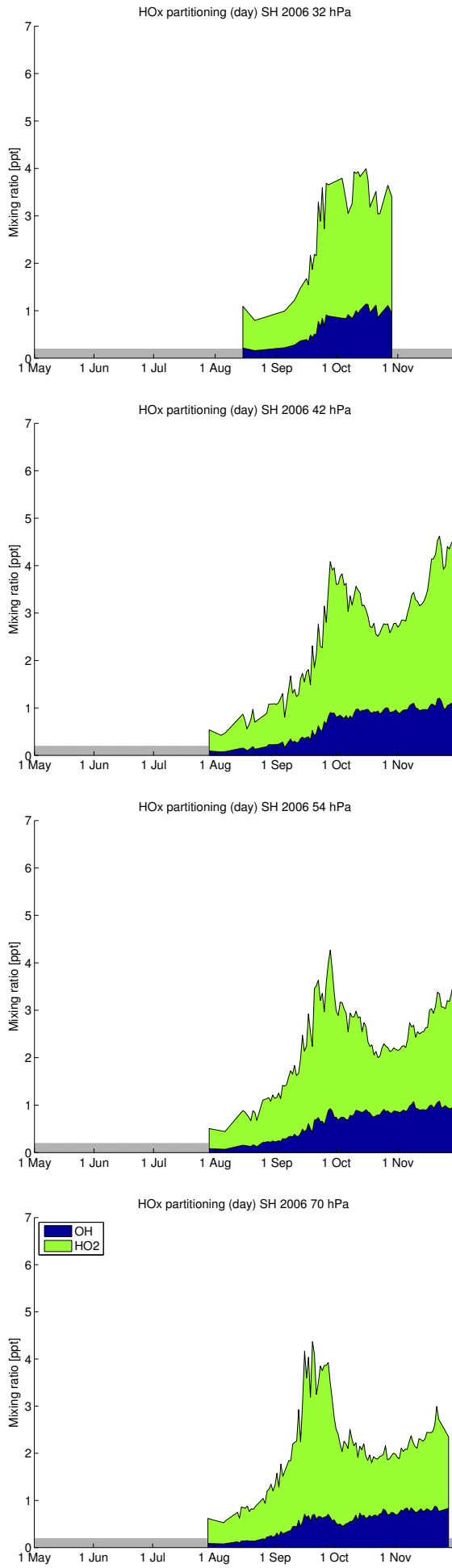


Figure 59: Vortex-averaged partitioning of HO_x species. Daytime averages (parts of the vortex where the solar zenith angle is smaller than 80°). Nighttime averages are near zero and not shown. Data: WRF-Chem (10°S–60°N, 10°–60°E) (see Fig. 1).

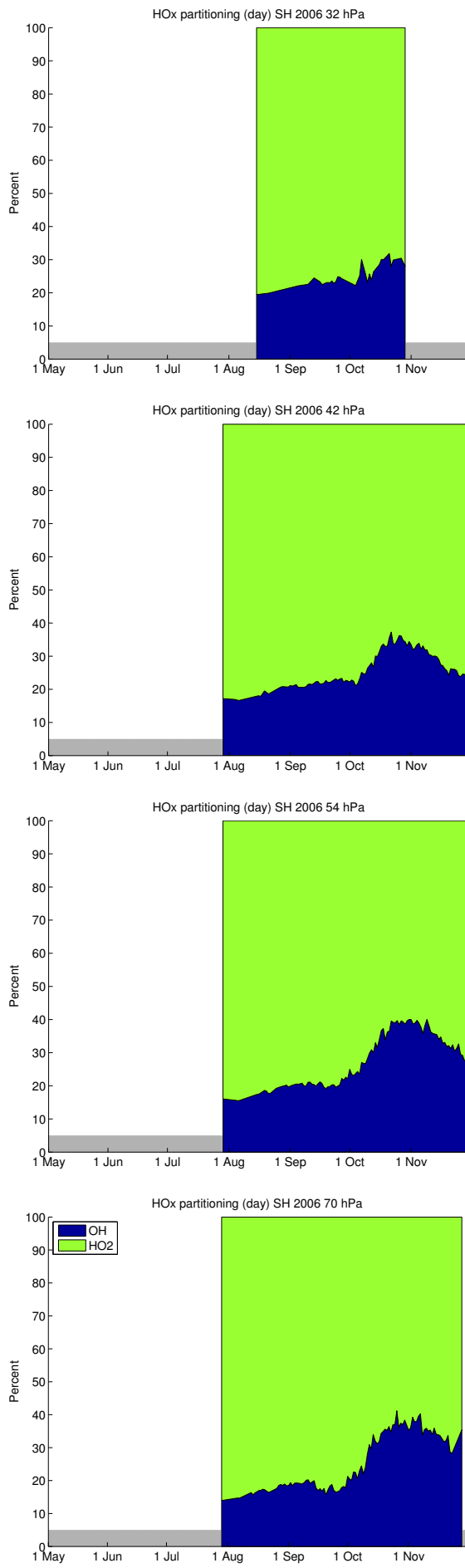


Figure 60: Same as Figure 59, but now in percentages and not in mixing ratios. Days without sufficient data for averaging are not shown (grey bars).

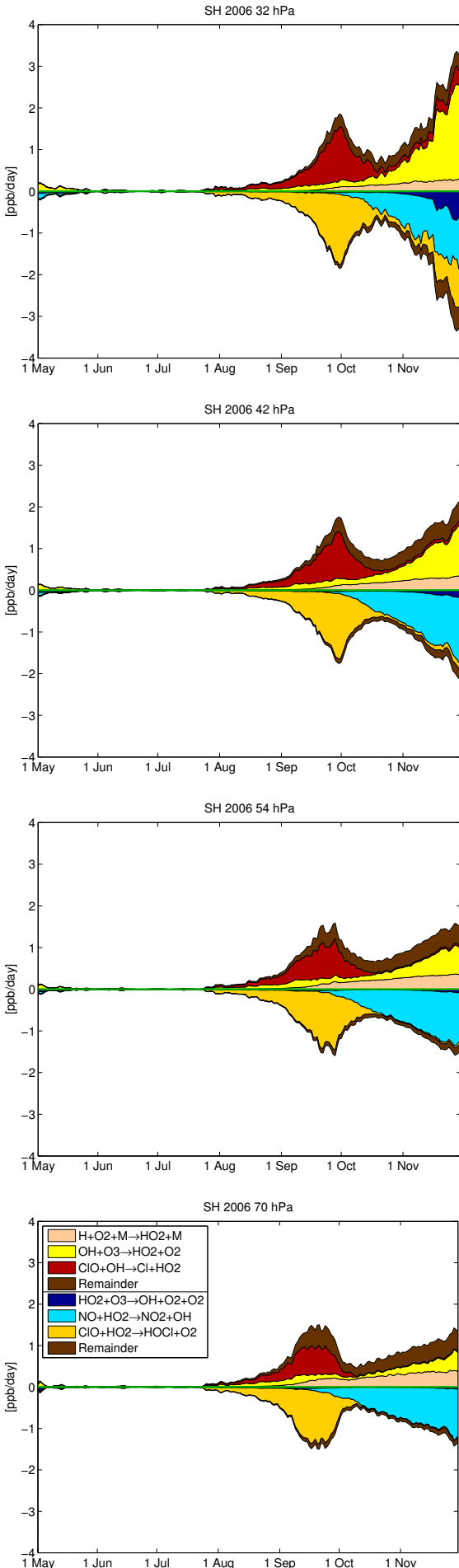


Figure 61: Vortex-averaged chemical reaction rates of reactions changing HO₂ to illustrate HO_x partitioning. Production reactions are shown positive and are separated by a line in the legend from the loss reactions, which are shown negative. The net change of HO₂ is shown as a green line.

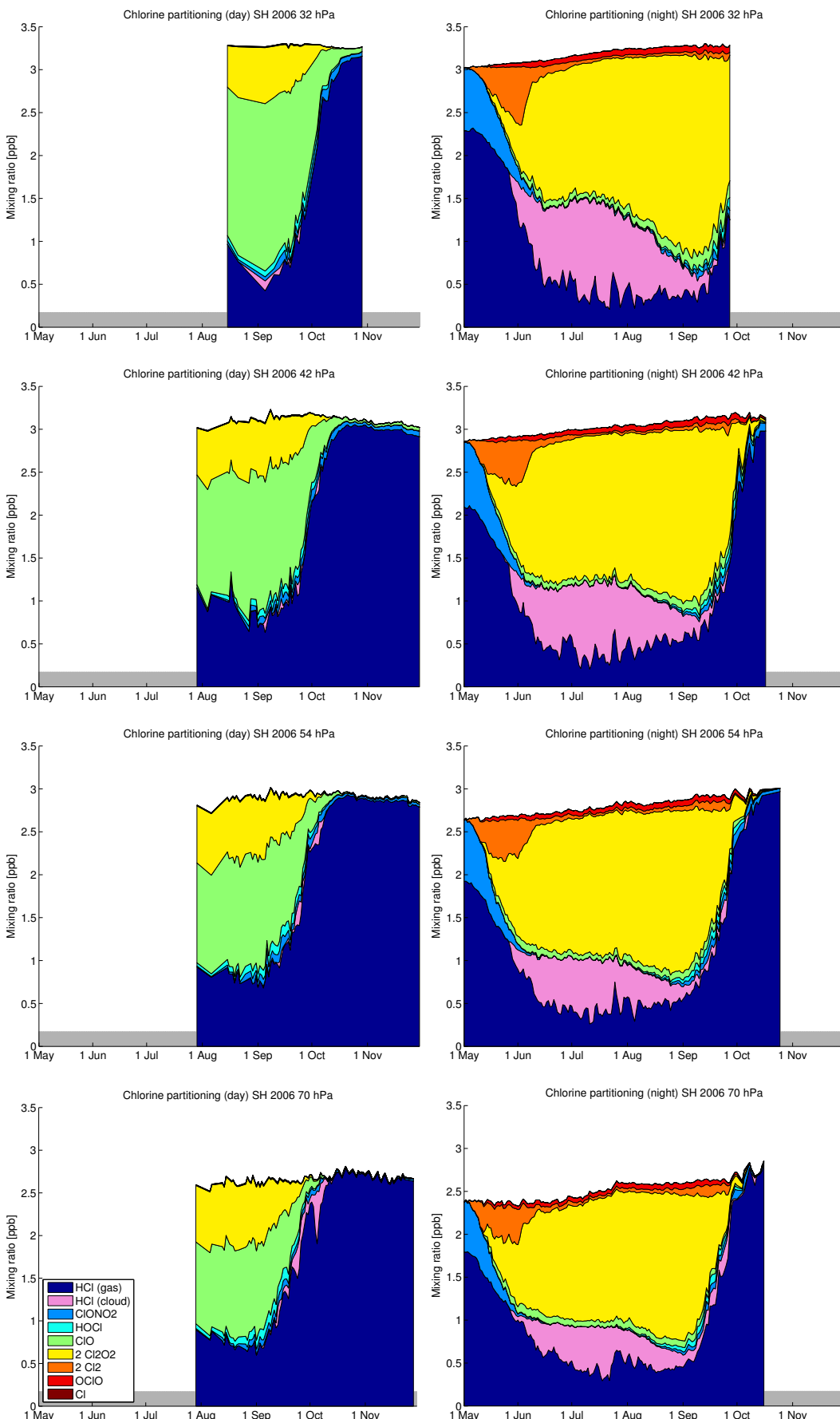


Figure 62: Vortex-averaged partitioning of inorganic chlorine species (Cl_y). Left: Daytime averages (parts of the vortex where the solar zenith angle is smaller than 80°). Right: Nighttime averages (parts of the vortex where the solar zenith angle is larger than 100°). Days without sufficient data for averaging are not shown (grey bars). Species ClNO_2 and BrCl are not shown due to their small mixing ratios. The area labeled “HCl (cloud)” shows HCl dissolved in STS droplets due to the applied correction to the HCl solubility.

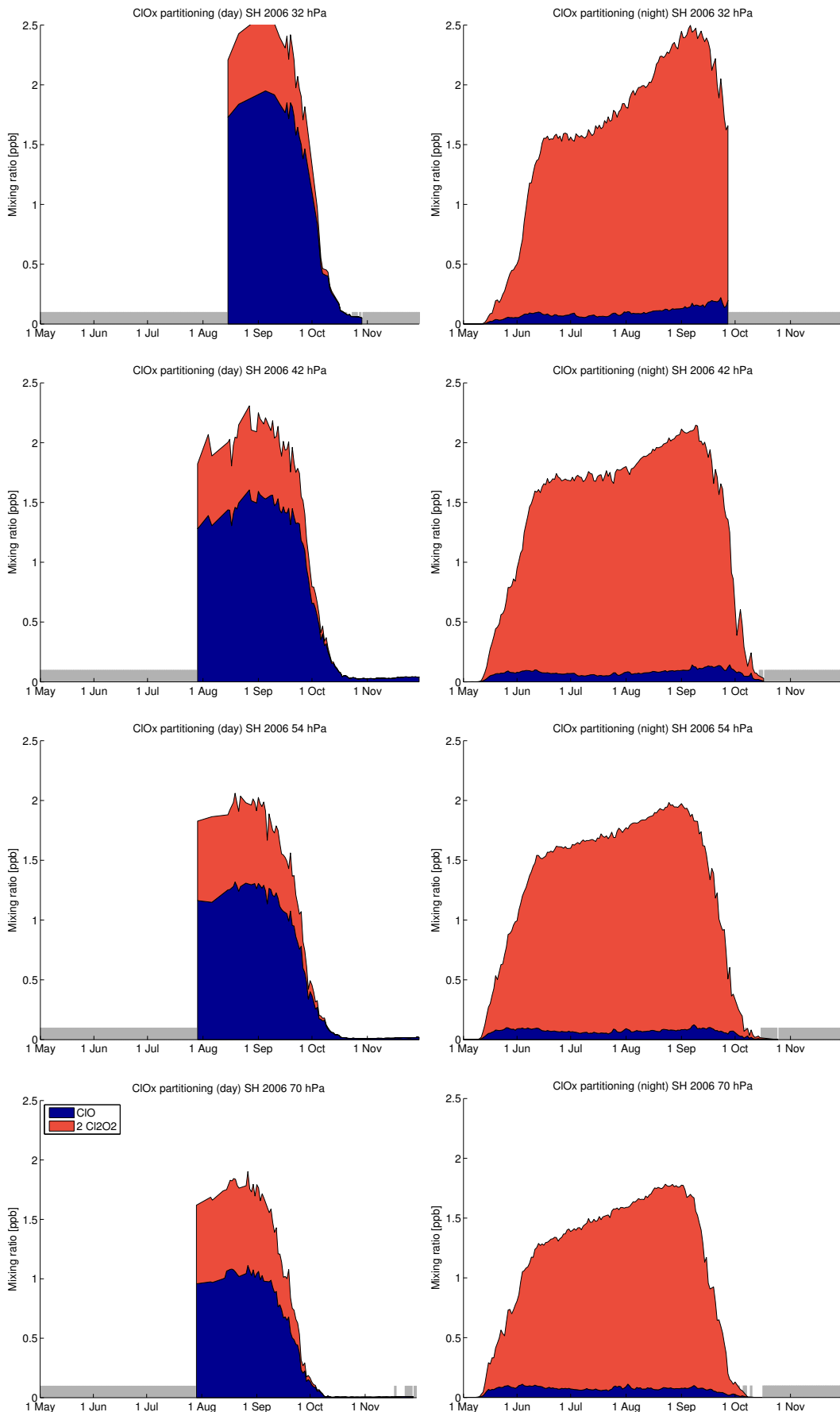


Figure 63: Vortex-averaged partitioning of ClO_x . Left: Daytime averages (parts of the vortex where the solar zenith angle is smaller than 80°). Right: Nighttime averages (parts of the vortex where the solar zenith angle is larger than 100°). Days without sufficient data for averaging are not shown (grey bars).

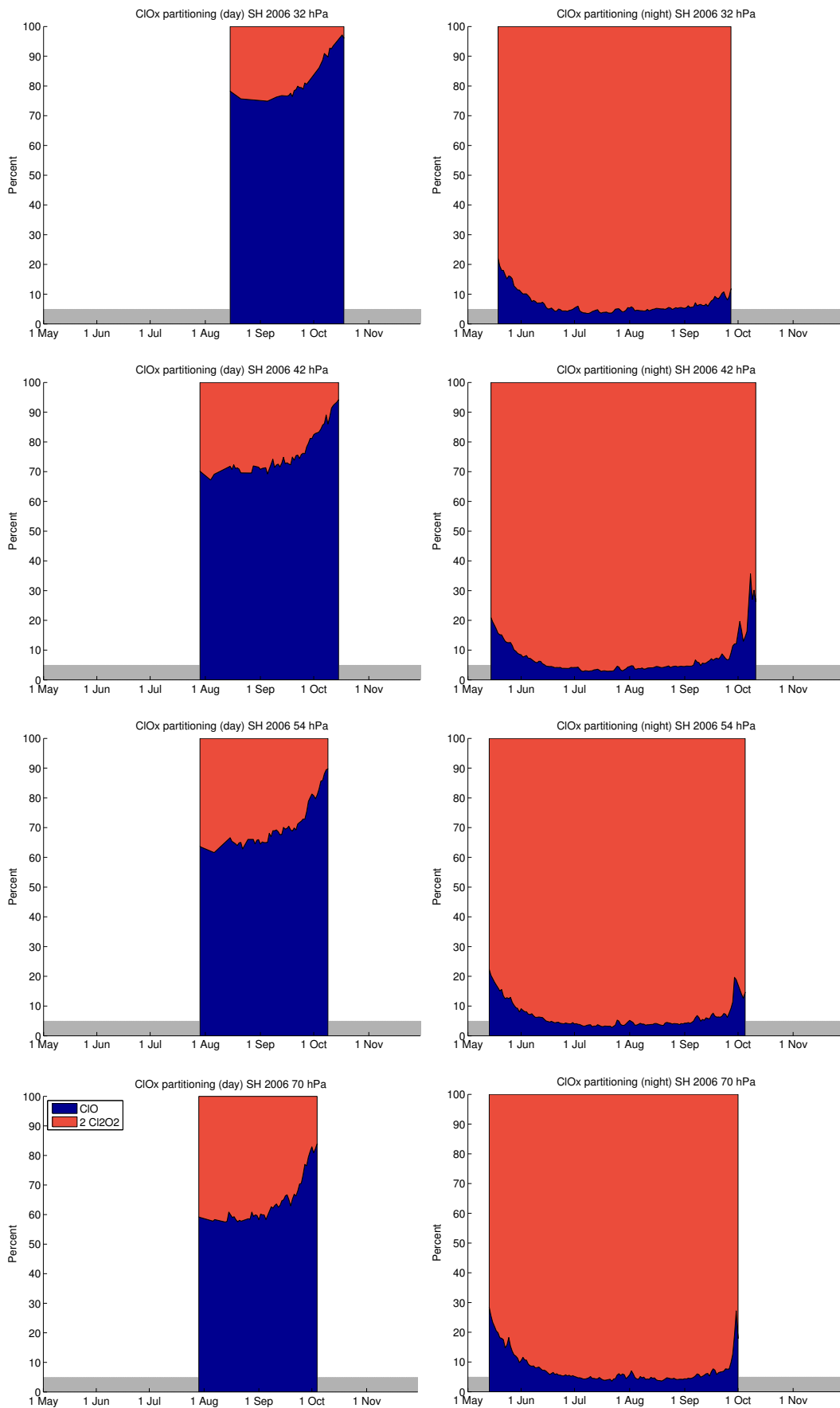


Figure 64: Same as Figure 63, but now in percentages and not in mixing ratios. Percentages are not shown for values of ClO_x below 0.1 ppb and for days without sufficient data for averaging (grey bars).

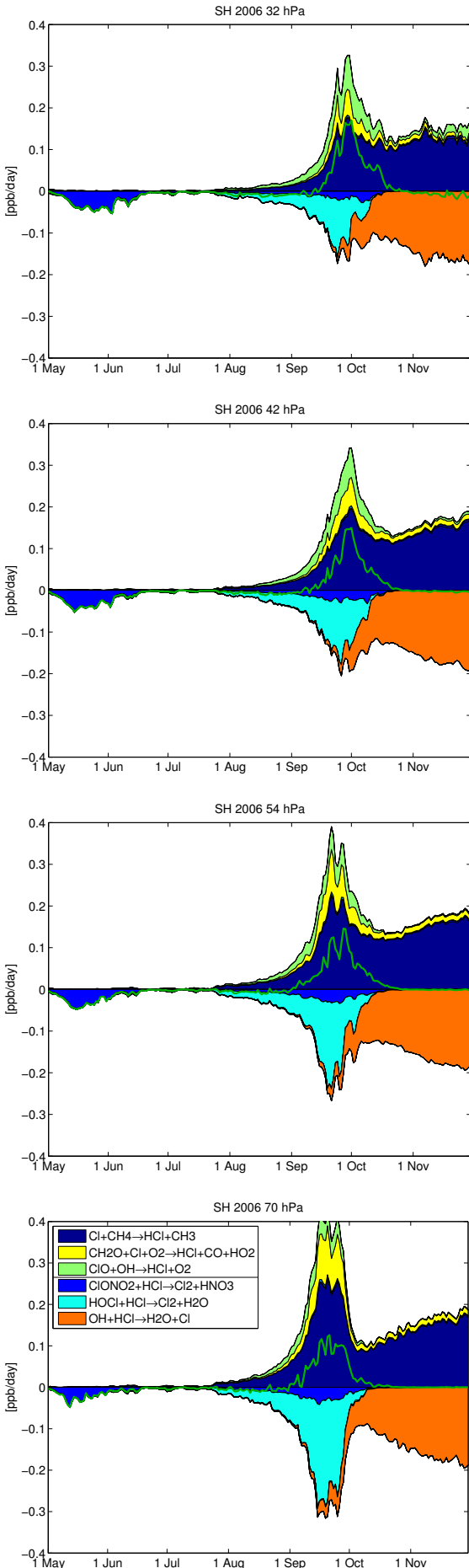


Figure 65: Vortex-averaged chemical reaction rates of reactions involving HCl. Production reactions are shown positive and are separated by a line in the legend from the loss reactions, which are shown negative. The net change of HCl is shown as a green line. Reactions with rates which cannot be distinguished from the zero line at plot resolution are not shown.

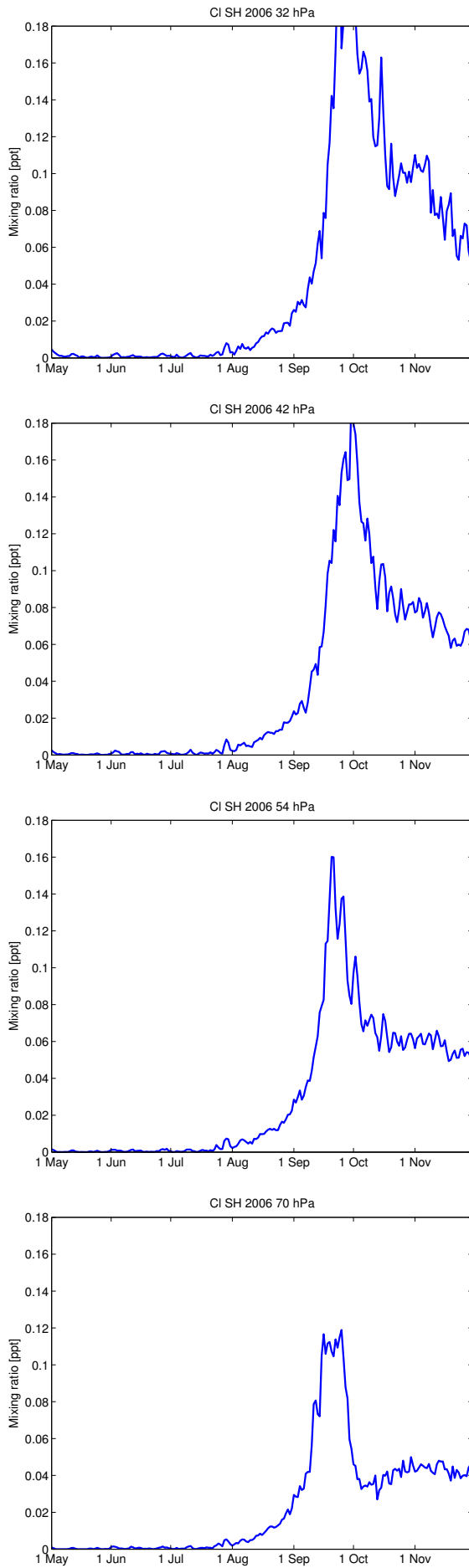


Figure 66: Vortex-averaged Cl mixing ratios.

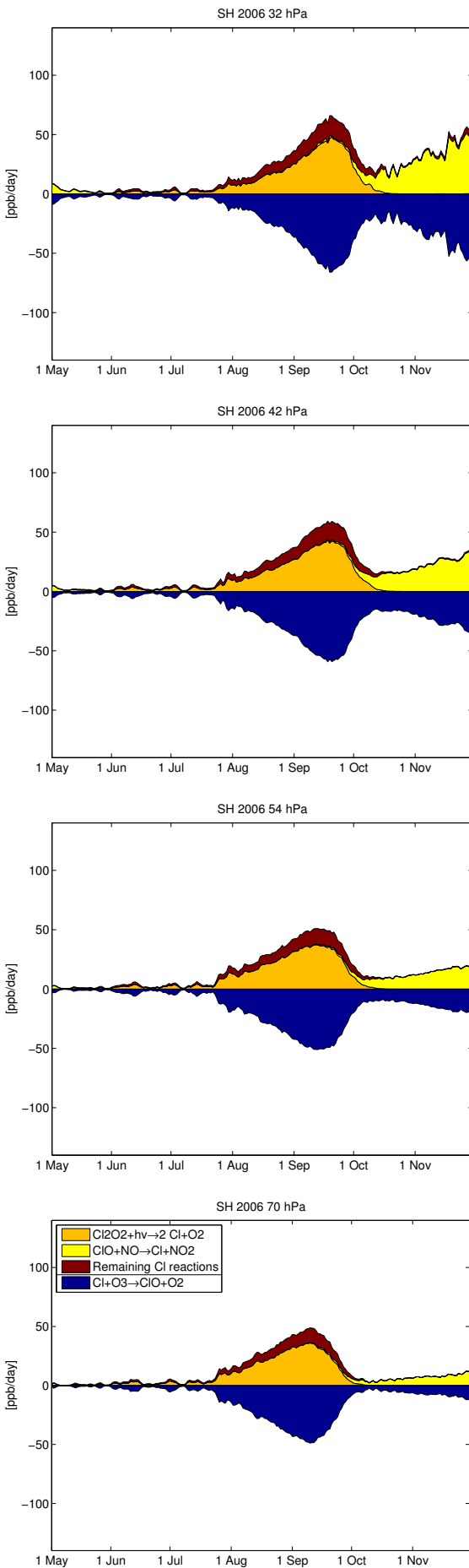


Figure 67: Vortex-averaged chemical reaction rates of reactions involving Cl. Production reactions are shown positive and are separated by a line in the legend from the loss reactions, which are shown negative.

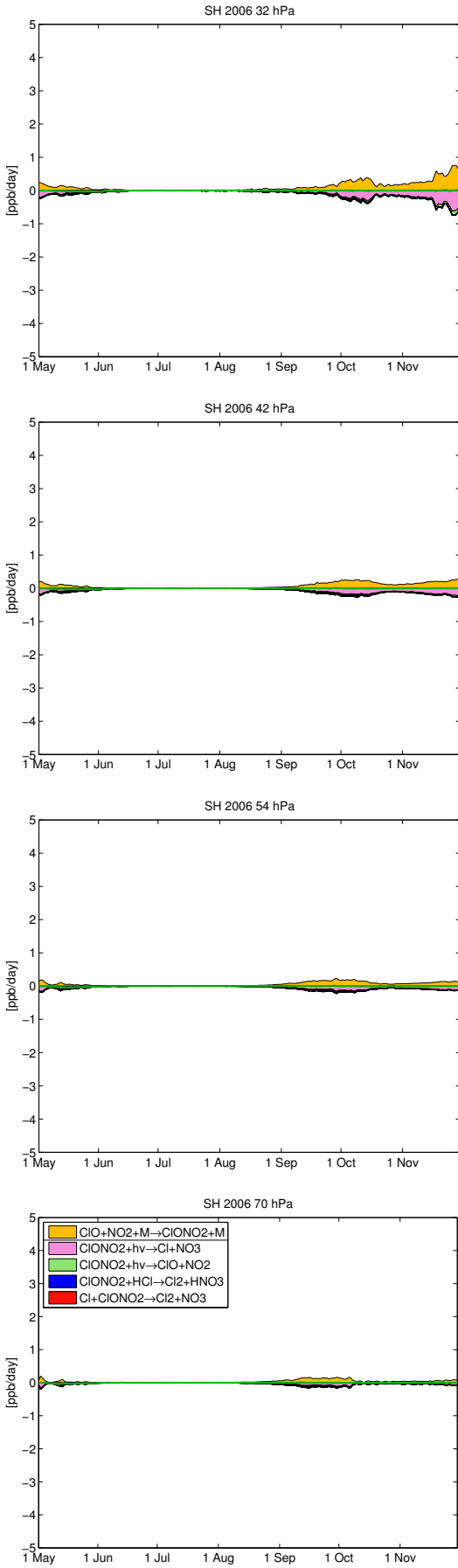


Figure 68: Vortex-averaged chemical reaction rates involving ClONO_2 . Production reactions are shown positive and are separated by a line in the legend from the loss reactions, which are shown negative. The net change of ClONO_2 is shown as a green line. Reactions with rates which cannot be distinguished from the zero line at plot resolution are not shown.

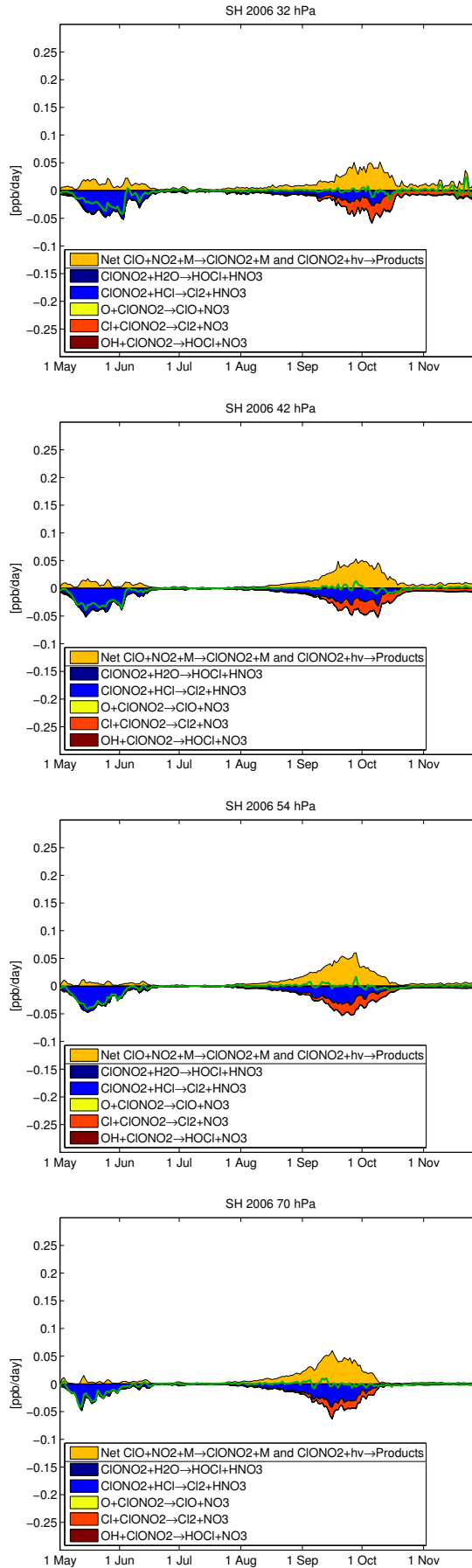


Figure 69: Vortex-averaged chemical reaction rates involving ClONO_2 . In contrast to Figure 68, the net production rate of the fast cycle $\text{ClONO}_2 + h\nu \rightarrow \text{Products} / \text{ClO} + \text{NO}_2 + \text{M} \rightarrow \text{ClONO}_2 + \text{M}$ is shown. This cycle is separated by a line in the legend from the loss reactions. The green line shows the net change of ClONO_2 by chemistry. Reactions with rates which cannot be distinguished from the zero line at plot resolution are not shown.

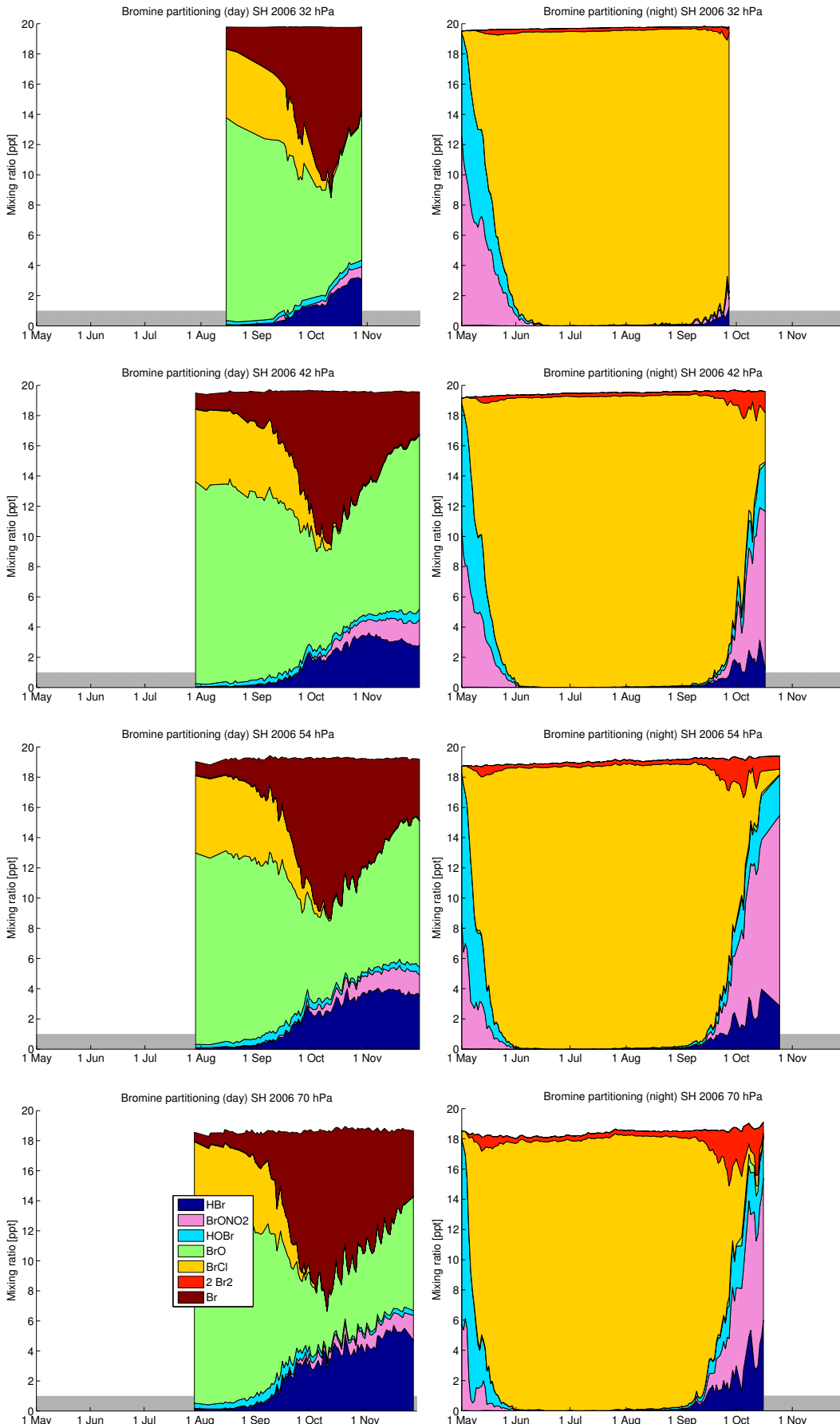


Figure 70: Vortex-averaged partitioning of inorganic bromine species. Left: Daytime averages (parts of the vortex where the solar zenith angle is smaller than 80°). Right: Nighttime averages (parts of the vortex where the solar zenith angle is larger than 100°). Days without sufficient data for averaging are not shown (grey bars).

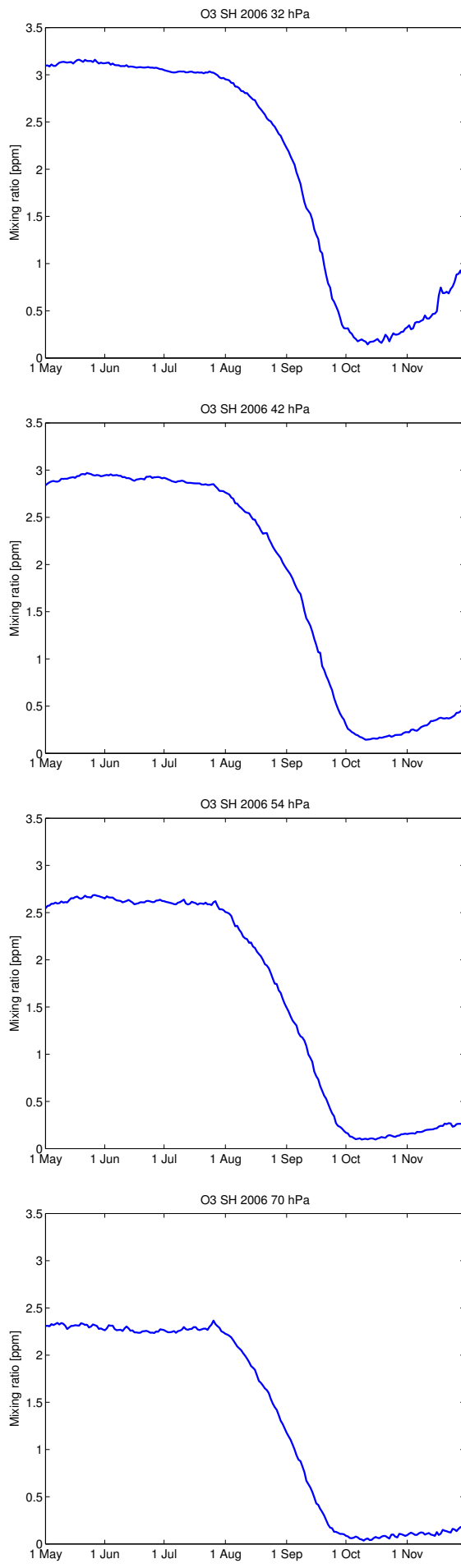


Figure 71: Vortex-averaged ozone mixing ratios.

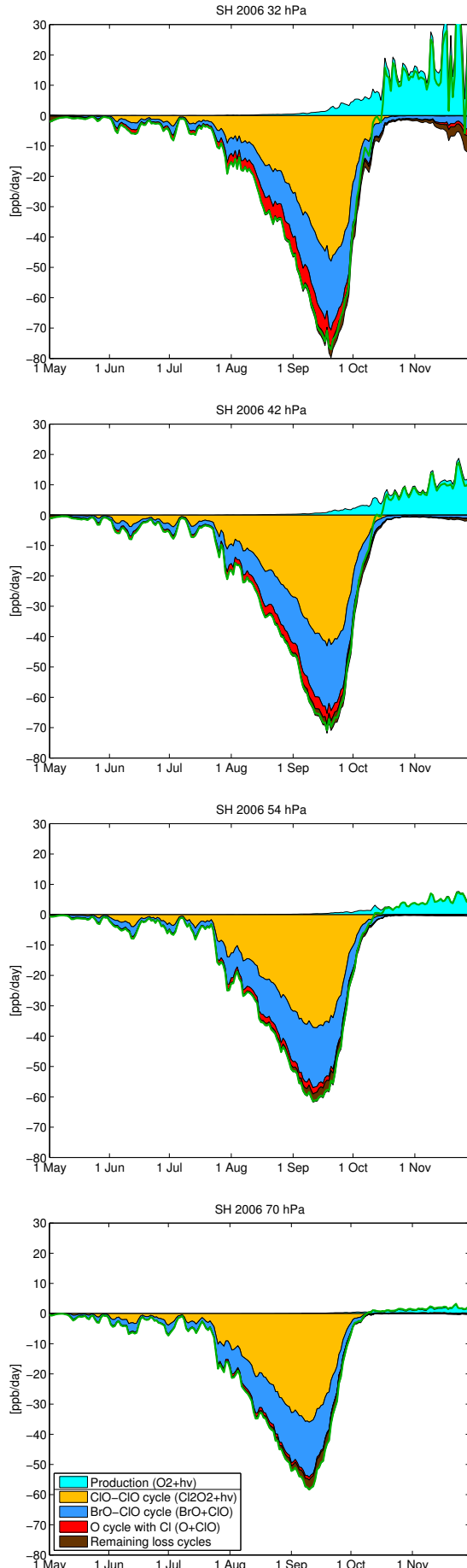


Figure 72: Vortex-averaged net chemical change of odd oxygen. The green line shows the net chemical change rate of ozone, which nearly equals the change rate of odd oxygen. The contribution of different catalytic cycles to the ozone loss is shown by the reaction rates of their rate limiting step. Only the three most important cycles are shown, the contribution of other cycles is small. Ozone production, which is almost exclusively by the $O_2 + h\nu$ reaction, is shown in cyan.

1.4 Southern Hemisphere 2011

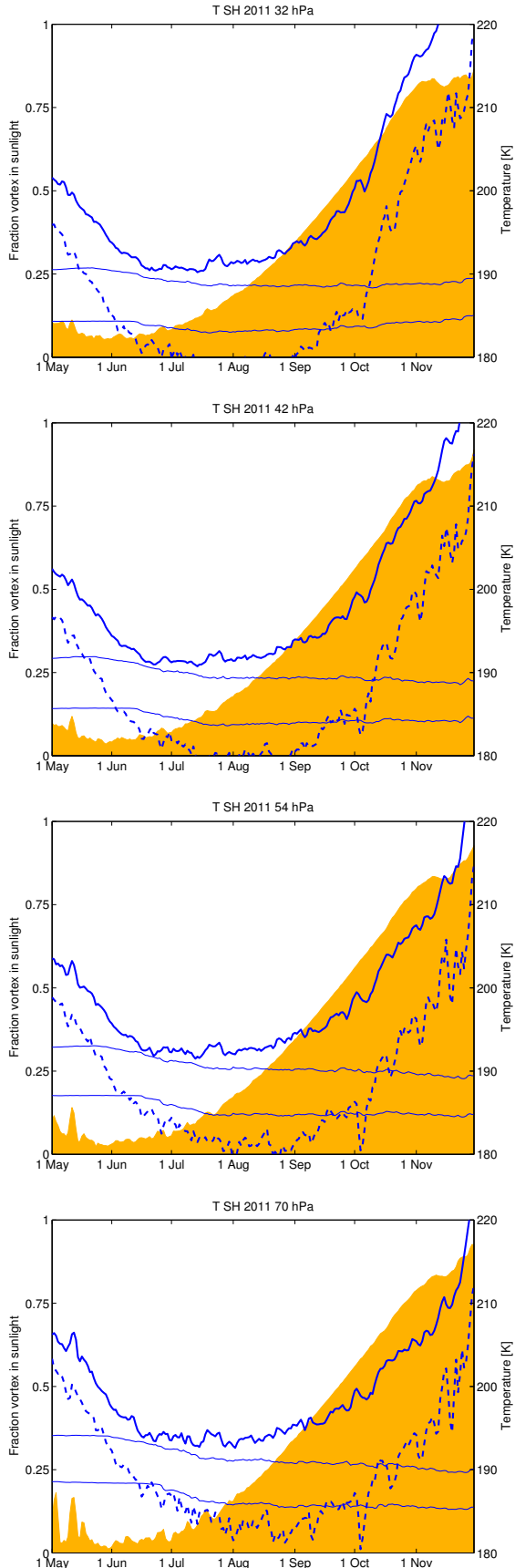


Figure 73: Vortex-averaged temperature (blue), vortex minimum temperature (dashed blue) and fraction of the vortex in sunlight (yellow). The upper thin blue line shows the threshold temperature for the formation of NAT clouds used in the model (based on vortex mean mixing ratios and considering supersaturation), and the lower thin blue line shows the same for ice clouds. The vortex tracer criterion is not applied (in contrast to all other figures).

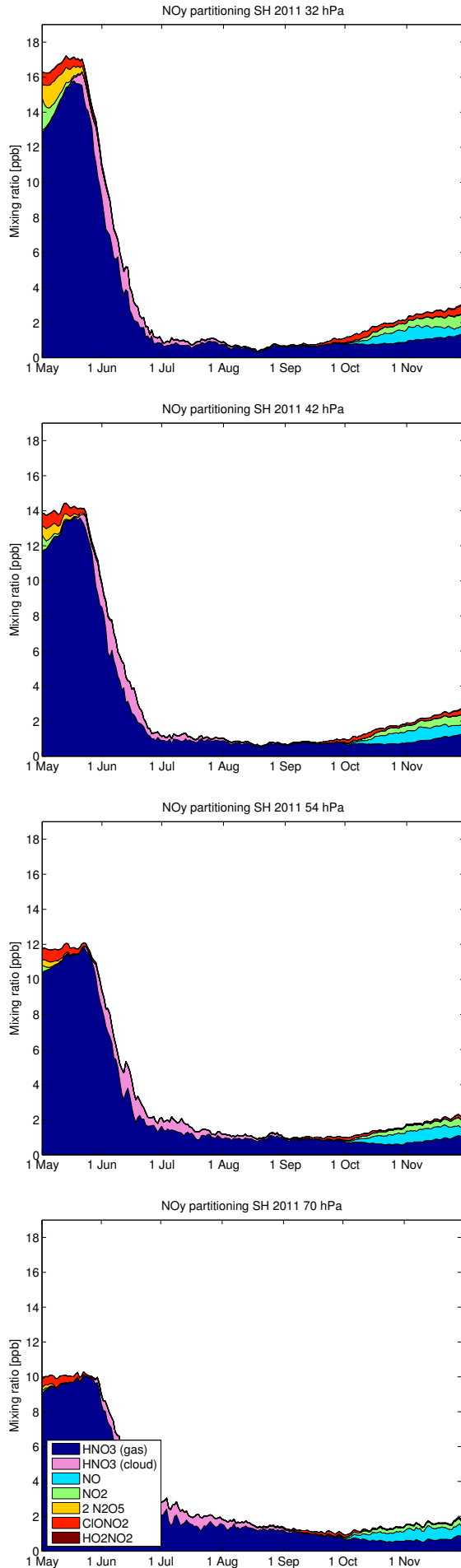


Figure 74: Vortex-averaged partitioning of NO_y species. Species NO₃, BrONO₂, ClONO₂ and N are not shown due to their small mixing ratios.

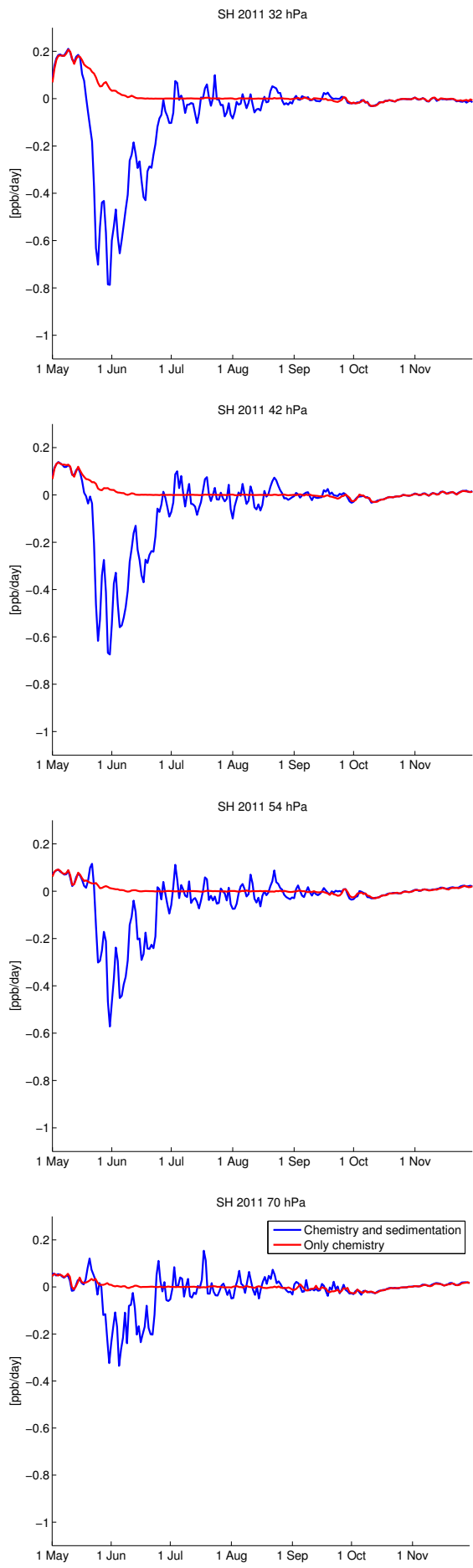


Figure 75: Vortex-averaged net chemical reaction rate of HNO_3 (red) and sum of the vortex-averaged change by sedimentation and the net chemical reaction rate (blue).

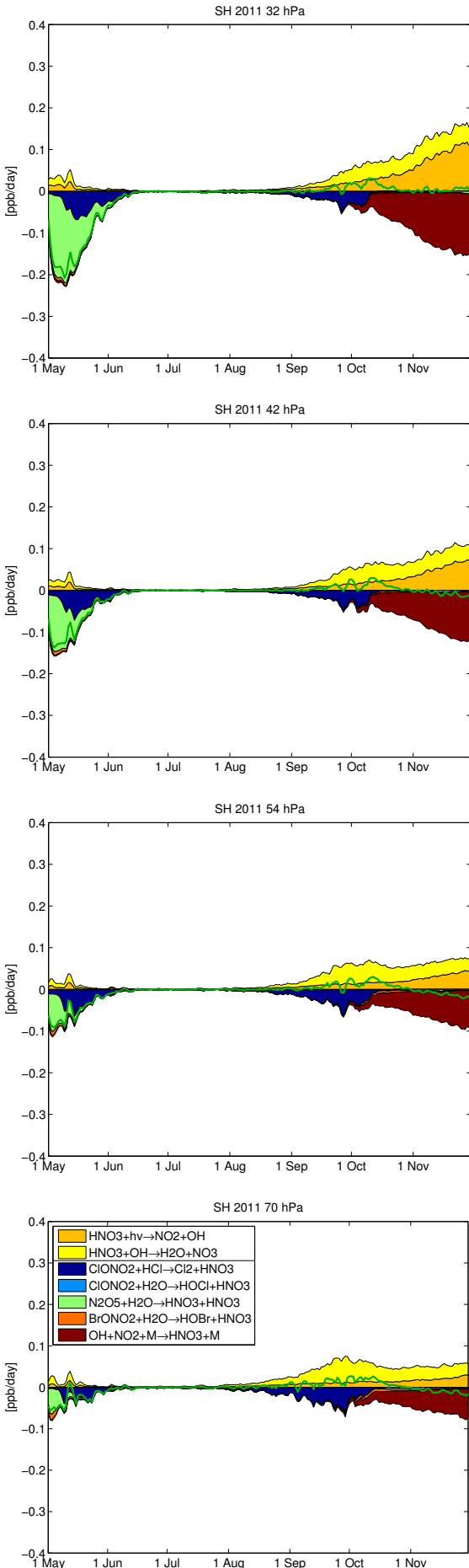


Figure 76: Vortex-averaged chemical reaction rates of reactions changing extended NO_x ($\text{NO} + \text{NO}_2 + \text{NO}_3 + 2\text{N}_2\text{O}_5 + \text{ClONO}_2 + \text{BrONO}_2 + \text{HO}_2\text{NO}_2$). Production reactions are shown positive and are separated by a line in the legend from the loss reactions, which are shown negative. The net change of extended NO_x is shown as a green line.

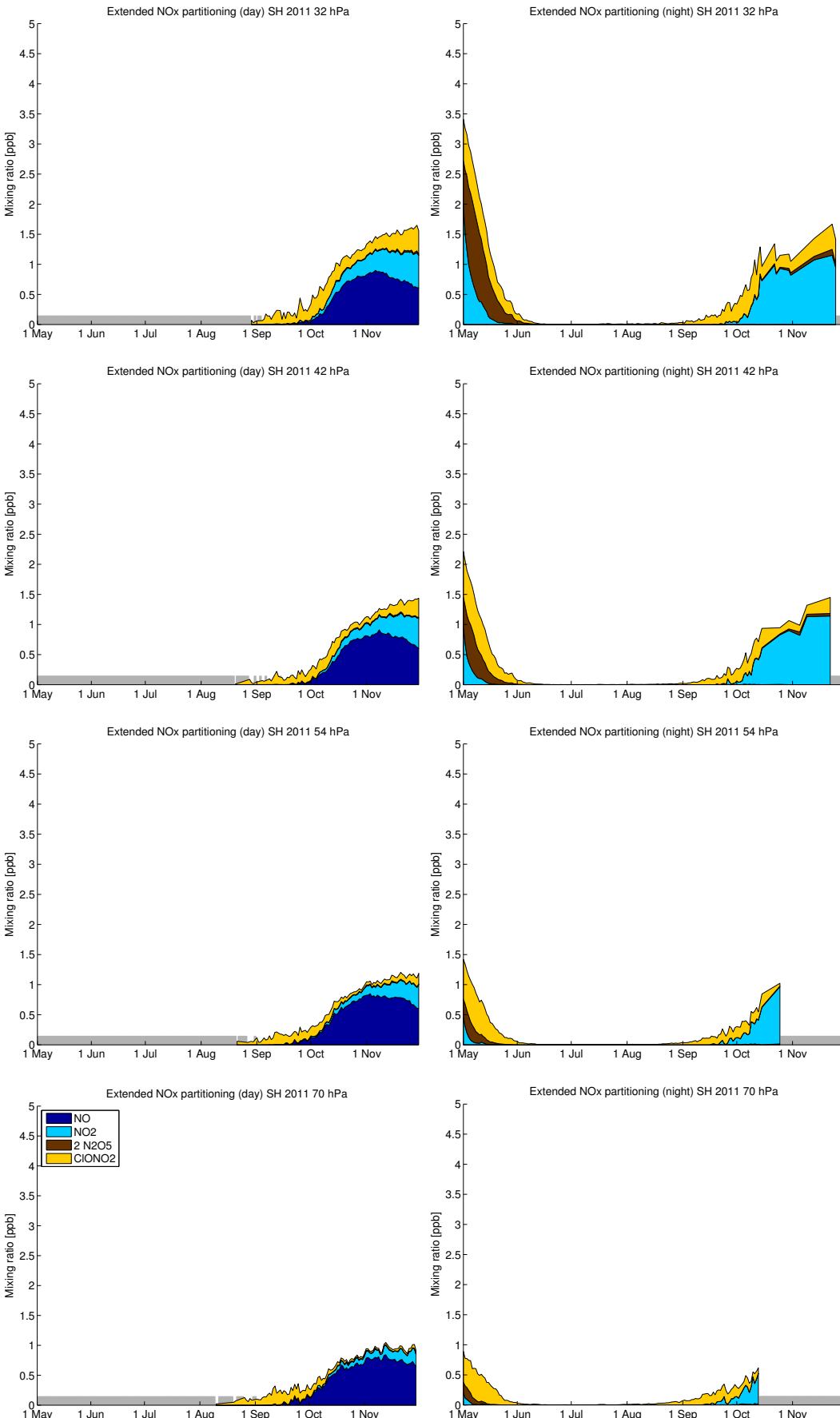


Figure 77: Vortex-averaged partitioning of extended NO_x species. Left: Daytime averages (parts of the vortex where the solar zenith angle is smaller than 80°). Right: Nighttime averages (parts of the vortex where the solar zenith angle is larger than 100°). Days without sufficient data for averaging are not shown (grey bars).

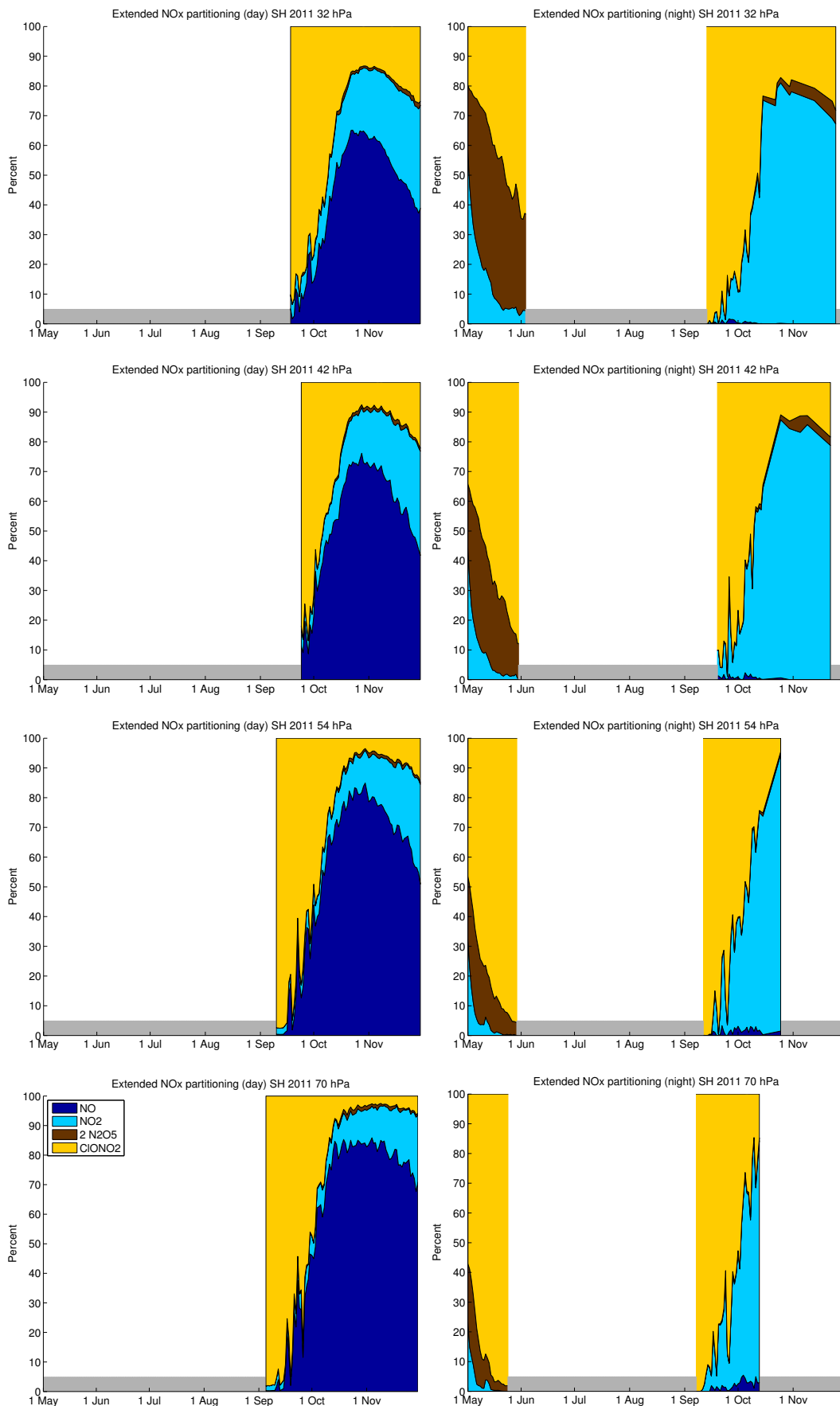


Figure 78: Same as Figure 77, but now in percentages and not in mixing ratios. Percentages are not shown for values of extended NO_x below 0.1 ppb and for days without sufficient data for averaging (grey bars).

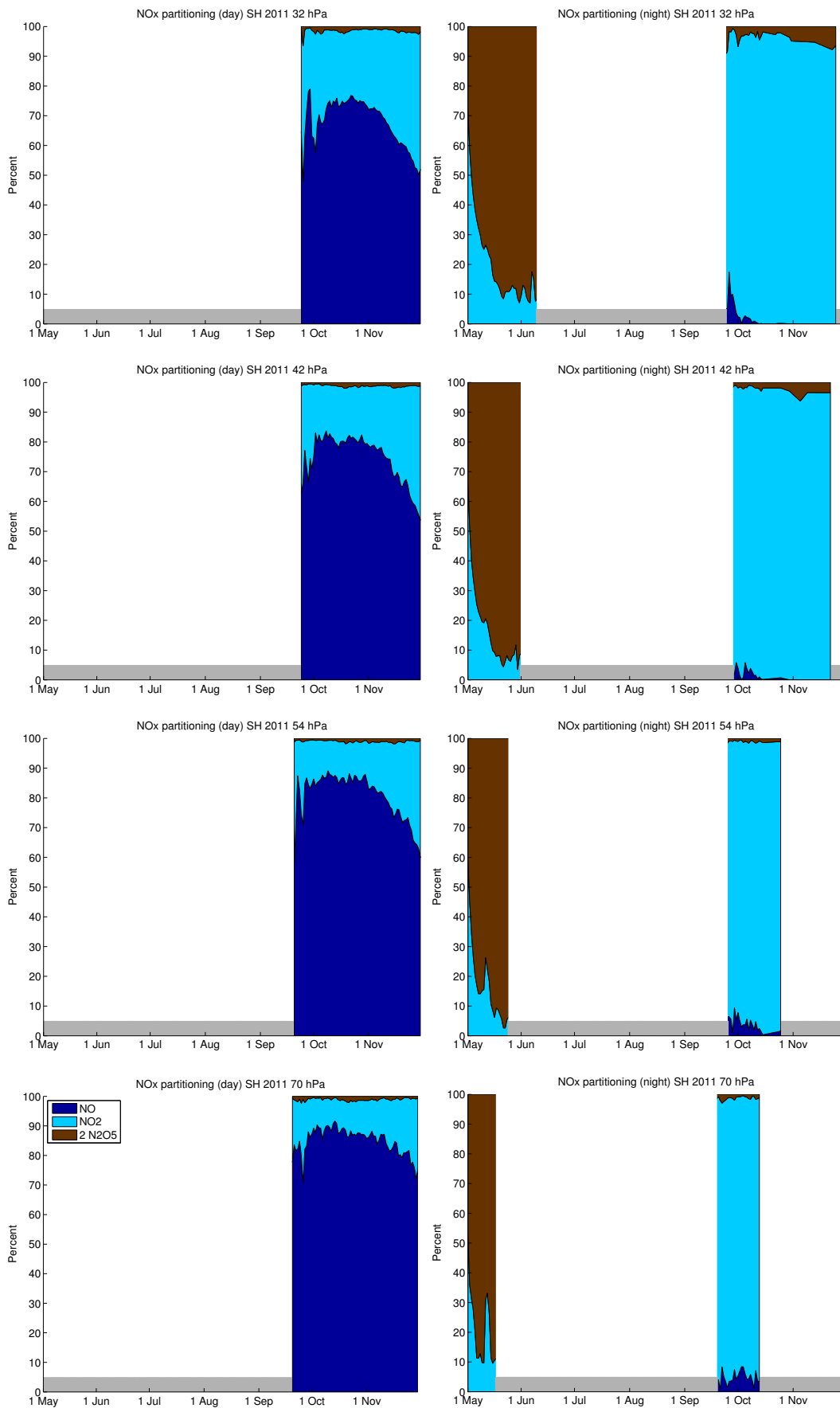


Figure 79: Same as Figure 78, but with only $\text{NO}_x = \text{NO} + \text{NO}_2 + 2\text{N}_2\text{O}_5$ partitioning. Percentages are not shown for values of NO_x below 0.01 ppb and for days without sufficient data for averaging (grey bars).

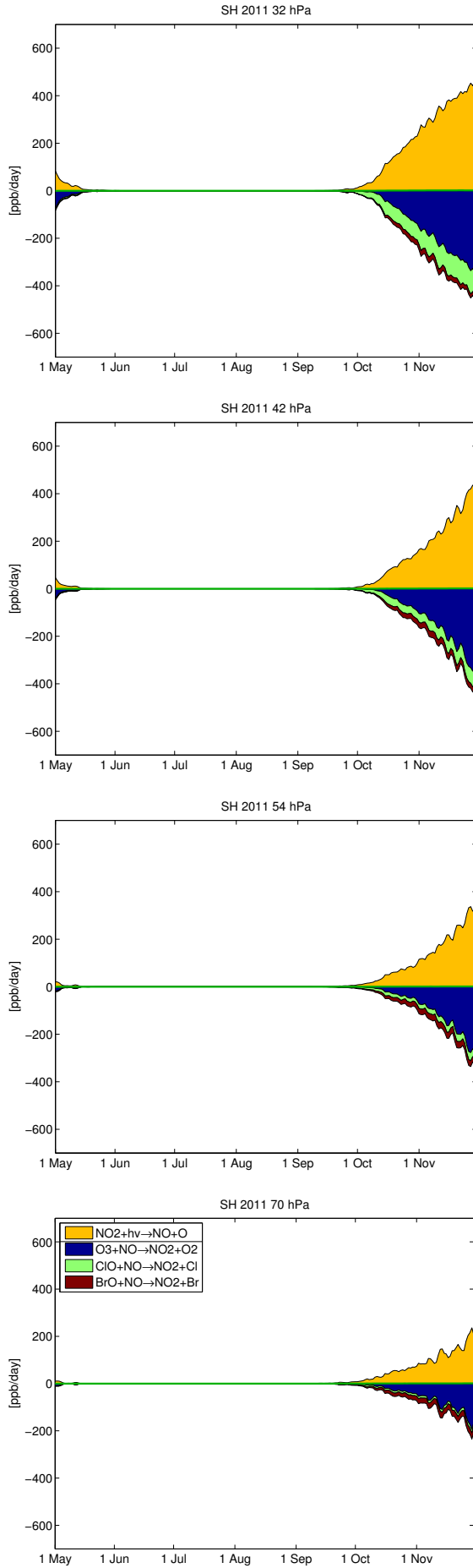


Figure 80: Vortex-averaged chemical reaction rates of reactions changing NO to illustrate NO_x partitioning. Production reactions are shown positive and are separated by a line in the legend from the loss reactions, which are shown negative. The net change of NO is shown as a green line.

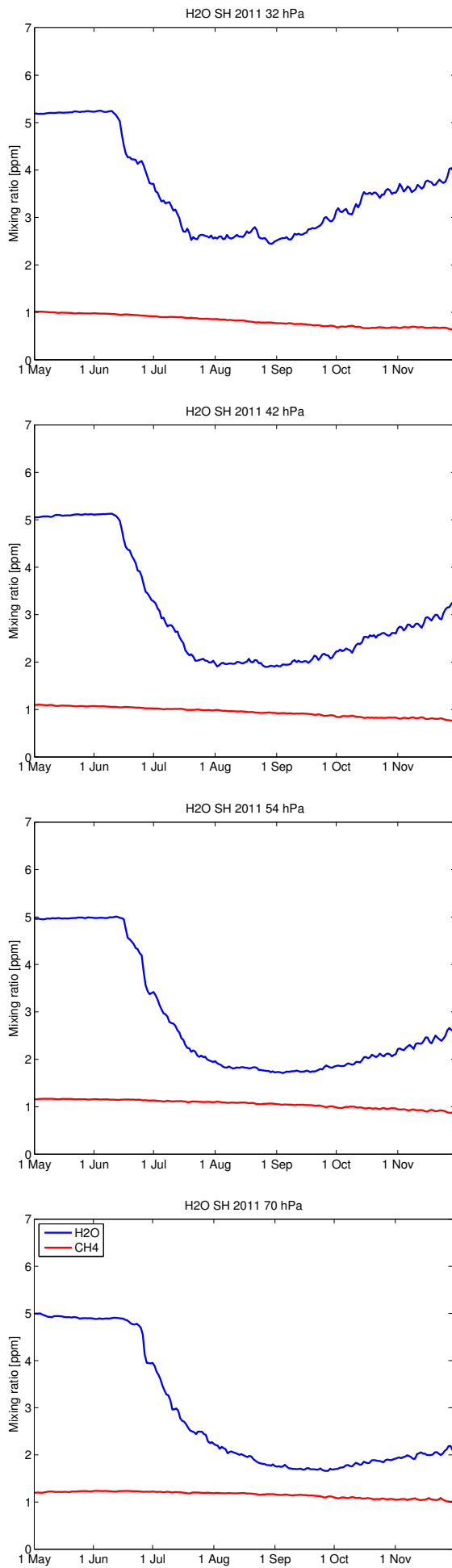


Figure 81: Vortex-averaged mixing ratios of H₂O and CH₄.

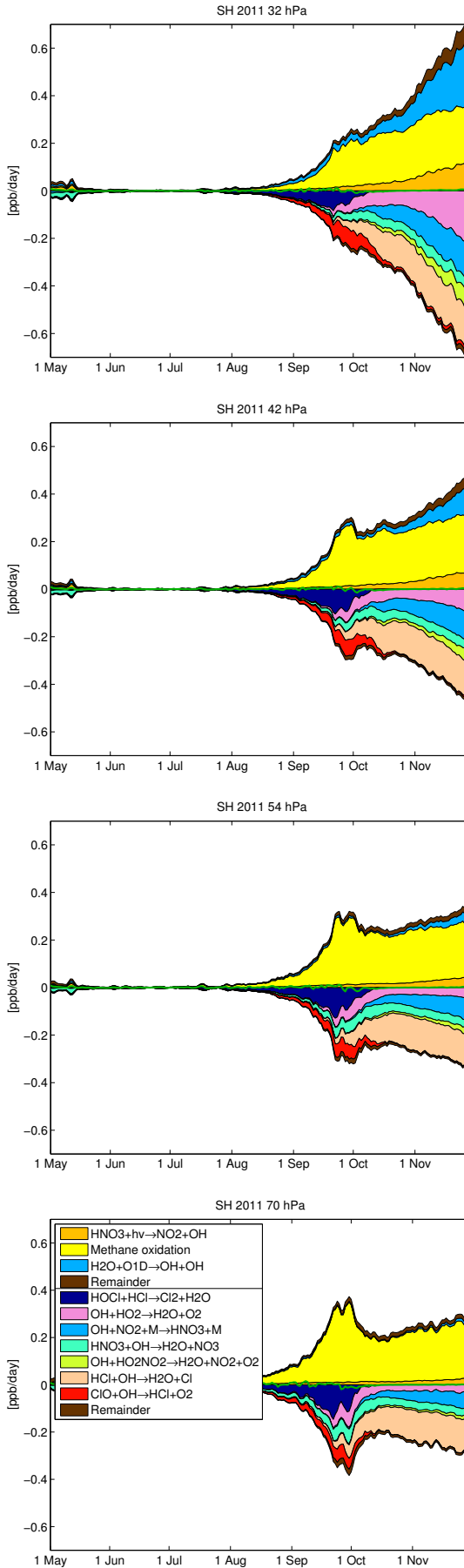


Figure 82: Vortex-averaged chemical reaction rates of reactions changing extended HO_x ($\text{OH} + \text{HO}_2 + \text{H} + \text{HOCl} + \text{HOBr} + \text{HO}_2\text{NO}_2$). Production reactions are shown positive and are separated by a line in the legend from the loss reactions, which are shown negative. The net change of extended HO_x is shown as a green line. Methane oxidation is modelled by simplified net reactions in ATLAS, the reactions denoted as methane oxidation in the legend are $\text{Cl} + \text{CH}_4 \rightarrow \text{HCl} + \text{CH}_2\text{O} + \text{HO}_2$ and $\text{Cl} + \text{CH}_2\text{O} \rightarrow \text{HCl} + \text{CO} + \text{HO}_2$.

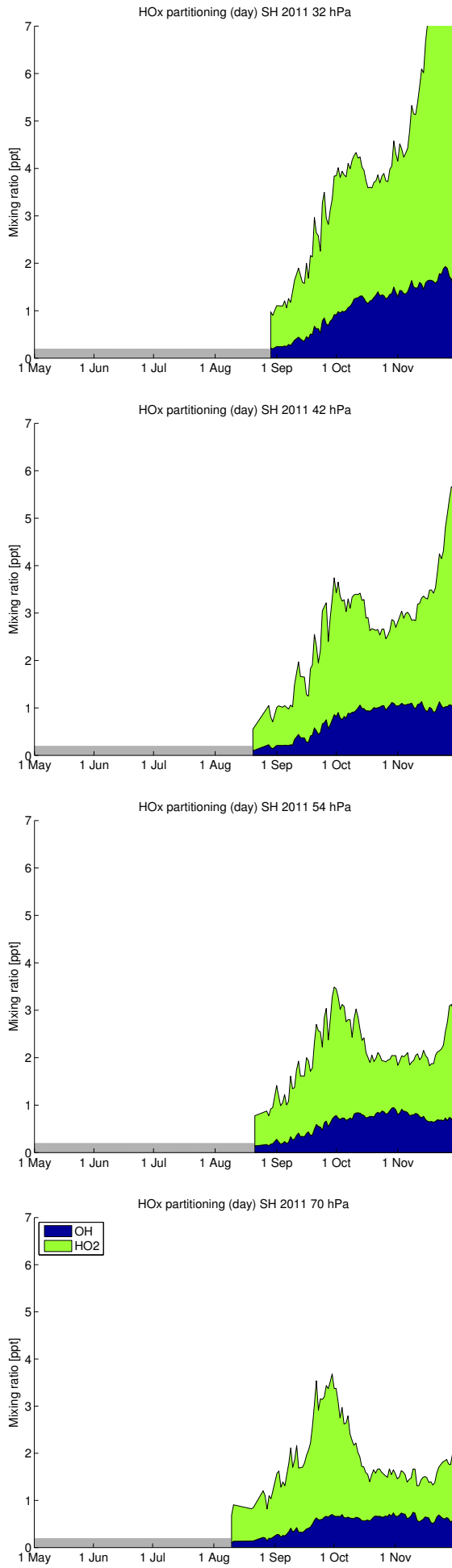


Figure 83: Vortex-averaged partitioning of HO_x species. Daytime averages (parts of the vortex where the solar zenith angle is smaller than 80°). Nighttime averages are near zero and not shown. Data: WRF-Chem (10°S–60°N, 10°–60°W, 10°–60°E) (see Fig. 1).

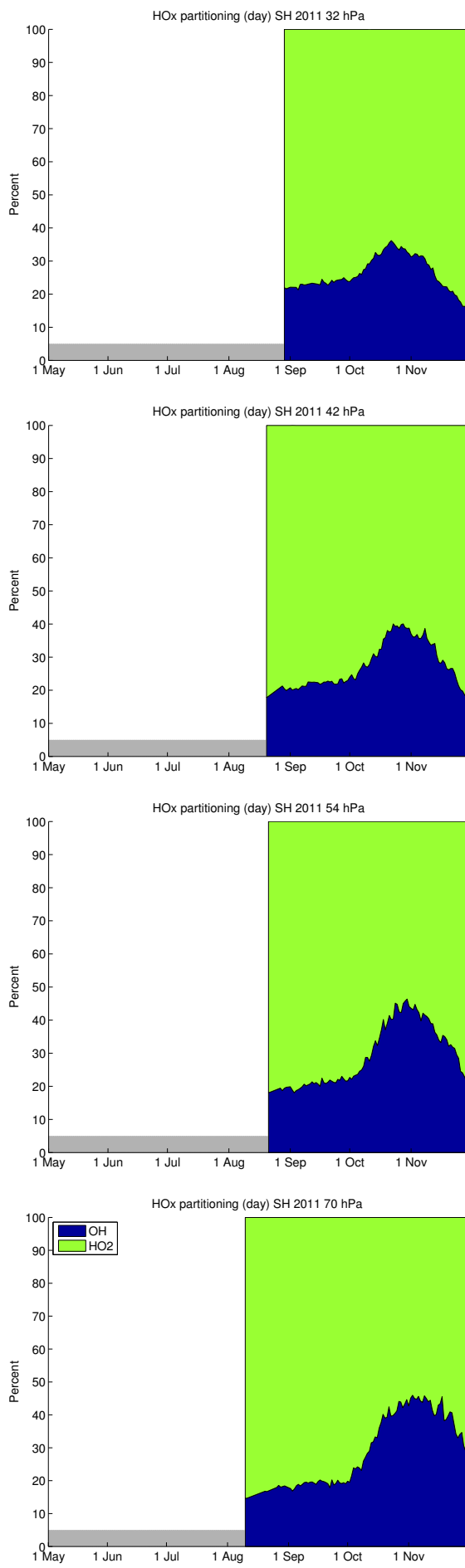


Figure 84: Same as Figure 83, but now in percentages and not in mixing ratios. Days without sufficient data for averaging are not shown (grey bars).

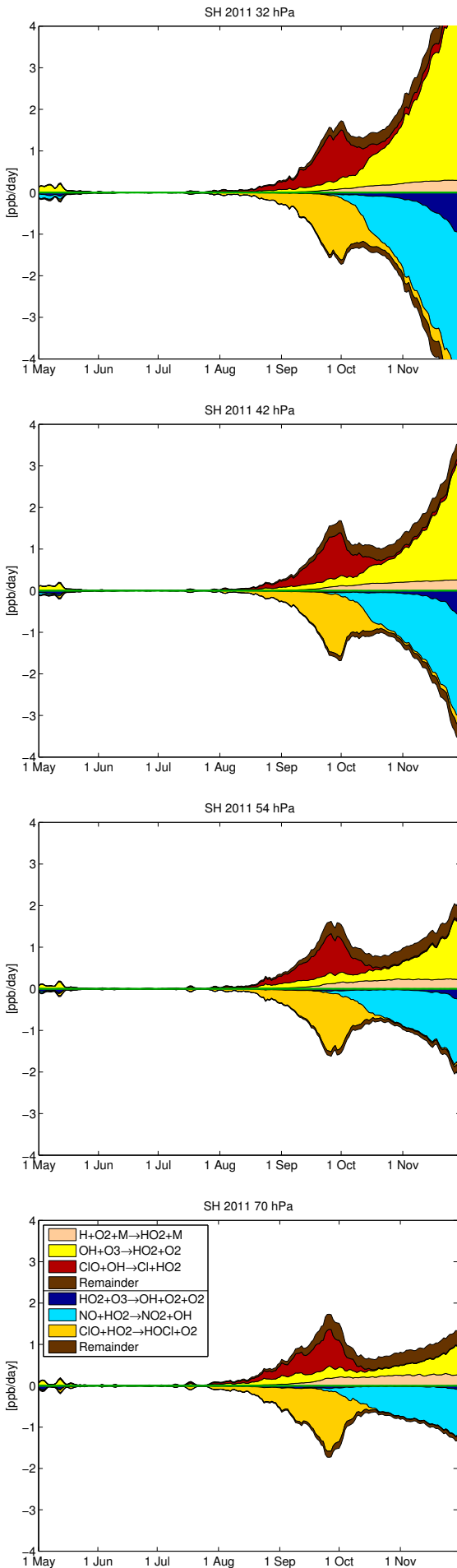


Figure 85: Vortex-averaged chemical reaction rates of reactions changing HO₂ to illustrate HO_x partitioning. Production reactions are shown positive and are separated by a line in the legend from the loss reactions, which are shown negative. The net change of HO₂ is shown as a green line.

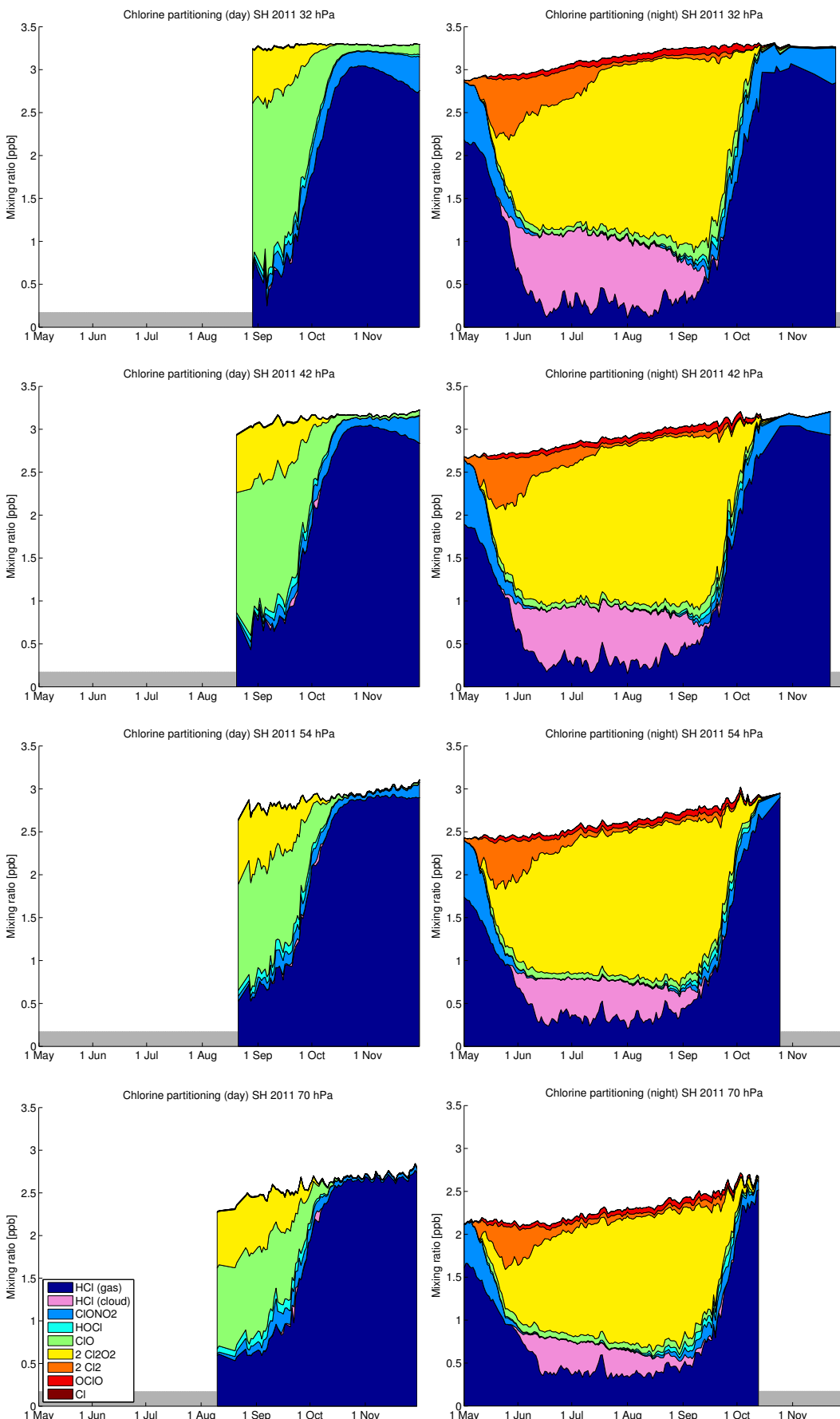


Figure 86: Vortex-averaged partitioning of inorganic chlorine species (Cl_y). Left: Daytime averages (parts of the vortex where the solar zenith angle is smaller than 80°). Right: Nighttime averages (parts of the vortex where the solar zenith angle is larger than 100°). Days without sufficient data for averaging are not shown (grey bars). Species ClNO_2 and BrCl are not shown due to their small mixing ratios. The area labeled “HCl (cloud)” shows HCl dissolved in STS droplets due to the applied correction to the HCl solubility.

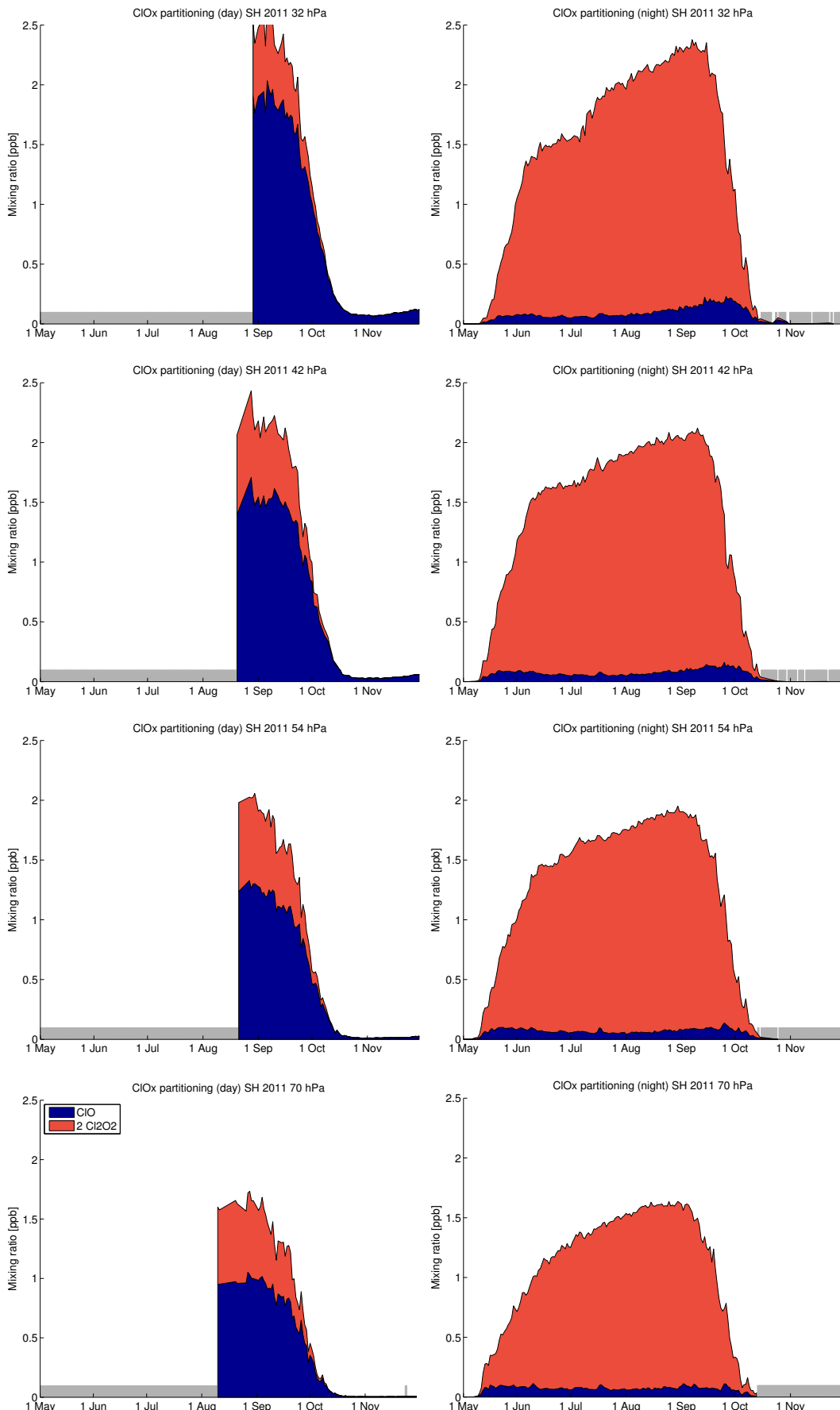


Figure 87: Vortex-averaged partitioning of ClO_x . Left: Daytime averages (parts of the vortex where the solar zenith angle is smaller than 80°). Right: Nighttime averages (parts of the vortex where the solar zenith angle is larger than 100°). Days without sufficient data for averaging are not shown (grey bars).

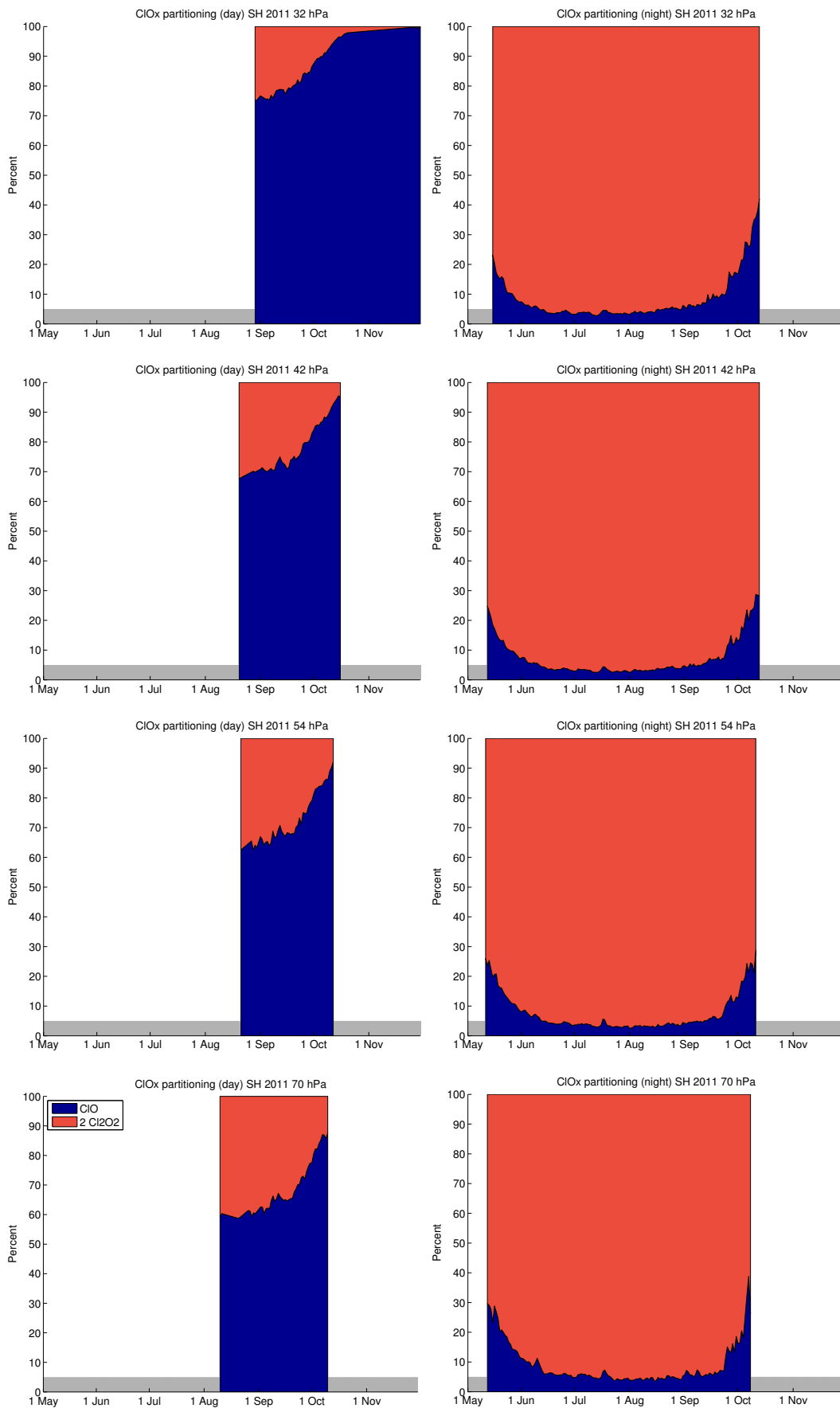


Figure 88: Same as Figure 87, but now in percentages and not in mixing ratios. Percentages are not shown for values of ClO_x below 0.1 ppb and for days without sufficient data for averaging (grey bars).

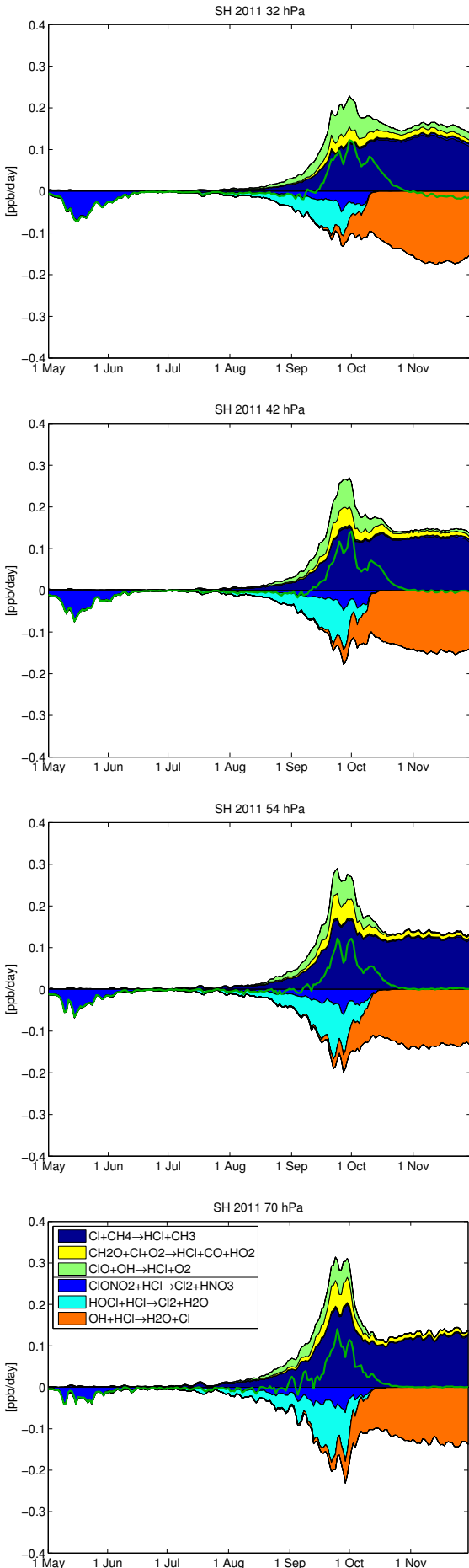


Figure 89: Vortex-averaged chemical reaction rates of reactions involving HCl. Production reactions are shown positive and are separated by a line in the legend from the loss reactions, which are shown negative. The net change of HCl is shown as a green line. Reactions with rates which cannot be distinguished from the zero line at plot resolution are not shown.

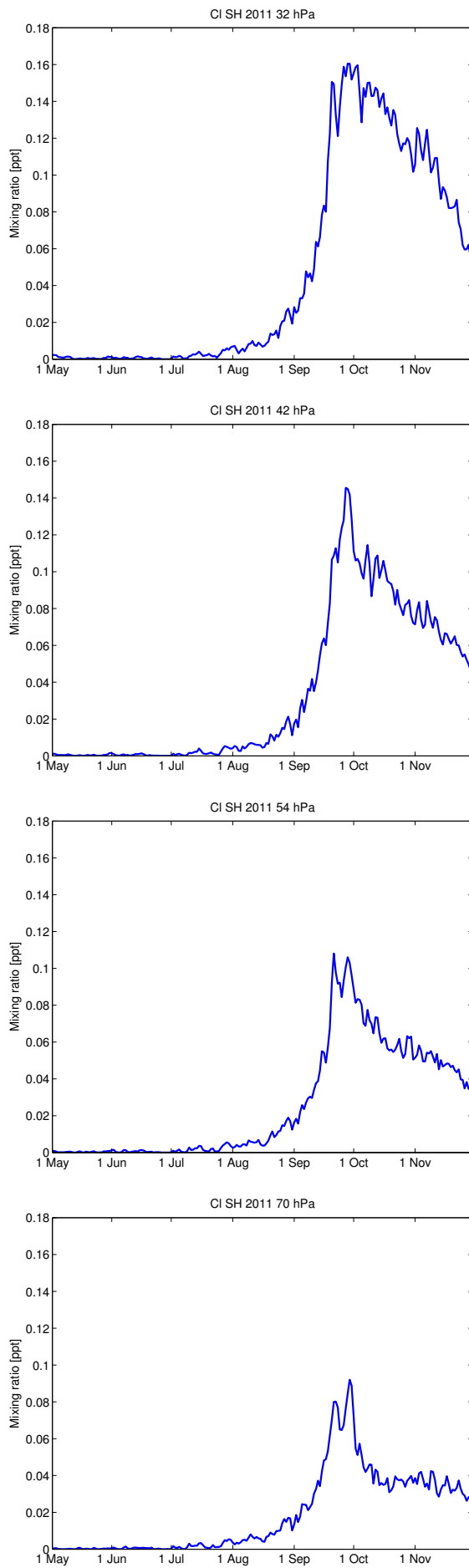


Figure 90: Vortex-averaged Cl mixing ratios.

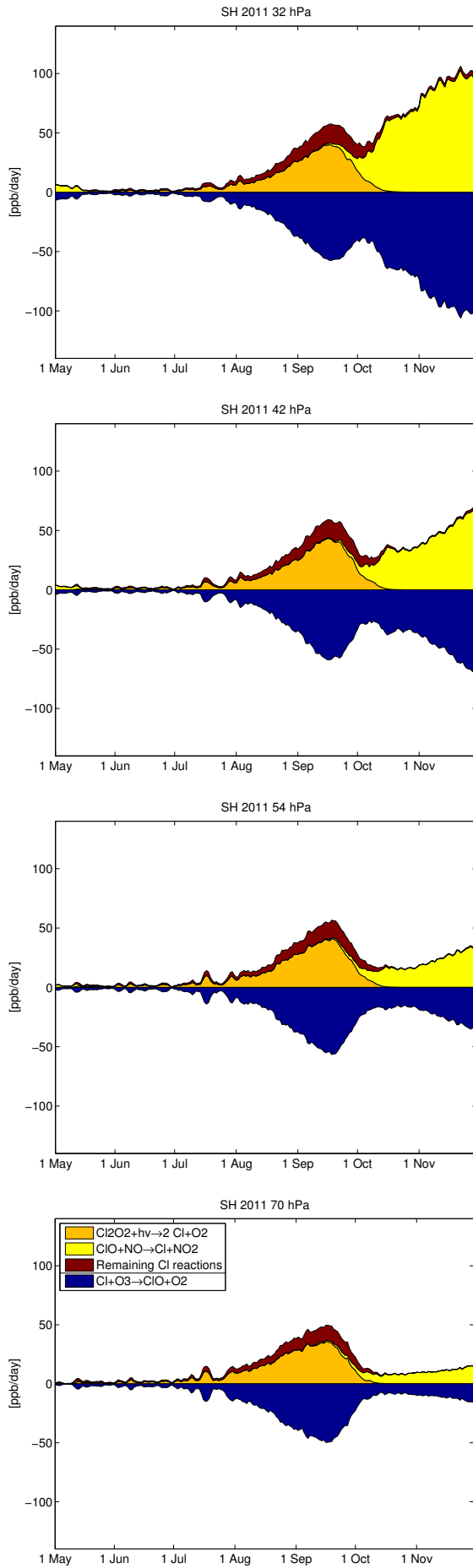


Figure 91: Vortex-averaged chemical reaction rates of reactions involving Cl. Production reactions are shown positive and are separated by a line in the legend from the loss reactions, which are shown negative.

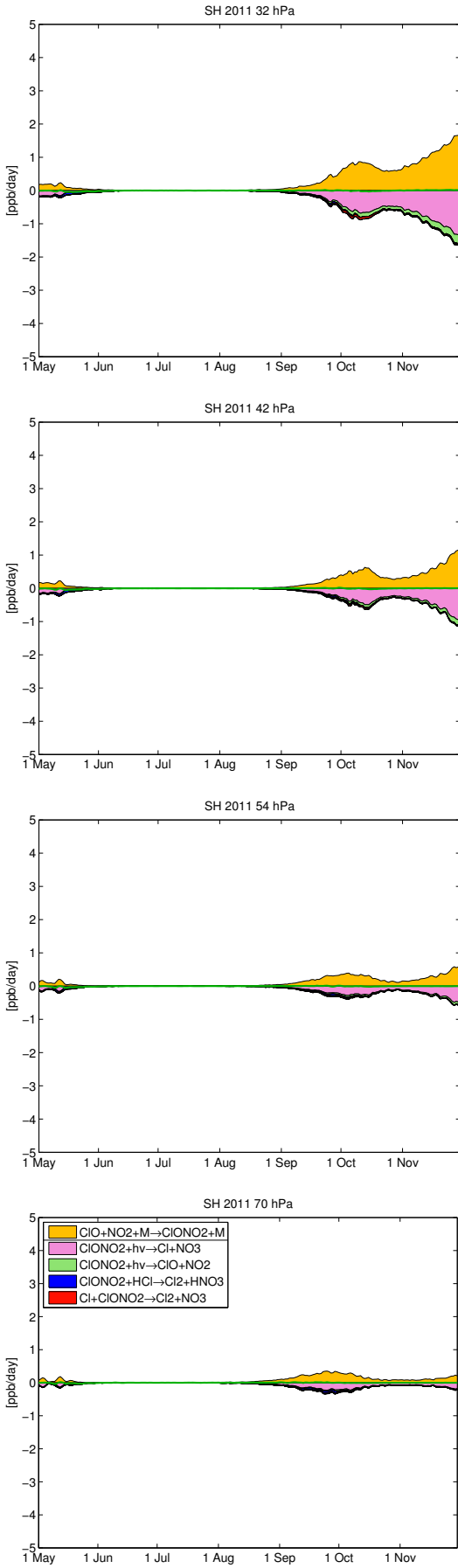


Figure 92: Vortex-averaged chemical reaction rates involving ClONO_2 . Production reactions are shown positive and are separated by a line in the legend from the loss reactions, which are shown negative. The net change of ClONO_2 is shown as a green line. Reactions with rates which cannot be distinguished from the zero line at plot resolution are not shown.

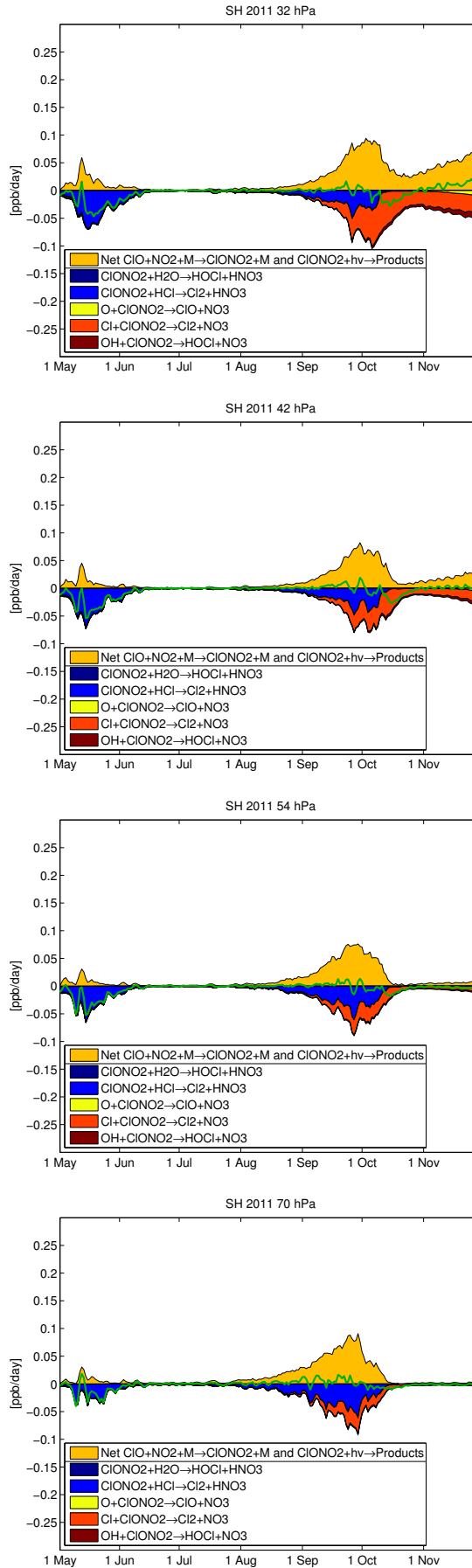


Figure 93: Vortex-averaged chemical reaction rates involving ClONO_2 . In contrast to Figure 92, the net production rate of the fast cycle $\text{ClONO}_2 + h\nu \rightarrow \text{Products} / \text{ClO} + \text{NO}_2 + \text{M} \rightarrow \text{ClONO}_2 + \text{M}$ is shown. This cycle is separated by a line in the legend from the loss reactions. The green line shows the net change of ClONO_2 by chemistry. Reactions with rates which cannot be distinguished from the zero line at plot resolution are not shown.

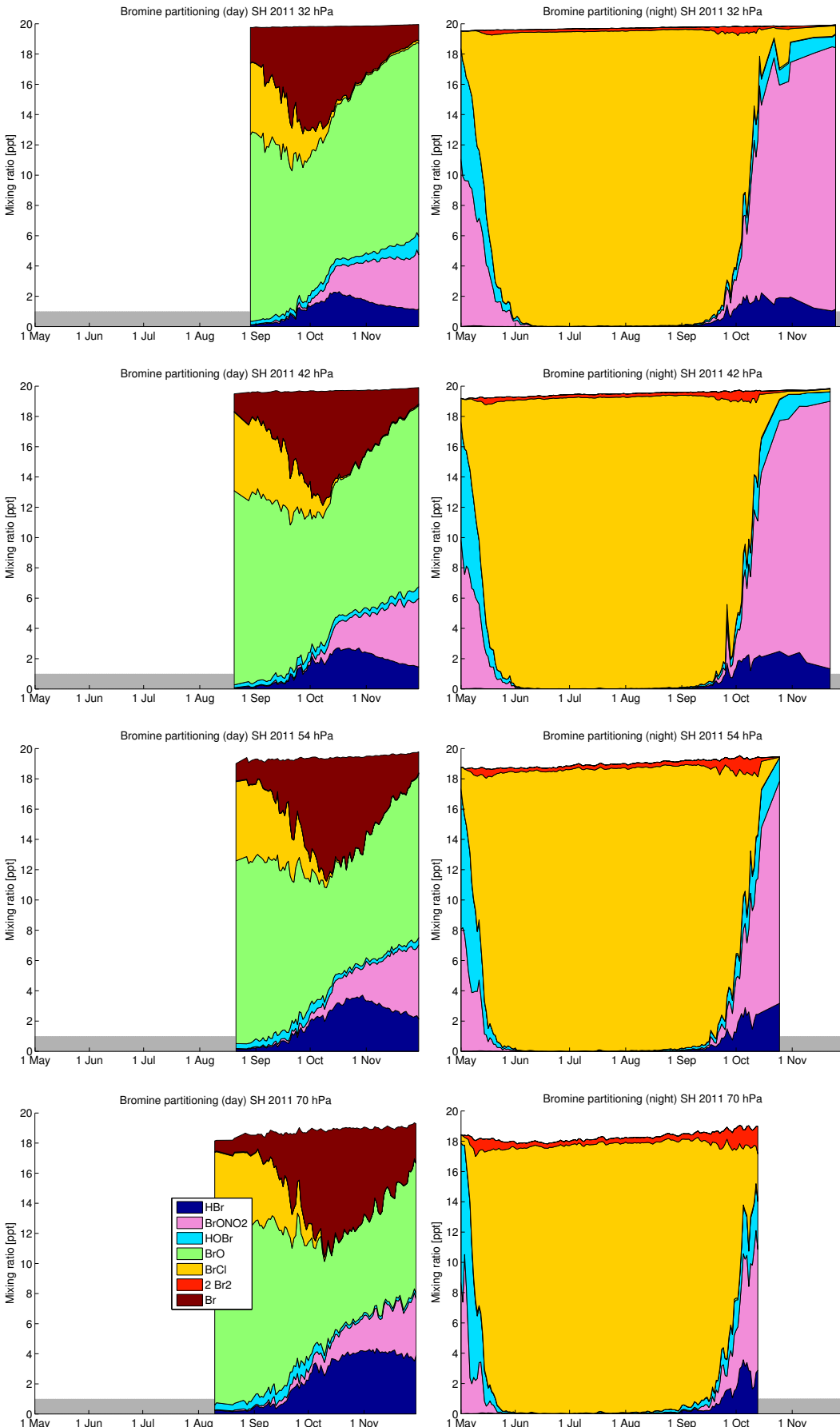


Figure 94: Vortex-averaged partitioning of inorganic bromine species. Left: Daytime averages (parts of the vortex where the solar zenith angle is smaller than 80°). Right: Nighttime averages (parts of the vortex where the solar zenith angle is larger than 100°). Days without sufficient data for averaging are not shown (grey bars).

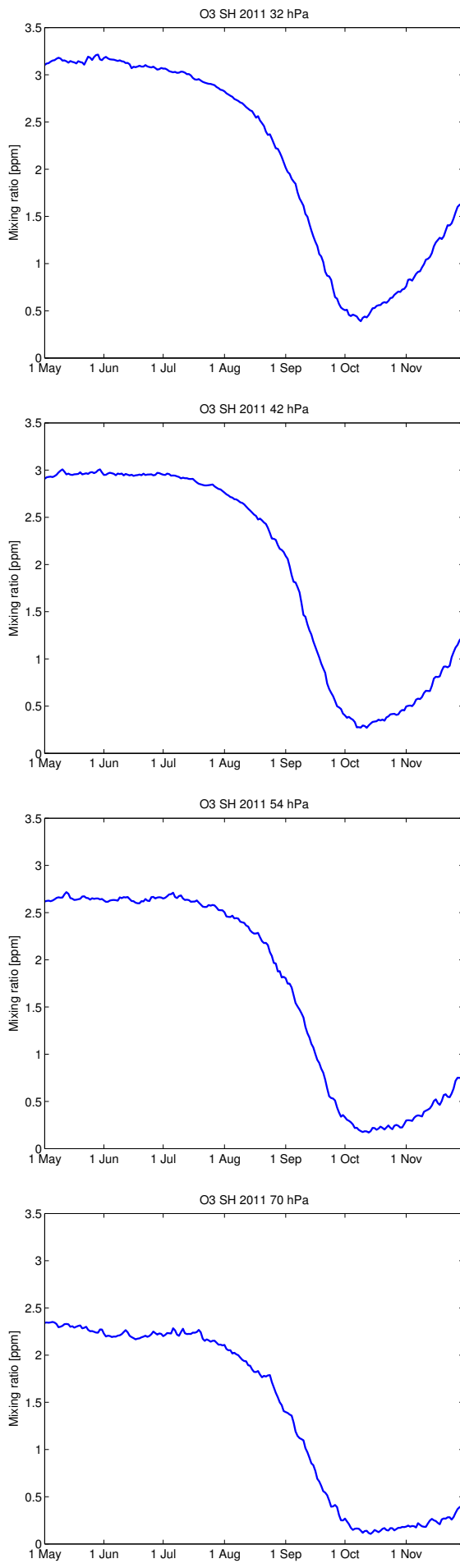


Figure 95: Vortex-averaged ozone mixing ratios.

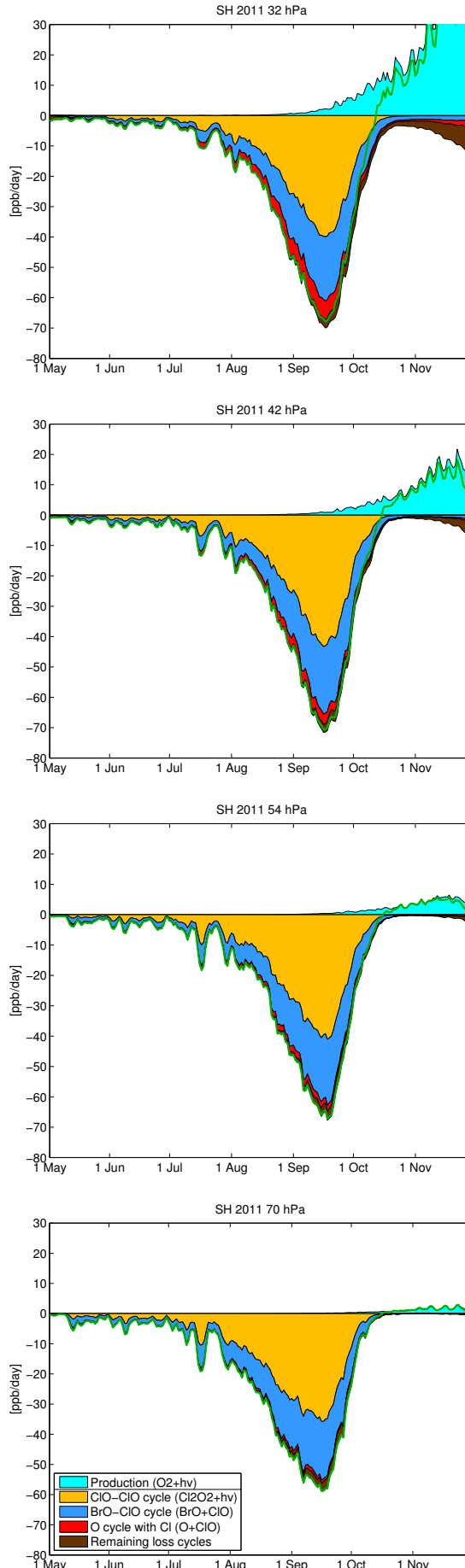


Figure 96: Vortex-averaged net chemical change of odd oxygen. The green line shows the net chemical change rate of ozone, which nearly equals the change rate of odd oxygen. The contribution of different catalytic cycles to the ozone loss is shown by the reaction rates of their rate limiting step. Only the three most important cycles are shown, the contribution of other cycles is small. Ozone production, which is almost exclusively by the $O_2 + h\nu$ reaction, is shown in cyan.

2 Results for runs not corrected for the HCl discrepancy

2.1 Northern Hemisphere 2004/2005 (Uncorrected run)

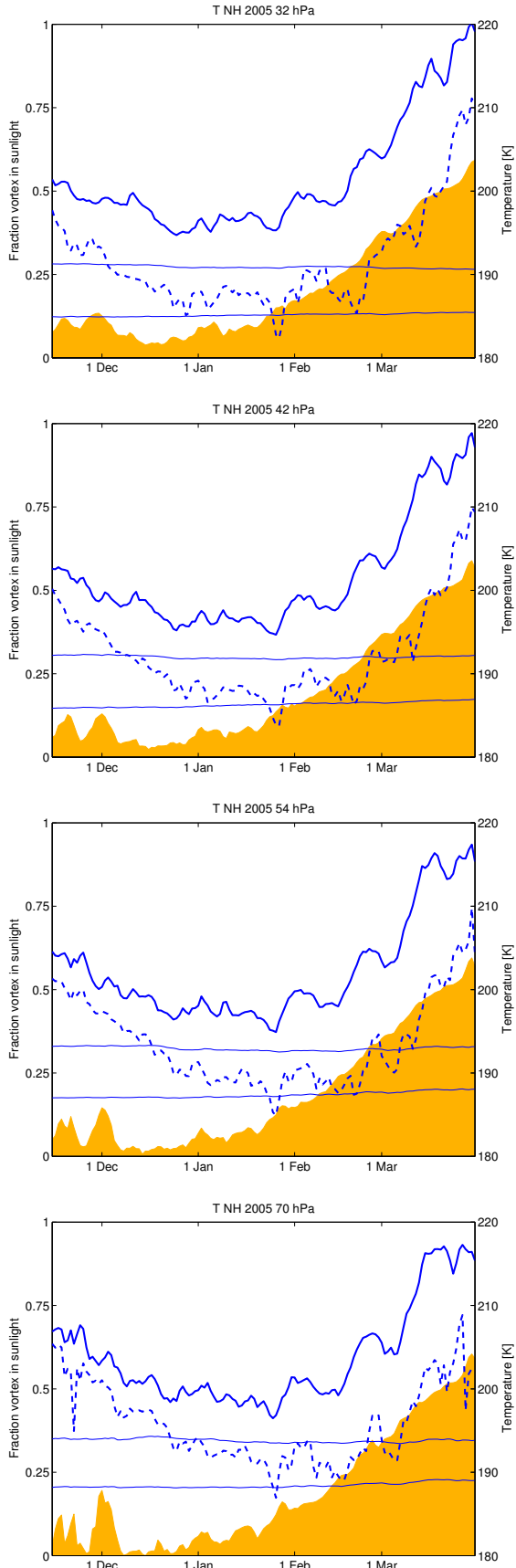


Figure 97: Vortex-averaged temperature (blue), vortex minimum temperature (dashed blue) and fraction of the vortex in sunlight (yellow). The upper thin blue line shows the threshold temperature for the formation of NAT clouds used in the model (based on vortex mean mixing ratios and considering supersaturation), and the lower thin blue line shows the same for ice clouds. The vortex tracer criterion is not applied (in contrast to all other figures).

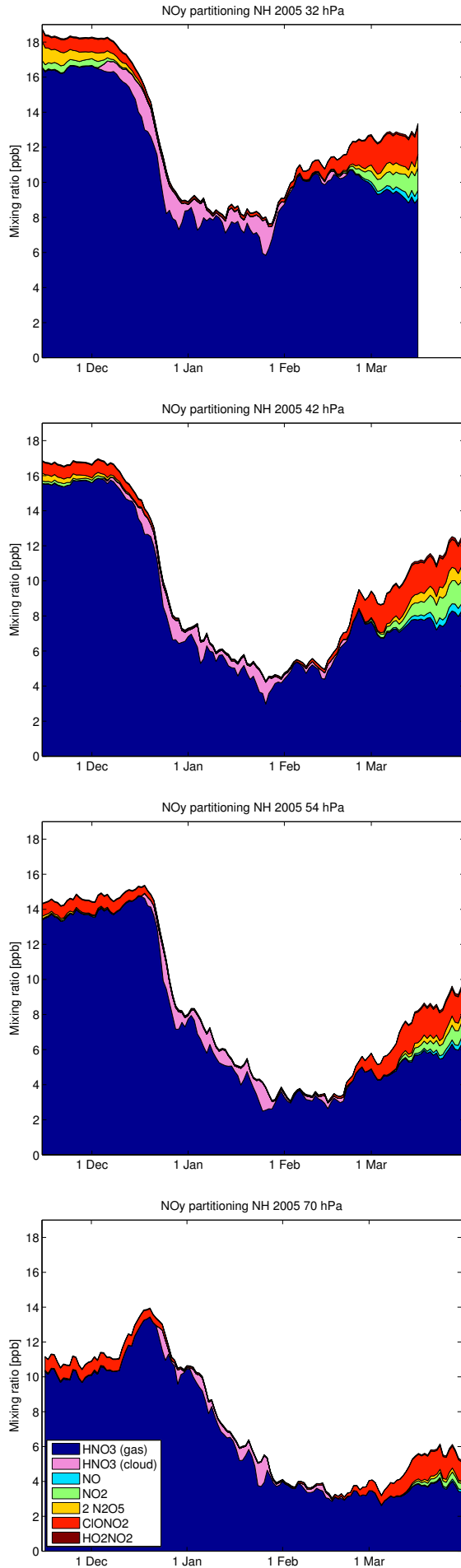


Figure 98: Vortex-averaged partitioning of NO_y species. Species NO₃, BrONO₂, ClONO₂ and N are not shown due to their small mixing ratios.

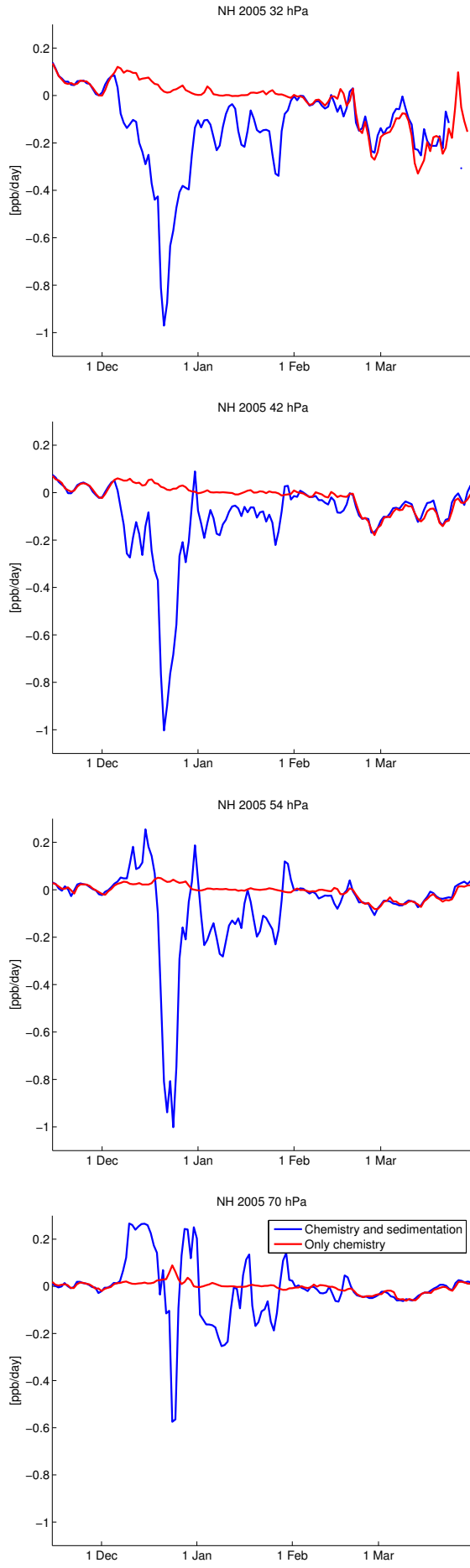


Figure 99: Vortex-averaged net chemical reaction rate of HNO₃ (red) and sum of the vortex-averaged change by sedimentation and the net chemical reaction rate (blue).

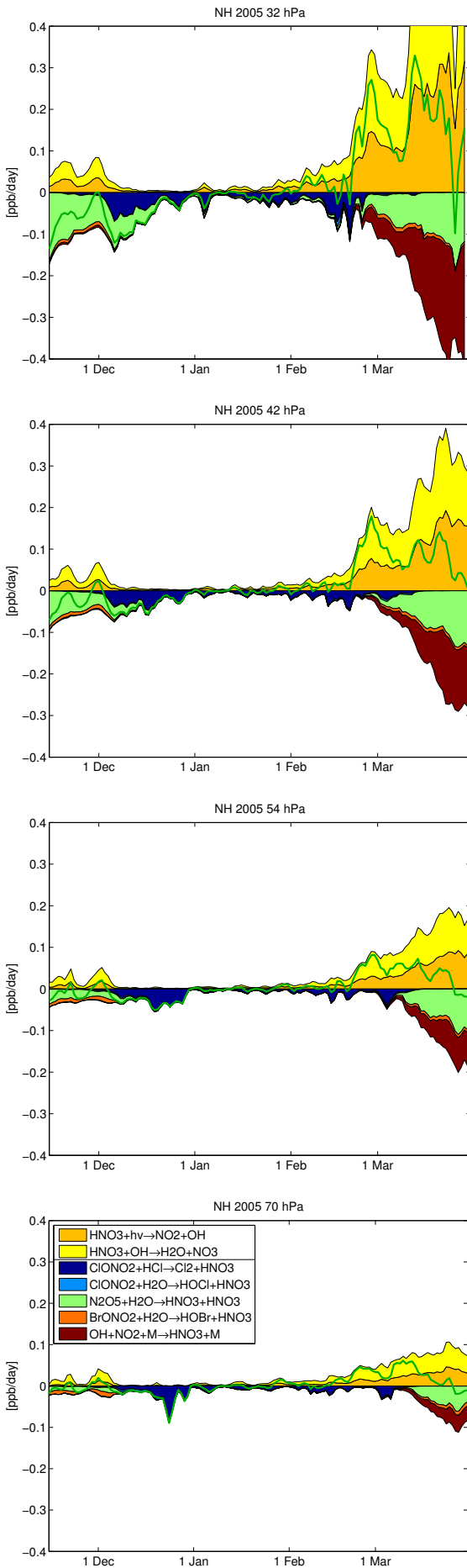


Figure 100: Vortex-averaged chemical reaction rates of reactions changing extended NO_x ($\text{NO} + \text{NO}_2 + \text{NO}_3 + 2\text{N}_2\text{O}_5 + \text{ClONO}_2 + \text{BrONO}_2 + \text{HO}_2\text{NO}_2$). Production reactions are shown positive and are separated by a line in the legend from the loss reactions, which are shown negative. The net change of extended NO_x is shown as a green line.

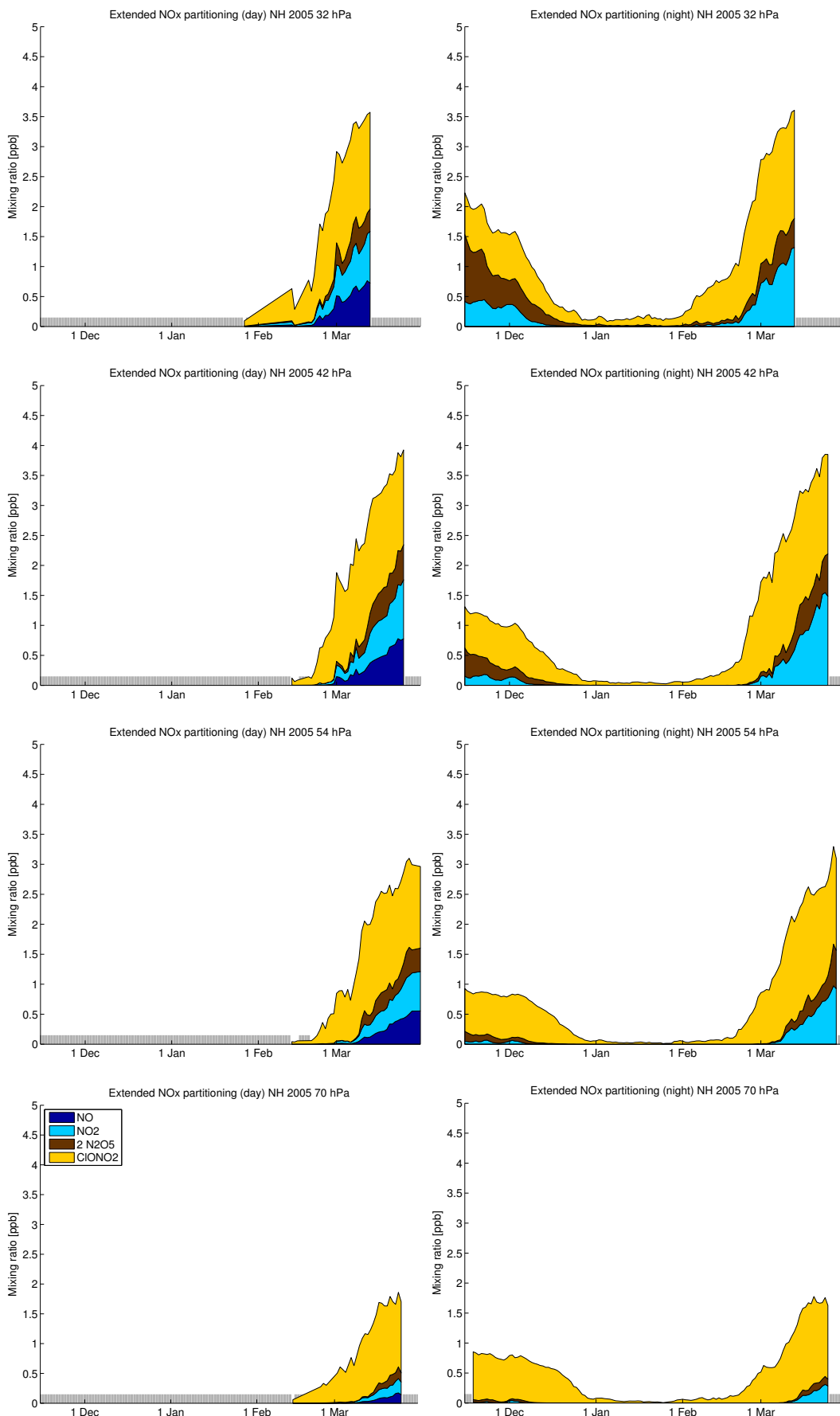


Figure 101: Vortex-averaged partitioning of extended NO_x species. Left: Daytime averages (parts of the vortex where the solar zenith angle is smaller than 80°). Right: Nighttime averages (parts of the vortex where the solar zenith angle is larger than 100°). Days without sufficient data for averaging are not shown (grey bars).

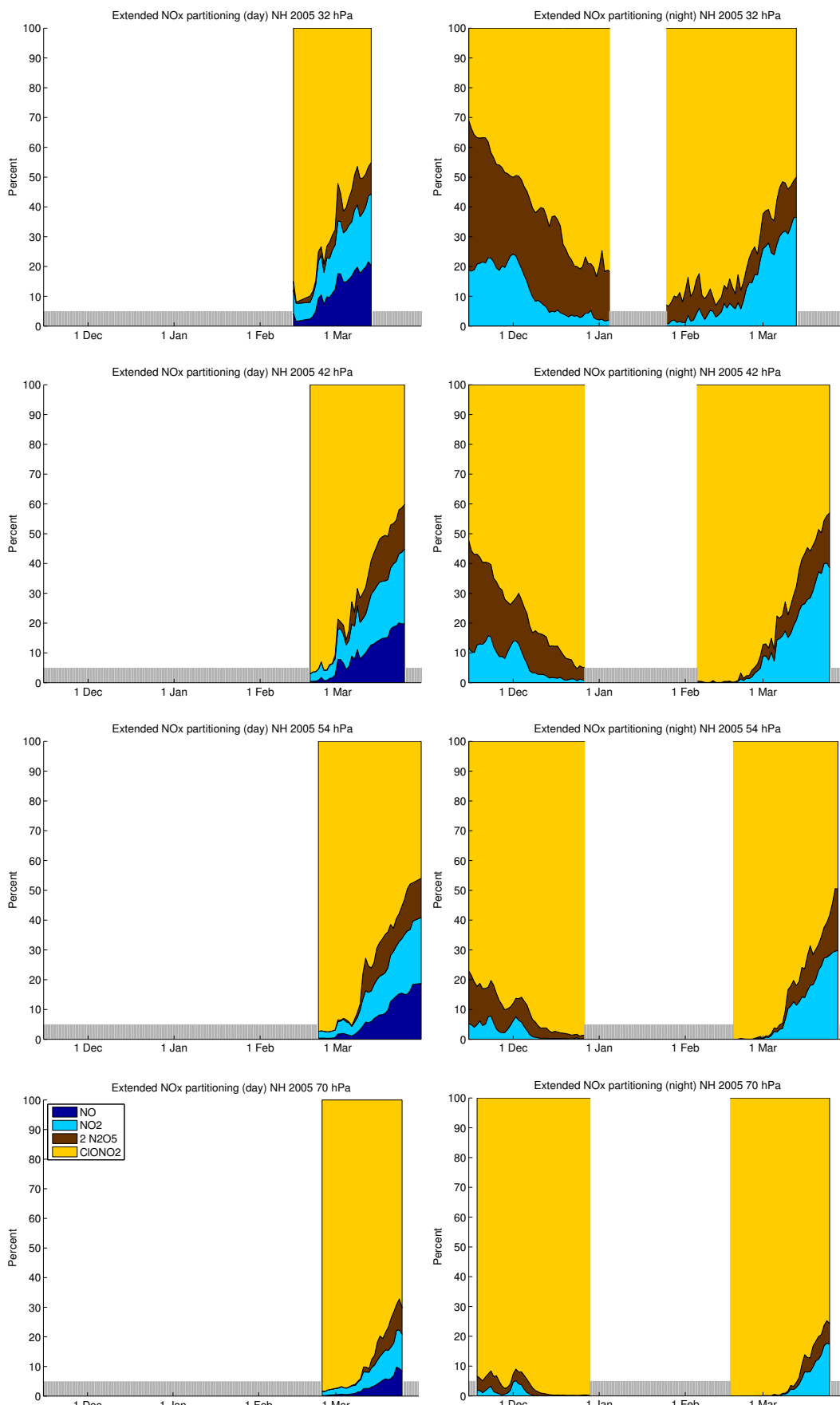


Figure 102: Same as Figure 101, but now in percentages and not in mixing ratios. Percentages are not shown for values of extended NO_x below 0.1 ppb and for days without sufficient data for averaging (grey bars).

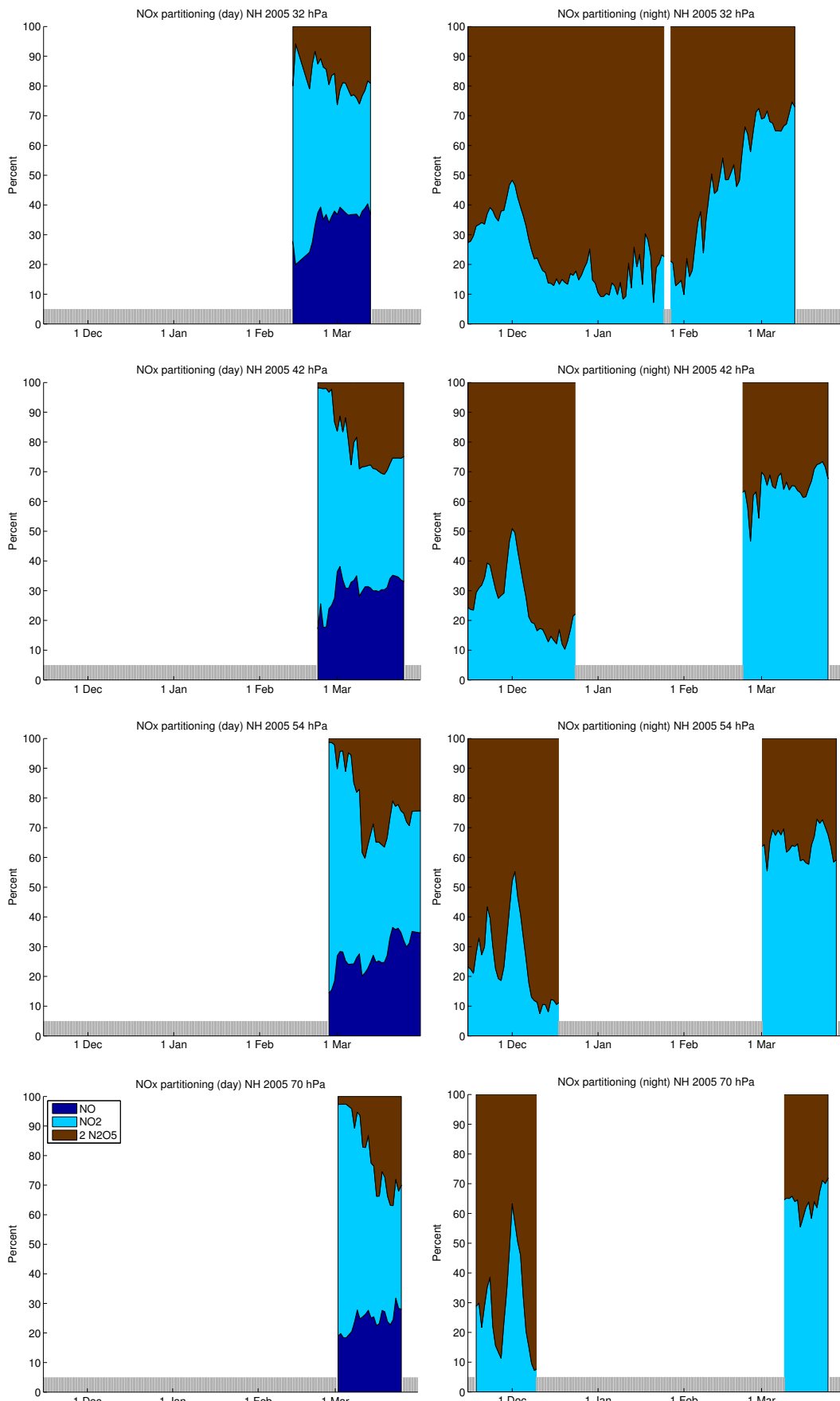


Figure 103: Same as Figure 102, but with only $\text{NO}_x = \text{NO} + \text{NO}_2 + 2\text{N}_2\text{O}_5$ partitioning. Percentages are not shown for values of NO_x below 0.01 ppb and for days without sufficient data for averaging (grey bars).

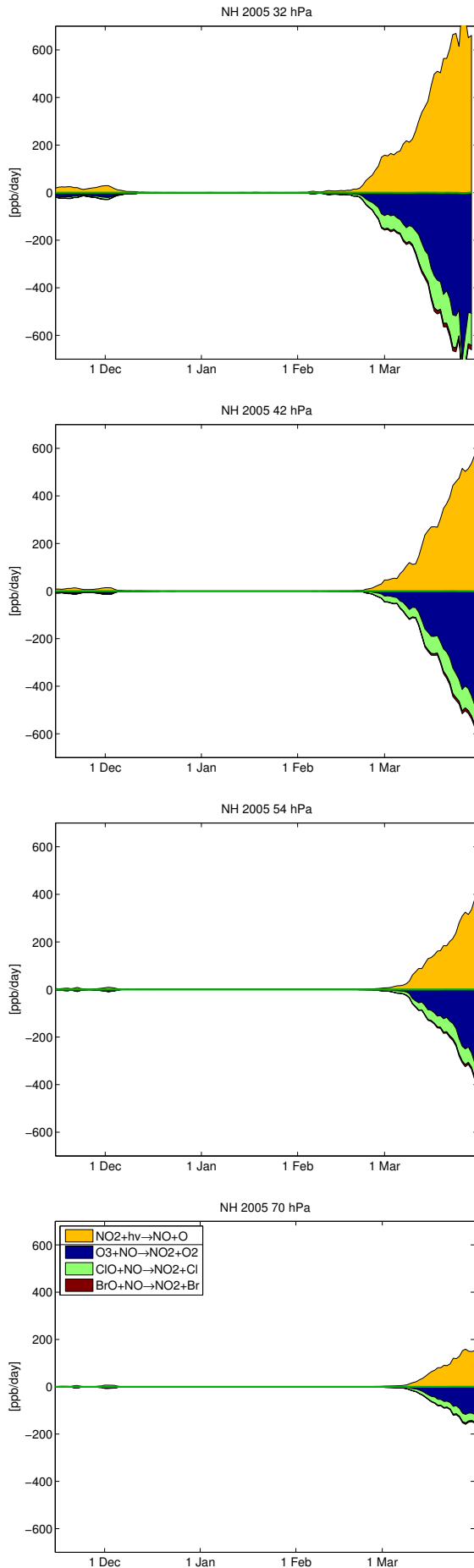


Figure 104: Vortex-averaged chemical reaction rates of reactions changing NO to illustrate NO_x partitioning. Production reactions are shown positive and are separated by a line in the legend from the loss reactions, which are shown negative. The net change of NO is shown as a green line.

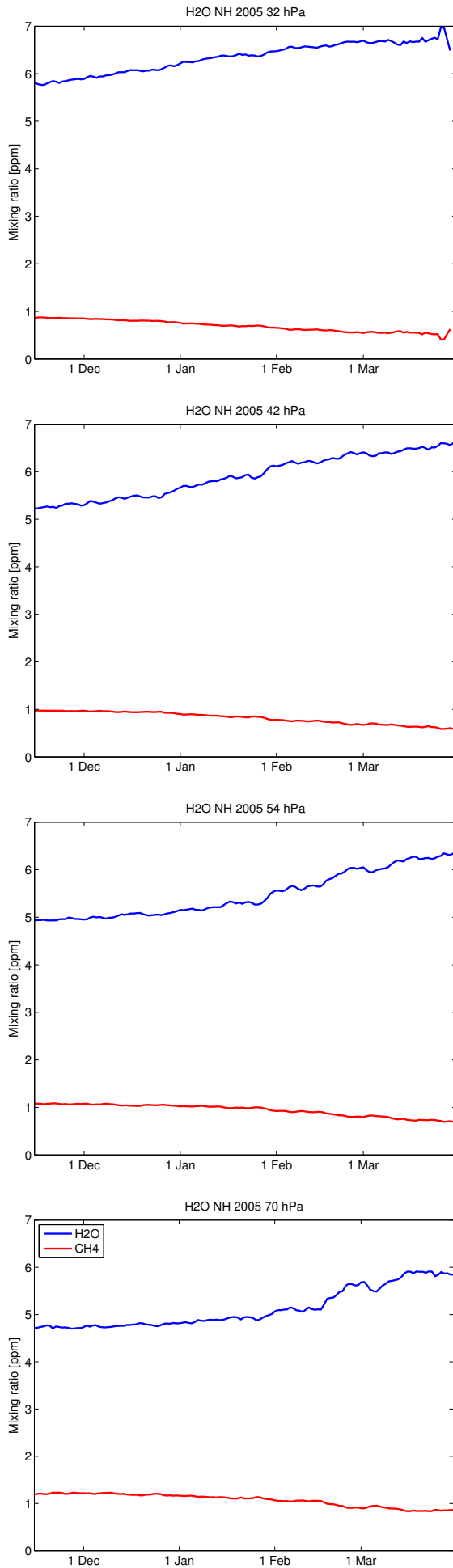


Figure 105: Vortex-averaged mixing ratios of H₂O and CH₄.

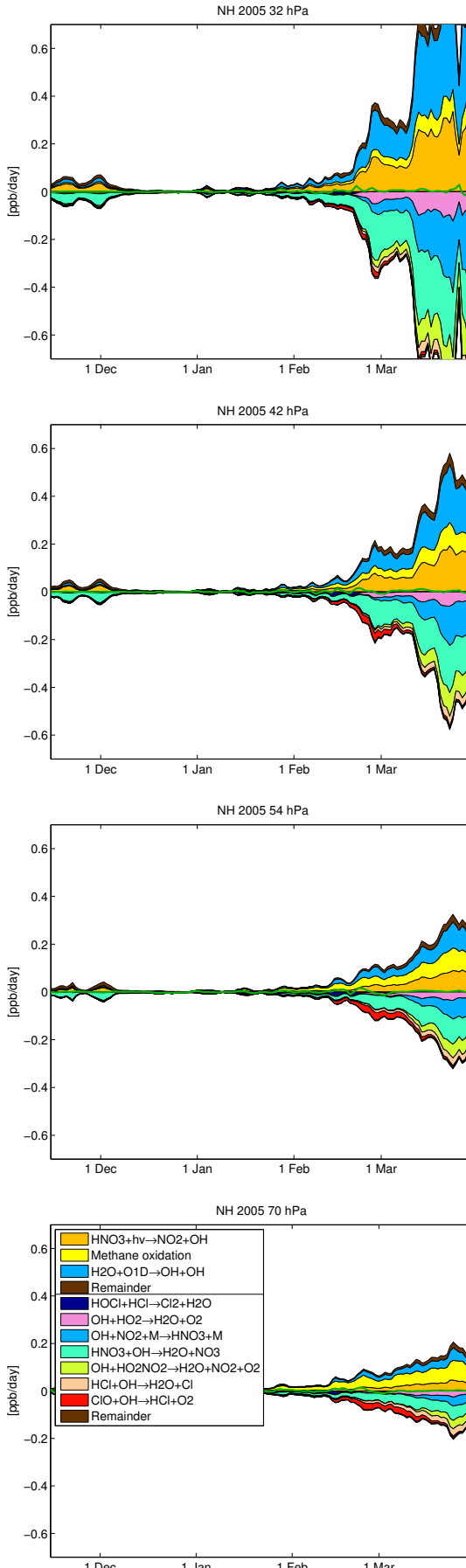


Figure 106: Vortex-averaged chemical reaction rates of reactions changing extended HO_x ($\text{OH} + \text{HO}_2 + \text{H} + \text{HOCl} + \text{HOBr} + \text{HO}_2\text{NO}_2$). Production reactions are shown positive and are separated by a line in the legend from the loss reactions, which are shown negative. The net change of extended HO_x is shown as a green line. Methane oxidation is modelled by simplified net reactions in ATLAS, the reactions denoted as methane oxidation in the legend are $\text{Cl} + \text{CH}_4 \rightarrow \text{HCl} + \text{CH}_2\text{O} + \text{HO}_2$ and $\text{Cl} + \text{CH}_2\text{O} \rightarrow \text{HCl} + \text{CO} + \text{HO}_2$.

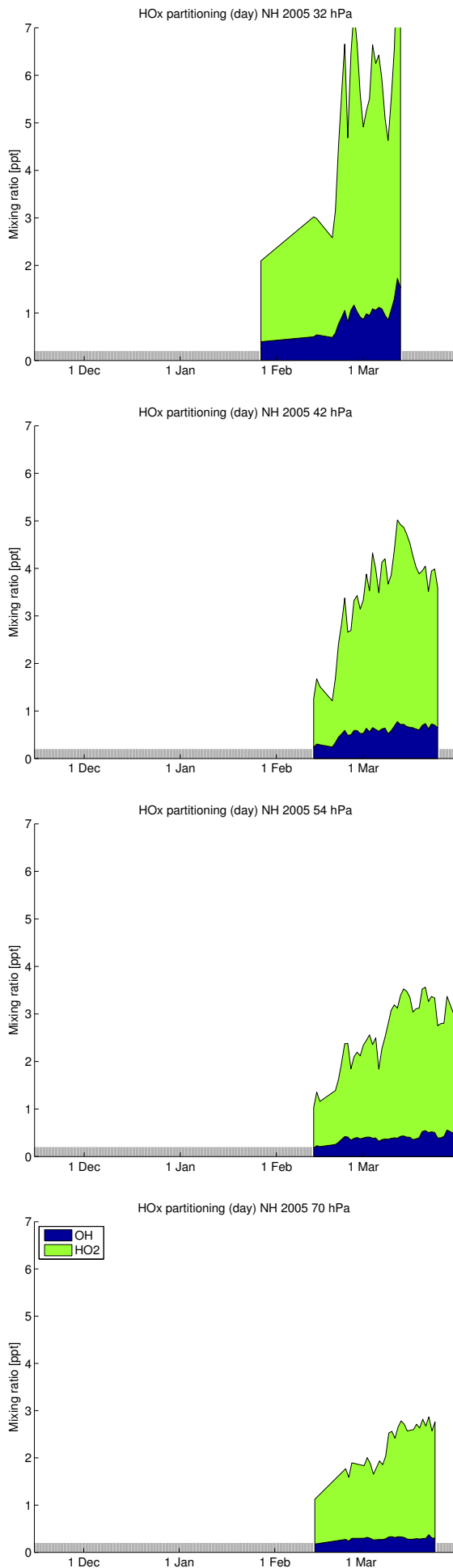


Figure 107: Vortex-averaged partitioning of HO_x species. Daytime averages (parts of the vortex where the solar zenith angle is smaller than 80°). Nighttime averages are near zero and not shown. Data: WMO (2005) (from the Tropospheric Ozone Budget (TOB) project).

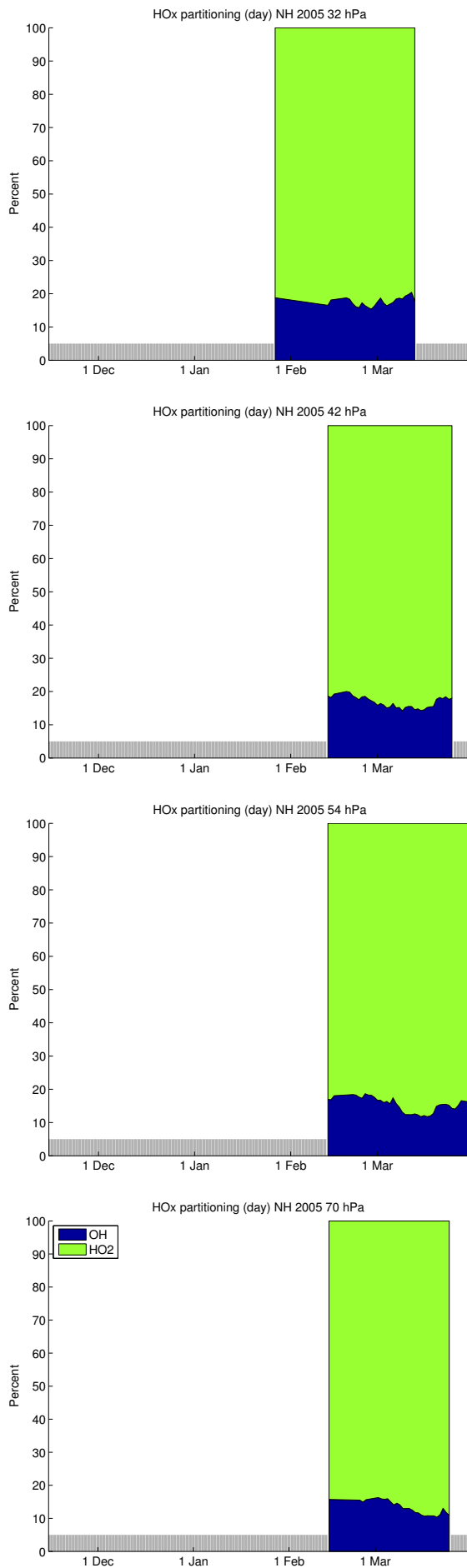


Figure 108: Same as Figure 107, but now in percentages and not in mixing ratios. Days without sufficient data for averaging are not shown (grey bars).

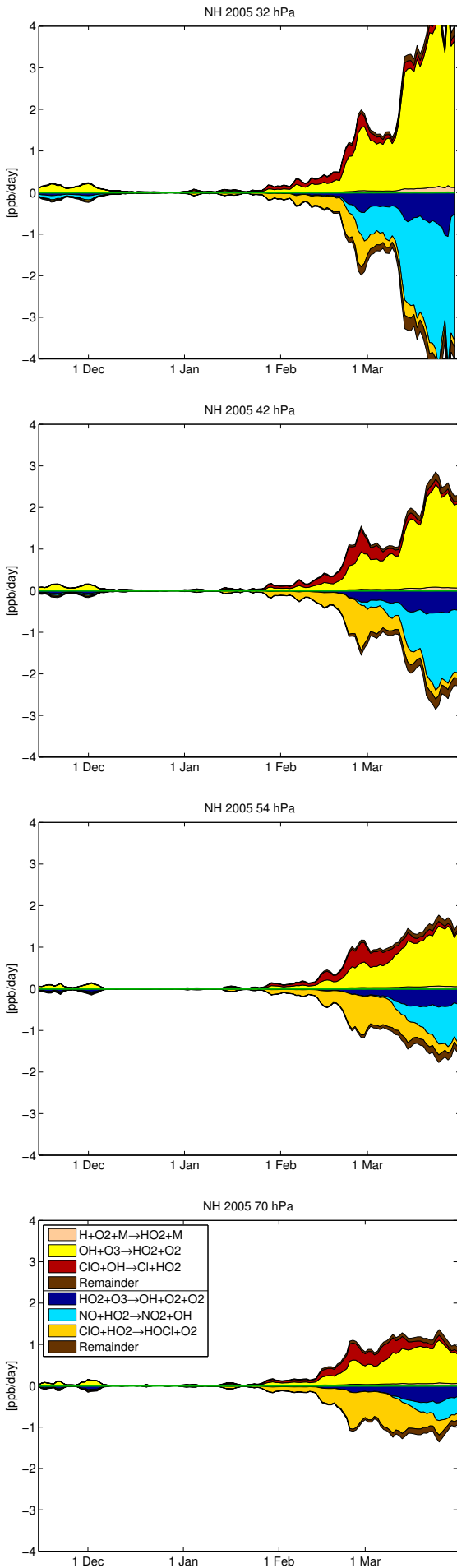


Figure 109: Vortex-averaged chemical reaction rates of reactions changing HO₂ to illustrate HO_x partitioning. Production reactions are shown positive and are separated by a line in the legend from the loss reactions, which are shown negative. The net change of HO₂ is shown as a green line.

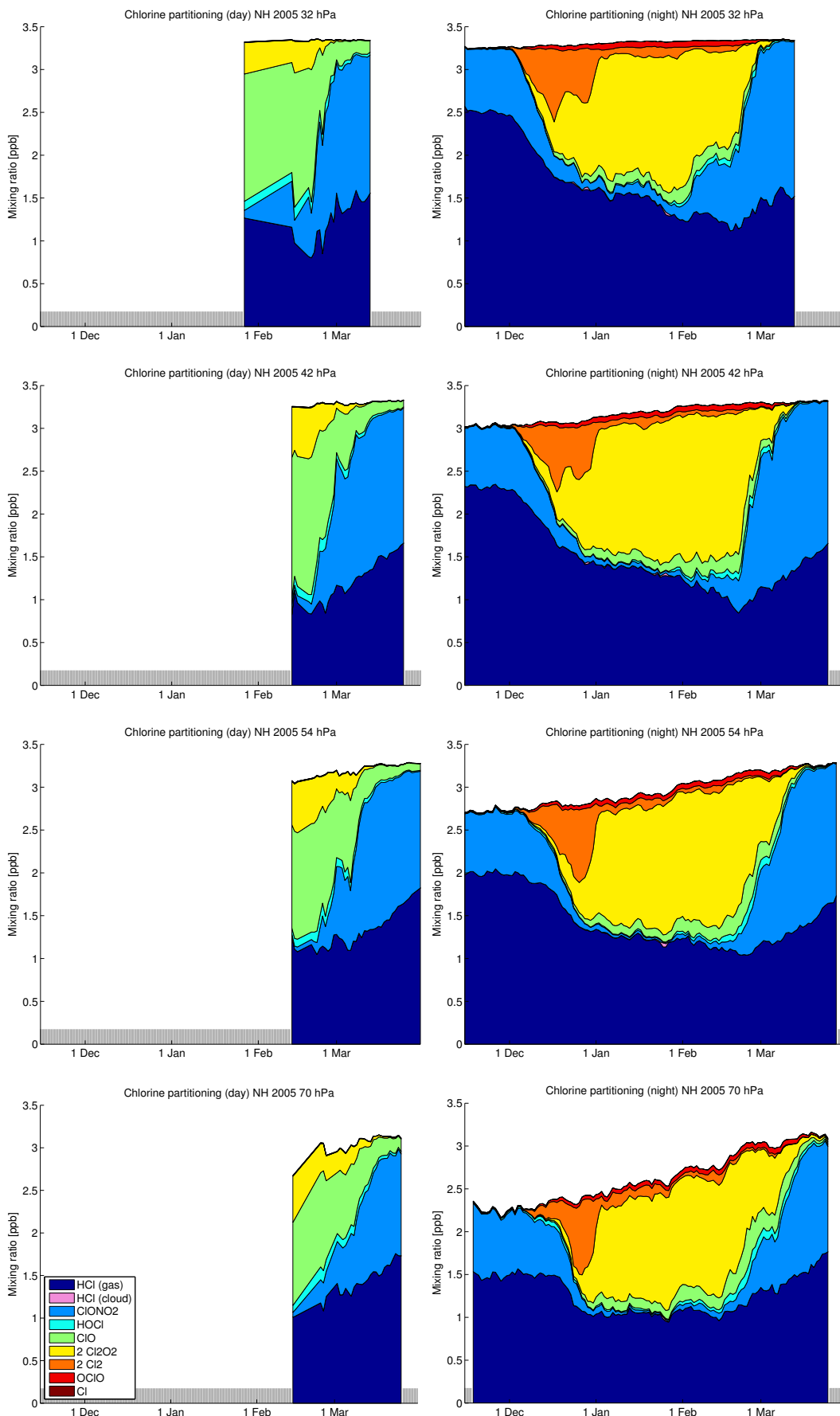


Figure 110: Vortex-averaged partitioning of inorganic chlorine species (Cl_y). Left: Daytime averages (parts of the vortex where the solar zenith angle is smaller than 80°). Right: Nighttime averages (parts of the vortex where the solar zenith angle is larger than 100°). Days without sufficient data for averaging are not shown (grey bars). Species ClNO_2 and BrCl are not shown due to their small mixing ratios. The area labeled "HCl (cloud)" shows HCl dissolved in STS droplets due to the applied correction to the HCl solubility.

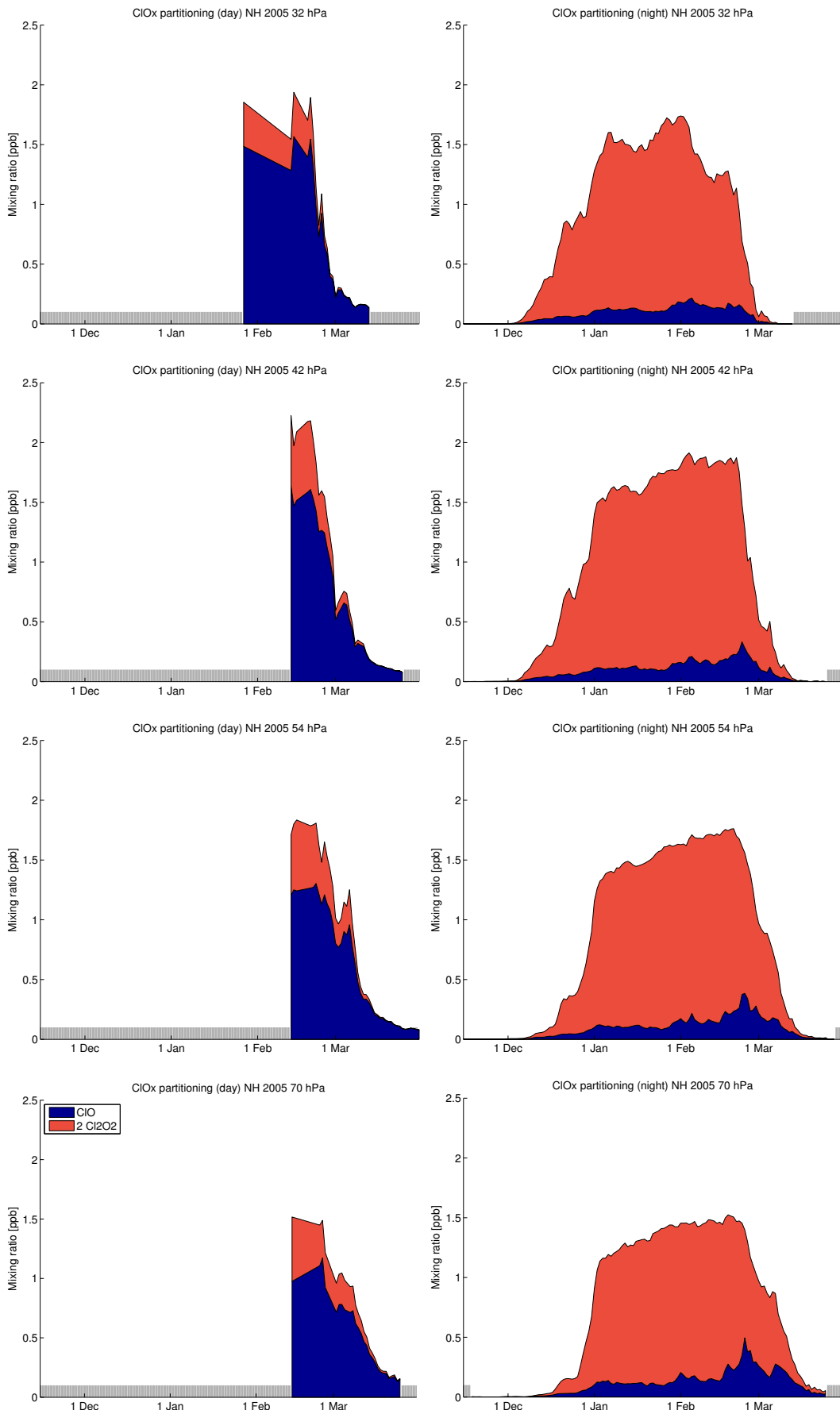


Figure 111: Vortex-averaged partitioning of ClO_x. Left: Daytime averages (parts of the vortex where the solar zenith angle is smaller than 80°). Right: Nighttime averages (parts of the vortex where the solar zenith angle is larger than 100°). Days without sufficient data for averaging are not shown (grey bars).

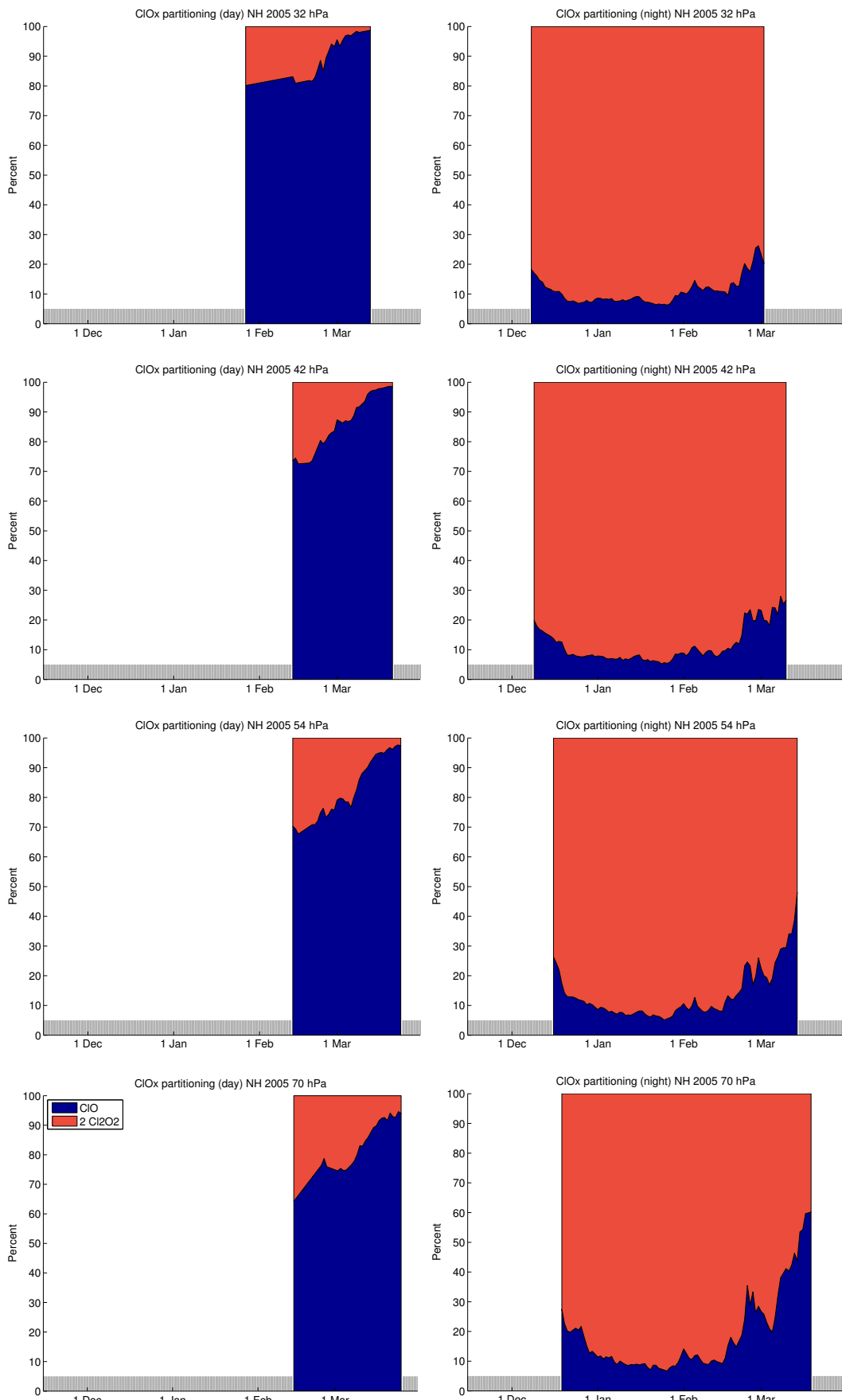


Figure 112: Same as Figure 111, but now in percentages and not in mixing ratios. Percentages are not shown for values of ClO_x below 0.1 ppb and for days without sufficient data for averaging (grey bars).

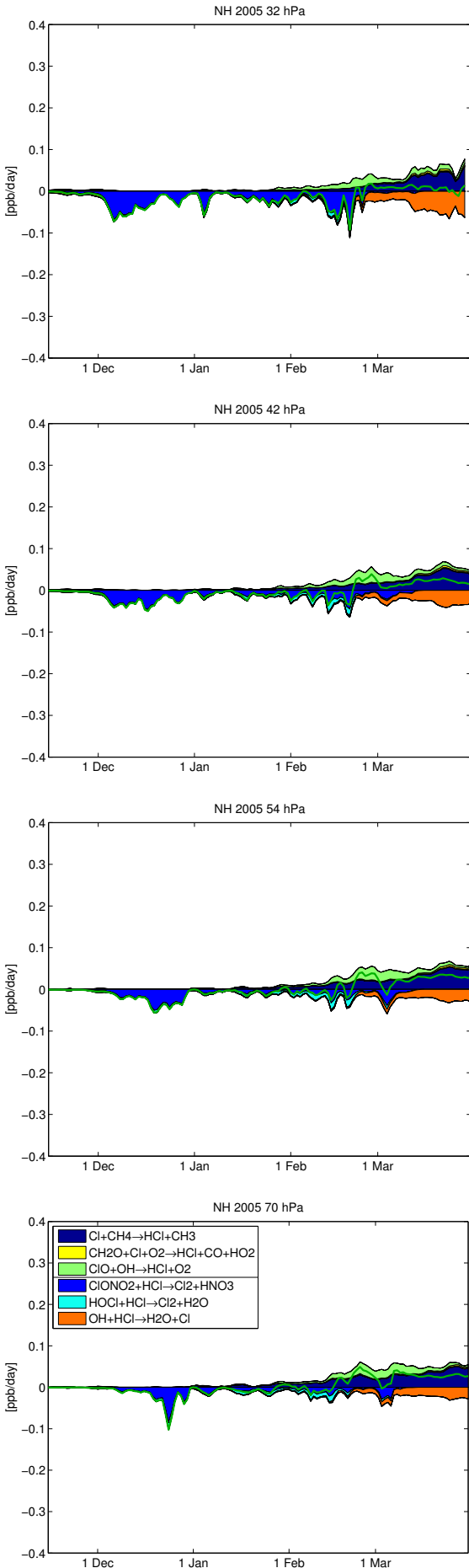


Figure 113: Vortex-averaged chemical reaction rates of reactions involving HCl. Production reactions are shown positive and are separated by a line in the legend from the loss reactions, which are shown negative. The net change of HCl is shown as a green line. Reactions with rates which cannot be distinguished from the zero line at plot resolution are not shown.

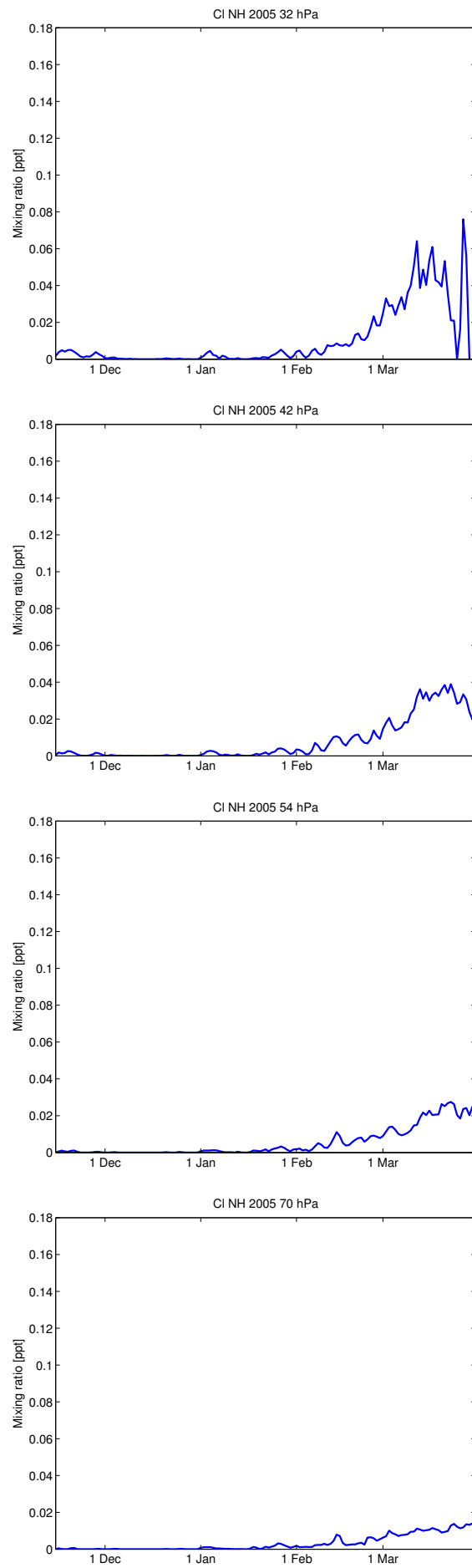


Figure 114: Vortex-averaged Cl mixing ratios.

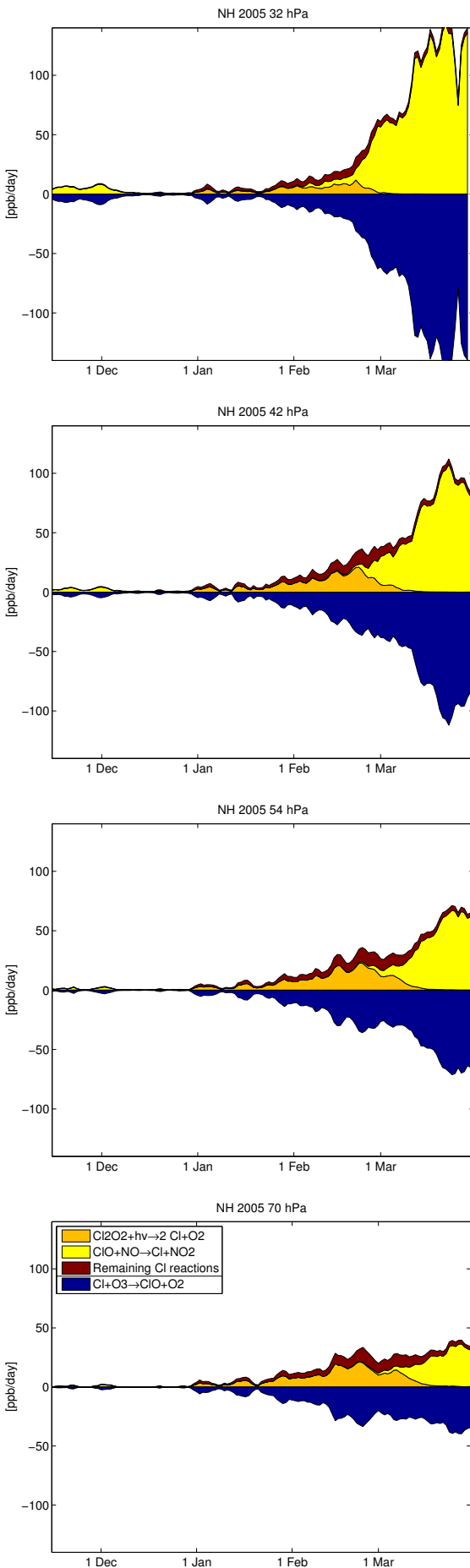


Figure 115: Vortex-averaged chemical reaction rates of reactions involving Cl. Production reactions are shown positive and are separated by a line in the legend from the loss reactions, which are shown negative.

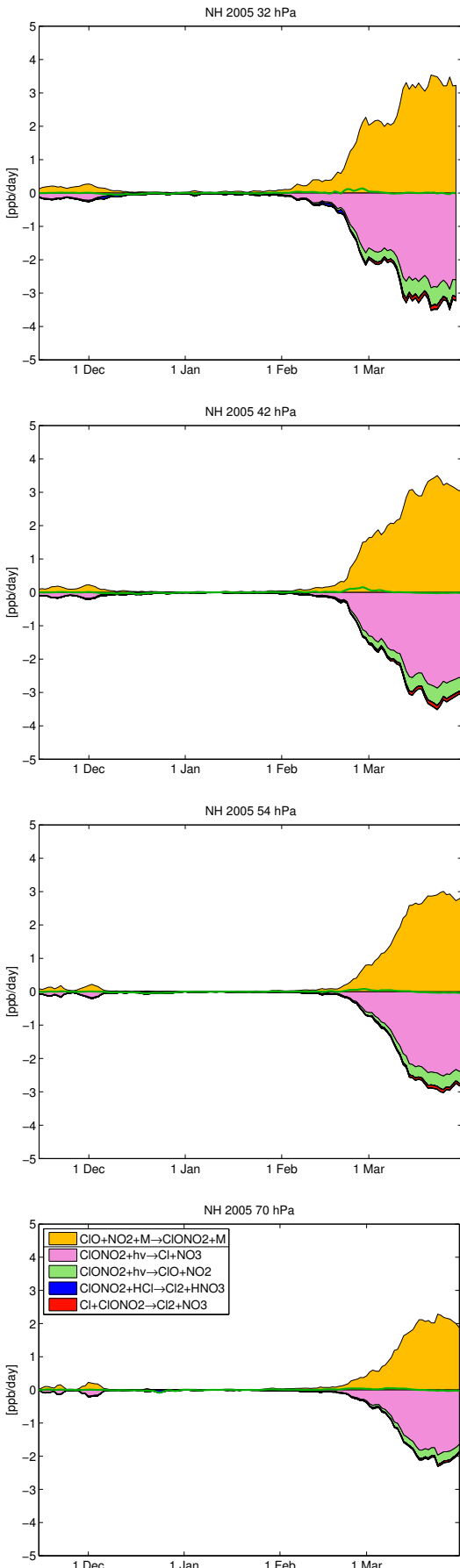


Figure 116: Vortex-averaged chemical reaction rates involving ClONO_2 . Production reactions are shown positive and are separated by a line in the legend from the loss reactions, which are shown negative. The net change of ClONO_2 is shown as a green line. Reactions with rates which cannot be distinguished from the zero line at plot resolution are not shown.

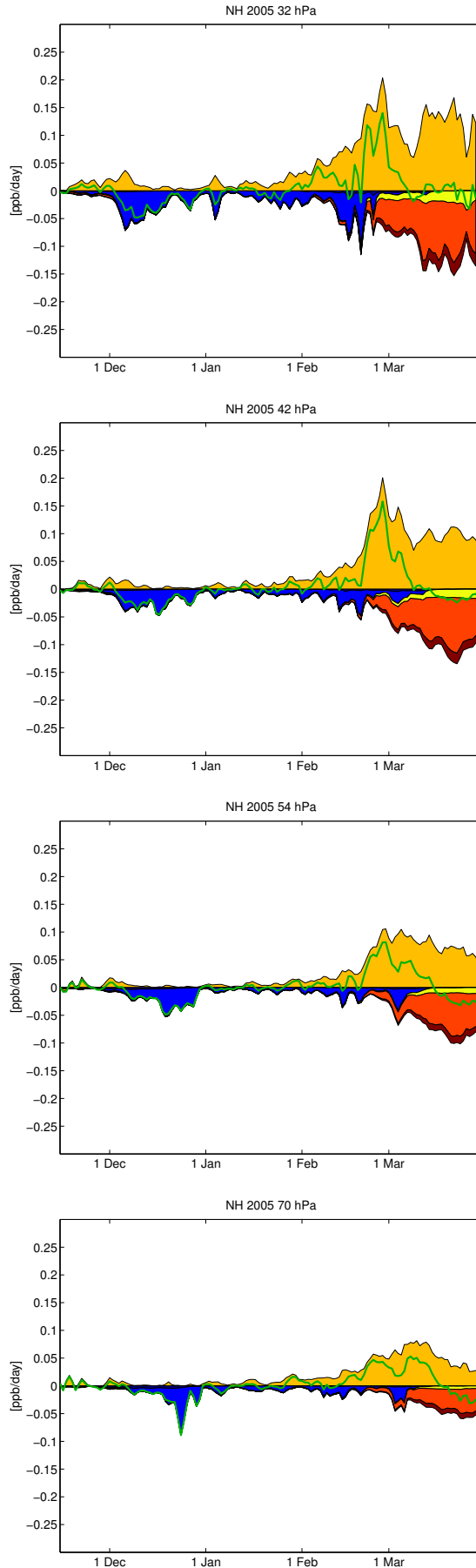


Figure 117: Vortex-averaged chemical reaction rates involving ClONO_2 . In contrast to Figure 116, the net production rate of the fast cycle $\text{ClONO}_2 + h\nu \rightarrow \text{Products} / \text{ClO} + \text{NO}_2 + \text{M} \rightarrow \text{ClONO}_2 + \text{M}$ is shown. This cycle is separated by a line in the legend from the loss reactions. The green line shows the net change of ClONO_2 by chemistry. Reactions with rates which cannot be distinguished from the zero line at plot resolution are not shown.

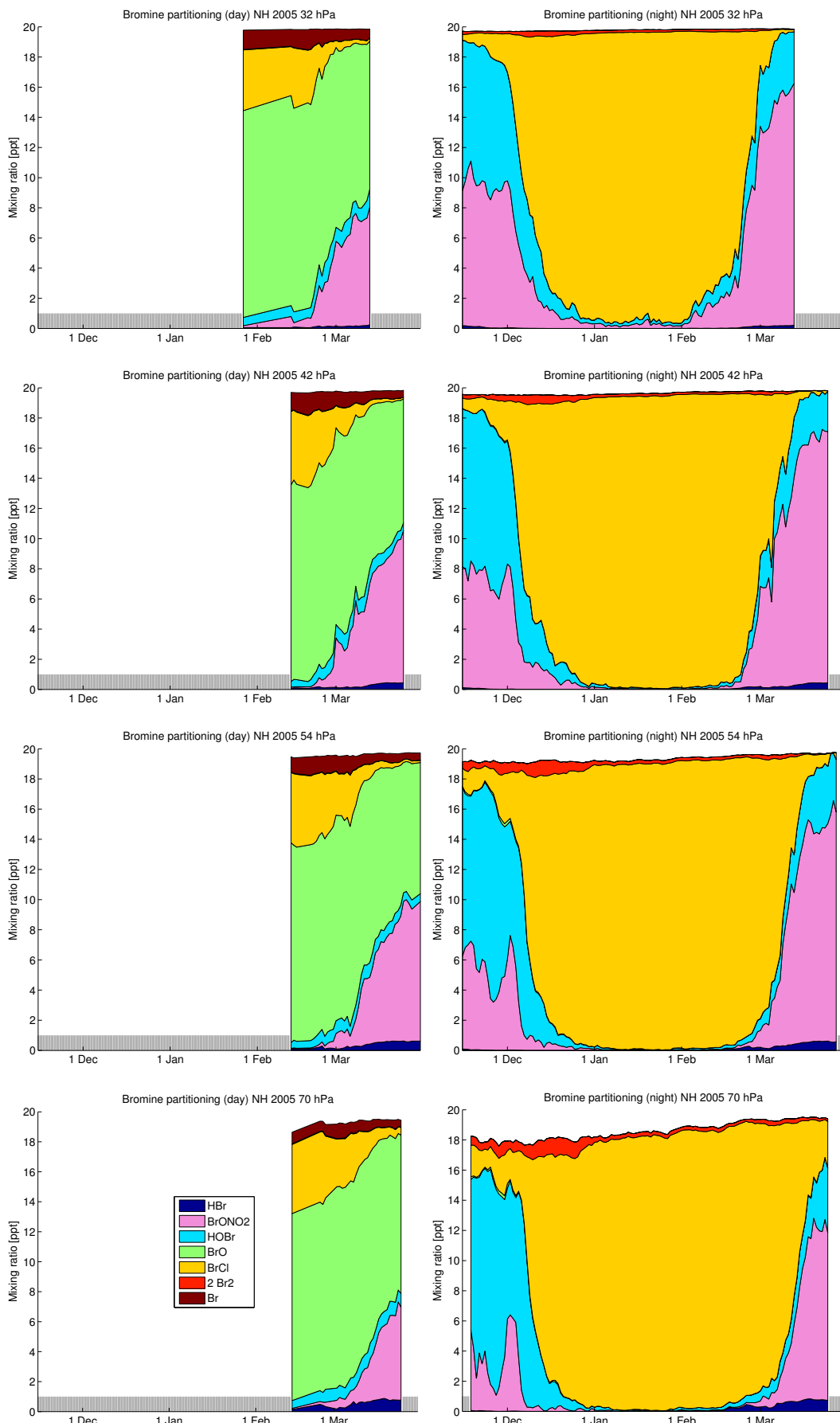


Figure 118: Vortex-averaged partitioning of inorganic bromine species. Left: Daytime averages (parts of the vortex where the solar zenith angle is smaller than 80°). Right: Nighttime averages (parts of the vortex where the solar zenith angle is larger than 100°). Days without sufficient data for averaging are not shown (grey bars).

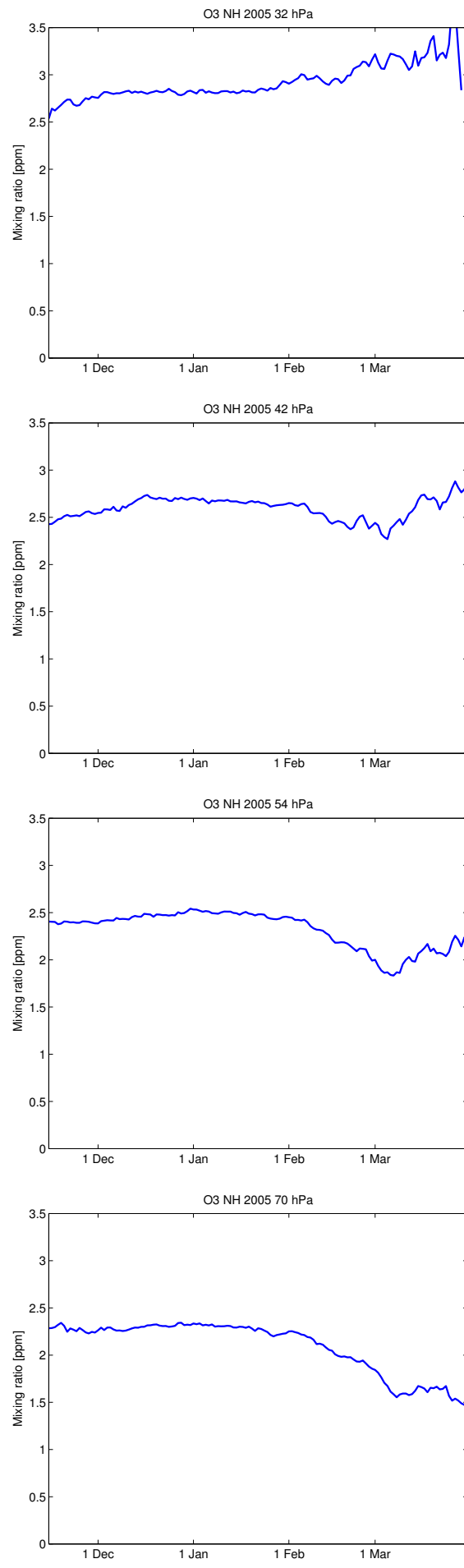


Figure 119: Vortex-averaged ozone mixing ratios.

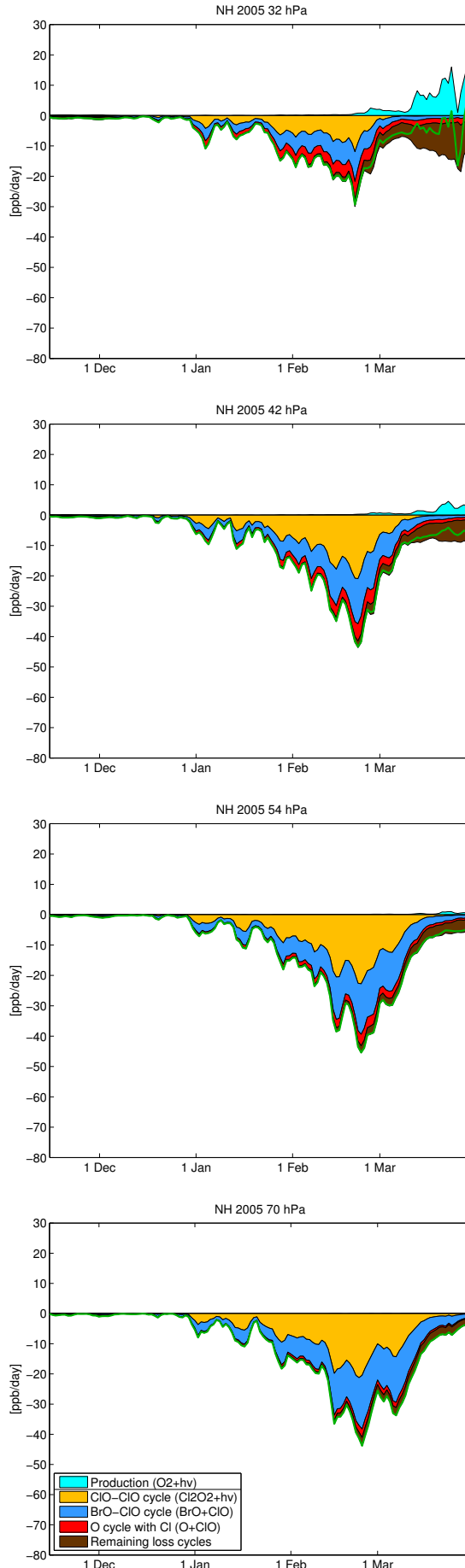


Figure 120: Vortex-averaged net chemical change of odd oxygen. The green line shows the net chemical change rate of ozone, which nearly equals the change rate of odd oxygen. The contribution of different catalytic cycles to the ozone loss is shown by the reaction rates of their rate limiting step. Only the three most important cycles are shown, the contribution of other cycles is small. Ozone production, which is almost exclusively by the $O_2 + h\nu$ reaction, is shown in cyan.

2.2 Southern Hemisphere 2006 (Uncorrected run)

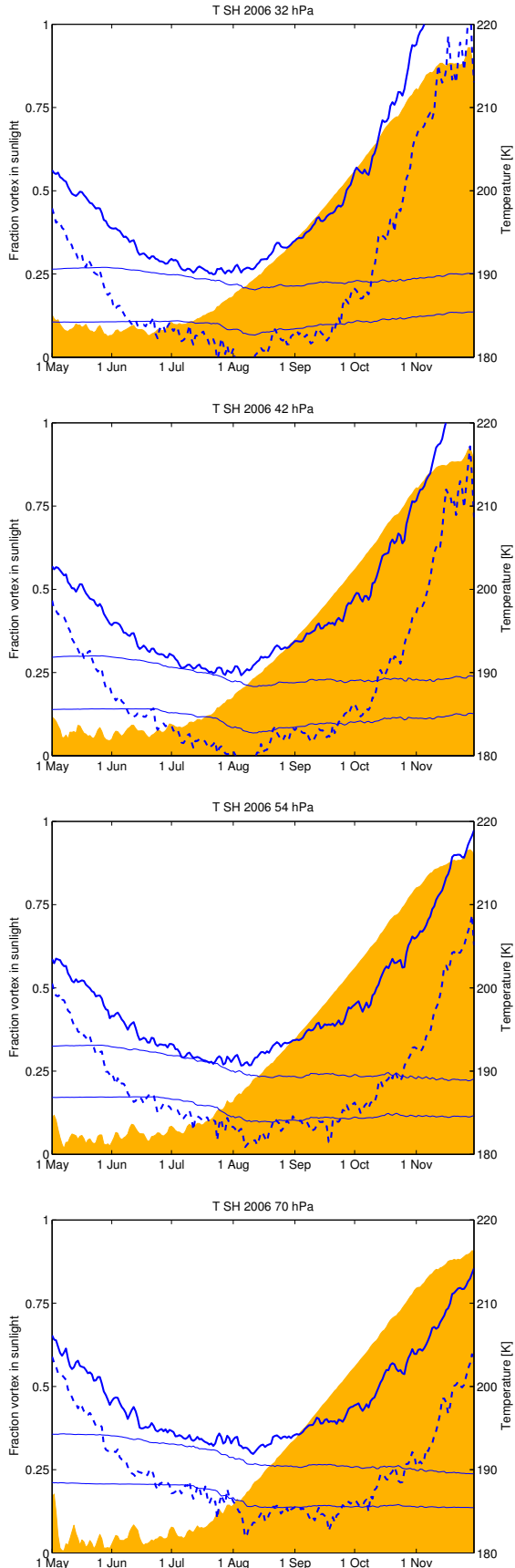


Figure 121: Vortex-averaged temperature (blue), vortex minimum temperature (dashed blue) and fraction of the vortex in sunlight (yellow). The upper thin blue line shows the threshold temperature for the formation of NAT clouds used in the model (based on vortex mean mixing ratios and considering supersaturation), and the lower thin blue line shows the same for ice clouds. The vortex tracer criterion is not applied (in contrast to all other figures).

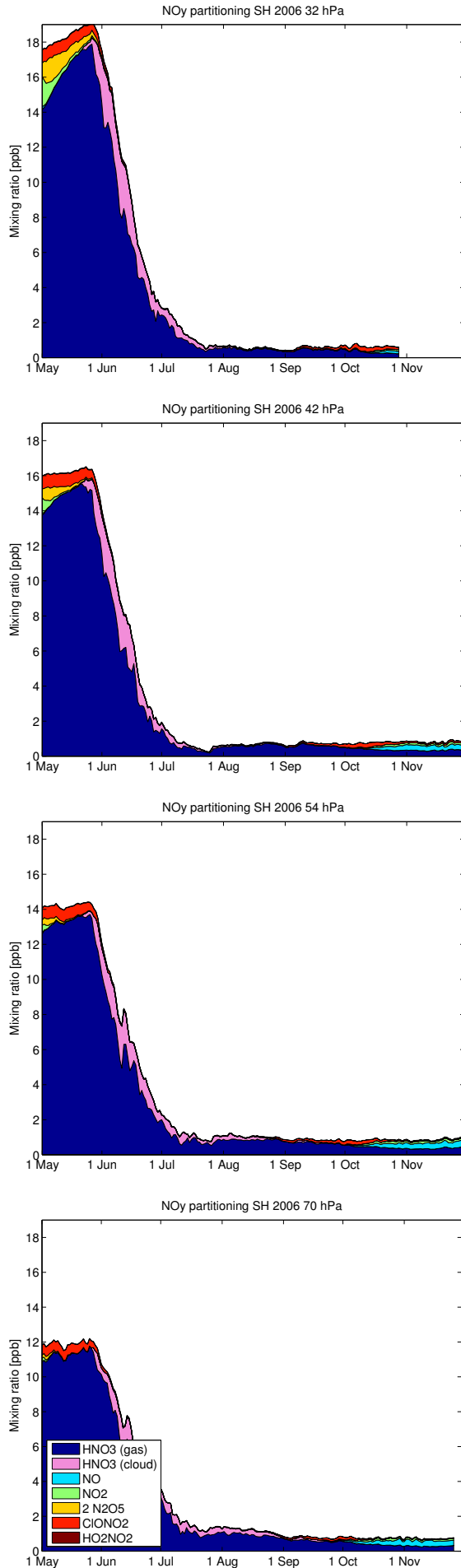


Figure 122: Vortex-averaged partitioning of NO_y species. Species NO₃, BrONO₂, ClONO₂ and N are not shown due to their small mixing ratios.

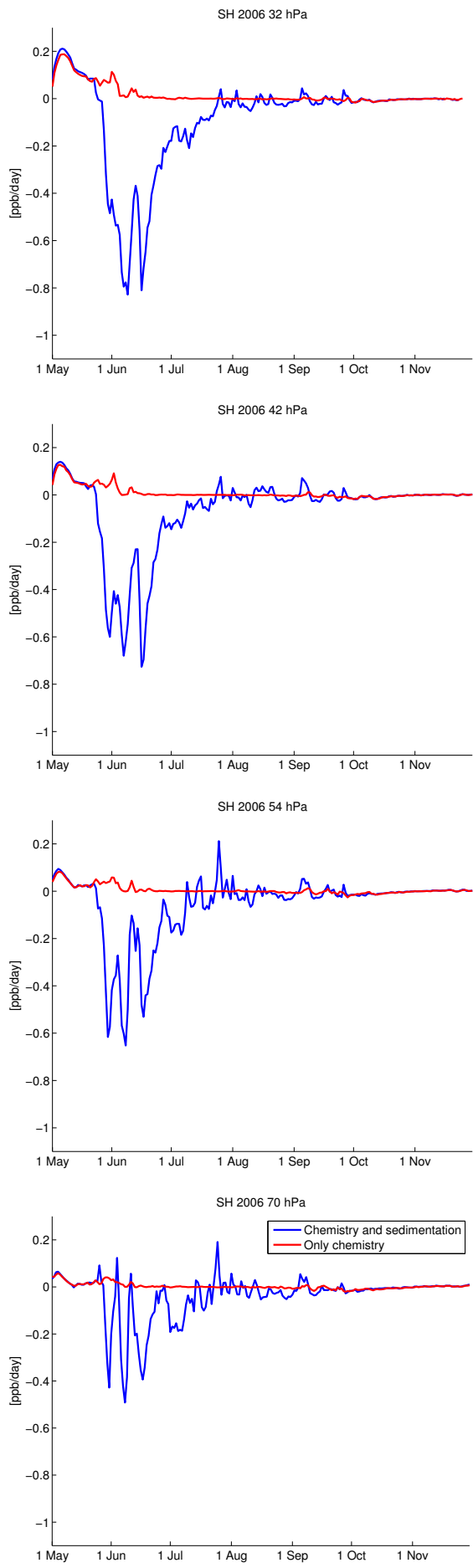


Figure 123: Vortex-averaged net chemical reaction rate of HNO_3 (red) and sum of the vortex-averaged change by sedimentation and the net chemical reaction rate (blue).

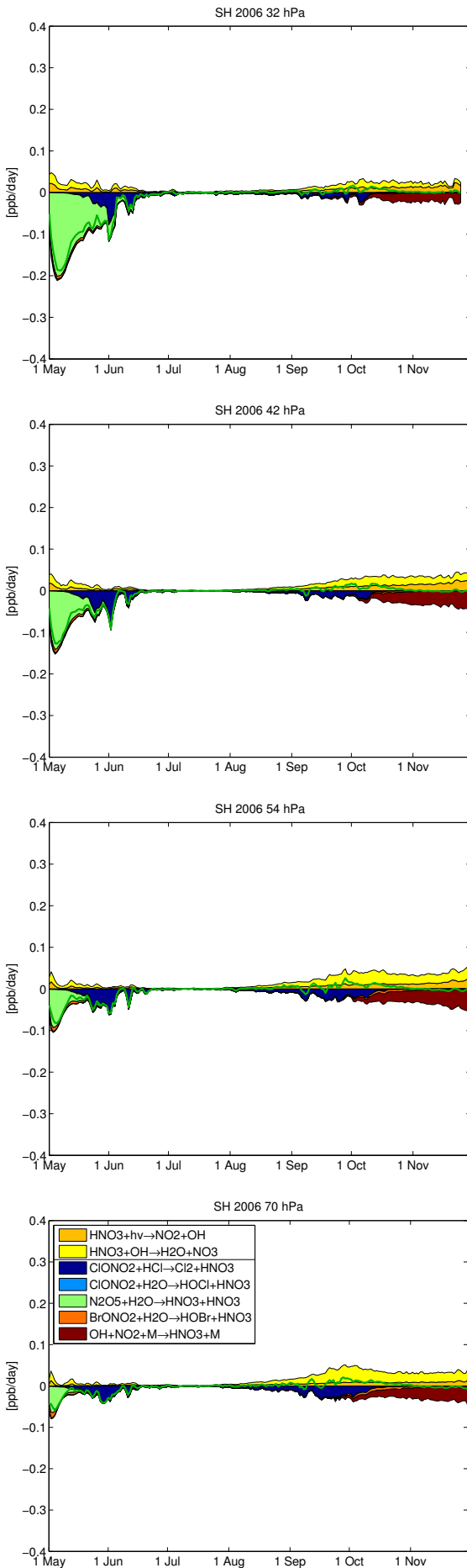


Figure 124: Vortex-averaged chemical reaction rates of reactions changing extended NO_x ($\text{NO} + \text{NO}_2 + \text{NO}_3 + 2\text{N}_2\text{O}_5 + \text{ClONO}_2 + \text{BrONO}_2 + \text{HO}_2\text{NO}_2$). Production reactions are shown positive and are separated by a line in the legend from the loss reactions, which are shown negative. The net change of extended NO_x is shown as a green line.

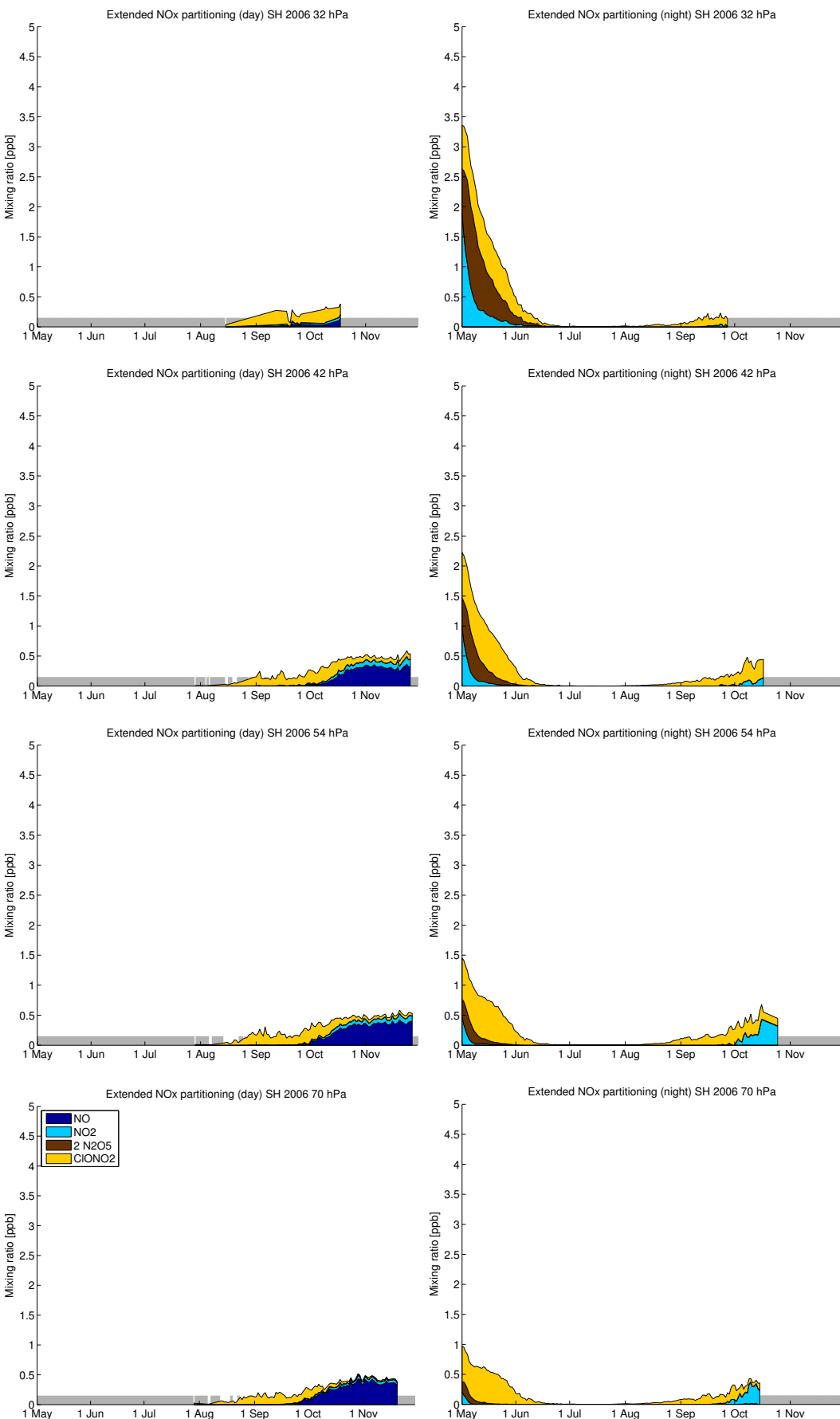


Figure 125: Vortex-averaged partitioning of extended NO_x species. Left: Daytime averages (parts of the vortex where the solar zenith angle is smaller than 80°). Right: Nighttime averages (parts of the vortex where the solar zenith angle is larger than 100°). Days without sufficient data for averaging are not shown (grey bars).

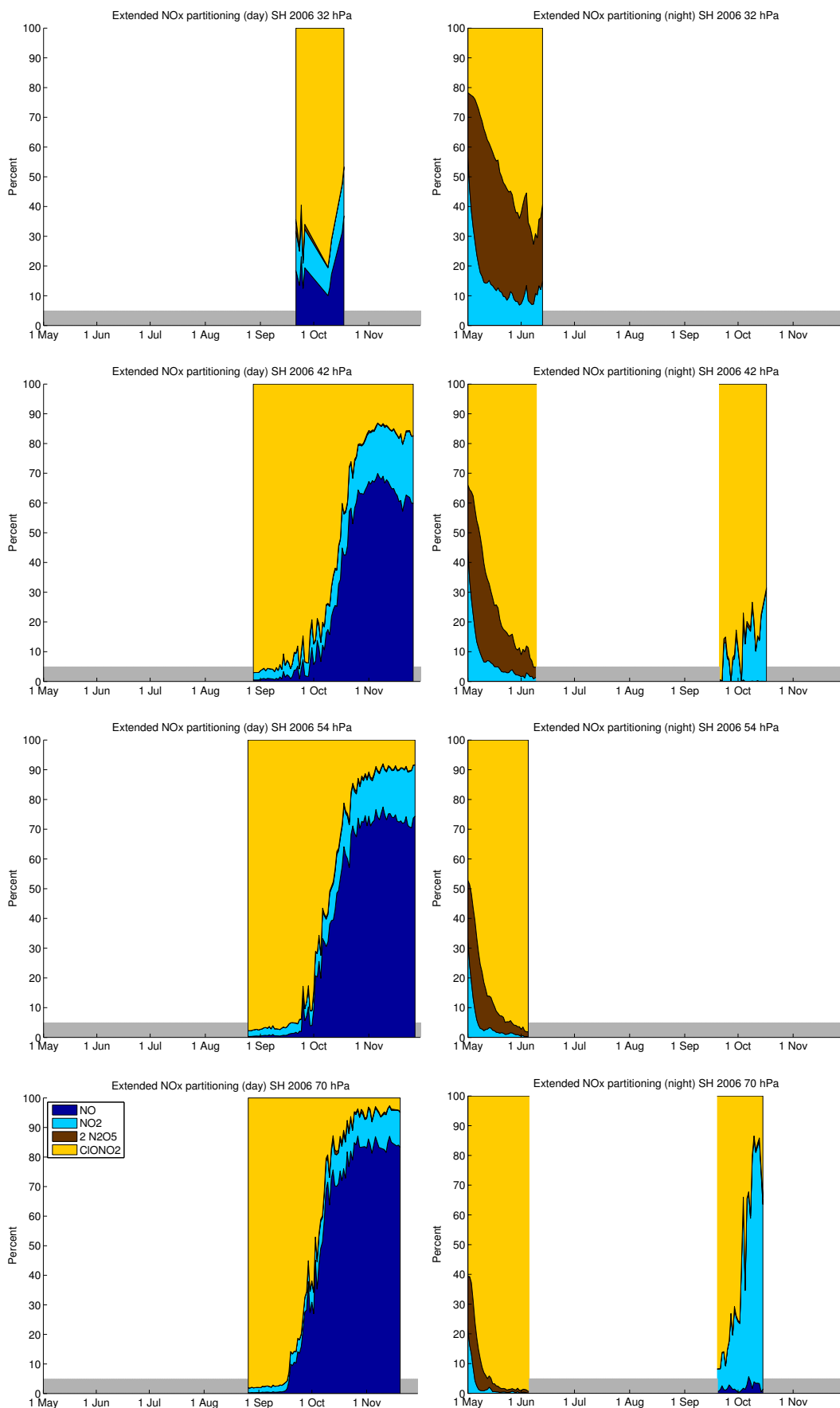


Figure 126: Same as Figure 125, but now in percentages and not in mixing ratios. Percentages are not shown for values of extended NO_x below 0.1 ppb and for days without sufficient data for averaging (grey bars).

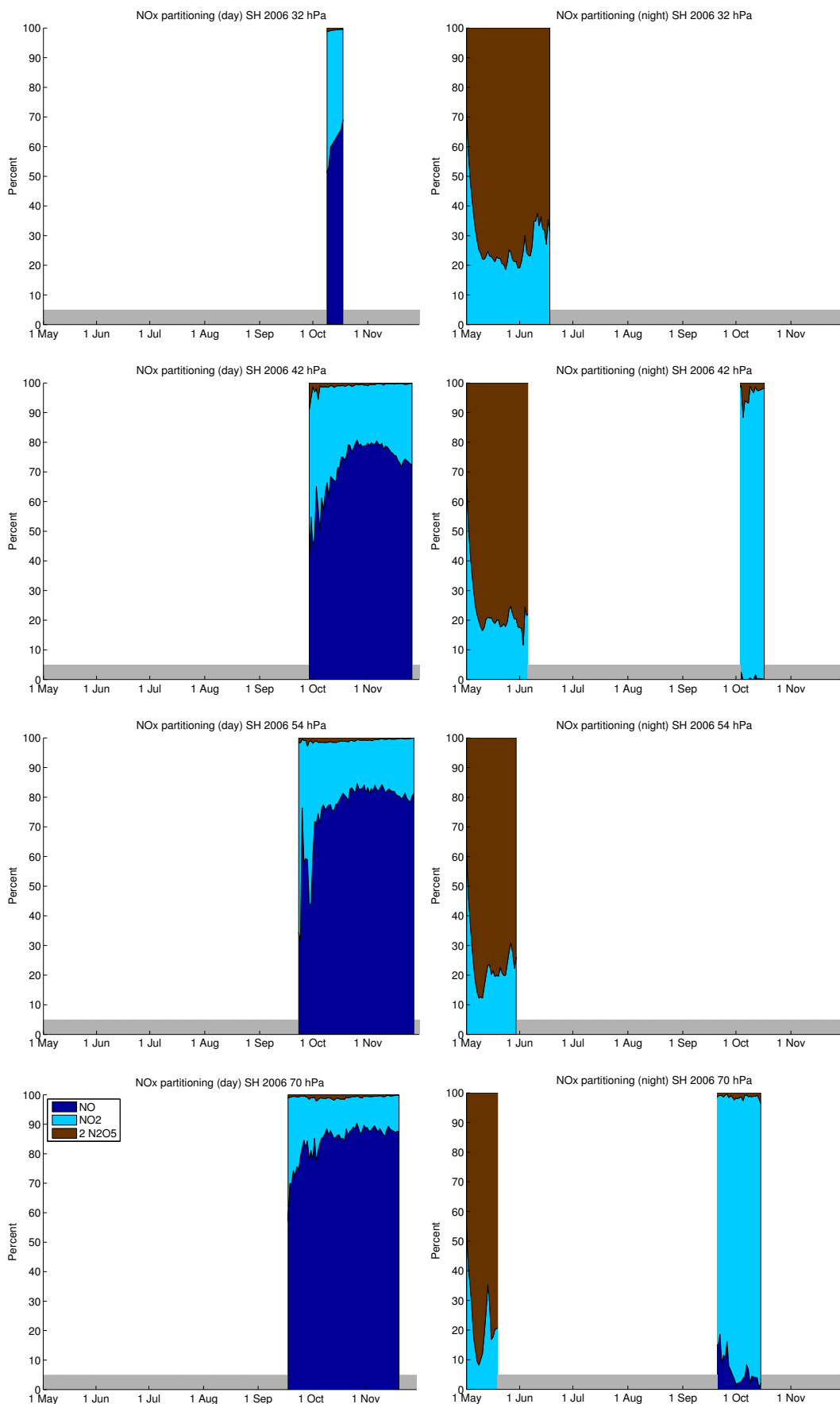


Figure 127: Same as Figure 126, but with only $\text{NO}_x = \text{NO} + \text{NO}_2 + 2\text{N}_2\text{O}_5$ partitioning. Percentages are not shown for values of NO_x below 0.01 ppb and for days without sufficient data for averaging (grey bars).

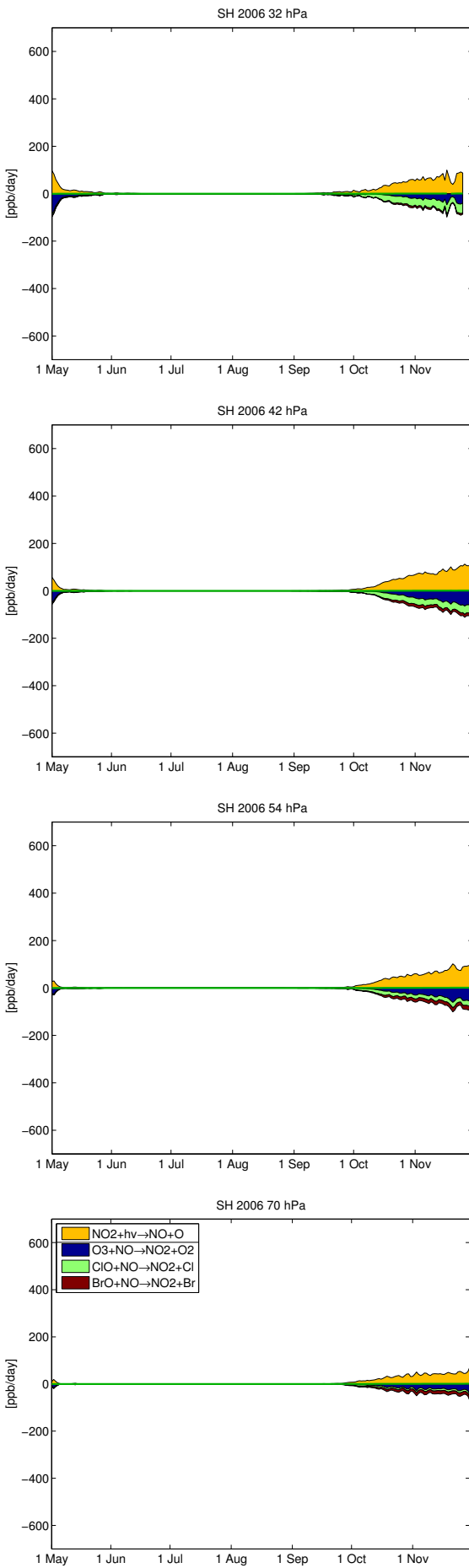


Figure 128: Vortex-averaged chemical reaction rates of reactions changing NO to illustrate NO_x partitioning. Production reactions are shown positive and are separated by a line in the legend from the loss reactions, which are shown negative. The net change of NO is shown as a green line.

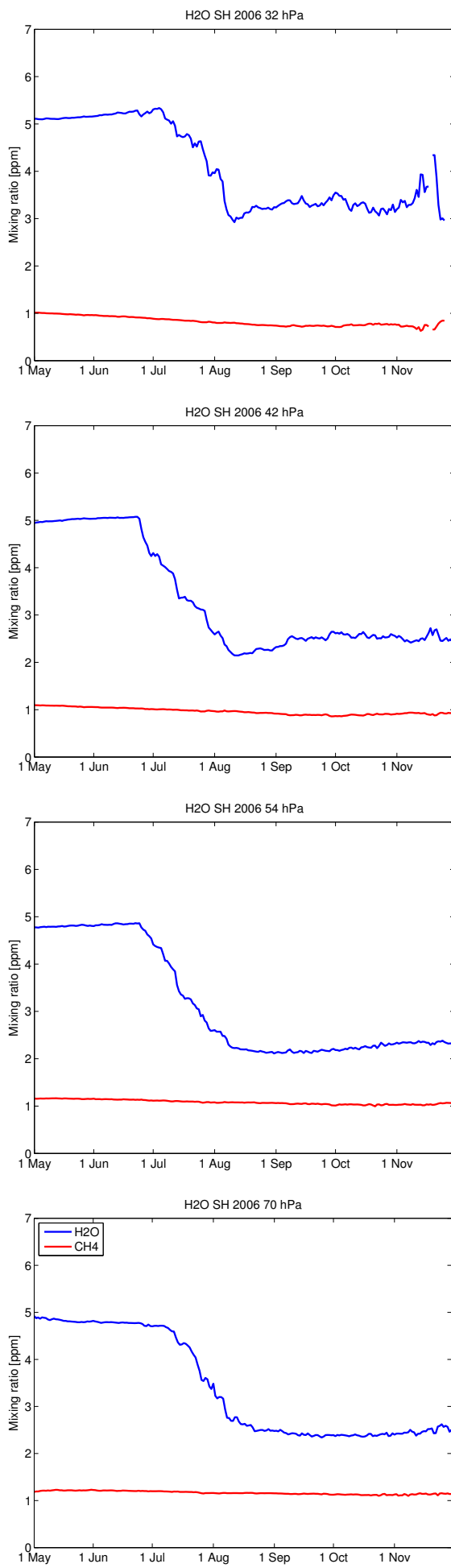


Figure 129: Vortex-averaged mixing ratios of H₂O and CH₄.

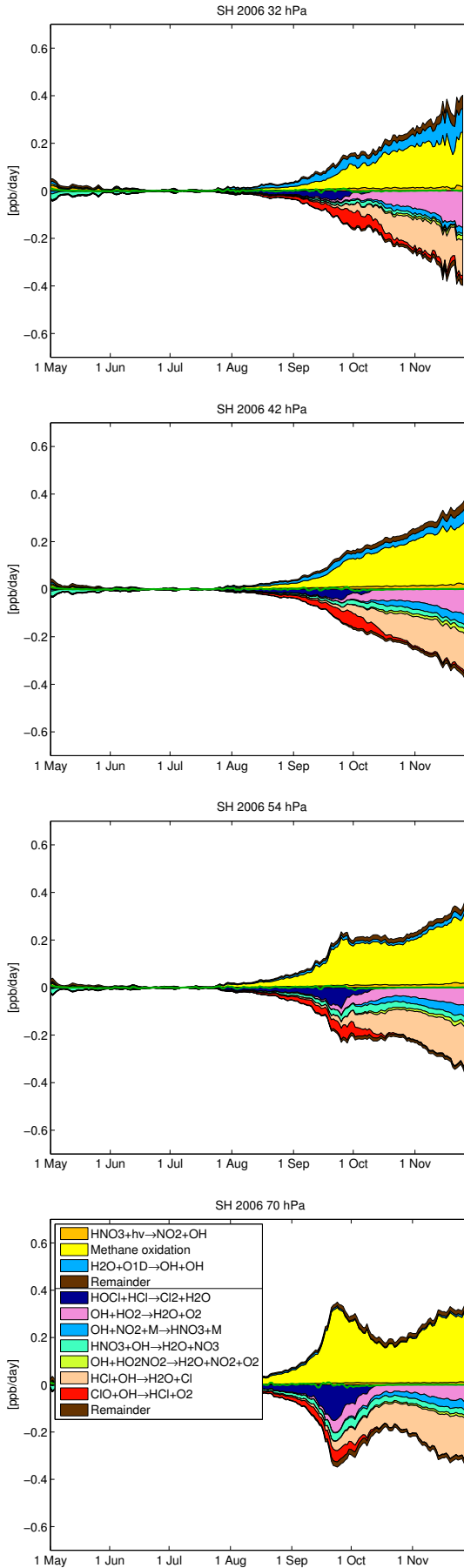


Figure 130: Vortex-averaged chemical reaction rates of reactions changing extended HO_x (OH + HO₂ + H + HOCl + HOBr + HO₂NO₂). Production reactions are shown positive and are separated by a line in the legend from the loss reactions, which are shown negative. The net change of extended HO_x is shown as a green line. Methane oxidation is modelled by simplified net reactions in ATLAS, the reactions denoted as methane oxidation in the legend are Cl + CH₄ → HCl + CH₂O + HO₂ and Cl + CH₂O → HCl + CO + HO₂.

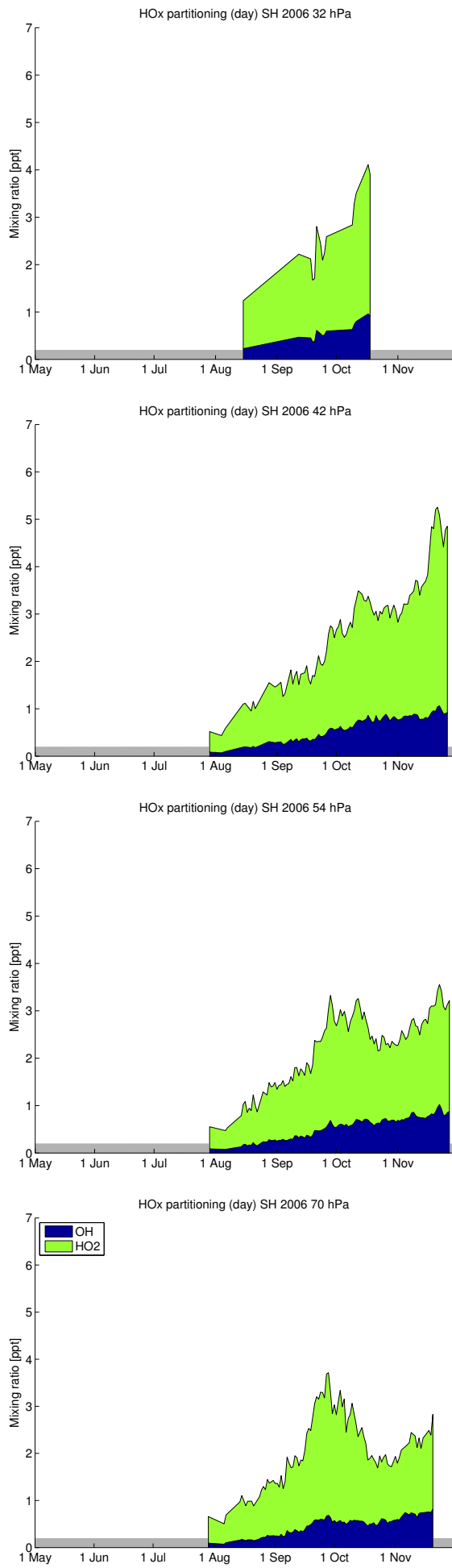


Figure 131: Vortex-averaged partitioning of HO_x species. Daytime averages (parts of the vortex where the solar zenith angle is smaller than 80°). Nighttime averages are near zero and not shown. Data: WMO (2006). Geopotential height of 1000 hPa (m) (not shown).

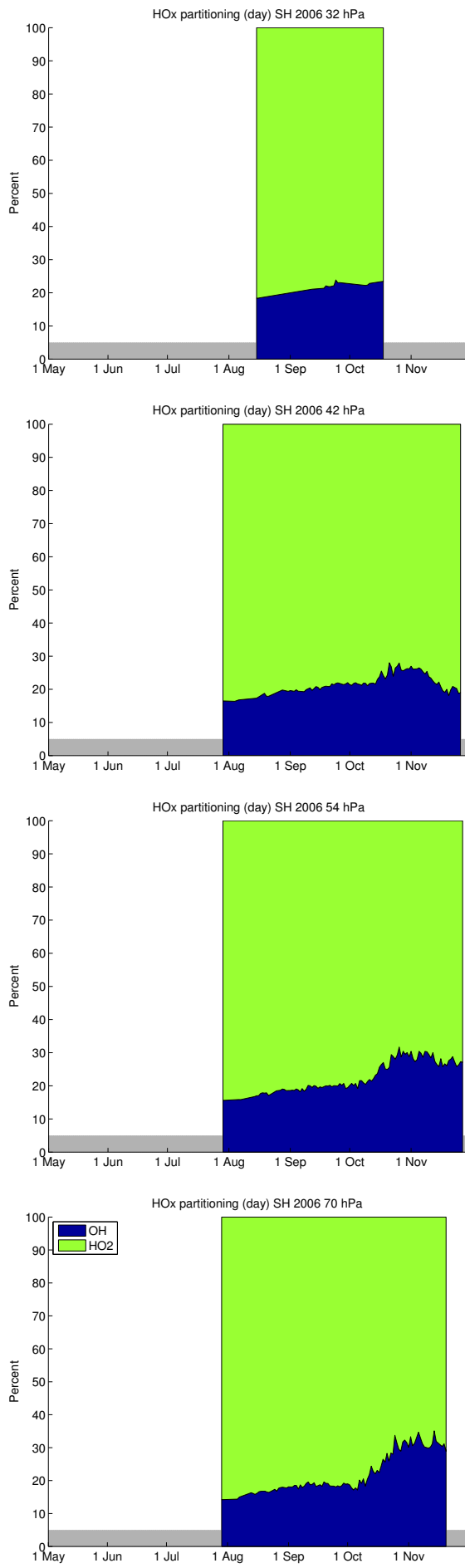


Figure 132: Same as Figure 59, but now in percentages and not in mixing ratios. Days without sufficient data for averaging are not shown (grey bars).

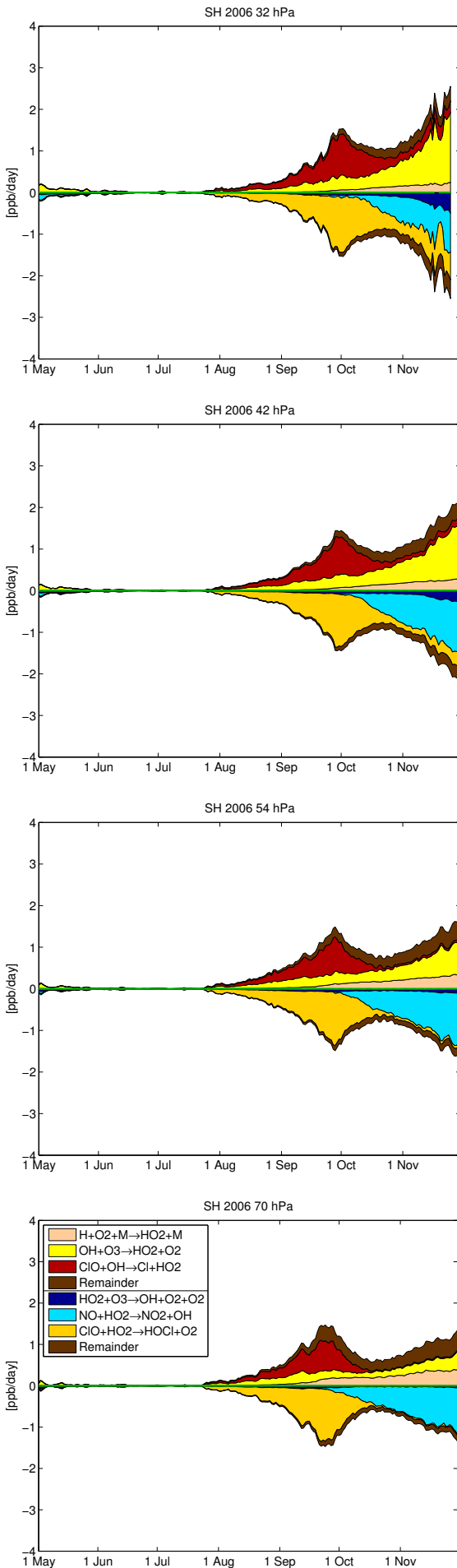


Figure 133: Vortex-averaged chemical reaction rates of reactions changing HO₂ to illustrate HO_x partitioning. Production reactions are shown positive and are separated by a line in the legend from the loss reactions, which are shown negative. The net change of HO₂ is shown as a green line.

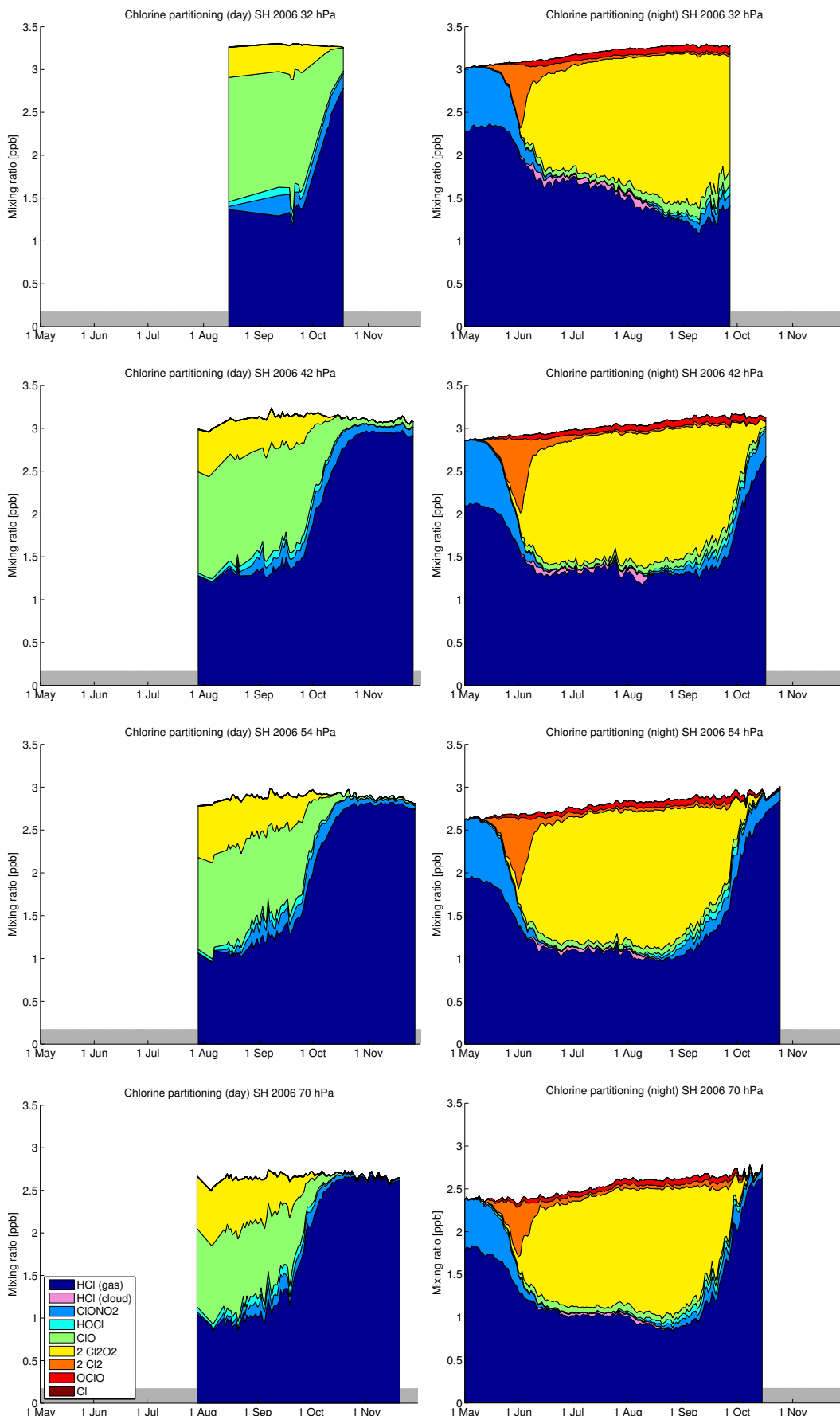


Figure 134: Vortex-averaged partitioning of inorganic chlorine species (Cl_y). Left: Daytime averages (parts of the vortex where the solar zenith angle is smaller than 80°). Right: Nighttime averages (parts of the vortex where the solar zenith angle is larger than 100°). Days without sufficient data for averaging are not shown (grey bars). Species ClNO_2 and BrCl are not shown due to their small mixing ratios. The area labeled "HCl (cloud)" shows HCl dissolved in STS droplets due to the applied correction to the HCl solubility.

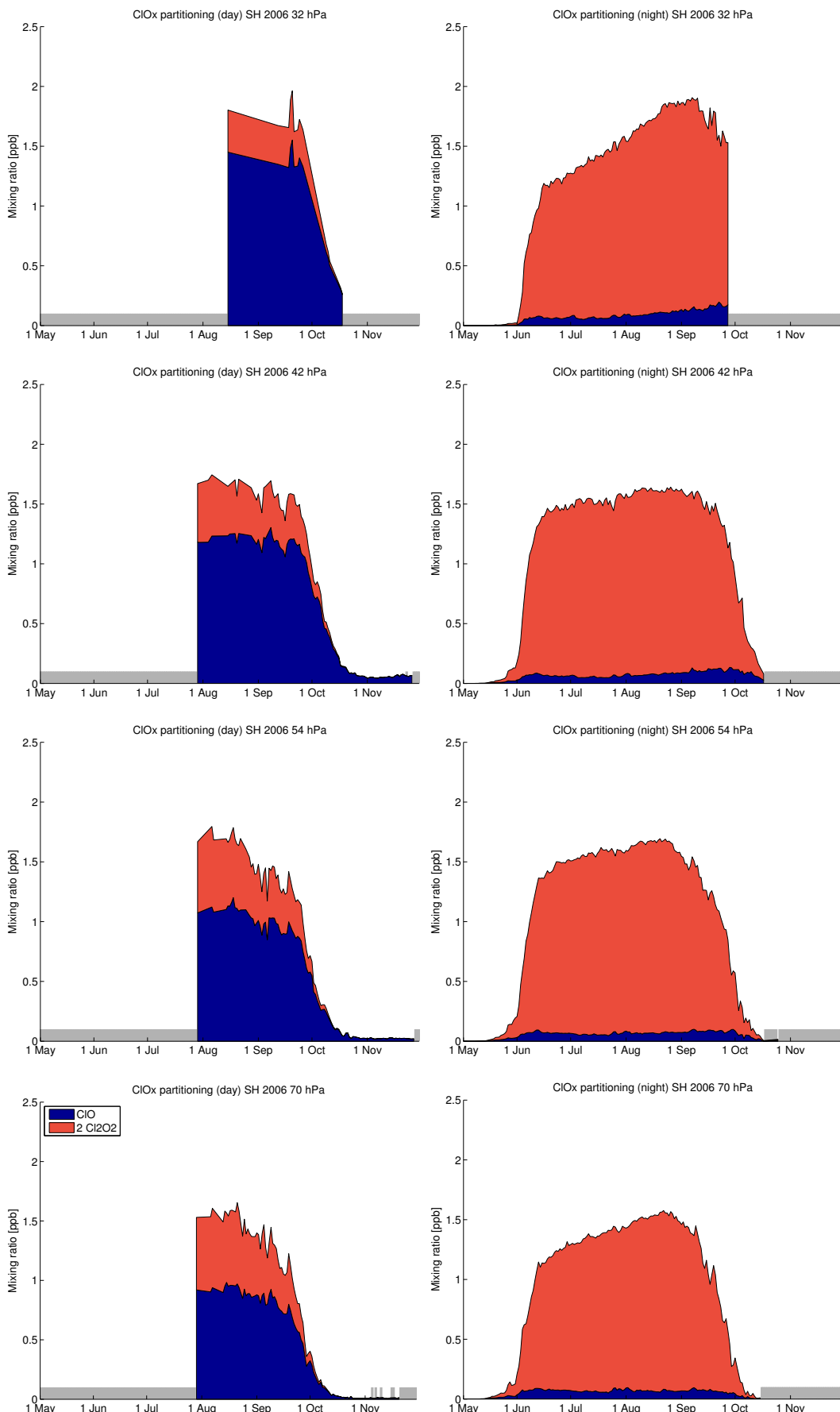


Figure 135: Vortex-averaged partitioning of ClO_x . Left: Daytime averages (parts of the vortex where the solar zenith angle is smaller than 80°). Right: Nighttime averages (parts of the vortex where the solar zenith angle is larger than 100°). Days without sufficient data for averaging are not shown (grey bars).

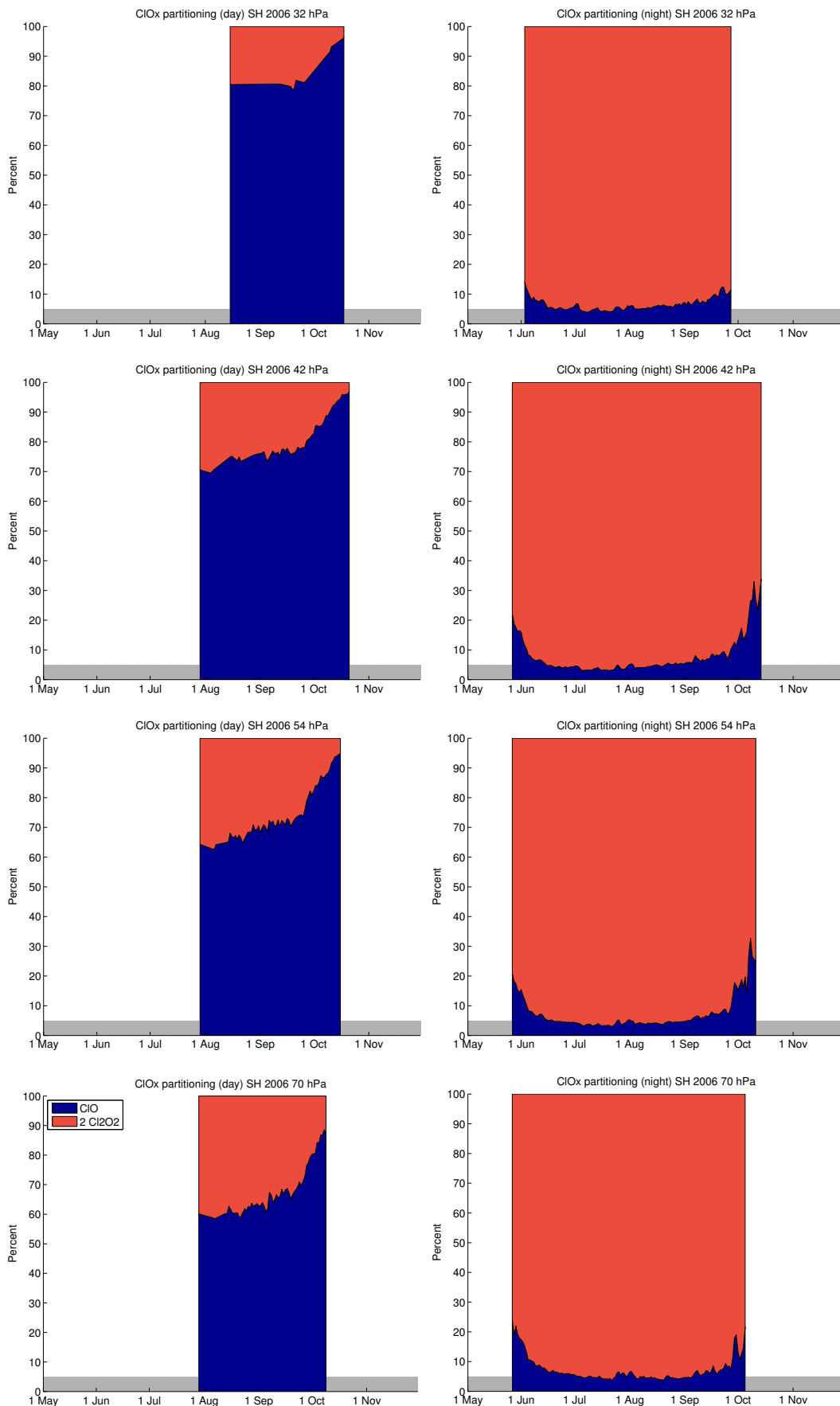


Figure 136: Same as Figure 135, but now in percentages and not in mixing ratios. Percentages are not shown for values of ClO_x below 0.1 ppb and for days without sufficient data for averaging (grey bars).

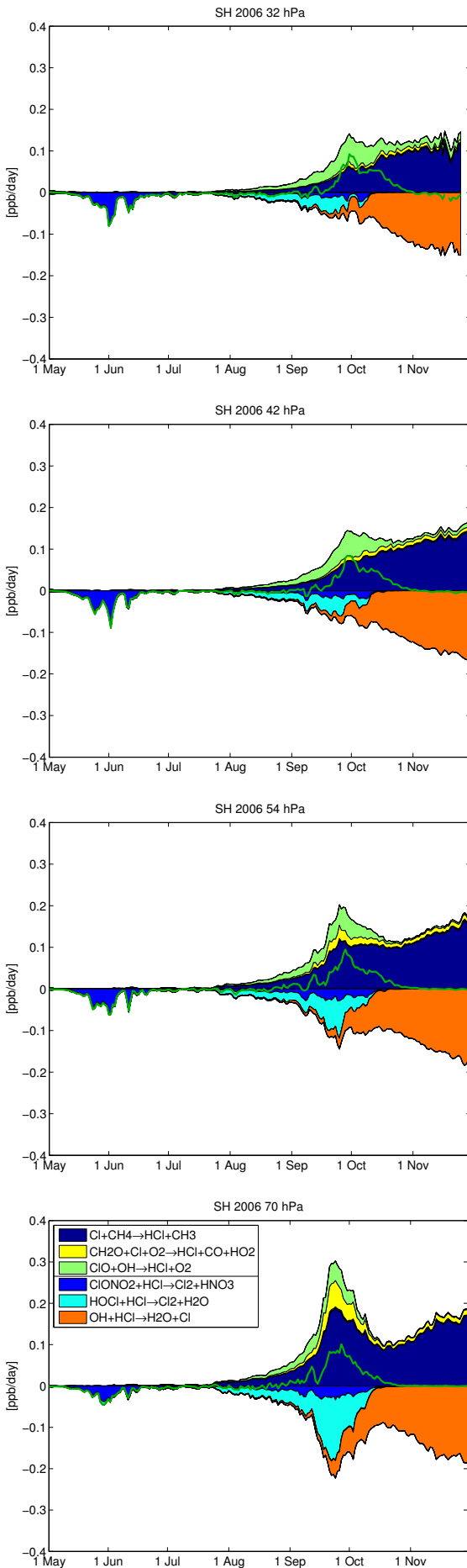


Figure 137: Vortex-averaged chemical reaction rates of reactions involving HCl. Production reactions are shown positive and are separated by a line in the legend from the loss reactions, which are shown negative. The net change of HCl is shown as a green line. Reactions with rates which cannot be distinguished from the zero line at plot resolution are not shown.

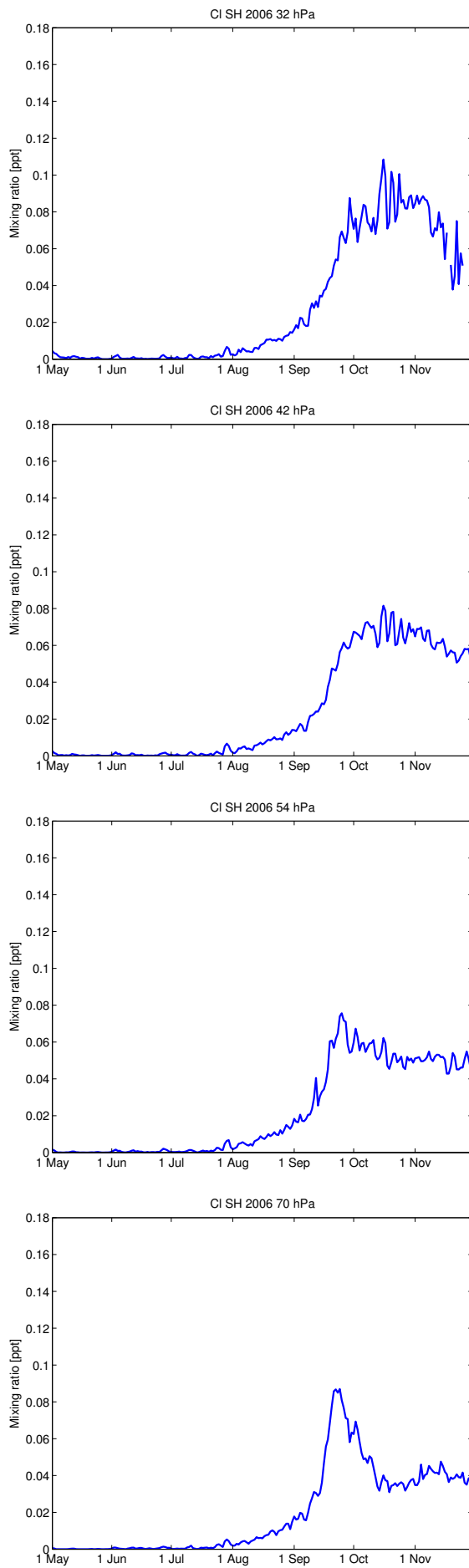


Figure 138: Vortex-averaged Cl mixing ratios.

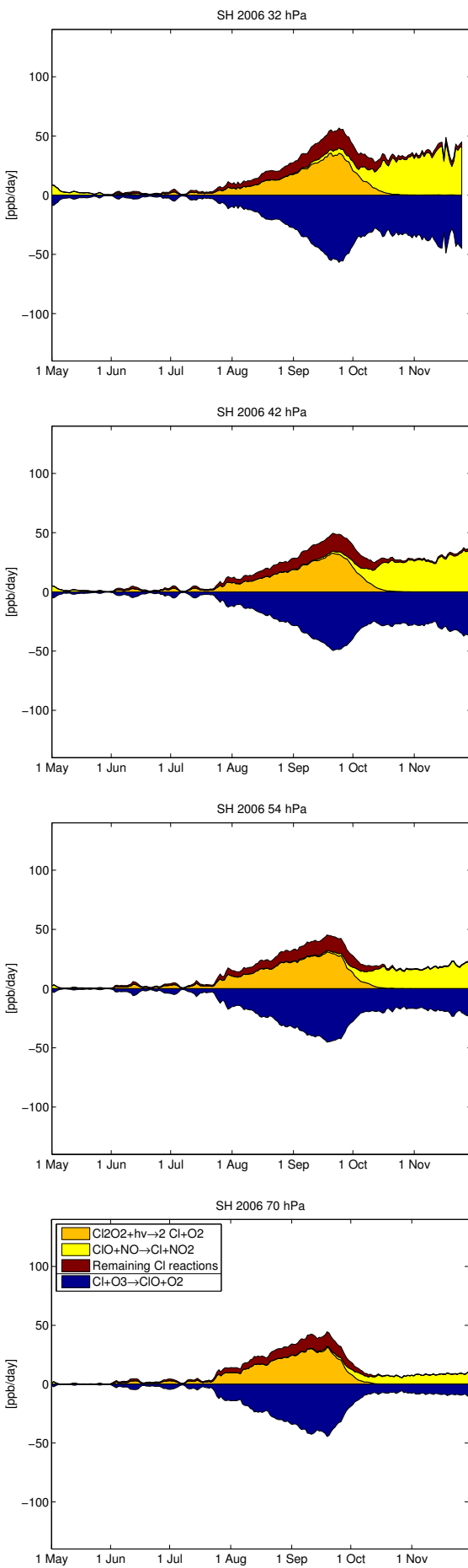


Figure 139: Vortex-averaged chemical reaction rates of reactions involving Cl. Production reactions are shown positive and are separated by a line in the legend from the loss reactions, which are shown negative.

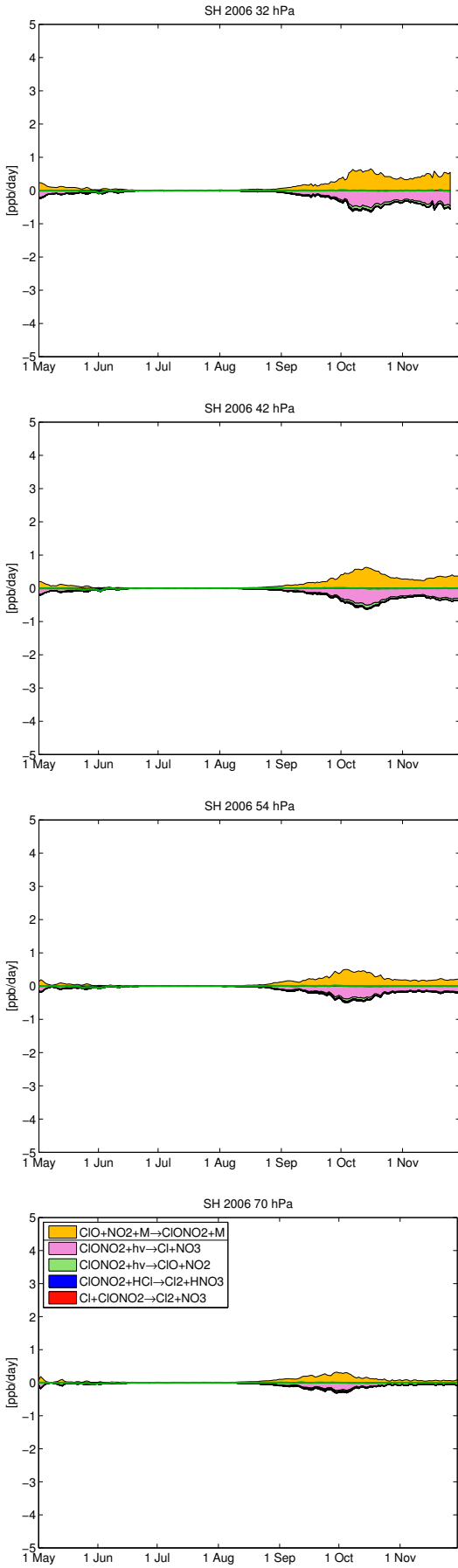


Figure 140: Vortex-averaged chemical reaction rates involving ClONO_2 . Production reactions are shown positive and are separated by a line in the legend from the loss reactions, which are shown negative. The net change of ClONO_2 is shown as a green line. Reactions with rates which cannot be distinguished from the zero line at plot resolution are not shown.

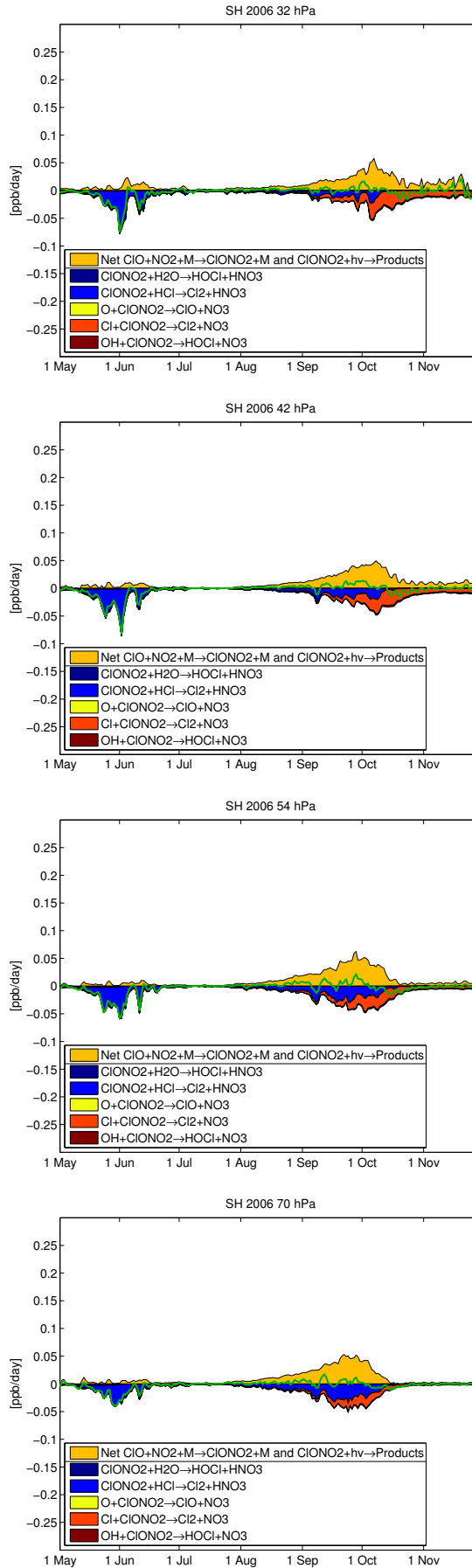


Figure 141: Vortex-averaged chemical reaction rates involving ClONO_2 . In contrast to Figure 140, the net production rate of the fast cycle $\text{ClONO}_2 + h\nu \rightarrow \text{Products} / \text{ClO} + \text{NO}_2 + \text{M} \rightarrow \text{ClONO}_2 + \text{M}$ is shown. This cycle is separated by a line in the legend from the loss reactions. The green line shows the net change of ClONO_2 by chemistry. Reactions with rates which cannot be distinguished from the zero line at plot resolution are not shown.

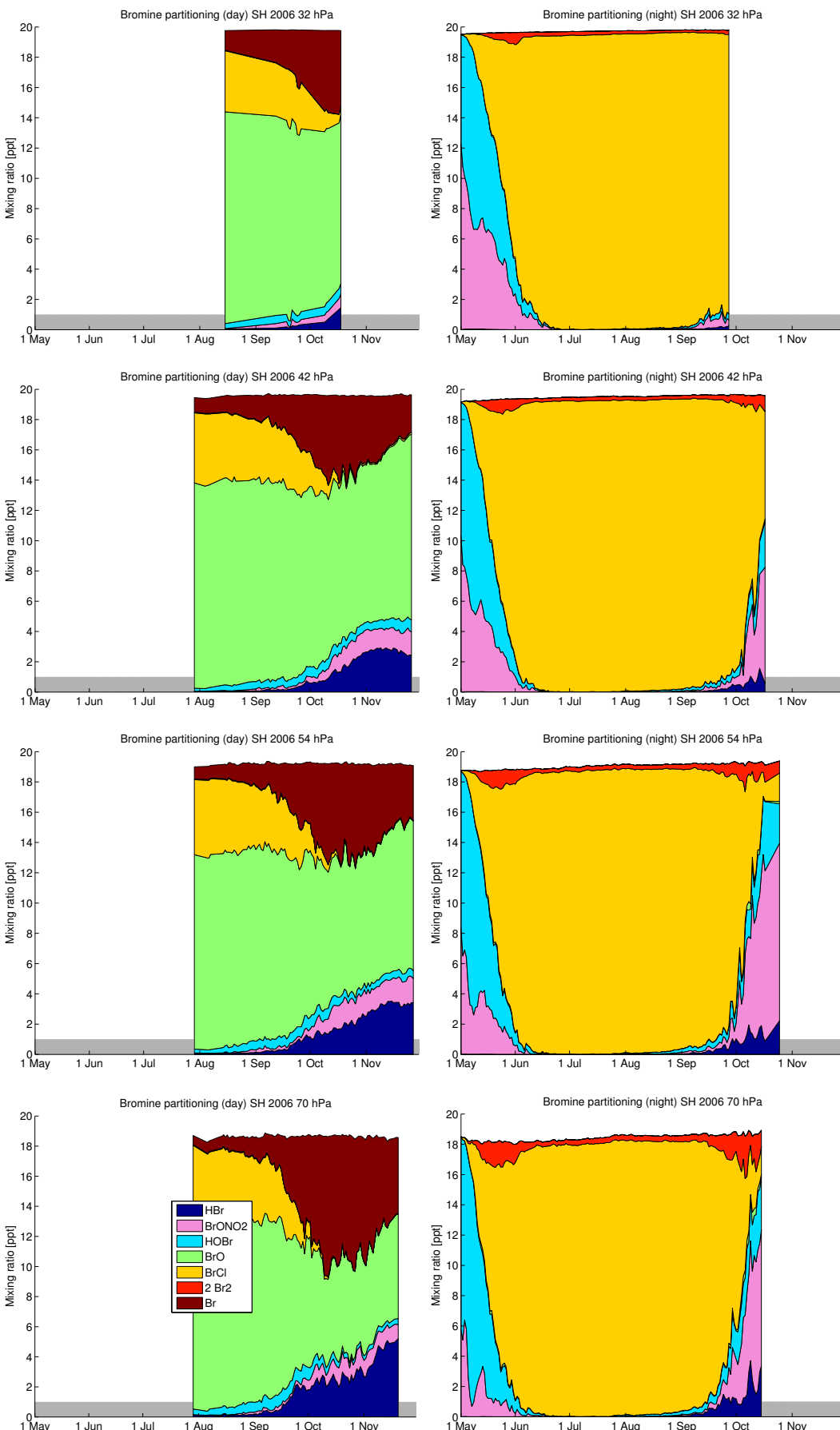


Figure 142: Vortex-averaged partitioning of inorganic bromine species. Left: Daytime averages (parts of the vortex where the solar zenith angle is smaller than 80°). Right: Nighttime averages (parts of the vortex where the solar zenith angle is larger than 100°). Days without sufficient data for averaging are not shown (grey bars).

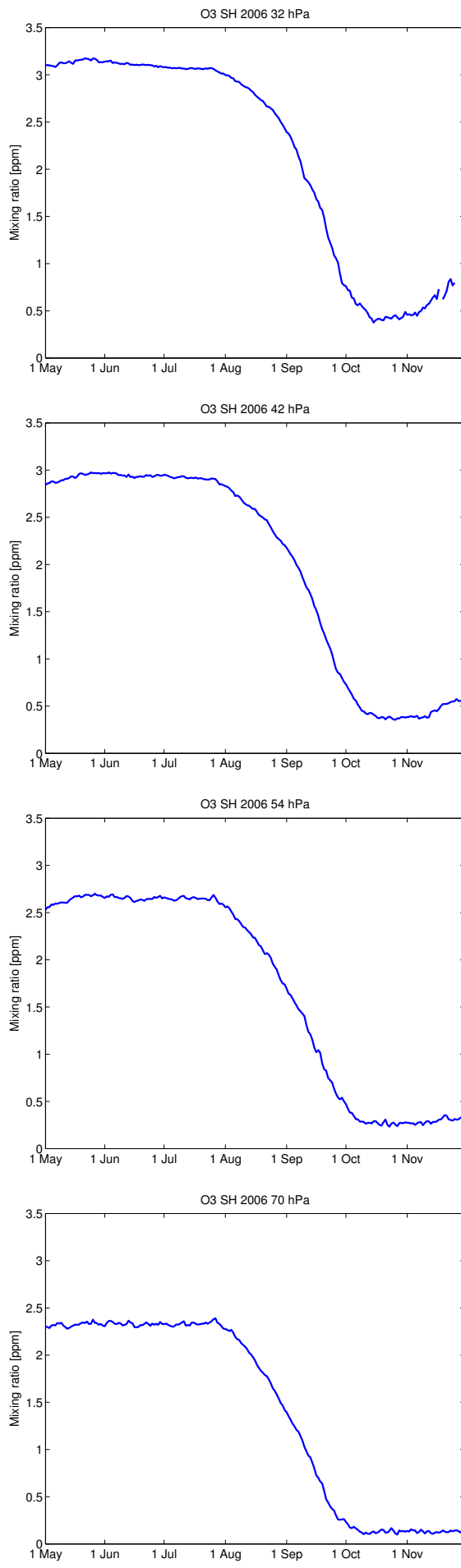


Figure 143: Vortex-averaged ozone mixing ratios.

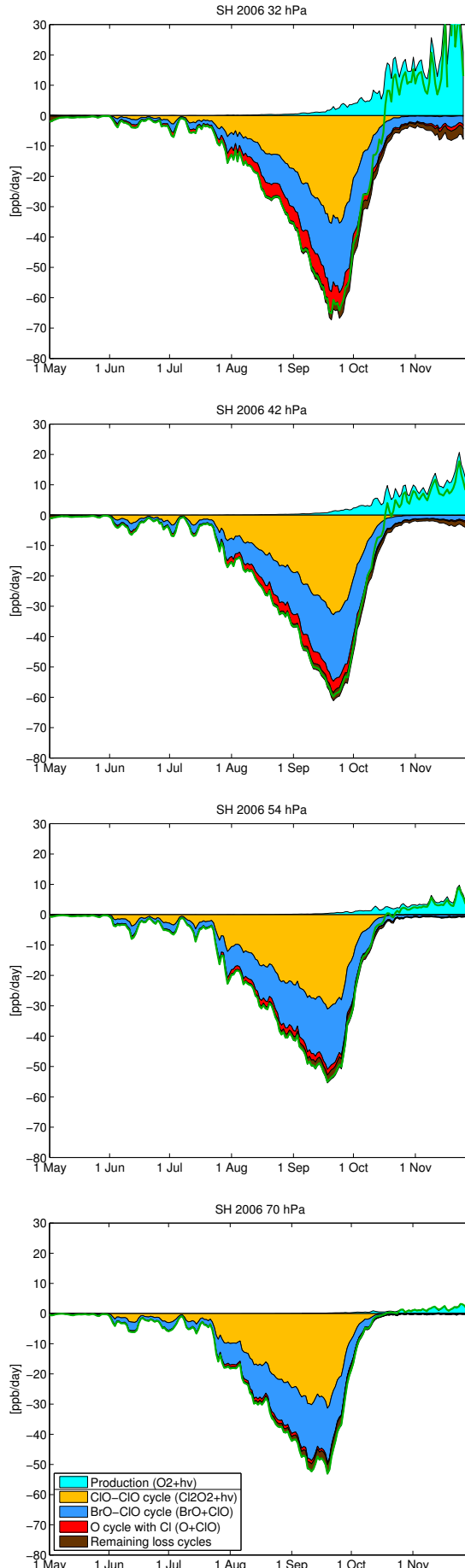


Figure 144: Vortex-averaged net chemical change of odd oxygen. The green line shows the net chemical change rate of ozone, which nearly equals the change rate of odd oxygen. The contribution of different catalytic cycles to the ozone loss is shown by the reaction rates of their rate limiting step. Only the three most important cycles are shown, the contribution of other cycles is small. Ozone production, which is almost exclusively by the $O_2 + h\nu$ reaction, is shown in cyan.

3 Comparison to measurements of MLS and ACE-FTS

Comparisons to MLS at 46 hPa (northern and southern hemisphere)

Backward trajectory calculations starting at the time and location of the satellite measurements of MLS (version 3 data) and ending at the time of the last model output before the measurement were performed for all measurements on the 15th of every month at 46 hPa and for the species ClO, HCl, H₂O, HNO₃, N₂O and O₃. Then, the chemical box model was initialized with the model data and the evolution of the species was calculated forward in time to obtain values to compare with the satellite measurements. Model results are shown on the left side and measurements on the right side.

Comparisons to ACE-FTS (southern hemisphere, all altitudes)

Comparisons with ACE-FTS were performed with the same method as for MLS. Since ACE-FTS is a solar occultation instrument, the number of measurements is limited and all measurements of a month are shown in the same plot as a function of equivalent latitude and altitude. Species are H₂O, O₃, CH₄, HCl, ClONO₂, N₂O, NO, NO₂, N₂O₅, HNO₃. Model results are shown on the left side and measurements on the right side.

3.1 Northern hemisphere 2004/2005

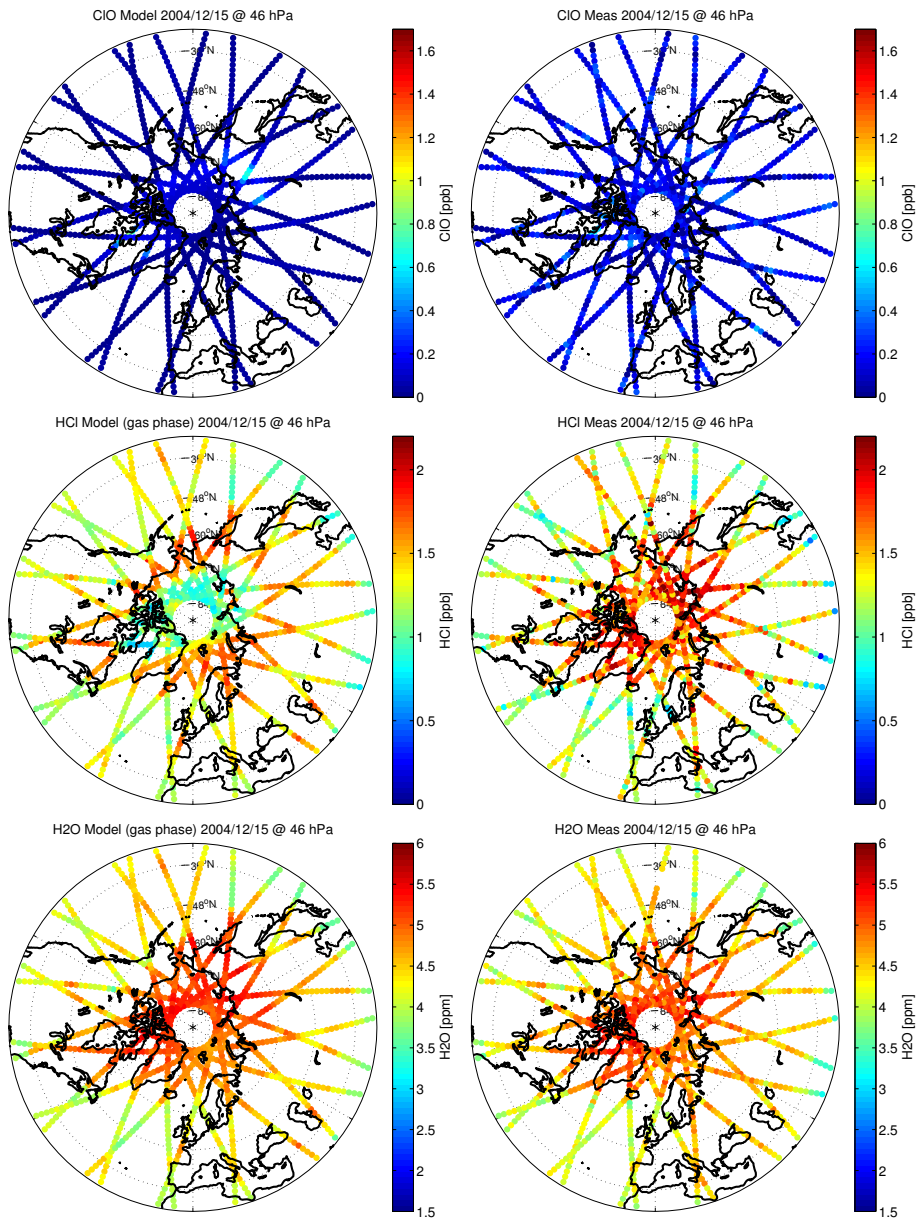


Figure 145: ClO, HCl and H₂O modelled by ATLAS (left) and measured by MLS (right) on 15 December 2004

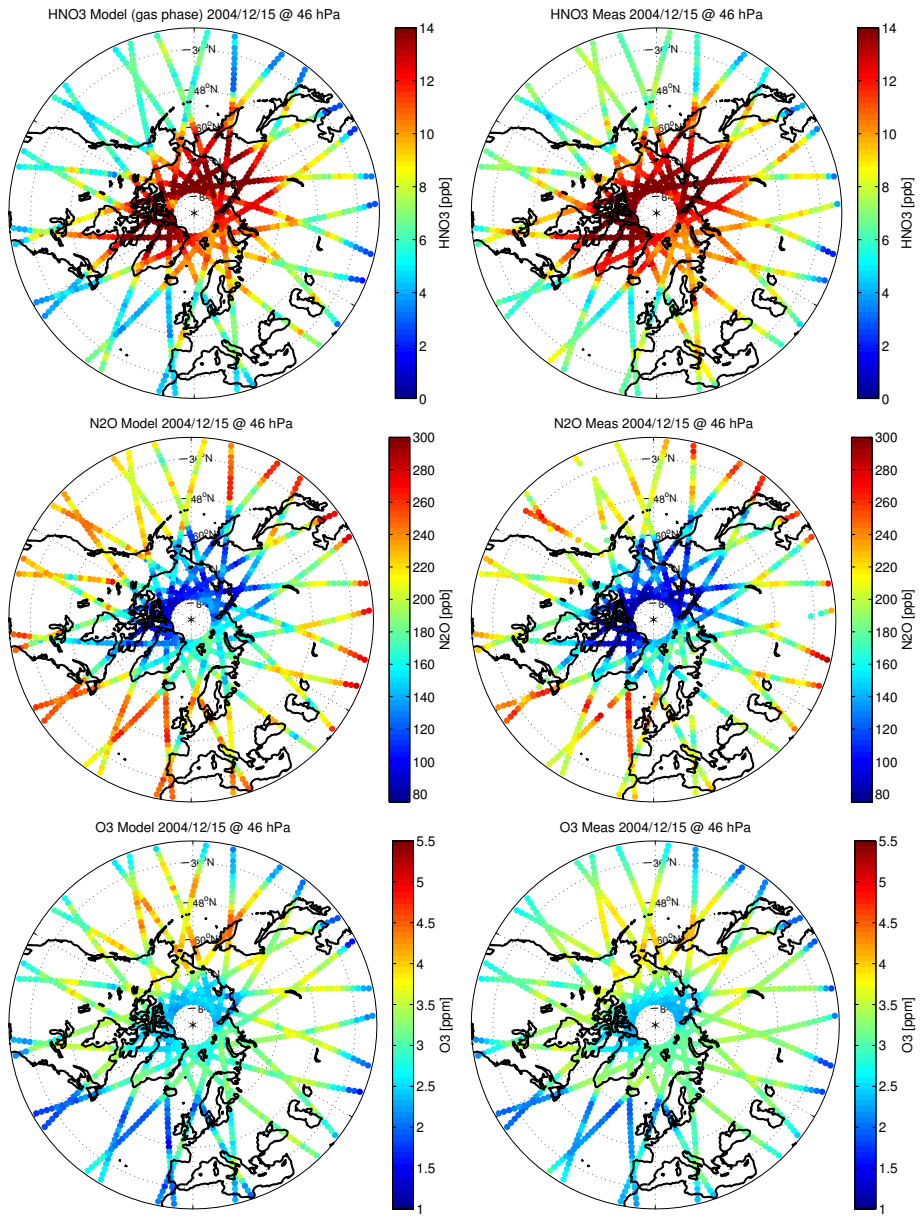


Figure 146: HNO₃, N₂O and O₃ at 46 hPa modelled by ATLAS (left) and measured by MLS (right) on 15 December 2004

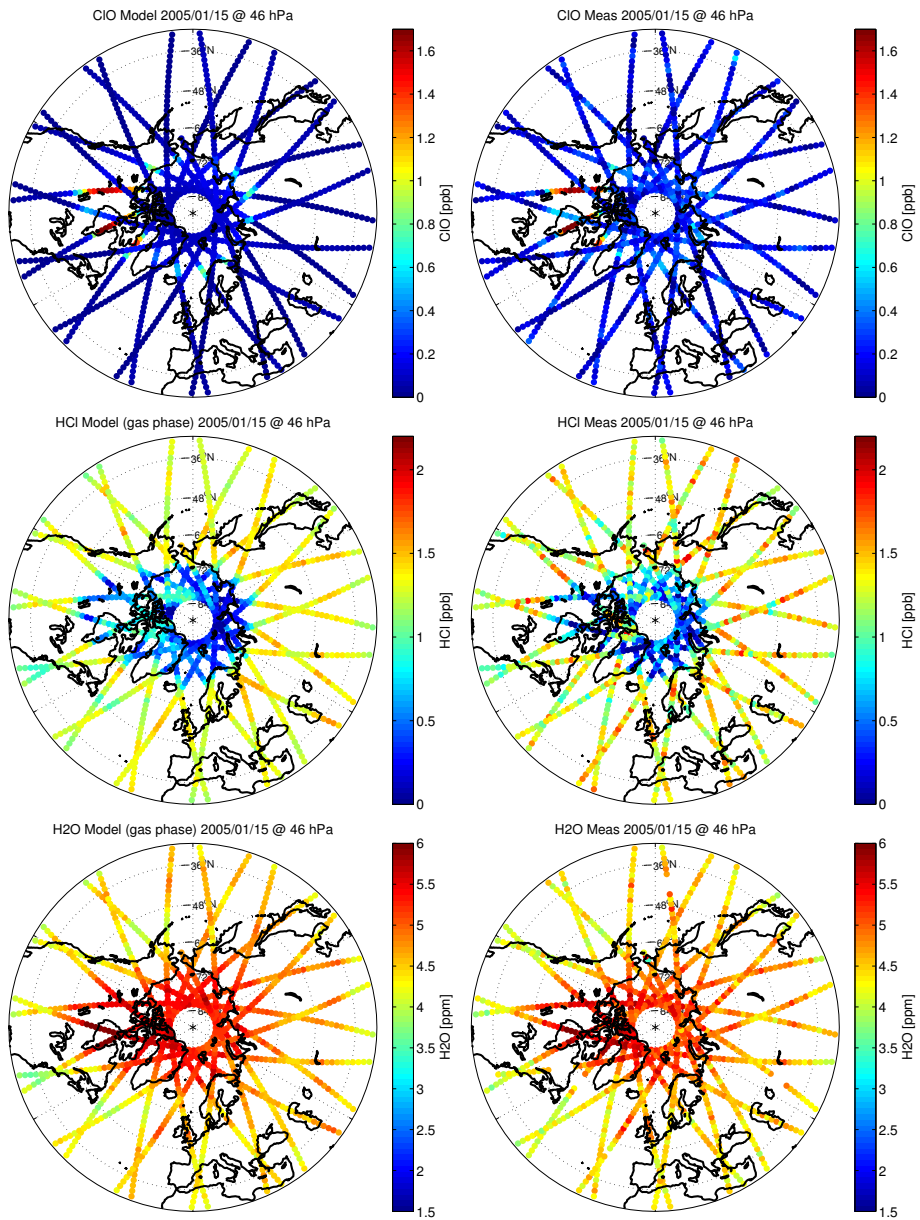


Figure 147: ClO, HCl and H₂O modelled by ATLAS (left) and measured by MLS (right) on 15 January 2005

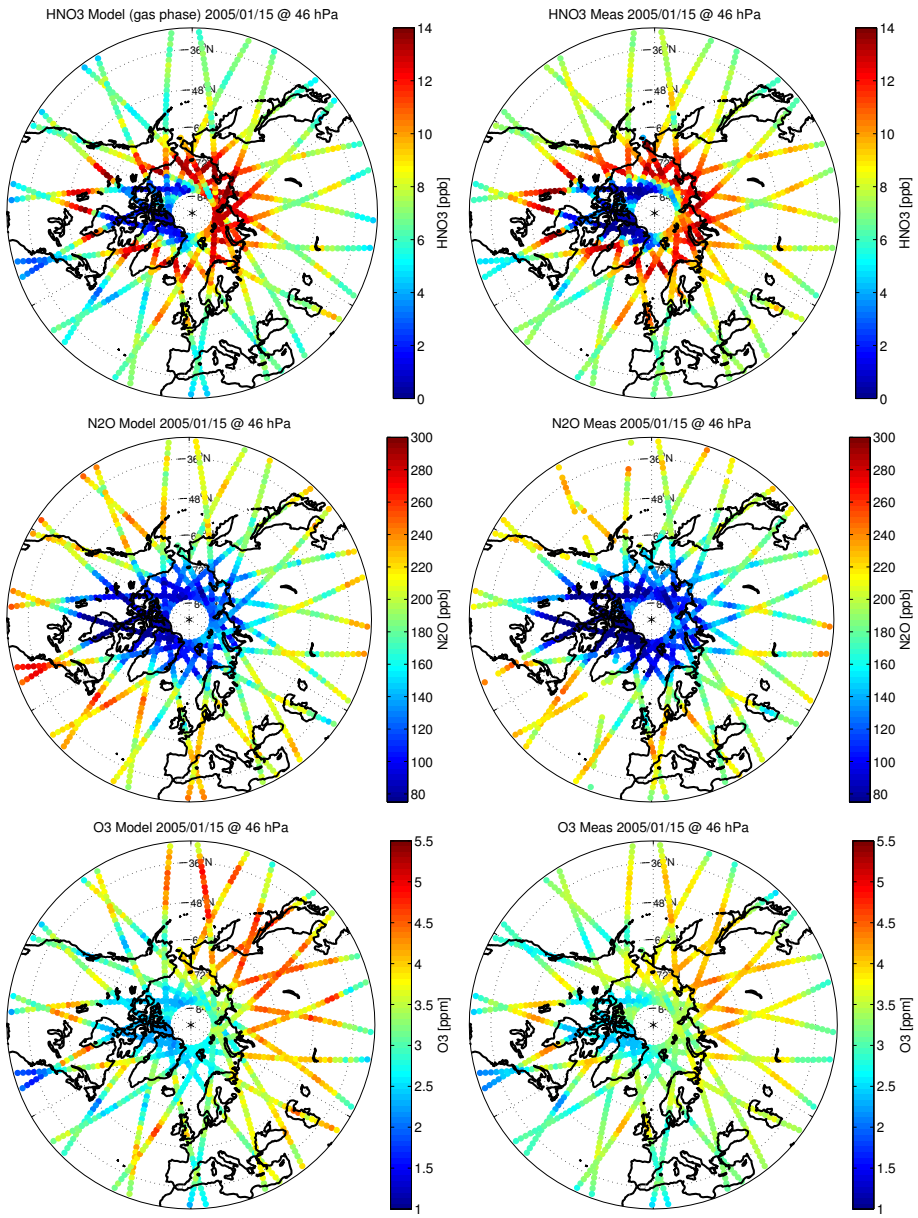


Figure 148: HNO₃, N₂O and O₃ at 46 hPa modelled by ATLAS (left) and measured by MLS (right) on 15 January 2005

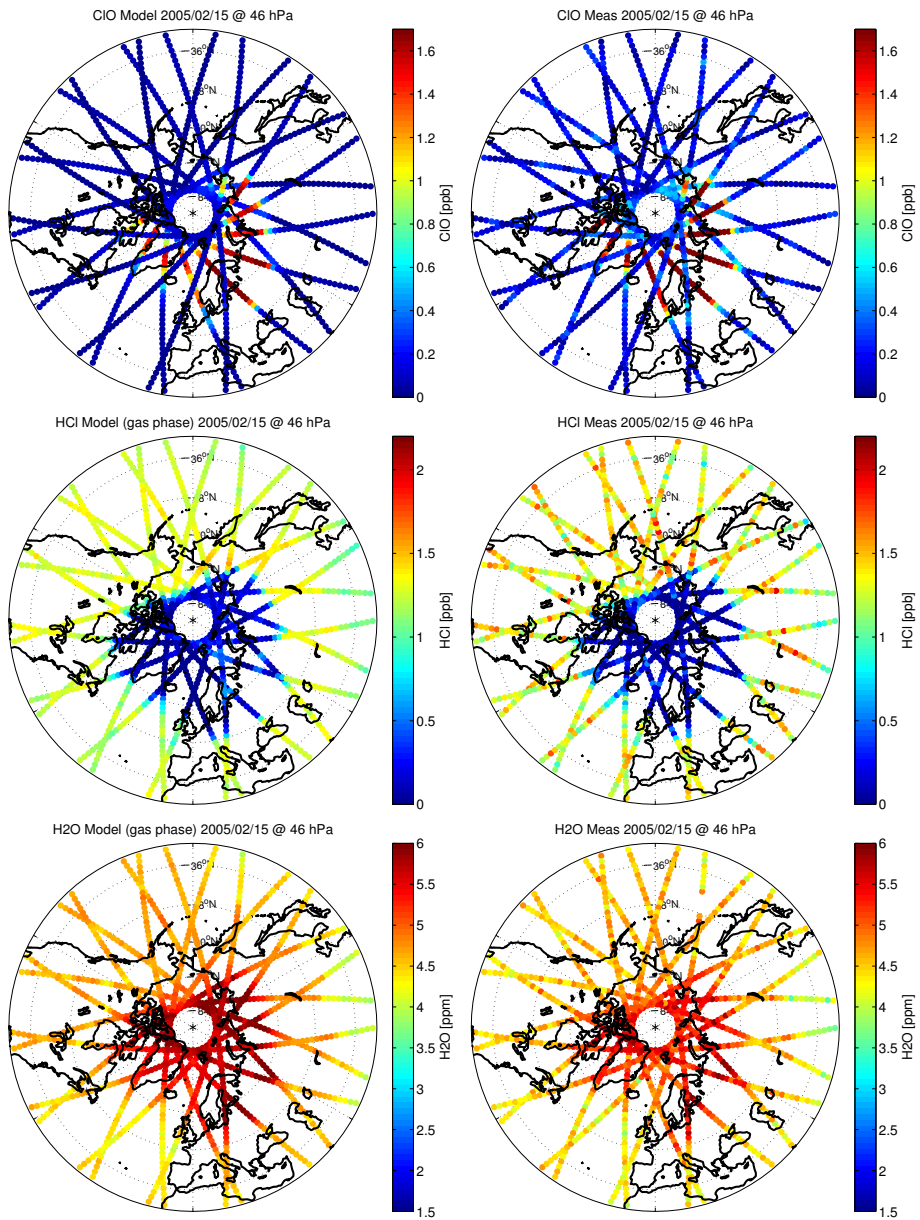


Figure 149: ClO, HCl and H₂O modelled by ATLAS (left) and measured by MLS (right) on 15 February 2005

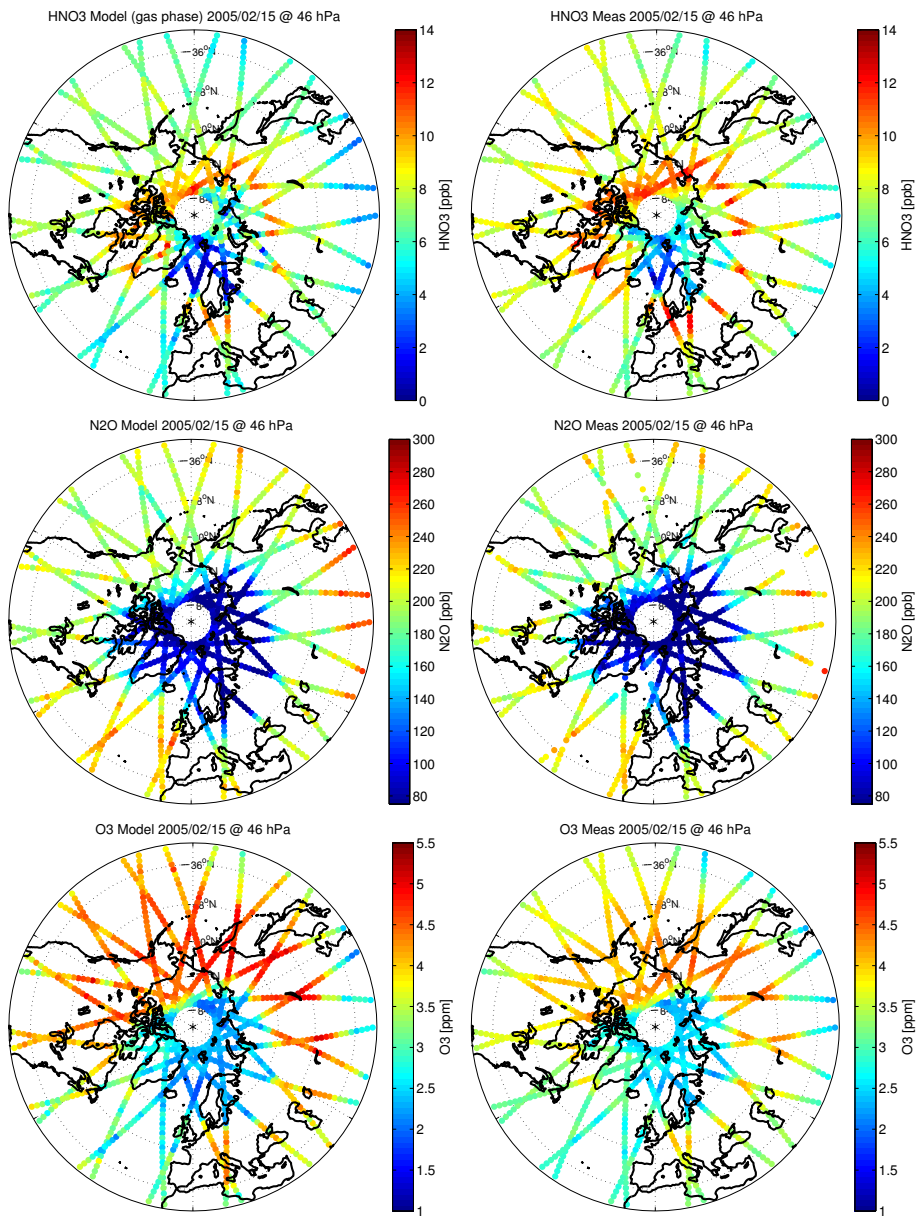


Figure 150: HNO₃, N₂O and O₃ at 46 hPa modelled by ATLAS (left) and measured by MLS (right) on 15 February 2005

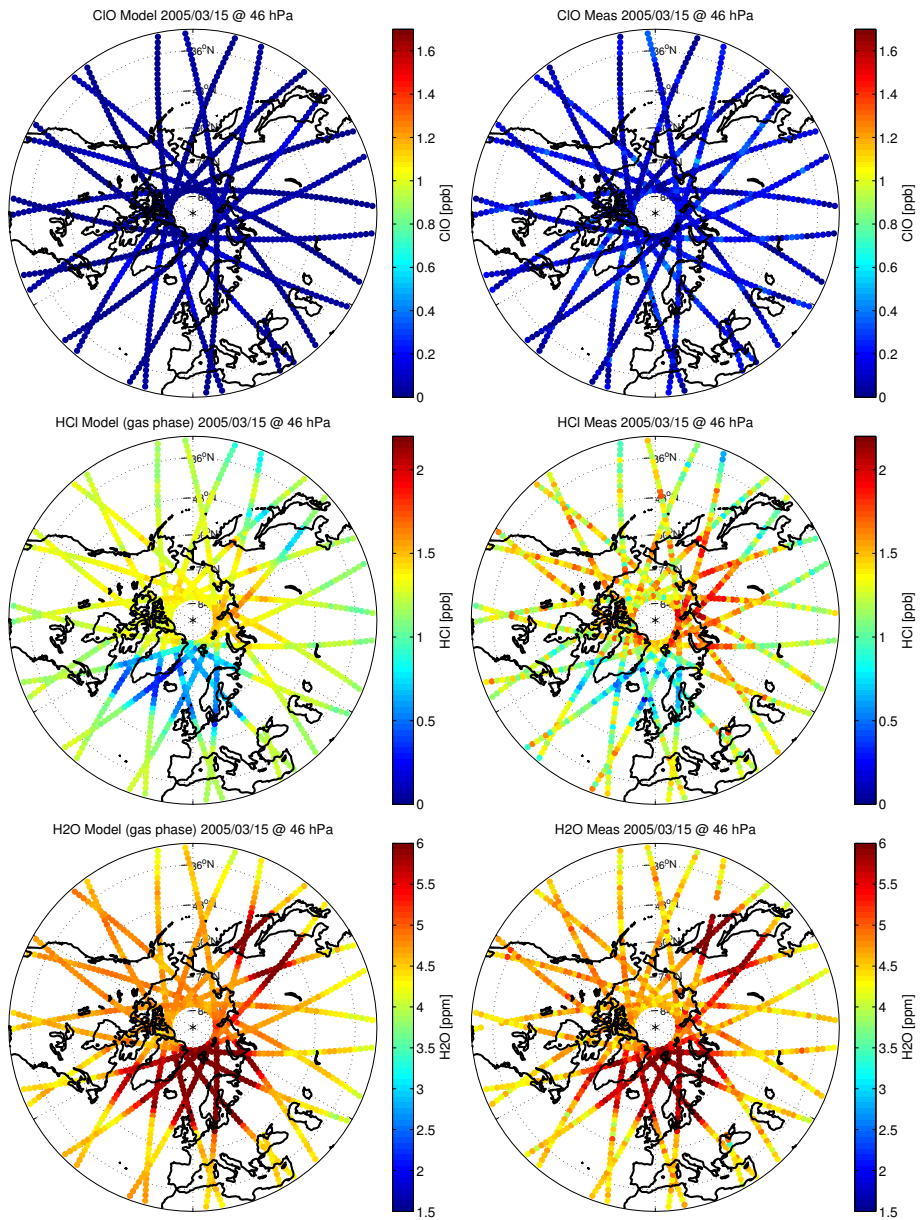


Figure 151: ClO, HCl and H₂O modelled by ATLAS (left) and measured by MLS (right) on 15 March 2005

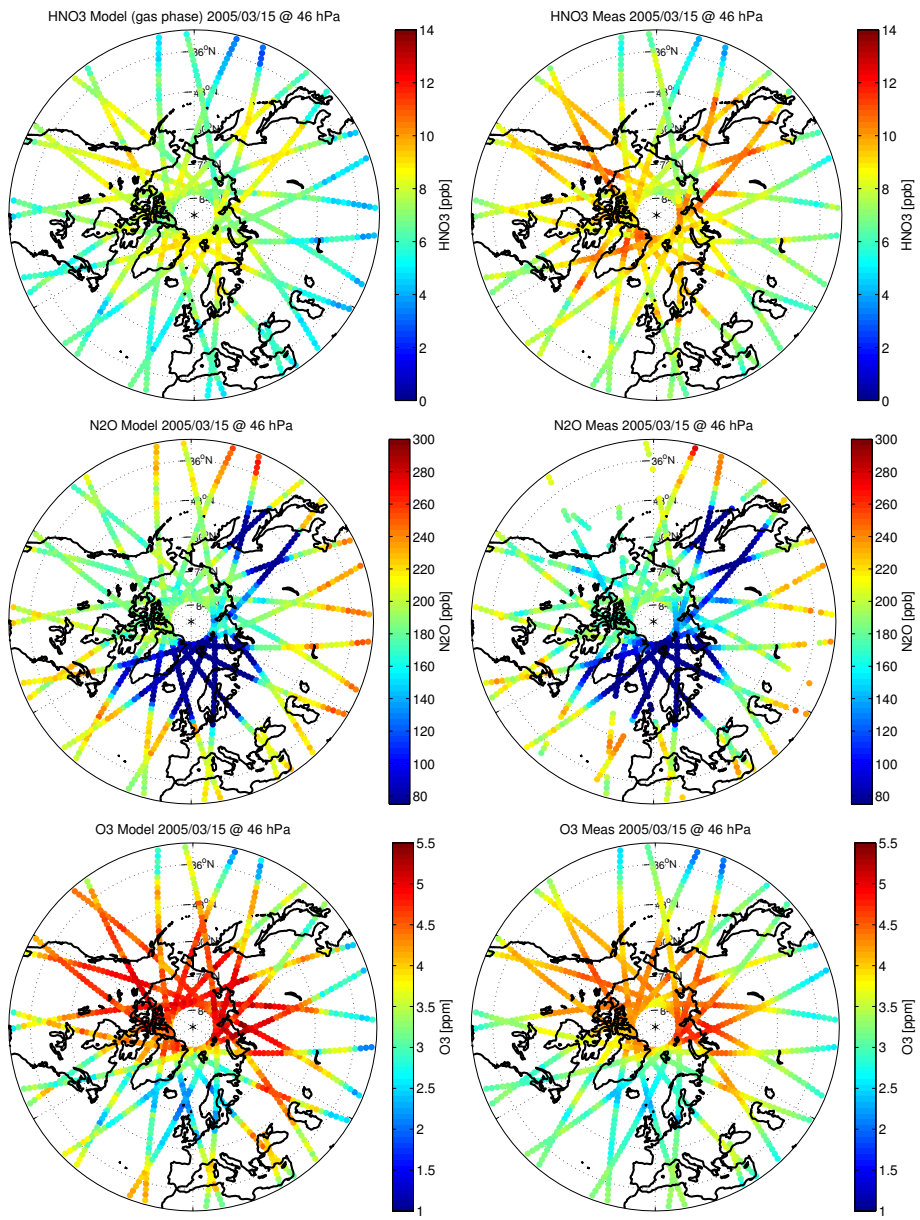


Figure 152: HNO₃, N₂O and O₃ at 46 hPa modelled by ATLAS (left) and measured by MLS (right) on 15 March 2005

3.2 Southern hemisphere 2006

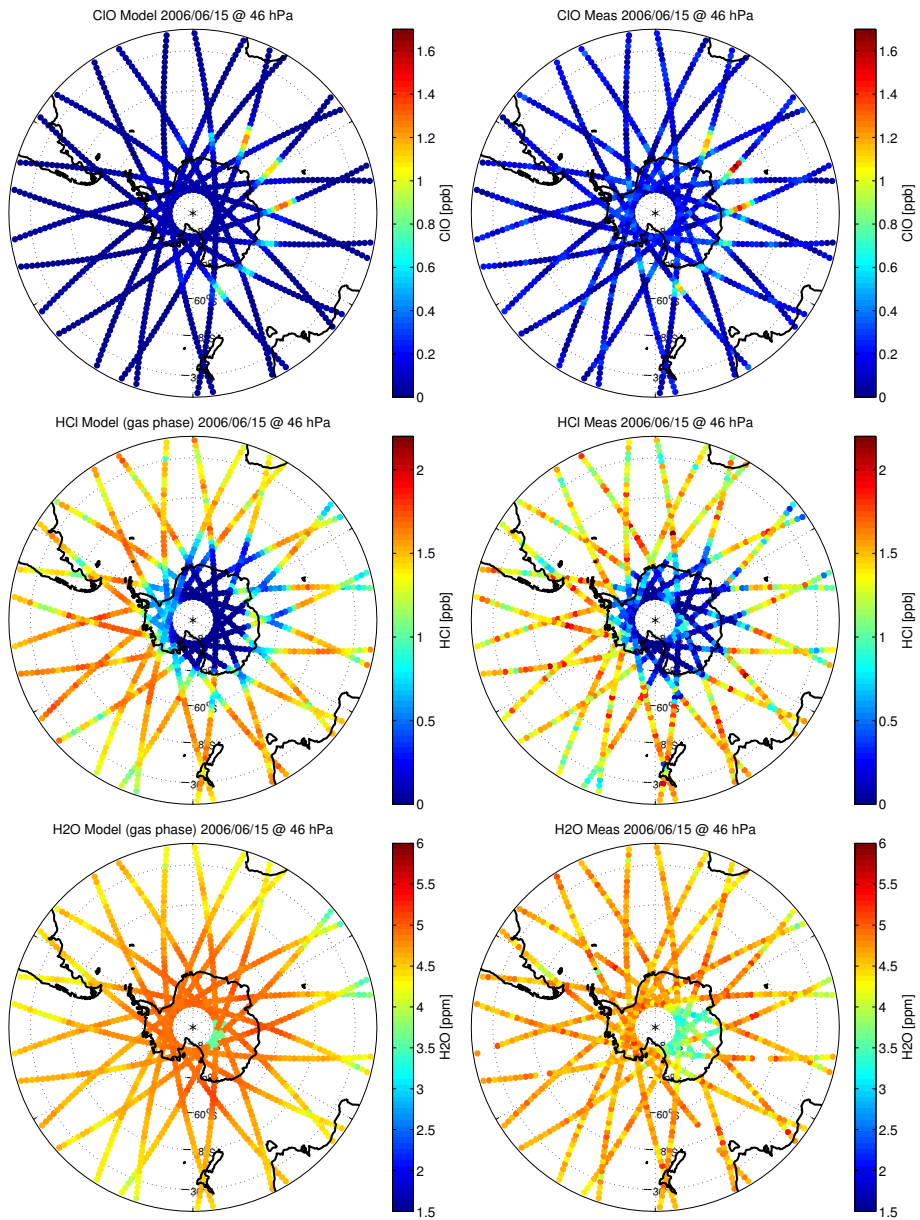


Figure 153: ClO, HCl and H₂O modelled by ATLAS (left) and measured by MLS (right) on 15 June 2006

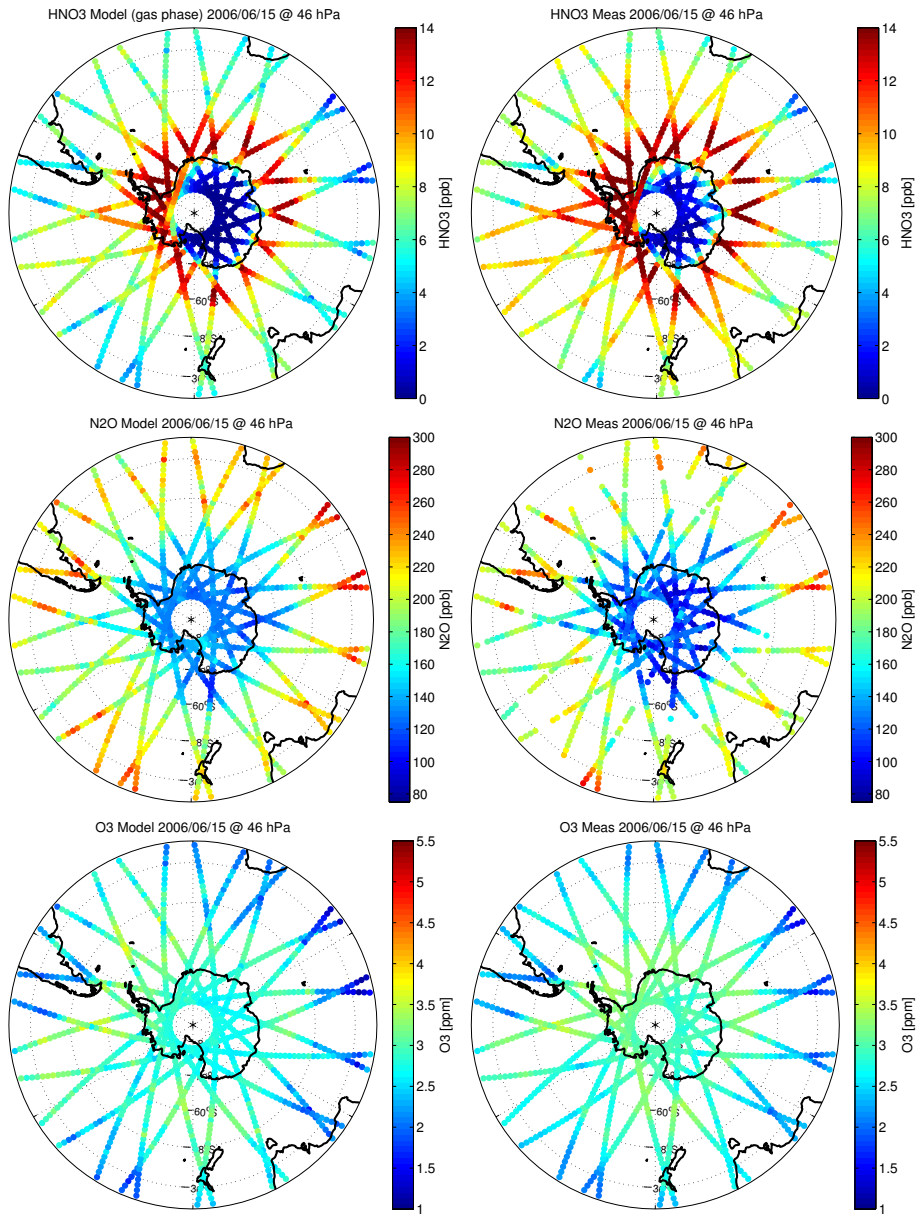


Figure 154: HNO₃, N₂O and O₃ at 46 hPa modelled by ATLAS (left) and measured by MLS (right) on 15 June 2006

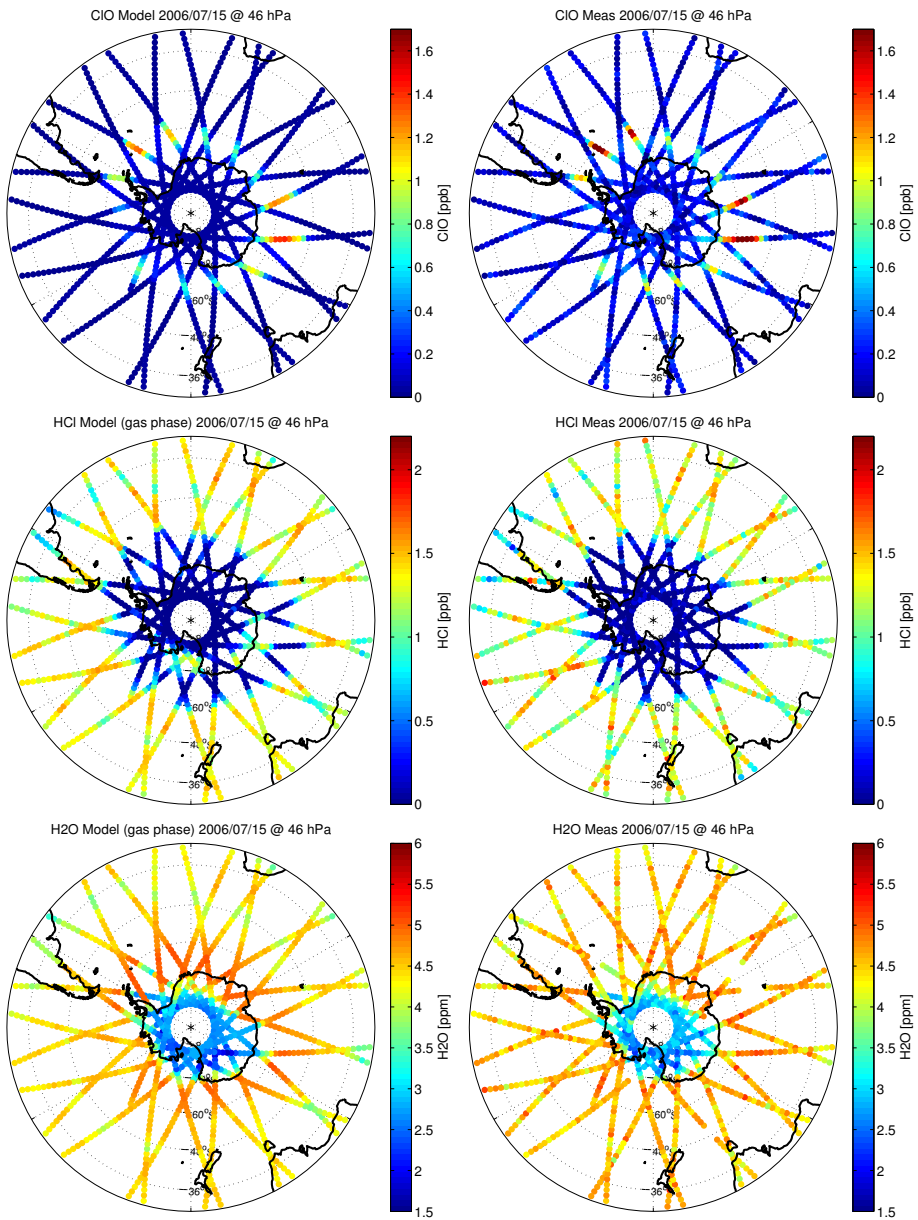


Figure 155: ClO, HCl and H₂O at 46 hPa modelled by ATLAS (left) and measured by MLS (right) on 15 July 2006

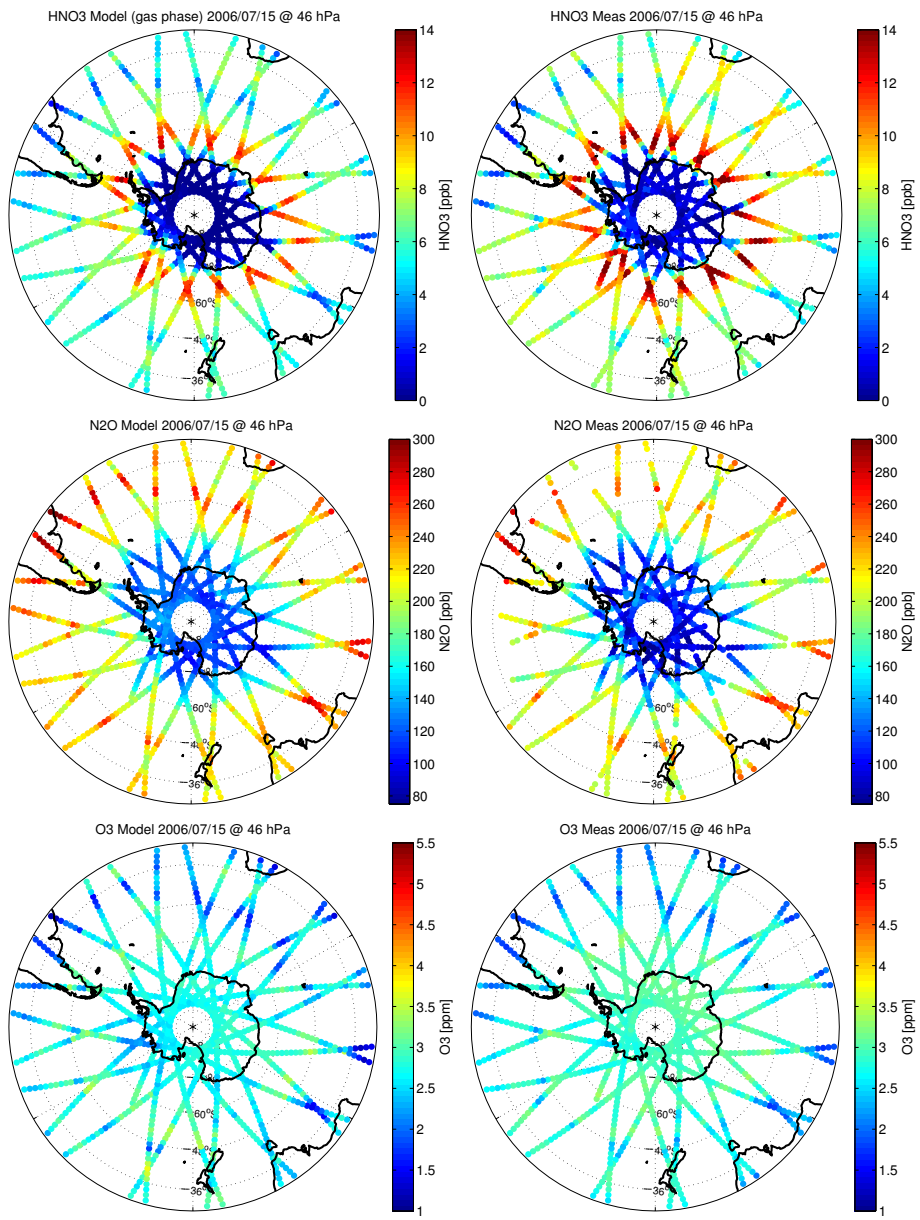


Figure 156: HNO₃, N₂O and O₃ at 46 hPa modelled by ATLAS (left) and measured by MLS (right) on 15 July 2006

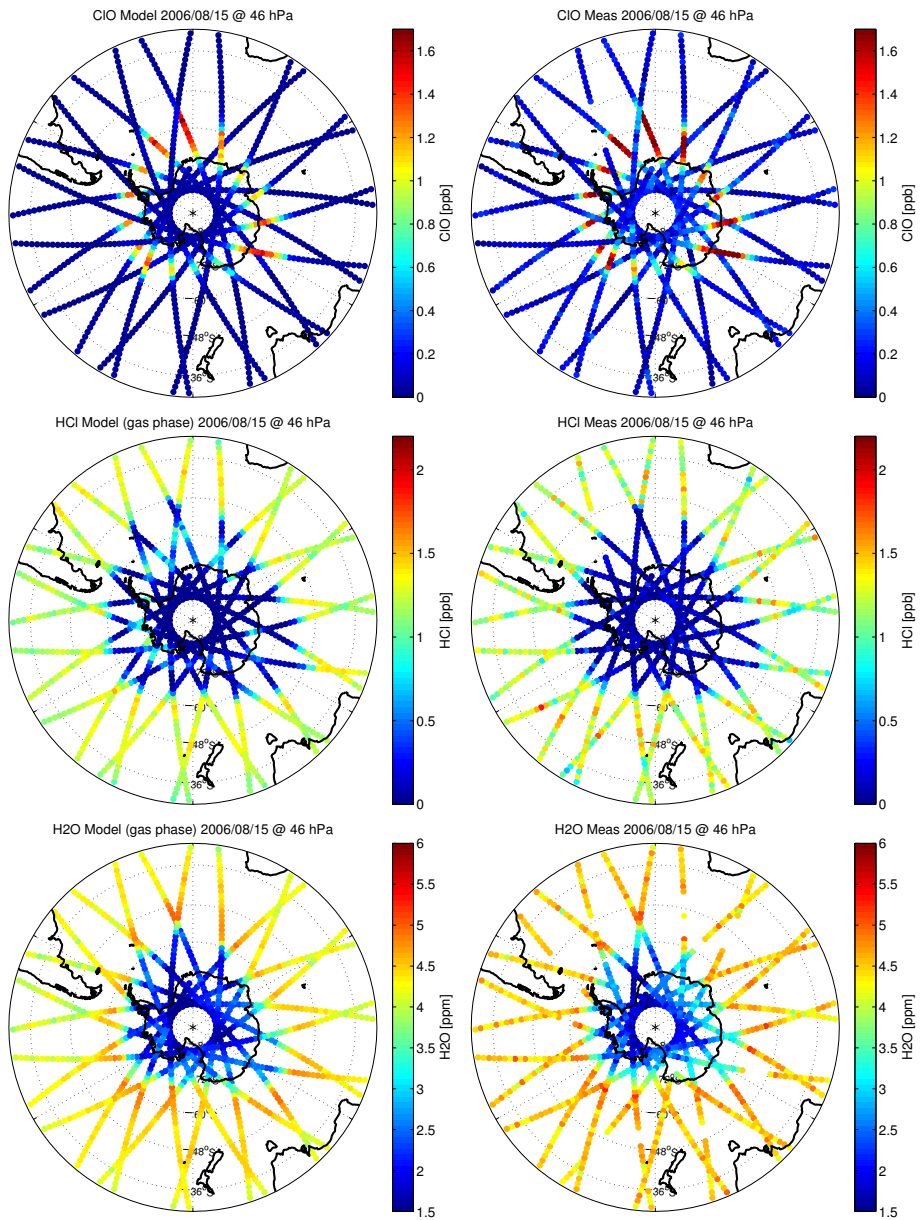


Figure 157: ClO, HCl and H₂O at 46 hPa modelled by ATLAS (left) and measured by MLS (right) on 15 August 2006

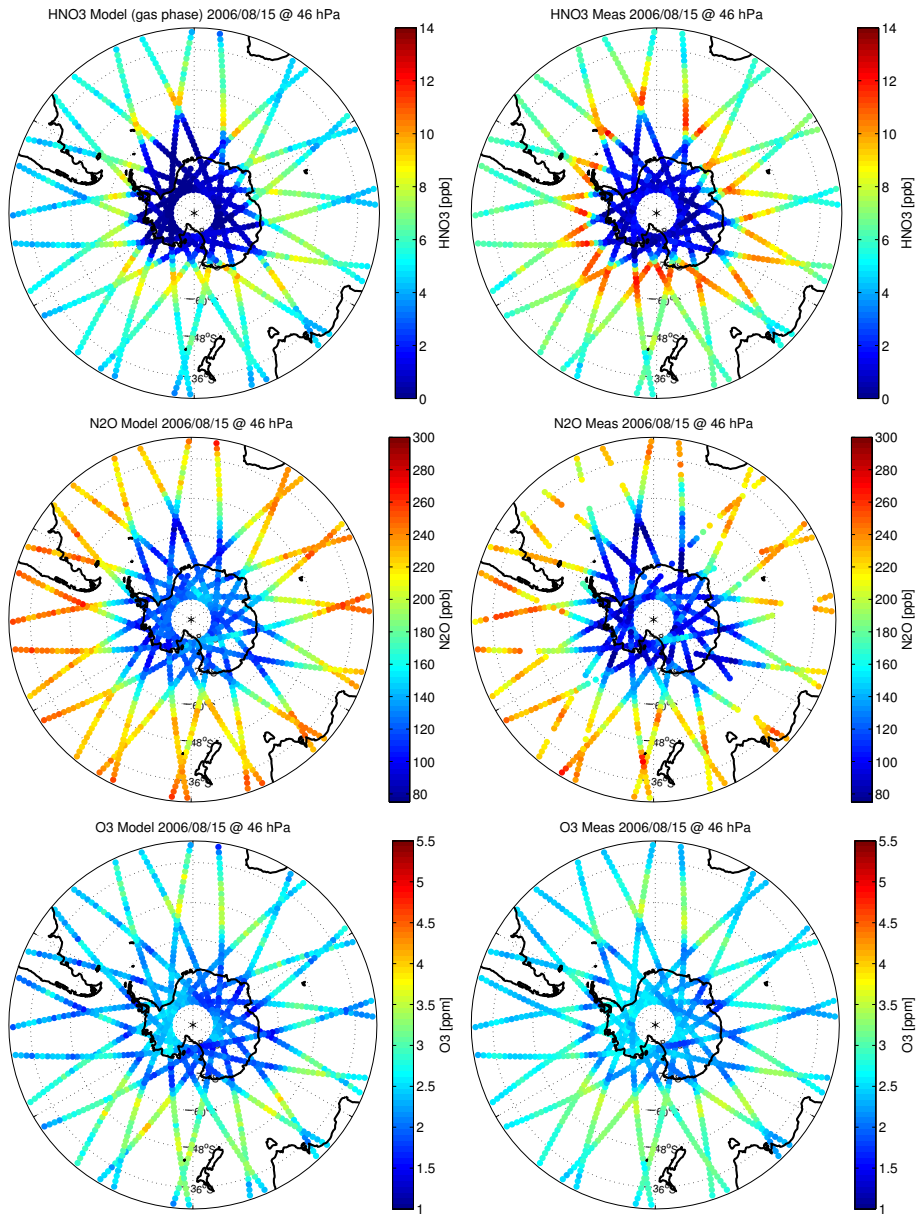


Figure 158: HNO₃, N₂O and O₃ at 46 hPa modelled by ATLAS (left) and measured by MLS (right) on 15 August 2006

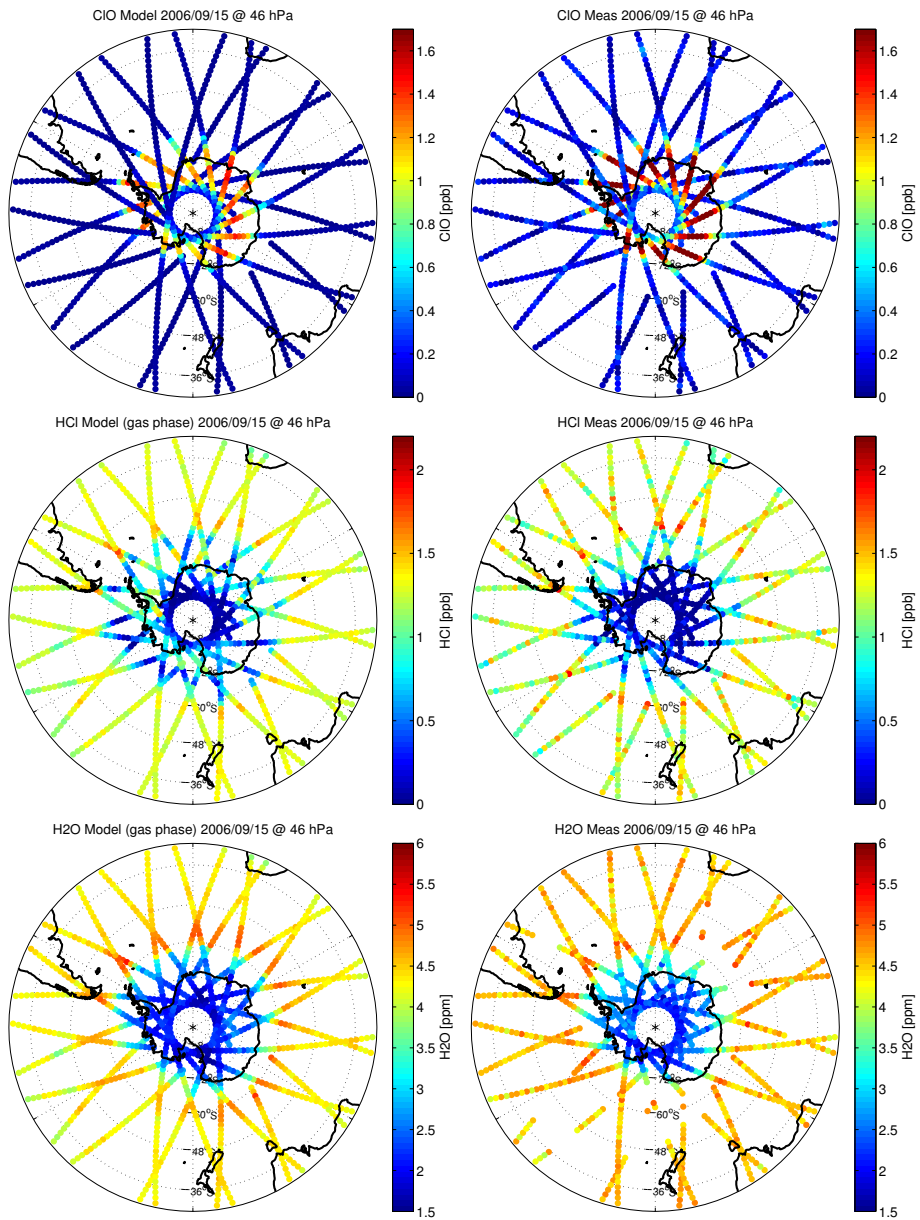


Figure 159: ClO, HCl and H₂O modelled by ATLAS (left) and measured by MLS (right) on 15 September 2006

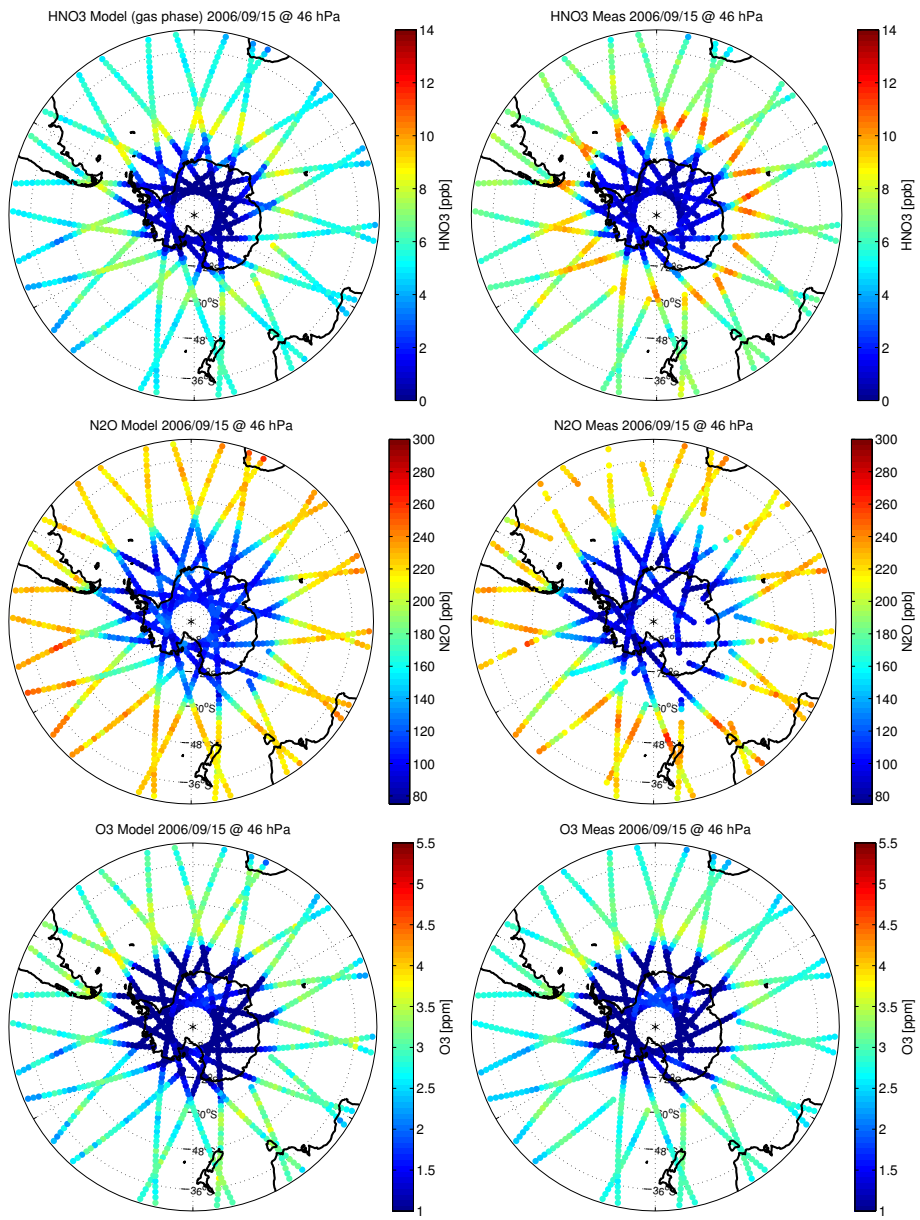


Figure 160: HNO₃, N₂O and O₃ at 46 hPa modelled by ATLAS (left) and measured by MLS (right) on 15 September 2006

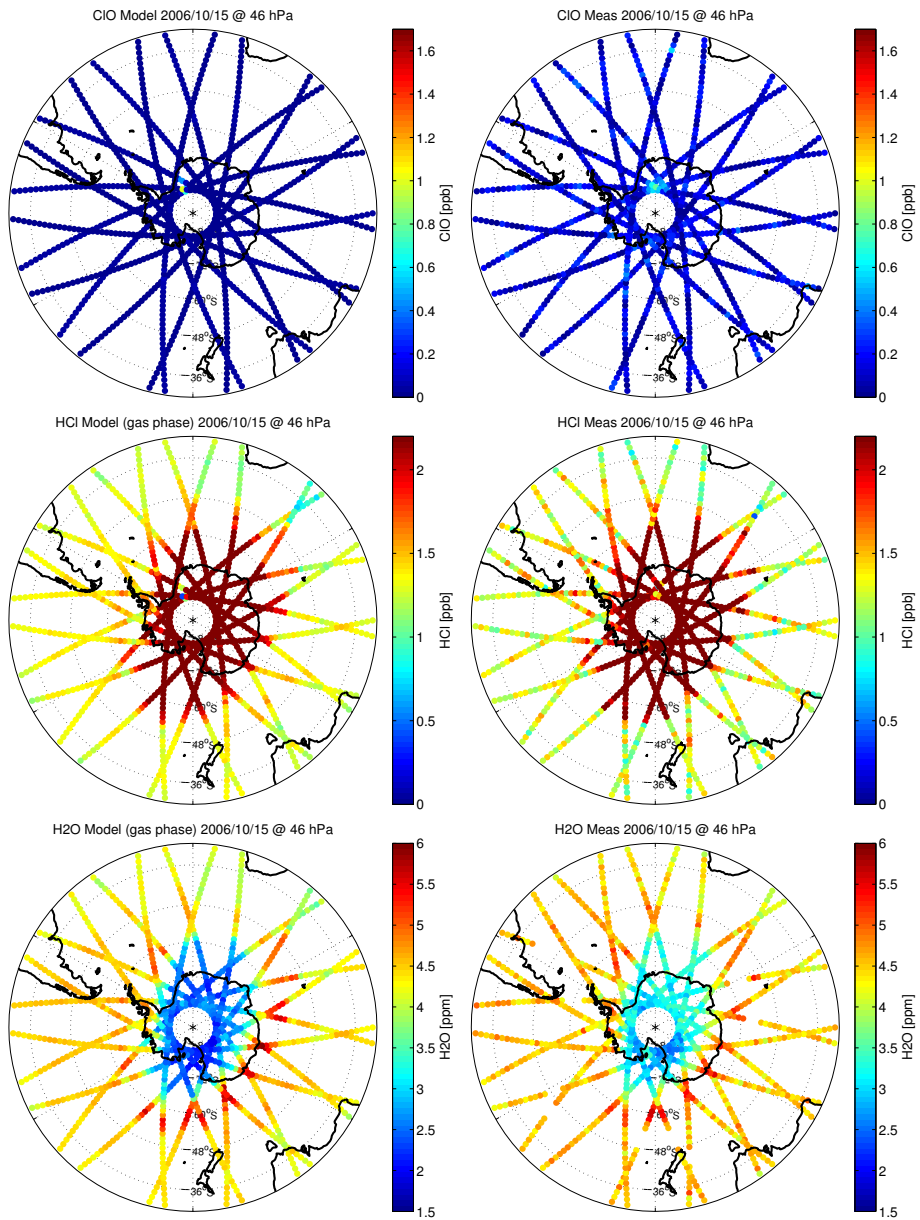


Figure 161: ClO, HCl and H₂O at 46 hPa modelled by ATLAS (left) and measured by MLS (right) on 15 October 2006

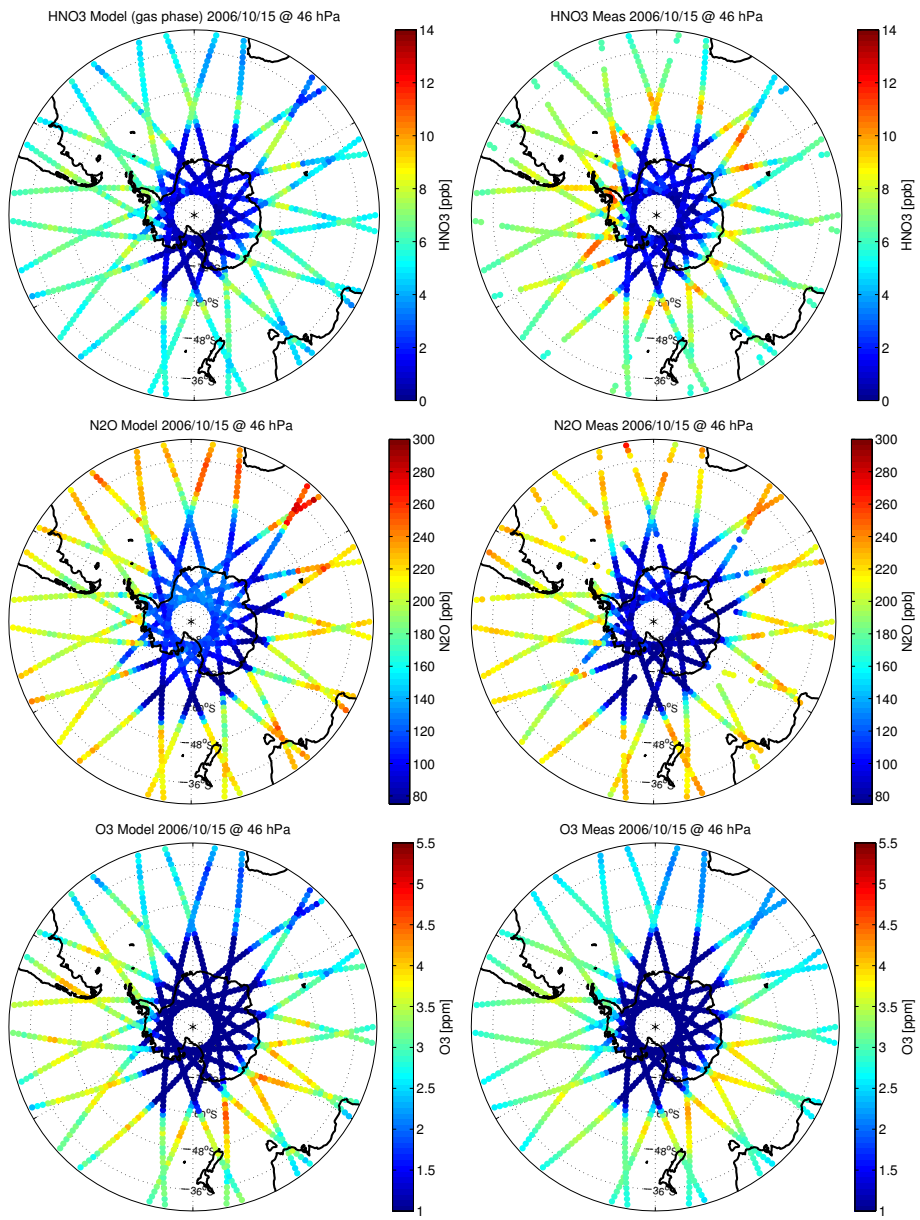


Figure 162: HNO₃, N₂O and O₃ at 46 hPa modelled by ATLAS (left) and measured by MLS (right) on 15 October 2006

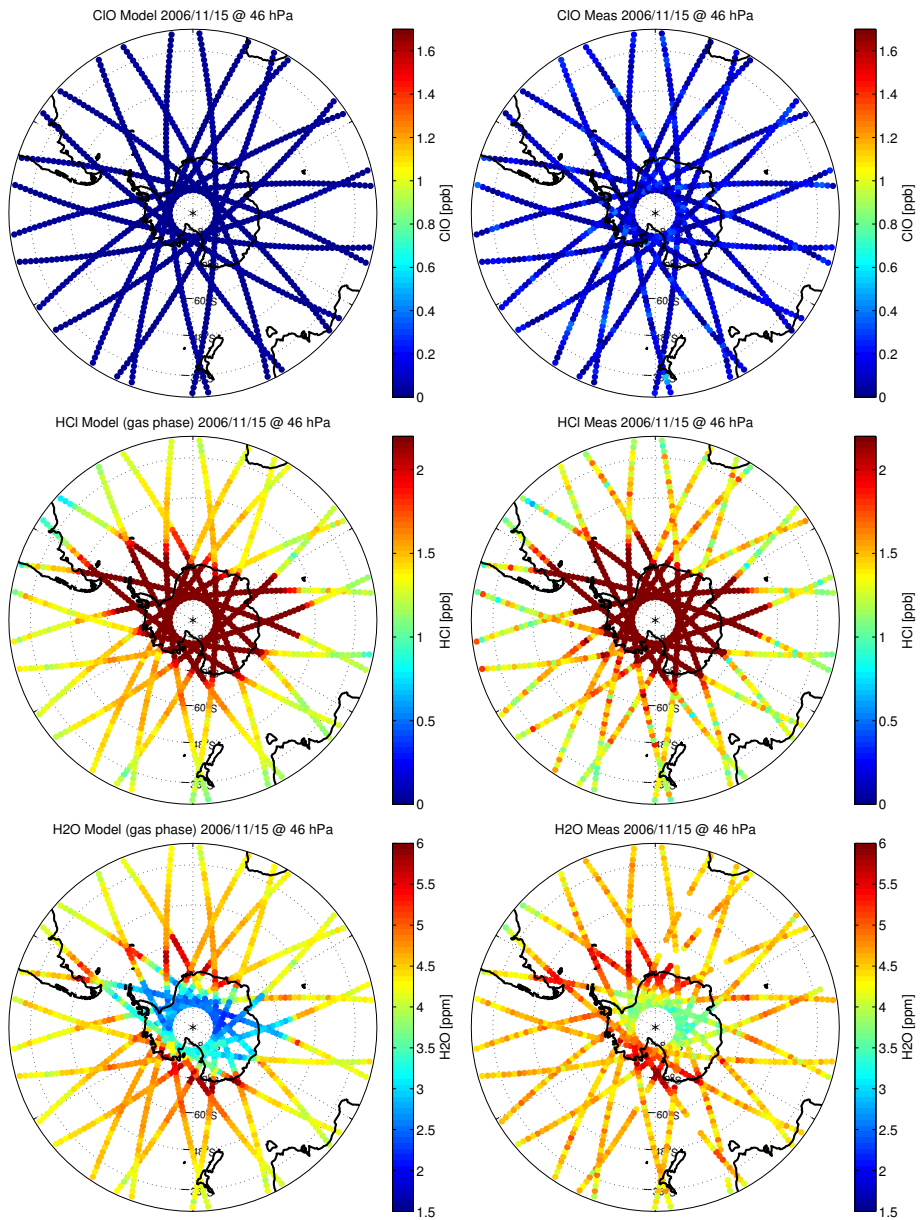


Figure 163: ClO, HCl and H₂O at 46 hPa modelled by ATLAS (left) and measured by MLS (right) on 15 November 2006

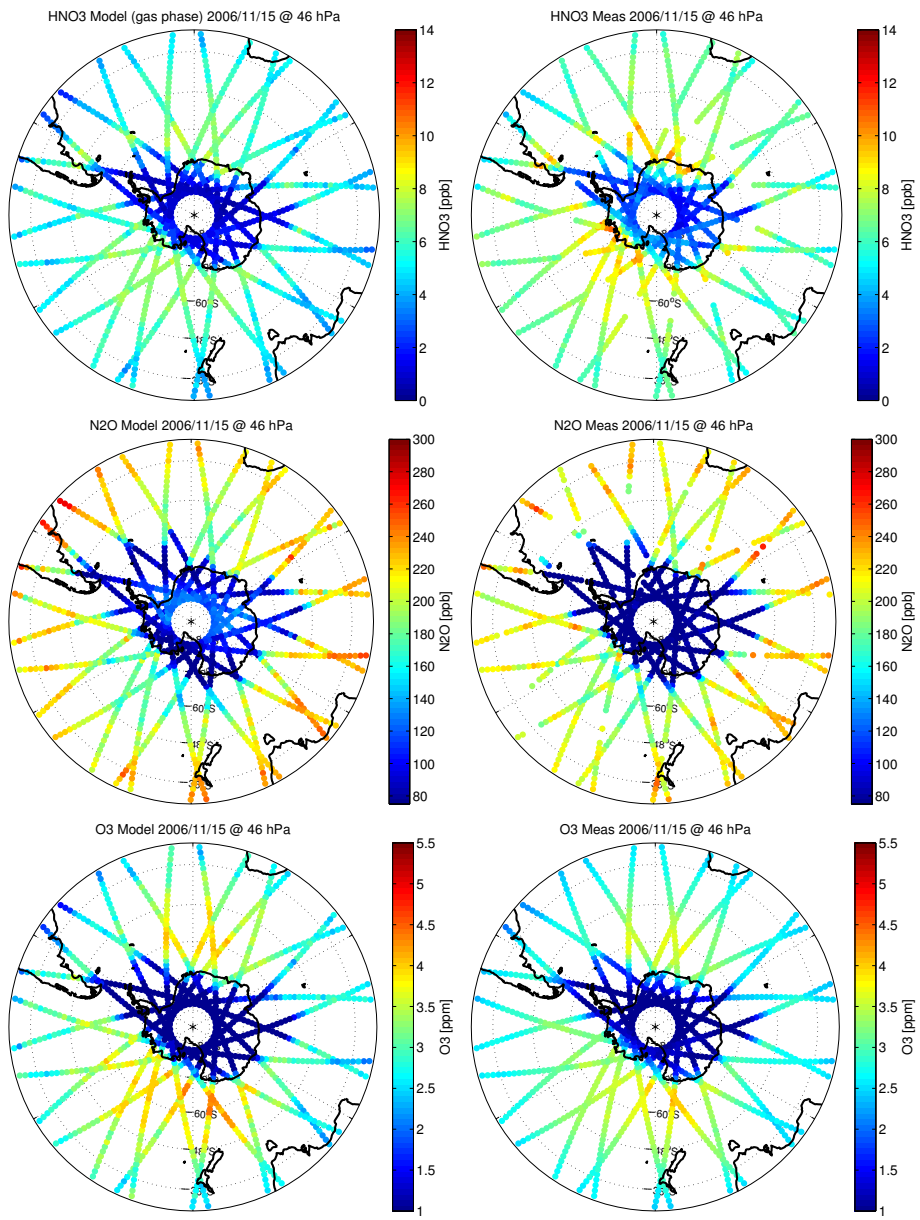


Figure 164: HNO₃, N₂O and O₃ at 46 hPa modelled by ATLAS (left) and measured by MLS (right) on 15 November 2006

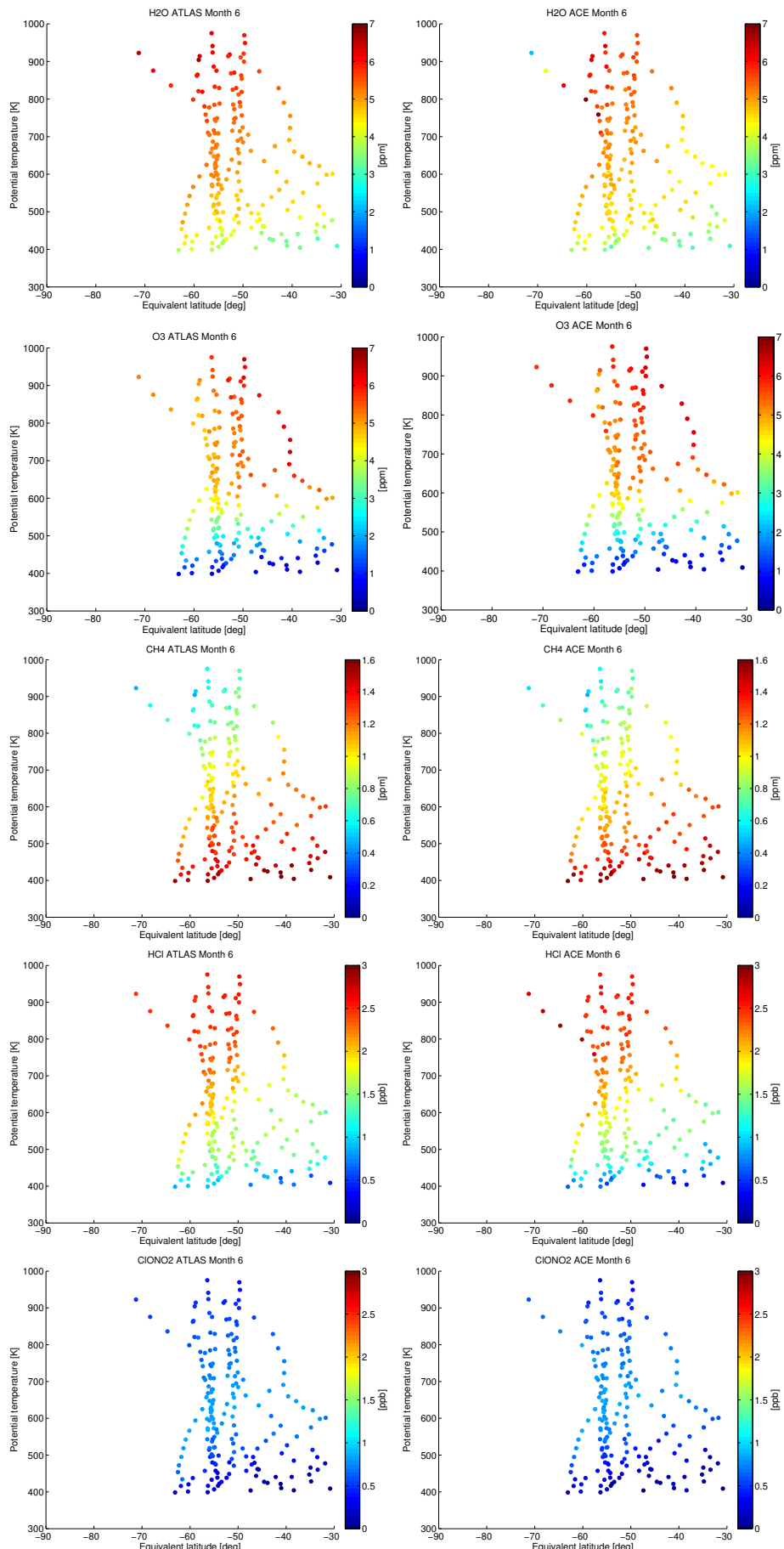


Figure 165: H₂O, O₃, CH₄, HCl, ClONO₂ modelled by ATLAS (left) and measured by ACE-FTS (right) for all measurements of June 2006

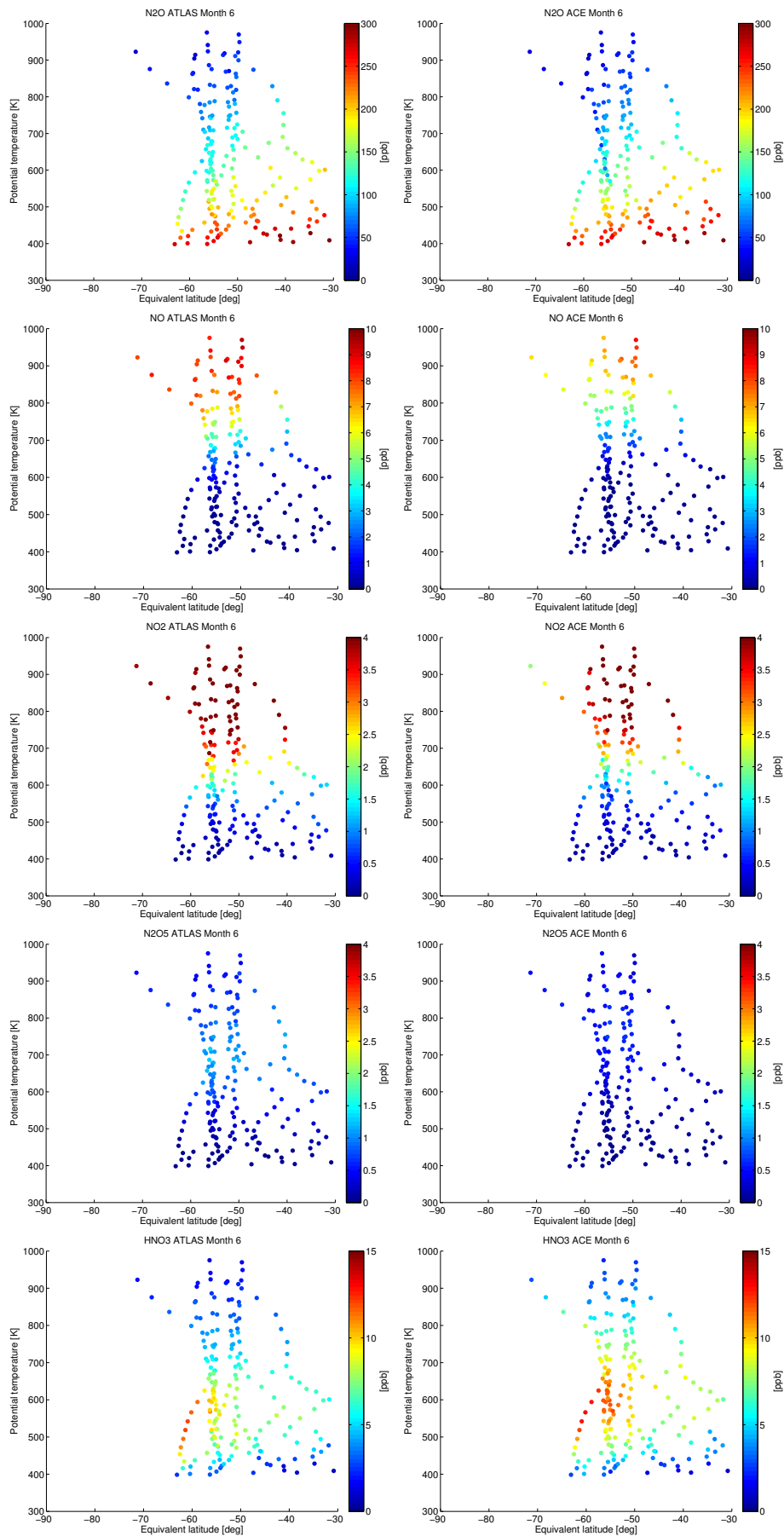


Figure 166: N₂O, NO, NO₂, N₂O₅, HNO₃ modelled by ATLAS (left) and measured by ACE-FTS (right) for all measurements of June 2006

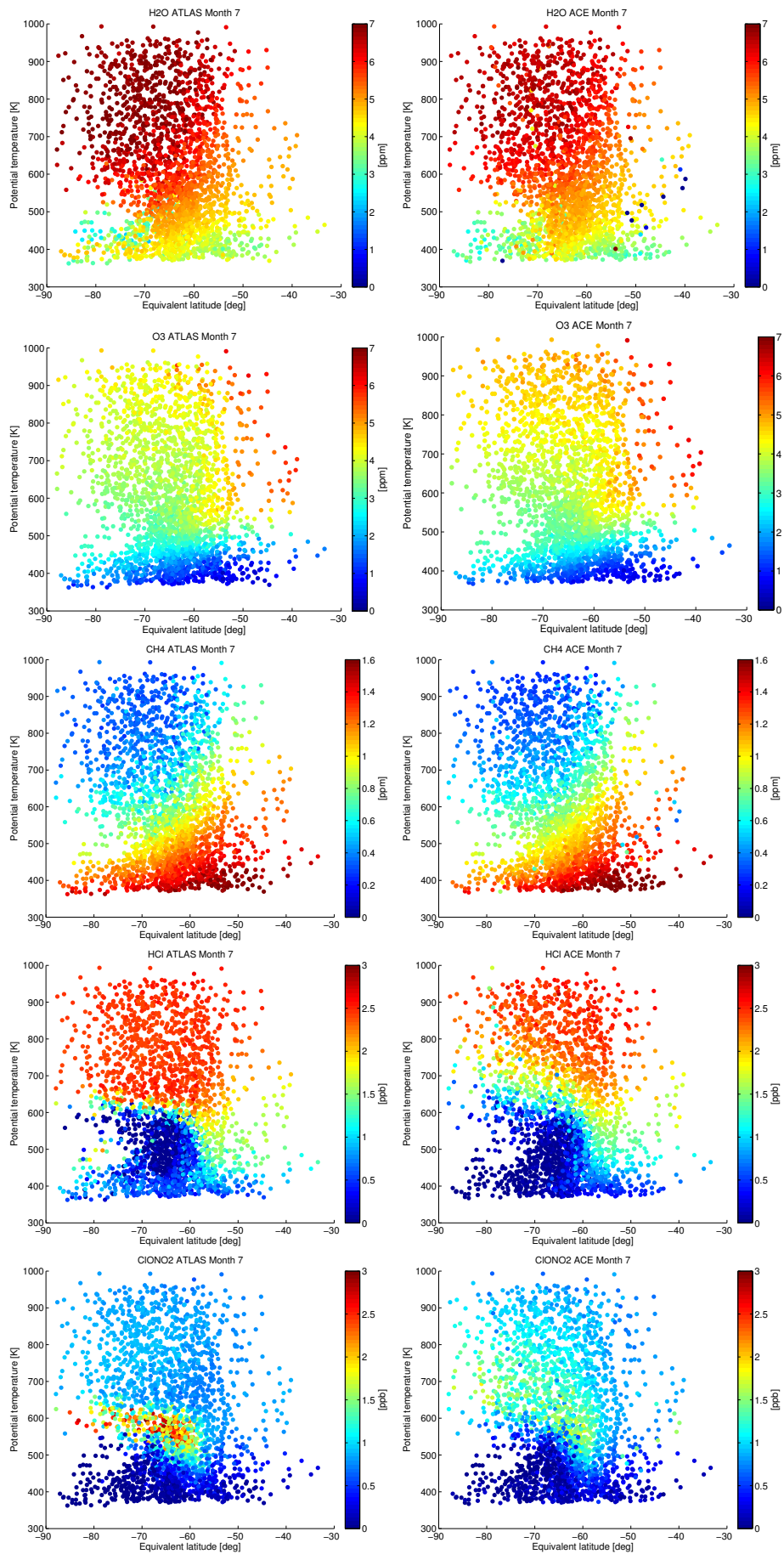


Figure 167: H₂O, O₃, CH₄, HCl, ClONO₂ modelled by ATLAS (left) and measured by ACE-FTS (right) for all measurements of July 2006

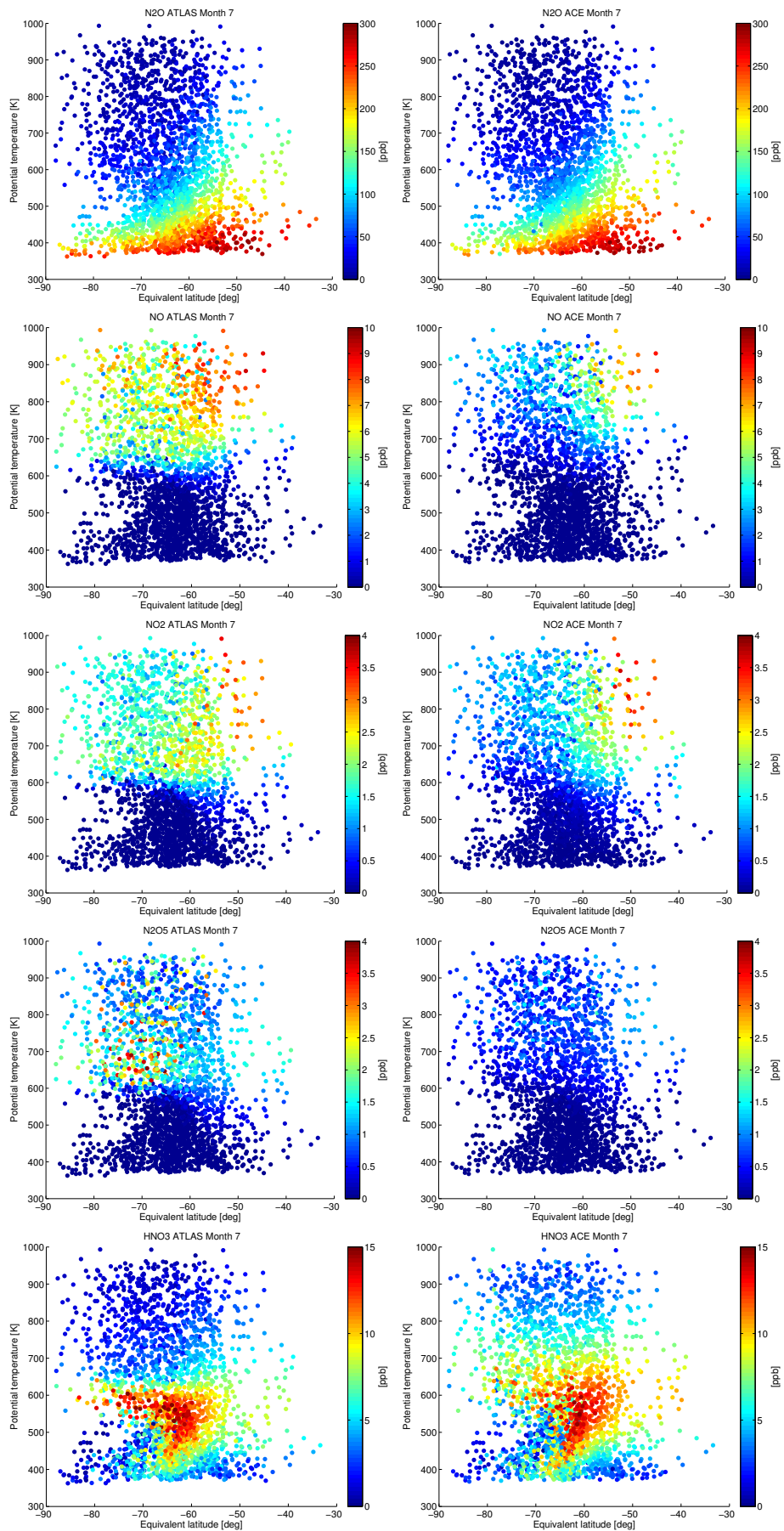


Figure 168: N₂O, NO, NO₂, N₂O₅, HNO₃ modelled by ATLAS (left) and measured by ACE-FTS (right) for all measurements of July 2006

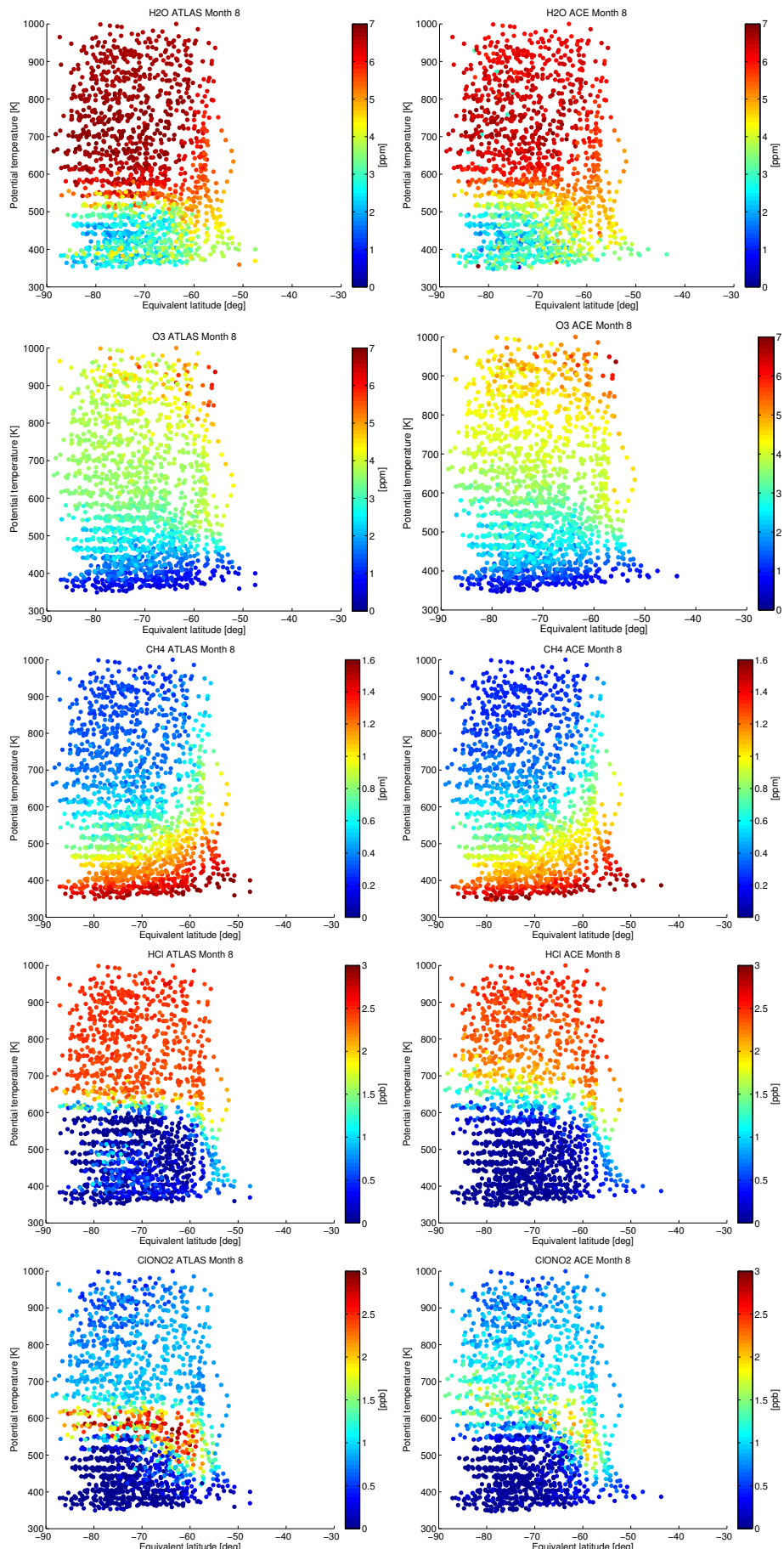


Figure 169: H₂O, O₃, CH₄, HCl, ClONO₂ modelled by ATLAS (left) and measured by ACE-FTS (right) for all measurements of August 2006

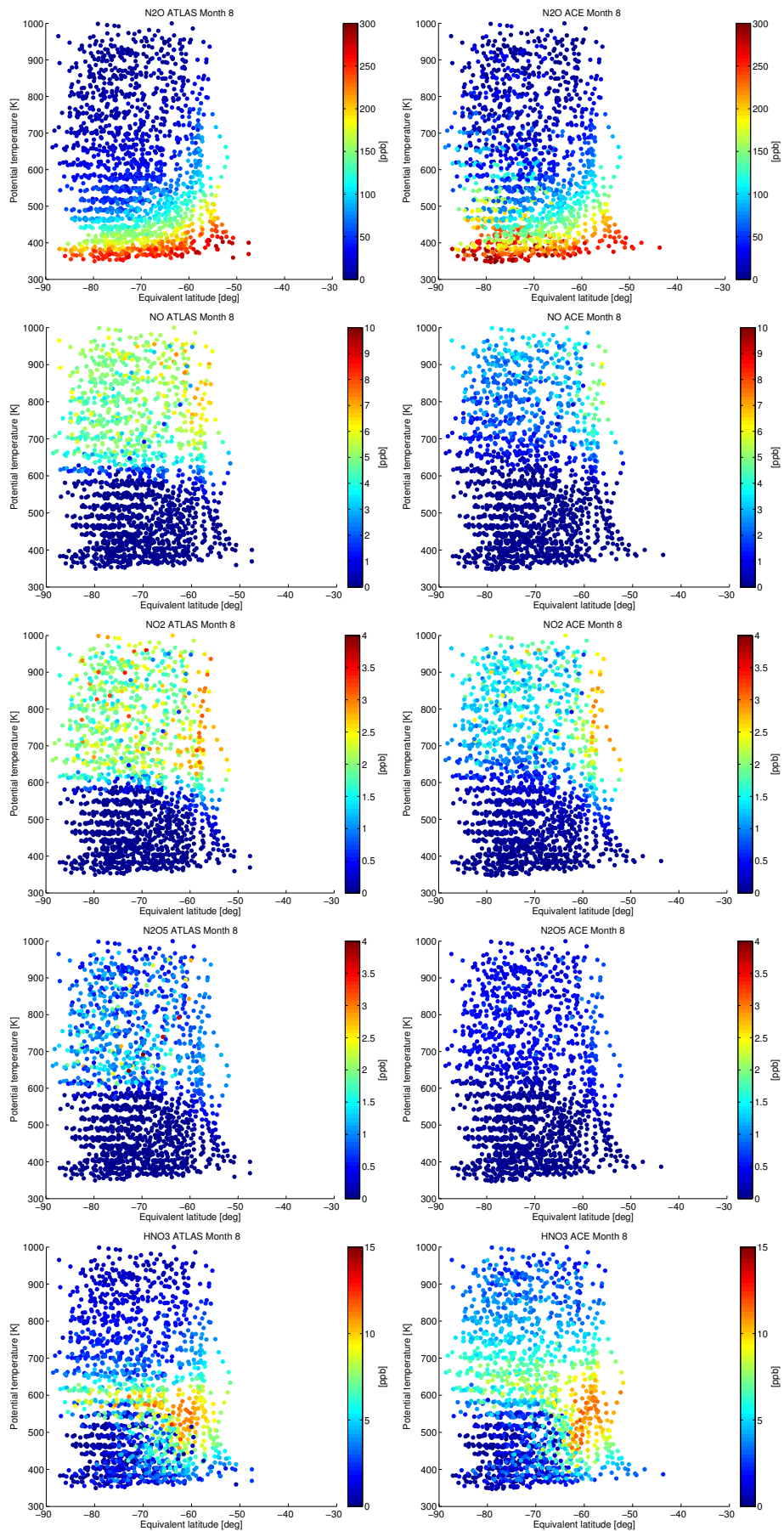


Figure 170: N₂O, NO, NO₂, N₂O₅, HNO₃ modelled by ATLAS (left) and measured by ACE-FTS (right) for all measurements of August 2006

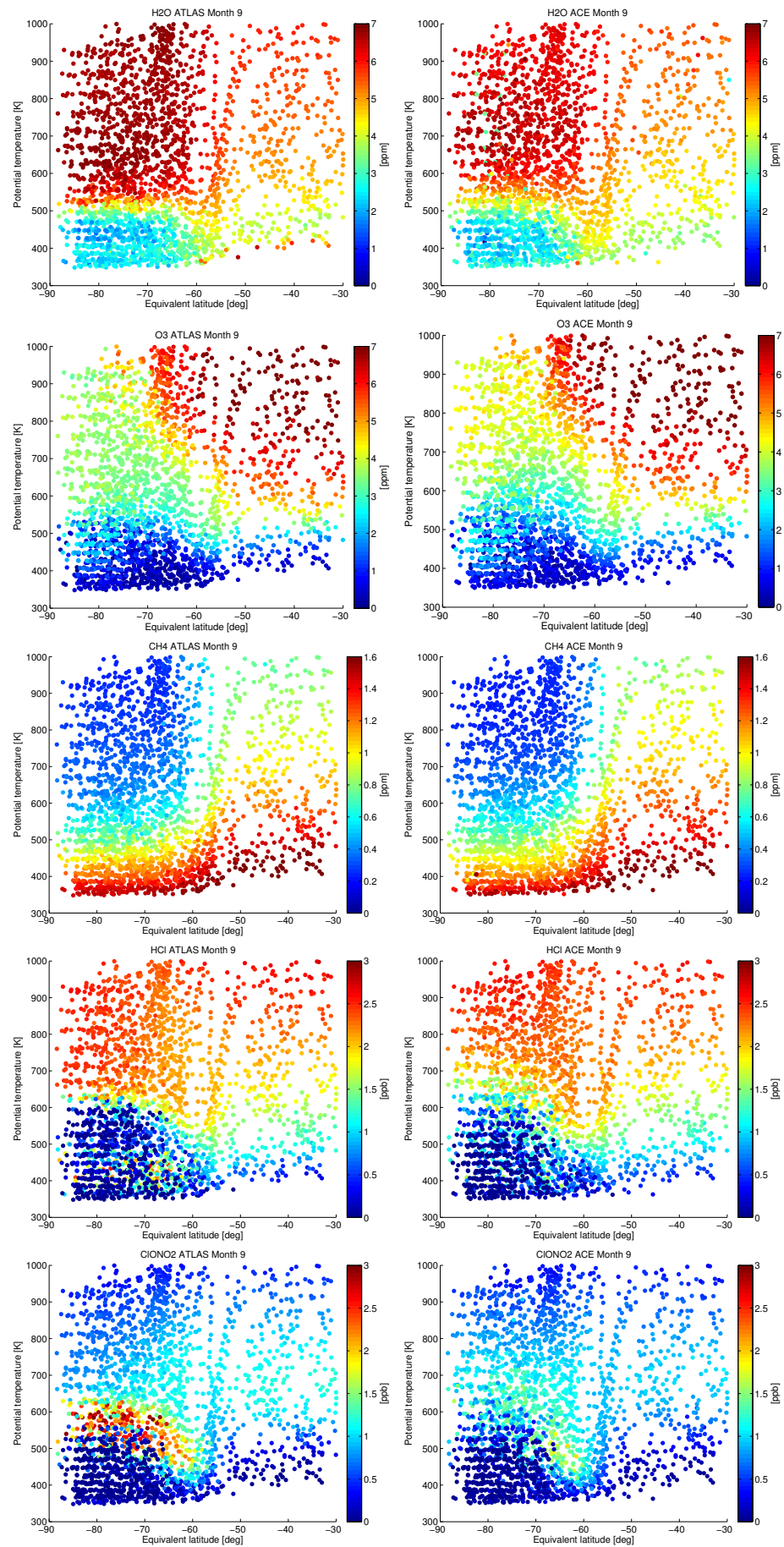


Figure 171: H₂O, O₃, CH₄, HCl, ClONO₂ modelled by ATLAS (left) and measured by ACE-FTS (right) for all measurements of September 2006

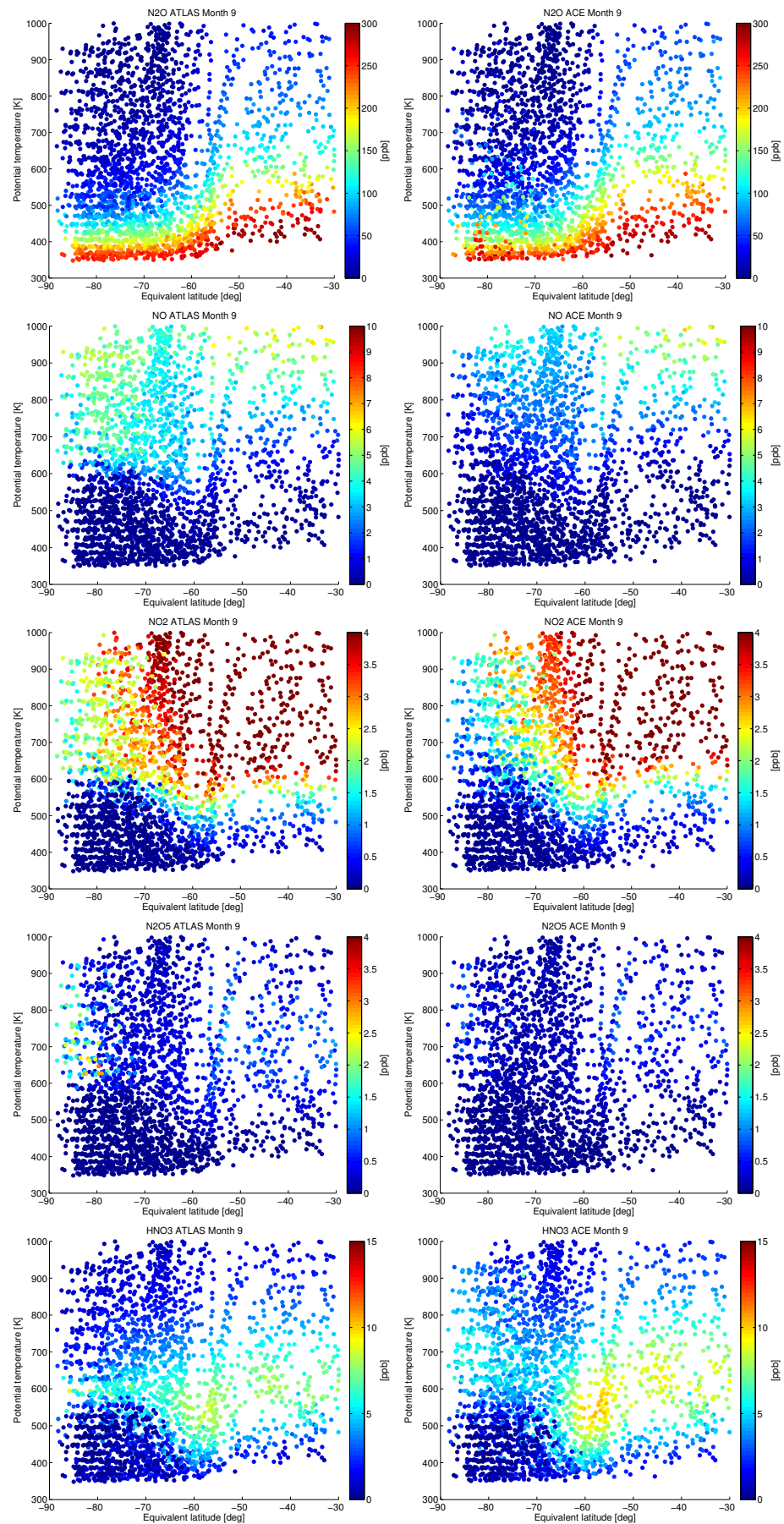


Figure 172: N₂O, NO, NO₂, N₂O₅, HNO₃ modelled by ATLAS (left) and measured by ACE-FTS (right) for all measurements of September 2006